Timothy Noël   *Editor*

Organometallic Flow Chemistry

Springer

57
Topics in Organometallic Chemistry

Aims and Scope

The series *Topics in Organometallic Chemistry* presents critical overviews of research results in organometallic chemistry. As our understanding of organometallic structure, properties and mechanisms increases, new ways are opened for the design of organometallic compounds and reactions tailored to the needs of such diverse areas as organic synthesis, medical research, biology and materials science. Thus the scope of coverage includes a broad range of topics of pure and applied organometallic chemistry, where new breakthroughs are being achieved that are of significance to a larger scientific audience.

The individual volumes of *Topics in Organometallic Chemistry* are thematic. Review articles are generally invited by the volume editors. All chapters from Topics in Organometallic Chemistry are published OnlineFirst with an individual DOI. In references, Topics in Organometallic Chemistry is abbreviated as Top Organomet Chem and cited as a journal.

More information about this series at http://www.springer.com/series/3418

Timothy Noël
Editor

Organometallic Flow Chemistry

With contributions by

C. Aymonier · C.A. Correia · K. Gilmore · K. Hellgardt ·
V. Hessel · K.K. (Mimi) Hii · H. Ishitani · S. Kobayashi ·
S. Marre · A. Nagaki · T. Noël · C.O. Kappe · B. Pieber ·
M.B. Plutschack · Y. Saito · P.H. Seeberger · Y. Su ·
P. Watts · J.-I. Yoshida

Springer

Editor
Timothy Noël
Micro Flow Chemistry
  and Process Technology
Eindhoven University of Technology
Eindhoven
The Netherlands

Preface

Continuous-flow chemistry is a relatively new field which has rapidly gained ground in the last couple of years. Especially, the use of microstructured devices has received a lot of attention as these devices provide novel and unprecedented opportunities to synthetic chemists with regard to reaction safety, mixing efficiency, and reproducibility. While this new field has met with skepticism in its advent ("we do not need another technique," "it's too complicated, let's stick with our round-bottom flasks"), more and more chemists have been convinced by the striking examples that have appeared in the literature. I do say chemists as engineers have embraced this technology from the very beginning.

However, caution is required with the euphoria surrounding continuous-flow chemistry in the present days. A microreactor is not something like a magical wand which transforms a shitty reaction with one flick into a high-impact transformation. It is important to realize that continuous-flow chemistry will definitely not solve all problems in chemistry. However, it can be very helpful in many cases. Notable examples are hazardous chemistries, unstable and reactive intermediate handling, gas-liquid reactions, and photochemical transformations. These are examples which are notoriously difficult for a chemist and where continuous microprocessing delivers a clear-cut advantage compared to classical batch processing.

Also in catalysis, many benefits from the small length scales can be envisioned. This volume of *Topics in Organometallic Chemistry* is dedicated to give an overview of the most important evolvements in the field. Hereto, I have assembled some of the leading figures in flow chemistry to contribute a review on their field of expertise.

Flow chemistry is not hard; however, it is important to know what you are doing. And yes, flow chemists do have to understand a minimum amount of engineering to get the maximum out of the technology. Therefore, the first chapter of this volume, written by Noël et al., is dedicated to give an overview of the most important engineering principles which you have to keep in mind when you are carrying out homogeneous catalysis in flow. This chapter provides also a unique guideline to assess which chemistries can benefit from flow processing. Photochemistry is another example which will profit from the small dimensions of microreactors.

This chapter, written by Gilmore et al., gives a nice overview of visible light photoredox catalysis using transition metal-based photocatalysts. Also gas-liquid reactions can be substantially accelerated in flow as the gas-liquid interfacial area is well defined. A nice overview of the use of different gases for transition metal catalysis in flow is provided by Watts. The use of oxygen in combination with flammable solvents is asking for problems when doing this in the lab, except when one is using a microreactor. Kappe et al. give a comprehensive overview on the use of oxygen for synthetic applications in flow. Yoshida et al. present a review on the generation and use of short-living organometallic species in microreactors. This is another outstanding example of challenging chemistries which are very difficult – if not impossible – to do in batch. Marre et al. describe the preparation of nanomaterials under supercritical conditions. Owing to the great control over different process parameters enabled by supercritical processing in microreactors, such materials can be reproducibly prepared which is a challenge for conventional batch techniques. Kobayashi et al. review the state of the art in enantioselective catalysis in flow reactors. This includes the immobilization of transition metal-based asymmetric catalysts providing opportunities for recycling. The last chapter in this volume is from the hand of Hii et al. A very interesting discussion on the leaching of metals in continuous-flow reactors is given. This chapter will be of great help to verify whether homogeneous or heterogeneous mechanisms are occurring.

As you can see, this volume of *Topics in Organometallic Chemistry* offers a versatile overview on the use of flow reactors for organometallic catalysis. Many of the aspects, which have brought flow chemistry to the forefront of R&D, are discussed in this book. It is my firm belief that this volume should be at the top of your reading list. I would like to express my gratitude to the colleagues and friends who contributed to this volume.

Enjoy and good luck with your own flow chemistry research!

Eindhoven, The Netherlands   T. Noël

Contents

Beyond Organometallic Flow Chemistry: The Principles Behind the Use of Continuous-Flow Reactors for Synthesis

Timothy Noël, Yuanhai Su, and Volker Hessel

Abstract Flow chemistry is typically used to enable challenging reactions which are difficult to carry out in conventional batch equipment. Consequently, the use of continuous-flow reactors for applications in organometallic and organic chemistry has witnessed a spectacular increase in interest from the chemistry community in the last decade. However, flow chemistry is more than just pumping reagents through a capillary and the engineering behind the observed phenomena can help to exploit the technology's full potential. Here, we give an overview of the most important engineering aspects associated with flow chemistry. This includes a discussion of mass-, heat-, and photon-transport phenomena which are relevant to carry out chemical reactions in a microreactor. Next, determination of intrinsic kinetics, automation of chemical processes, solids handling, and multistep reaction sequences in flow are discussed. Safety is one of the main drivers to implement continuous-flow microreactor technology in an existing process and a brief overview is given here as well. Finally, the scale-up potential of microreactor technology is reviewed.

Keywords Continuous flow · Continuous manufacturing – synthesis · Flow chemistry · Microreactors

T. Noël (✉)
Micro Flow Chemistry and Process Technology, Eindhoven University of Technology, Building 14, Helix, room STW 1.48, De Rondom 70, 5612 AP Eindhoven, The Netherlands

Department of Organic Chemistry, Ghent University, Krijgslaan 281 (S4), 9000 Ghent, Belgium
e-mail: t.noel@tue.nl

Y. Su and V. Hessel
Micro Flow Chemistry and Process Technology, Eindhoven University of Technology, Building 14, Helix, room STW 1.48, De Rondom 70, 5612 AP Eindhoven, The Netherlands

Contents

1   Introduction

Continuous-flow reactors have been increasingly used in synthetic organic chemistry to facilitate chemistries which are otherwise difficult to carry out. This includes gas–liquid reactions, photochemical transformations, chemistries utilizing hazardous compounds, extreme reaction conditions, and multistep reaction sequences. While many chemists understand the chemistry behind flow chemistry really well, the engineering aspects of the field are less understood. This seems initially not to be a major hurdle, but a thorough understanding of the engineering principles behind the observations would allow one to get the maximum out of the technology. In this chapter, we give an overview of the most important engineering aspects, which are relevant for continuous-flow chemistry in microreactors. The deeper meaning of these principles is further explained by giving relevant examples. It is our hope that this overview will aid the reader to recognize where continuous-flow reactors might actually make a difference for their chemistry and to exploit its full potential.

2   Continuous Manufacturing in the Pharmaceutical Industry

The use of continuous manufacturing is very common in the petrochemical industry, whereas in the pharmaceutical industry, the most used manufacturing principle remains batch processing. However, in recent years, continuous manufacturing has been recognized as one of the key green engineering research areas by the ACS GCI Pharmaceutical Roundtable [1]. Researchers from Eli Lilly and Company compared the use of a batch and flow process for a high-pressure asymmetric hydrogenation [2]. For this process, a high hydrogen pressure of 70 bar is required to provide high TON and TOF of the expensive catalyst. They concluded that a flow

Table 1 Main drivers for the implementation of continuous-flow processing in the pharmaceutical industry [2]

Logistics/quality	Chemistry/process	Safety
Higher throughput	Extreme reaction conditions (high p, T)	Exothermic reactions
Speed of implementation	Unstable intermediates	Reaction at high pressure with hazardous gases
Minimization of stock inventory	Demanding separations	No vapor headspace
		Toxic reagents or products

protocol was the best compromise as it provided a more practical, safe, fast, and flexible alternative for traditional batch manufacturing. Due to the high attrition rate in the pharmaceutical industry, the capital cost is a major driver. The flow plant would cost about 10 times less and was more flexible with regard to production rate. Furthermore, the development of a large-scale high-pressure autoclave (1,000 L) would be time consuming for the process engineers. The batch protocol was considered as a high-risk operation due to the use of hydrogen at elevated pressure, while the corresponding hydrogenation in flow was categorized as a much lower risk because of the small liquid and gas holdup and the reduction of the upper explosion limit. This example shows that there is indeed a need for continuous manufacturing in the pharmaceutical industry and several drivers for its implementation have been identified and categorized in three main groups: logistics/quality, chemistry/process, and safety (Table 1) [2, 3]. One of the main reasons why the pharmaceutical industry has not changed its entire production processes to continuous flow is the requirement of special equipment (investment cost). In addition, specialized equipment is of high risk as the company has typically only a few people who are familiar with continuous manufacturing and who can troubleshoot in case of failure [4]. However, most companies have established small continuous-flow research groups as they recognize the importance of the technology [5]. As such, continuous-flow processing will slowly but definitely gain ground, eventually displacing established batch techniques. This is also called "disruptive innovation," a term coined by Cristensen [6].

Researchers from the Novartis-MIT Center for Continuous Manufacturing demonstrated that it is indeed feasible to prepare complex active pharmaceutical ingredients in a continuous-flow process [7]. A fully operational pilot plant was developed for the preparation of aliskiren and integrated all required processes including synthesis, purification, formulation, and tableting. The process could be operated for 10 days, which included startup and the stabilization of key processes, and produced 45 g/h of aliskiren. Interestingly, the number of unit operations could be largely reduced from 21 in batch to 14 in flow. The total processing time could be reduced from 300 h in batch to 47 h in flow. However, it must be noted that the reaction was reengineered to avoid solids handling and solvent swaps.

The change to continuous-flow processing fits also with the current trends in Process Intensification [8, 9]. The aim of Process Intensification is to have a drastic

improvement of the equipment performance and process efficiency. One of the most popular Process Intensification technologies is microreactor, as it allows to intensify heat transport, mass transport, and photon-transport phenomena [10]. This mainly arises from the large surface-to-volume ratios in microreactors [11]. In addition, the chemistry can be further accelerated by using extreme reaction conditions, such as elevated reaction temperatures and pressures. This concept of using unusual reaction conditions is also called novel process windows, coined by Hessel [12–14]. The use of microreactor technology further provides enhanced process safety, high control over the reaction conditions, and increasing throughput by controlled scalability. According to a detailed investigation of Roberge et al., 50% of the reactions in the pharmaceutical and fine chemical industry could benefit from a continuous process [15]. For most of these reactions, the use of a microreactor would be actually the preferred device. However, solid-forming reactions were categorized as unsuitable for microreactor technology, thus reducing the total amount of suitable reactions significantly. In recent years, a lot of progress has been made to overcome the hurdles of microreactor clogging [16].

3 Mass Transport Phenomena

The overall performance of a reaction is determined by the intrinsic kinetics of the reaction and the transport properties in the reactor. The reaction rate and selectivity are substantially influenced by the mass transfer rate. A fundamental understanding of the reaction kinetics and the mass transfer characteristics is required to design a suitable reactor and scale up the chemistry from laboratory to full production scale.

The degree of mixing influences the outcome of the reaction. The mixing efficiency is directly related to the flow regime, which is characterized by the Reynolds number (Re):

$$Re = \frac{\rho D_{\mathrm{h}} u}{\mu} \tag{1}$$

where ρ is the fluid density, u the fluid velocity, D_{h} the hydraulic diameter of the channel, and μ the dynamic viscosity. The Reynolds number describes the ratio between the inertial and viscous forces. At high Re ($Re > 2,500$), the flow regime is turbulent and fluid elements exhibit a random motion, which facilitates convective mass transport. At low Re ($Re \ll 1,500$), a laminar flow regime is observed. Hereby, the fluid elements flow in parallel lamellae and mixing is governed by molecular diffusion only.

At macroscale, mixing is typically achieved by inducing a turbulent flow regime. However, owing to the small length scales, often only a laminar flow profile is observed in microchannels ($Re < 100$) [17–19]. This means that mixing is achieved by diffusion of molecules from one lamella to a neighboring one. The characteristic mixing time (t_{m}) can be calculated by the Einstein–Smoluchowski equation:
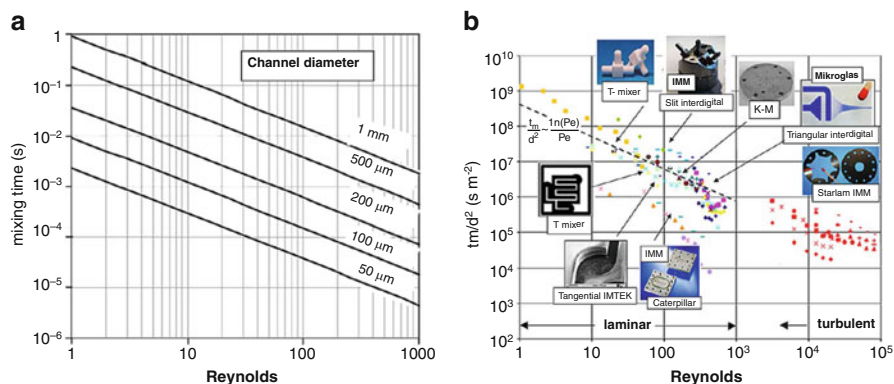
Fig. 1 (**a**) Theoretical diffusional mixing times versus Re in microchannels with varying diameters (water, $Sc = 1,000$). (**b**) Ratio of the mixing time to the square of the characteristic flow dimension versus Re for various micromixers. Reprinted with permission from Elsevier [20]

$$t_{\mathrm{m}} = \frac{L^2}{D} \quad (2)$$

where L is the diffusion distance and D is the molecular diffusivity. From this equation, it is evident that smaller dimensions lead to faster mixing. This insight has led to the development of micromixers in which the diffusion distance is reduced by splitting two reaction streams in several lamellae which are subsequently recombined (e.g., interdigital micromixer) (Fig. 1). Such passive micromixers utilize flow energy (originates from the pump) to facilitate micromixing. Other passive micromixers are, for example, T- and Y-shaped micromixers, split-and-recombine micromixers, packed-bed microchannels, and caterpillar micromixers [21]. Such a mixing process is called chaotic advection, in which fluid elements are mixed by a net transport of matter [22]. Chaotic advection is much more efficient than molecular diffusion and can be used to speed up the mixing efficiency. Active micromixers utilize external energy to introduce flow perturbations and thus to facilitate mixing. Suitable energy sources for active micromixers are ultrasound, electrohydrodynamics, pressure disturbances, magnetohydrodynamics, and thermal energy.

The ratio between the characteristic mixing time (t_{m}) and the reaction time (t_{r}) is given by the second Damköhler number (Da_{II}):

$$Da_{\mathrm{II}} = \frac{t_{\mathrm{m}}}{t_{\mathrm{r}}} \quad (3)$$

To eliminate mass transfer effects, Da_{II} should be smaller than 1 (reaction rate-controlled regime). When $Da_{\mathrm{II}} > 1$, a concentration gradient exists, which might lead to by-product formation (mass transfer controlled regime). It is therefore a good practice to start with calculating the Da_{II} for a given chemical reaction to

verify whether mixing effects occur and, consequently, if the use of more advanced mixers or reactors is required. An example of this principle is competitive consecutive reactions, in which the selectivity is governed by the rate constants of the two reactions and the mixing efficiency [23]. When $Da_{II} > 1$, disguised chemical selectivity occurs [24]. An excellent example of this effect is the monolithiation of dibromoaryls with n-BuLi [25]. Poor mixing results in the formation of higher amounts of dilithiated species than what could be expected from the kinetically based selectivity. Such observations can be rationalized by local higher concentrations of n-BuLi or accumulated monolithiated species, which give rise to fast formation of dilithiated compounds (Scheme 1). This problem can be overcome essentially via two strategies. The first one is to slow down the reaction kinetics by lowering the reaction temperature as governed by the Arrhenius equation:

$$k = A\exp\left(-\frac{E_{a}}{RT}\right) \tag{4}$$

where k is the reaction rate constant, A is the pre-exponential factor, E_{a} is the activation energy, R is the universal gas constant, and T is the reaction temperature. This is a typical strategy employed by chemists when working with batch reactors. The reaction is cooled down sufficiently so that the mixing time becomes faster than the reaction time ($Da_{II} < 1$). A second option is to increase the mixing efficiency in flow by using a micromixer. This allows to carry out the reaction at higher reaction temperatures than those typically used under conventional batch techniques (see Scheme 1). Other examples in synthetic organic chemistry where a flow strategy was used to overcome disguised chemical selectivity are the Friedel–Crafts aminoalkylation of aromatic compounds [26], anionic polymerization [27], and mono-BOC protection of diamines [28].

Calculating the Damköhler number is not always easy as it requires knowledge of the rate constants and the kinetic model. Recently, Jensen et al. have proposed an estimation of the Damköhler number based on the Fourier number (Fo) and a coefficient χ which depends on the kinetics and feed ratios [29]. The Fourier number (Fo) describes the transient mass transfer by diffusion:

$$Fo = \frac{\text{residence time}}{\text{transverse diffusion time}} = \frac{4D\tau}{d_{t}^{2}} \tag{5}$$

where D is the diffusivity, τ the residence time, and d_{t} the channel diameter. Based on this, the Damköhler number becomes

$$Da_{II} = \frac{\chi d_{t}^{2}}{4\tau D} = \frac{\chi}{Fo} \tag{6}$$

Values for the coefficient χ can be estimated by using analogous deviations for common kinetic models, allowing to rapidly estimate the value of Da_{II}.
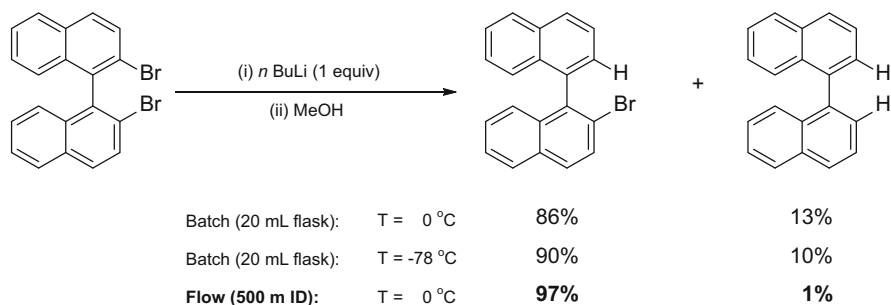
**Scheme 1** Selective monolithiation of dibromoaryl compounds in flow

Flow profiles in microchannels are considered to be laminar, yet microreactors are often described as plug flow reactors. However, this statement is only valid when the radial diffusion is much faster than convective mass transport along the channel length. Deviations from the plug flow behavior can be determined via the Taylor–Aris dispersion model [30, 31]. The Bodenstein number (Bo) describes the ratio of convection to dispersion and provides an estimation for the deviation from plug flow behavior:

$$Bo = \frac{\bar{u}L}{\mathbf{D}} = \frac{4\beta D\tau}{d_t^2} \tag{7}$$

where $\bar{u}$ is the average flow velocity, L the length of the tube, and $\mathbf{D}$ the Taylor dispersion coefficient which typically is equal to the axial diffusivity ($D_{v,a}$) in small-scale flow systems (diffusion in the direction of the flow path). In particular, the parameter β is dependent on the channel geometry, which is 48 for circular tubes and approximately 30 for square channels. For systems with $Bo > 100$, small deviations from plug flow are seen, while with $Bo < 100$, large deviations from plug flow can be observed. Figure 2 gives an overview of the different flow regimes as a function of the channel diameter and the residence time according to Eq. (7).

The effect of dispersion for flow chemistry applications is especially important for multistep reactions. Reagent plugs are sequentially injected in the reaction stream and this addition needs to be matched in terms of concentration and thus stoichiometry to obtain high conversions and selectivities. Due to the dispersion effect, the plug broadens substantially and it is difficult to predict accurately its extent (Fig. 3a). This effect is even more pronounced when using packed-bed microreactors with immobilized reagents or catalysts. Ley et al. have developed an inline infrared monitoring tool which can determine the dispersion effect of the reaction stream (Fig. 3b) [32]. LabVIEW software is subsequently used to control the flow rates of the pumps to inject reactants in real time based on the required stoichiometry. This allows to reduce the total amount of reactants required for a given transformation.

Fig. 2 Deviation of plug flow behavior due to dispersion effects in a capillary in function of the tube diameter and the residence time (diffusion coefficient $D = 10^{-9}$ m^2/s). Reprinted with permission from [29]. Copyright (2012) American Chemical Society
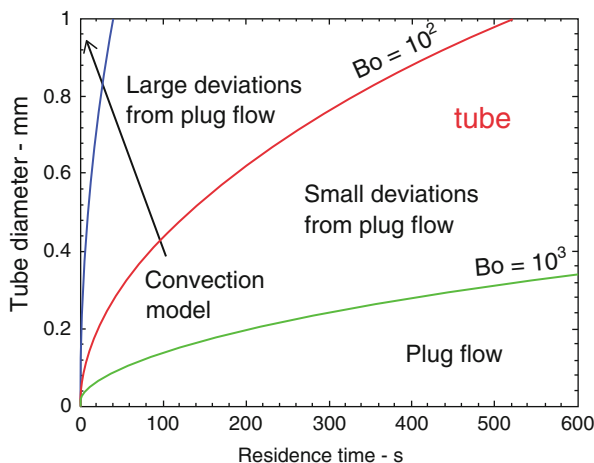
One efficient strategy to overcome dispersion effects is the use of a second immiscible phase, which generates a segmented flow regime. Such flow regime is characterized by alternating liquid segments, which are separated by bubbles of an immiscible liquid or gas. In such segments and bubbles, toroidal circulation patterns are established due to a two-phase slip. These patterns improve the mass and heat transfer and minimize the dispersion effect [33, 34]. Segmented flow regimes are often considered to be optimal plug flow reactors. Consequently, communication between the liquid slugs and segments is minimized, which is a handy tool to carry out a large number of isolated reactions in series. This strategy was used to screen different catalytic systems for the oxidation of methane with oxygen (Fig. 4) [35]. Each catalytic system was compartmentalized in an aqueous droplet and separated by an immiscible fluorous carrier fluid. The segmented flow was pumped in a tube-in-tube microreactor, to which methane and oxygen gas was dosed via diffusion through the inner PFA capillary wall. Indicator plugs, which changed color when methanol was generated, were used to obtain a semiquantitative data. Using this strategy, hundreds of reactions could be carried out in a time- and cost-efficient way, utilizing only a minimal amount of reactants. In addition, the applications of a segmented flow regime in microfluidic channels have been extended to different fields, such as the measurement of fast reaction kinetics parameters [36], protein crystallization [37], and the synthesis of nanoparticles [38].

Multiphase reactions, such as hydrogenations, oxidations, carbonylations and halogenations, are mainstay in the chemical industry [39]. In such reactions, one of the reactants is a gas and thus mass transfer of gaseous compounds from the gas to the liquid phase often constitutes the rate-determining step. It is therefore of great importance that the interfacial area is large and well defined. Conventional multiphase reactors, such as bubble columns, trickle-bed reactors, and mechanically stirred vessels, provide poor interfacial areas and are difficult to scale up while maintaining the mass transfer and reaction characteristics. With regard to hydrogenation and oxidation chemistry, the scalability problem is further aggravated due to
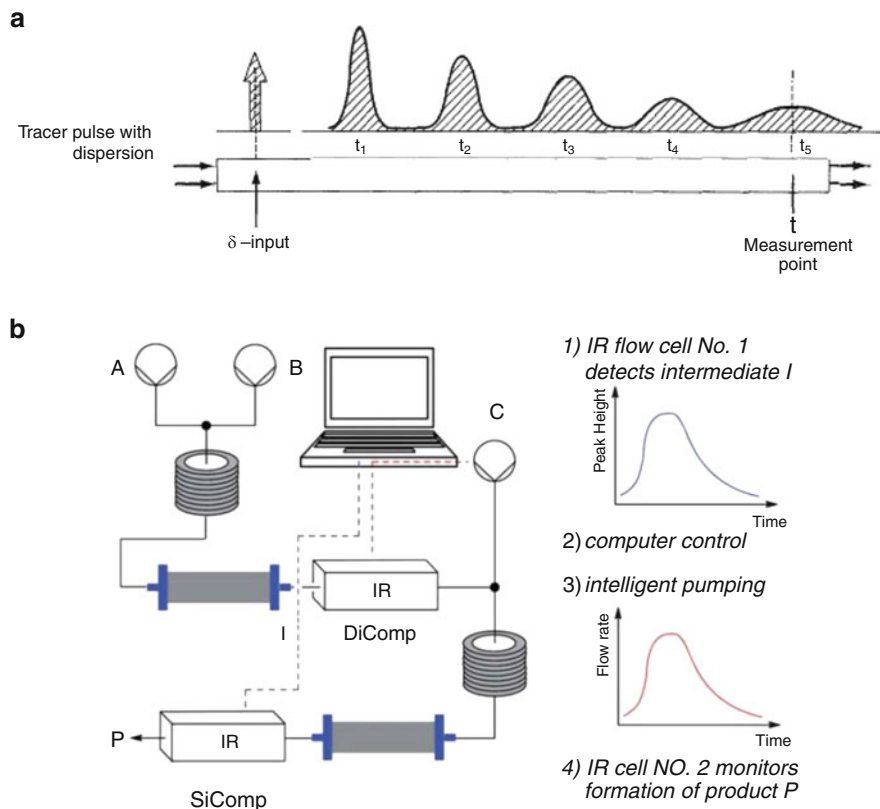
Fig. 3 (**a**) Peak broadening due to dispersion effects. Reproduced with permission from Pearson Education [30]. (**b**) Inline IR measurement in combination with LabVIEW software enables the precise control of the flow rates to match the reaction stoichiometry. Reprinted with permission from [32]. Copyright (2011) Royal Society of Chemistry

concomitant safety risks [40, 41]. Microstructured reactors provide much higher surface-to-volume ratios than conventional reactors (see Table 2). This is especially important to stimulate the mass transfer between the two immiscible phases and thus accelerate the corresponding mass transport-controlled reactions.

The mass transfer in multiphase reactions can be described with the so-called two-film model (see Fig. 5). A gaseous reactant A is diffusing from the gas phase to liquid phase where it can undergo a chemical reaction to yield a target product. The driving force for this mass transfer phenomenon is the existence of a concentration gradient. In the two-film model, two stagnant zones (gas and liquid layer) can be distinguished, where a vapor–liquid equilibrium is established. The bulk of the liquid and the gas phase is considered to be well mixed. With the two-film model, the calculation of a mass transfer coefficient (k_L) for segmented flow regime in microreactors can be simplified.
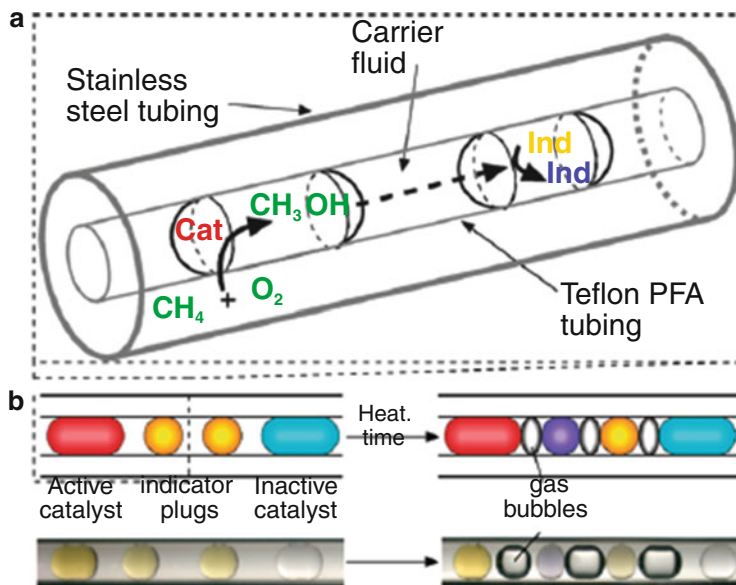
Fig. 4 A segmented flow regime enabling rapid screening of different catalysts for the oxidation of methane with oxygen. (**a**) schematic representation of the tube in tube concept in which the gas mixture diffuses through the gas permeable Teflon tubing. (**b**) Indicator plugs separate catalysts plugs and allow for identification of active catalysts. A color change to purple represents that an active catalyst is present in the adjacent catalyst plug. Reprinted with permission from [35]. Copyright (2010) American Chemical Society

Table 2 Comparison of mass transfer parameters and interfacial areas for microreactors and conventional reactors

Type of reactor/contactor	$k_L a \times 10^2$ (s^{-1})	$k_L \times 10^2$ (m s^{-1})	a (m^2/m^3)
Bubble column	0.5–24	10–40	50–600
Couette–Taylor flow reactor	3–21	9–20	200–1,200
Impinging jet absorber	2.5–122	29–66	90–2,050
Packed column	0.04–102	4–60	10–1,700
Spray column	1.5–2.2	12–19	75–170
Static mixer	10–250	100–450	100–1,000
Stirred tank	3–40	0.3–80	100–2,000
Tube reactor	0.5–70	10–100	50–700
Microreactor	30–2,100	40–160	3,400–9,000

Mass transfer efficiency is often represented by the liquid-side volumetric mass transfer coefficient ($k_L a$), which is the product between the mass transfer coefficient (k_L) and the interfacial area (a). In microreactors, the liquid-side volumetric mass transfer coefficient ($k_L a$) and the interfacial area can, respectively, reach up to 21 s^{-1} and 9,000 m^2/m^3. The $k_L a$ values are at least one to two orders of magnitude higher than those values obtained in conventional reactors (Table 2). Furthermore, increasing the flow rates results in a higher $k_L a$ as the recirculating secondary flow
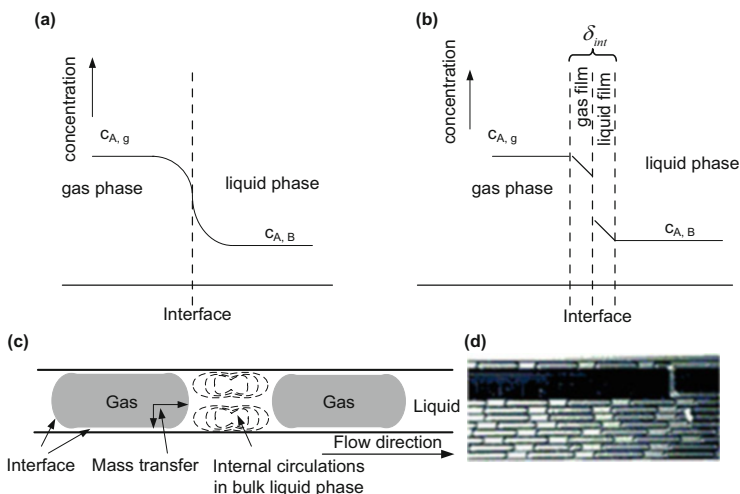
Fig. 5 (**a**) Physical representation of absorption and reaction, (**b**) schematic representation of the two-film model, (**c**) sketch of the mass transfer process in a Taylor flow regime in microchannels, and (**d**) a picture of Taylor flow for gas–liquid selective oxidation of cyclohexane with oxygen in a microreactor. Reprinted with permission from [40]. Copyright (2015) Royal Society of Chemistry

motions are further intensified. This feature can be used to facilitate fast reactions with short-living species, e.g., singlet oxygen.
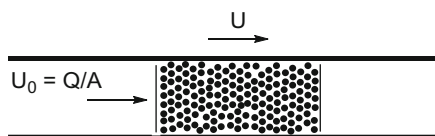
The importance of high surface-to-volume ratios and high $k_L a$ for biphasic reaction conditions can be best shown via an example involving phase-transfer catalysis [42]. A phase-transfer alkylation of phenylacetonitrile with *n*-butyl bromide in the presence of triethylbenzylammonium chloride was carried out in a PEEK capillary (ID 250 μm). By changing the aqueous-to-organic-phase volumetric flow ratio, Schouten et al. varied systematically the interfacial area from 3,000 to 5,900 m^2/m^3 at a constant total flow rate (Table 3). This resulted in an overall increase of the $k_L a$ value from 0.24 to 0.47 s^{-1} and, consequently, in a substantial enhancement of the conversion from 40% to 99%.

The high reproducibility of the interfacial area and the flexibility of biphasic microreactors have been used to evaluate the "on-water" effect for the cycloaddition of olefins with diethyl azodicarboxylate [43]. The precise control over important process parameters, e.g., interfacial area, flow rate, and residence time, allowed to study the kinetics and the activation energies of this reaction with high precision. This is very difficult to achieve with classical multiphase reactors as there is little to no control over the interfacial area.

A further increase in interfacial area can be obtained by using packed-bed microreactors (Fig. 6). These reactors often have characteristic dimensions of several millimeters but the interstitial voids between the particles can be categorized as microchannels. The superficial velocity U_0, i.e., the velocity in the open tube, can be easily calculated by dividing the volumetric flow rate with the cross-sectional area. The interstitial velocity, i.e., the velocity of the fluid in the pores of

Table 3 Influence of the surface-to-volume ratio and the $k_L a$ on the conversion of phase-transfer alkylation of phenylacetonitrile with *n*-butyl bromide

Aqueous-to-organic-phase volumetric flow ratio	Average organic slug length (μm)	Average surface-to-volume ratio (m^2/m^3)	$k_L a$ (m$_l^3$m$_r^{-3}$s^{-1})	Conversion (%)
1.0	467	3,000	0.24	40
2.3	330	4,500	0.36	74
4.0	295	5,100	0.41	92
6.1	265	5,900	0.47	99

Fig. 6 Schematic representation of a packed-bed microreactor and the difference between superficial velocity and interstitial velocity

the bed, will be much higher due to fluid continuity. If the porosity is isotropic, the relation between superficial velocity and the interstitial velocity can be calculated with the knowledge of the void fraction or porosity (ε):

$$U = \frac{U_0}{\varepsilon} \tag{8}$$

With a porosity of 0.3, it can be easily calculated that a 50 μL/min volumetric flow rate results in an interstitial flow rate of 167 μL/min. This is a substantial increase, which results improved mass transfer characteristics for multiphase flow compared to a segmented flow regime [44–46]. The immiscible fluids flow into confined interstices at high flow rates. This causes an increased shear between the fluids and results in a good dispersion, resulting in higher mixing efficiency and mass transfer rates [44, 46]. A modified Reynolds number (Re_{PB}) can be identified, which is used to identify the boundaries of the different flow regimes in a packed bed:

$$Re = \frac{\rho d_p U_0}{\mu (1 - \varepsilon)} \tag{9}$$

where d_p is the spherical particle diameter, ρ is the density of the fluid, μ is the viscosity of the fluid, and ε is the porosity. The boundaries for the different flow regimes in a packed-bed microreactor include a laminar regime ($Re_{PB} < 10$), a transitional regime ($10 < Re_{PB} < 300$), and a turbulent regime ($Re_{PB} > 300$) [47].

Packed-bed microreactors have been widely used to reduce the reaction times in multiphase reaction conditions. The bed is typically an inert material which is merely used to intensify the surface area between the two immiscible phases. Examples using organometallic catalysts in biphasic packed-bed microreactors are Buchwald–Hartwig aminations [48], α-arylations [49], Suzuki–Miyaura cross-coupling reactions [50, 51], nitration [45], and adipic acid synthesis [52, 53]. The packed bed can also be made out of catalysts, reactants, or scavengers [54]. This results often in a high increase of the reaction rate as a large excess is available [55]. One point of attention is the activity of the bed which can decrease over time due to catalyst leaching or degradation [56], deposition of by-products, or complete consumption of the immobilized reagents [57]. The packed bed can even be used as a heating device via inductive heating [58] or microwave heating [59], which allows very fast heating of the reaction mixture.

In packed-bed microreactors, a high resistance for fluid flow is encountered, which results in a high pressure drop over the bed. It is important to understand that a higher pressure drop requires a higher energy input from the pumps to overcome this barrier, e.g., HPLC pumps are suitable in most cases. The pressure drop over the packed bed can be calculated according to Darcy's law:

$$\frac{\Delta P}{L} = \frac{\mu Q}{\kappa A} \tag{10}$$

where Δp is the pressure drop, Q is the volumetric flow rate, L is the length of the bed, μ is the viscosity of the fluid, κ is permeability of the bed, and A is the cross section. From this equation, it is clear that the pressure drop will increase linearly with increasing flow rates and lengths of the packed bed. Further, the pressure drop will decrease with increasing permeability of the bed. In other words, smaller particles will result in high pressure drops as the porosity of the bed decreases with decreasing particle size. It is also important to have a narrow particle size distribution to ensure a high permeability; smaller particles can fill up the pores between larger particles resulting in a lower permeability of the bed. Large pore volumes (1–2 mL/g) can be found in monolith microreactors, where the permeability is high and the fluid encounters low resistance [60, 61].

For gas–liquid and liquid–liquid biphasic reaction conditions, the Hatta number (Ha) can be calculated which compares the rate of reaction in the liquid film to the rate of diffusion through the film:

$$Ha = \frac{\sqrt{\frac{2}{m+1} k_{m,n} (c_{A,i})^{m-1} (c_{B,bulk})^n D_A}}{k_L} \tag{11}$$

where $k_{m,n}$ is the reaction rate constant, $C_{A,i}$ is the concentration of A at the interface, $C_{B,bulk}$ is the concentration of component B in the bulk of the liquid, D_A is the diffusivity of A, and k_L is the liquid-side mass transfer coefficient. The value of Ha can be used to evaluate the extent of mass transfer limitations from the
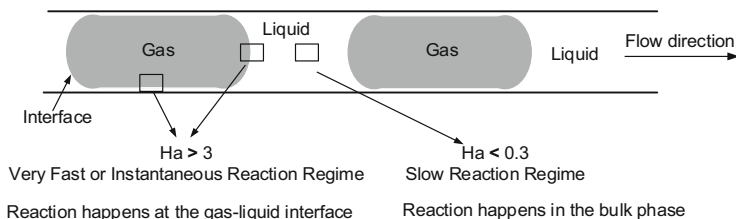
Fig. 7 Schematic representation of the different reaction regimes for gas–liquid reaction in flow according to the Hatta number. Reprinted with permission from [62]. Copyright (2014) Wiley-VCH, Weinheim

gas to the liquid phase. Two main regimes can be distinguished (Fig. 7). When $Ha < 0.3$, the reaction is in the slow reaction regime and the reaction takes place in the bulk phase. There is no gas–liquid mass transfer limitation in this regime. When $Ha > 3$, the reaction is in the instantaneous regime and the reaction occurs at the gas–liquid interface. This reaction regime occurs when the diffusion time is more than an order of magnitude longer than the reaction time.

Noël et al. have calculated Ha for the photocatalytic aerobic oxidation of thiols to disulfides and found that the value was lower than 0.06 [63]. This low value indicates that the reaction occurs in the bulk phase and that no mass transfer limitations are present in this gas–liquid photocatalytic process. The absence of mass transfer limitations allows one to determine intrinsic kinetics with microreactor technology. A similar observation was made in the aerobic oxidation of cyclohexane [64].

4 Heat Transport Phenomena

An adequate energy management is crucial in the design of any reactor to guarantee a high yield and selectivity [65]. This is especially mandatory for highly exothermic reactions, in which uncontrolled heat generation can lead to thermal runaways and ultimately to explosions. For any chemical reaction, the classical heat balance can be used without considering the effect of axial dispersion:

$$\frac{dT}{dV} = \frac{dT}{S \cdot dz} = \frac{r \cdot (-\Delta H_R)}{mC_P} - \frac{U \cdot a \cdot (T - T_c)}{mC_P} \tag{12}$$

where T is the temperature of reaction mixture, V is the reactor volume, S is the cross-sectional area, z is the reactor length along the flow direction, a is the specific heat-exchange surface, ΔH_R is the reaction enthalpy, C_P is the mean specific heat capacity of the reaction mixture, and U is the global heat-transfer coefficient. The first item on the left describes the variation of the temperature along the flow direction. The first item on the right describes the rate of heat generated through

reaction and the second item represents the rate of heat removed through the channel wall.

One of the most important design parameters for a chemical reactor is the adiabatic temperature rise (ΔT_{ad}), which represents the worst-case scenario of heat generation. ΔT_{ad} is the increase in reaction temperature as a result of an exothermic reaction in the absence of any heat dissipation to the environment. In other words, this is the maximum temperature increase one can expect and its value is used to design the chemical reactor and to incorporate appropriate safety measures. ΔT_{ad} is given by the following equation:

$$\Delta T_{ad} = \frac{c_{s,0}(-\Delta H_R)}{\rho C_p} \tag{13}$$

where $c_{s,0}$ is the inlet concentration of the substrate and ρ is the mean density of the reaction mixture.

The temperature profile in a chemical reactor is in reality depending on the global heat-transfer coefficient (U), which accumulates all heat-transfer resistances and can be expressed as follows:

$$\frac{1}{U} = \frac{1}{h_{in}} + \left(\frac{d_{out} - d_h}{2\lambda_{wall}}\right)\frac{a}{a_m} + \frac{1}{h_{out}}\frac{a}{a_{out}} \tag{14}$$

The first item describes the resistance between the channel wall and reaction mixture, the second item represents the resistance of channel wall, and the third item expresses the resistance located between the outer wall and the cooling fluid. The convective heat-transfer coefficients (h_{in} and h_{out}) are related to the hydrodynamics and the hydraulic diameter of reactors, which can be calculated through the Nusselt number (Nu): [66]

$$h_{in} = Nu \cdot \lambda_{fluid}/d_h = \left[3.65 + \frac{0.19(Re \cdot Pr \cdot d_h)^{0.8}}{1 + 0.117(Re \cdot Pr \cdot d_h)^{0.467}}\right] \cdot \lambda_{fluid}/d_h \tag{15}$$

According to this correlation, a reduction of the hydraulic diameter (d_h) will result in an increase of the heat-transfer coefficient (Fig. 8). This in combination with the large heat-transfer surface area makes that microreactors are ideally suited for heat-exchange purposes. This was already realized in 1981 by Tuckerman and Pease in their landmark paper on micro heat exchange [67]. They reported that heat dissipation up to 790 W/cm^2 was possible for a single-phase water-cooling system, which was used for cooling integrated circuits. Since then many different applications of micro heat exchangers have been realized, e.g., in automotive industry, electronic industry, and microreactor technology [68].

To ensure a proper energy balance within the chemical reactor, it is crucial to ensure that the heat removal rate is at least equal to the heat generation rate. This
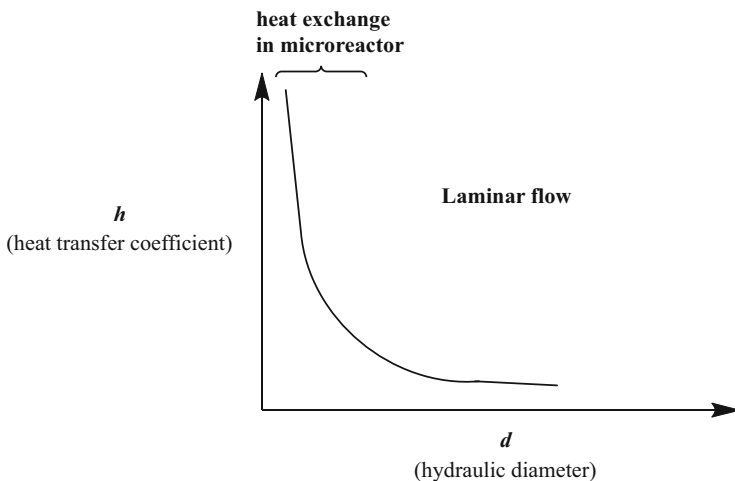
Fig. 8 Effect of the hydraulic diameter d on the heat-transfer coefficient h

means that the ratio of heat generation rate to the heat removal rate should be lower than 1:

$$\beta = \frac{\text{heat generation rate}}{\text{heat removal rate}} = \frac{-r\Delta H_R d_h}{6\Delta T_{ad} h_{in}} \leq 1 \tag{16}$$

Due to the high surface-to-volume ratio, material properties and surface characteristics of the microchannels play a dominant role in the heat-exchange efficiency [69]. Circular channels give the best thermal and hydrodynamic performance, while rectangular channels are still often used due to the ease of manufacturing. The heat-exchange efficiency can further be intensified by increasing the surface area through heat pin-fins or channel curvature [70]. But also the channel material is important as described in Eq. (14); higher conductivities result in a higher global heat-transfer coefficient (U) (Table 4). The choice of material is given in by (1) the availability and cost of the material, (2) the ease of handling of the material and manufacturing process, (3) the thermal conductivity, (4) the surface roughness of the material, and (5) the operational conditions. Stainless steel is often used to make microreactors as it is cheap and can resist high pressure and temperature [71]. It provides a high heat conductivity; however, it is not compatible with acidic media due to corrosion. Silicon microreactors are used owing to their favorable thermal conductivity and ease of manufacturing [72]. The latter can be attributed to a broad availability of micromachining techniques from the silicon and computing industry. Silicon microreactors can withstand high temperatures and pressures and provide chemical resistance to a broad range of chemicals. However, strong alkaline reaction mixtures can erode the channels, which can be overcome by special surface treatments [34]. The use of polymer-based microreactors, such as the widespread PFA and FEP capillaries, are less suited for heat-exchange purposes considering

Table 4 Thermal conductivity of some materials commonly employed for the fabrication of microreactors

Material	Thermal conductivity [W m^{-1} K^{-1}]
PFA	0.195
FEP	0.19–0.24
Glass	1
Stainless steel	12–45
Silicon	149
Aluminum	237 (pure)
	120–180 (alloy)
Silicon carbide	120–490
Copper	401

their low thermal conductivity. However, they are still used a lot in micro flow chemistry applications as a result of their easy fabrication, low cost, and high chemical stability. Furthermore, due to the optimal light transparency properties, the use of polymeric microreactors is advantageous for photochemical applications [62, 73]. Aluminum alloys are mostly used to fabricate micro heat exchangers in the automotive and thermal industry by virtue of their lower weight compared to stainless steel [74]. Silicon carbide has a very high thermal conductivity and an exceptional chemical stability [75]. However, this material is quite expensive and brittle. Therefore, it is mainly used for highly exothermic reactions, where a high heat dissipation rate is desired.

The use of microreactors is especially interesting for fast and highly exothermic reactions $(-\Delta H_R > 50$ kJ/mol) [76]. In batch, such reactions are typically conducted under suboptimal reaction conditions, meaning that the reaction is cooled substantially to slow down the reaction kinetics and thus to minimize the concomitant heat generation (see discussion Da_{II}). Intriguing examples, where the reaction can be carried out at higher temperatures in flow, are transmetallation reactions. As can be seen from Fig. 9, the monolithiation of 1,2-dibromobenzene needs careful temperature control to provide high selectivity [77]. Hot-spot formation leads in batch to the formation of benzyne and derived by-products. Consequently, the reaction needed to be cooled down to $-100°C$ to obtain decent yields. In flow, the reaction could be carried out at $-70°C$ to $-75°C$ thanks to the improved heat and mass transfer characteristics by using stainless steel micromixers and reactor coils. The heat production is the highest at the mixing zone where the reactants are merged. Depending on the exothermicity of the reaction (ΔT_{ad}), the formation of hot spots is still possible with instantaneous reactions even when one is using a microreactor. An interesting strategy to avoid formation of hot spots is to spread the heat production by multi-injection of the reactants along the reactor length [78]. The extent of the hot spot can be minimized by increasing the amount of injections. An application of this multi-injection protocol was the Grignard reaction between phenylethylmagnesium bromide and 2-chloropropionyl chloride [79]. A four-injection strategy was sufficient to temper the exotherm of the reaction and allowed to increase the selectivity of the reaction up to 50% yield. Furthermore, the heat management in microreactor systems can also be improved by applying a
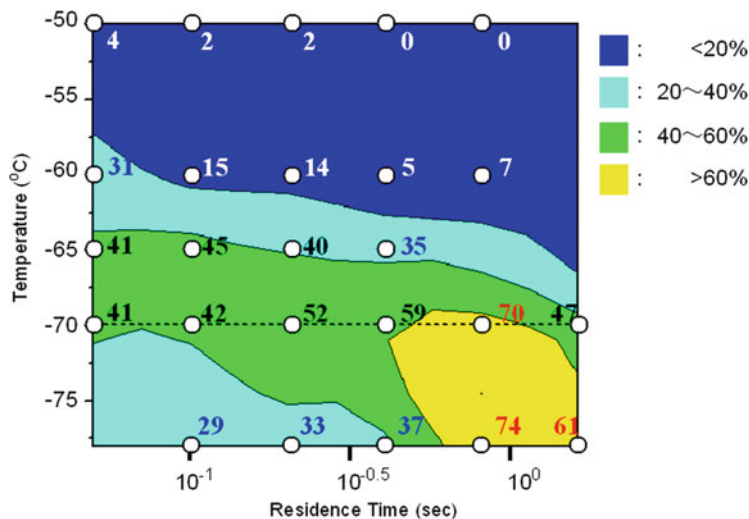
Fig. 9 Contour plot which visualizes the correlation between the reaction temperature, residence time, and the yield of bromobenzene. Reprinted with permission from [77]. Copyright (2007) American Chemical Society

multistage temperature ramping approach [53]. The main characteristics of this approach are to use various temperatures in different sections of the reactor according to the reaction properties. This strategy allows to avoid hot spot formation throughout the microreactor, which is particularly useful for reactions involving thermal decomposition of reactants (e.g., adipic acid synthesis from cyclohexene and hydrogen peroxide). The use of multiphase reaction streams, e.g., segmented flow, can also intensify the heat dissipation which provides a high degree of control over the selectivity of the reaction. Notable examples are oxidations [53], hydrogenations [80], nitrations [81], hydroformylations [82], and direct fluorinations [83, 84].
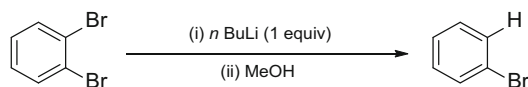
Some organic reactions need harsh conditions, including high temperatures and pressures, to provide substantial conversions. In batch, such reactions were typically carried out in autoclaves or microwave reactors [85, 86]. However, the use of an autoclave involves complex reactor design and raises important safety issues. The use of microwave reactors remains limited as scalability is hampered because of the limited penetration depth of the irradiation [87]. In microreactors, often a rapid heating can be achieved due to the small characteristic length scales. The fast heat transfer even allows to carry out reactions in the absence of any solvent, highlighting the green aspect of continuous-flow processing in microreactors [88–

90]. An even faster heat transfer can be achieved by using microwave [91] or induction heaters [92]. Microwave heating is enabled by absorbance of the energy due to interaction of dipoles with the microwaves. The rate of microwave heating is determined by the dielectric constant of the solvent. Selective heating can also occur through coupling with immobilized catalysts, which are either deposited on the reactor walls or used as a packed bed [59, 93]. The use of microwave heating can be beneficial for heating mesoscale flow reactors (>1 mm) as the efficiency of microwave energy transfer increases with larger diameters [94, 95]. Induction heating can heat packed-bed reactors very fast due to generation of eddy currents in electrically conducting objects via a constantly changing electromagnetic field (joule heating). The magnetic nanoparticles can be decorated with catalysts and thus selective heating takes place where the reaction occurs [58]. Interestingly, by using back-pressure regulators, reaction solvents can be heated above their boiling point (super heating). Furthermore, solvents or gases can be heated and pressurized above their critical point furnishing supercritical reaction conditions [96–98]. Supercritical conditions provide reduced viscosity and interfacial tension, improved diffusivities, and increased gas solubility.

5   Photon Transport Phenomena

The use of photons to initiate chemical reactions has been known for decades in organic synthetic chemistry [99–101]. It provides opportunities to carry out remarkable reactions which are otherwise difficult to realize with classical thermochemical approaches. In recent years, a new wave in photochemistry has emerged in which visible light photoredox catalysis has been recognized as a mild and selective way of small molecule activation [102–104]. The use of photons as "traceless reagents" abides to the green chemistry principles; in the absence of any reaction, the starting material can be recovered when it returns to its ground state. Nevertheless, many engineering challenges are associated with photochemical processes and these can be often attributed to the Lambert–Beer limitation (attenuation effect of photon transport) [105]. Many of these issues can be overcome by using continuous-flow photomicroreactors [62, 73, 106–109].

Photochemical processes are initiated by the absorption of photons. Thus, conversion and yield are highly depending on the energy distribution within the reactor. In photochemical reactors, a gradient in photon absorption exists which is due to absorption or light scattering. In order to maximize the efficiency of the photochemical reactor, it is important that the radiation distribution is as homogeneous as possible. The radiation distribution can be represented by the spectral specific intensity (I) and gives the amount of irradiative energy through a unit area per unit wavelength per unit time:

$$I\left(s,\ \underline{\Omega},\ t,\lambda\right) = \lim_{dA,\,d\Omega,\,dt,\,d\lambda}\left(\frac{dE_\lambda}{dA\cos\theta d\underline{\Omega}dtd\lambda}\right) \tag{17}$$

where dE_λ is the total amount of irradiative energy passing through a unit area in the time dt and within a wavelength range between λ and $\lambda+d\lambda$. Integrating the spectral specific intensity over the reactor surface provides the incident radiation (G_λ):

$$G_\lambda(s,t) = \int_{\underline{\Omega}} I_{\lambda,\underline{\Omega}}(s,t)d\underline{\Omega} \tag{18}$$

The local volumetric rate of energy absorption (LVRPA) is an important parameter depending on the design of the photoreactor, the light source intensity, and the photophysical properties of the reaction mixture. Due to absorption and light scattering, the LVRPA is not uniform. Considering the small length scales, the nonuniformity of the LVRPA can be minimized in a microreactor:

$$LVRPA_\lambda(s,t) = \kappa_\lambda G_\lambda(s,t) \tag{19}$$

where κ_λ is the volumetric absorption coefficient that represents the fraction of the incident radiation that is absorbed by the matter per unit length along the path of the beam. However, even when the photons are absorbed by the reaction medium, not every absorbed photon will give rise to one reaction event. The excited state can return to its ground state through radiative or non-radiative (e.g., heat generation) processes. The efficiency of the photochemical process can be given by the quantum yield:

$$\phi = \frac{\text{number of } P \text{ molecules formed}}{\text{number of photons absorbed by reactive medium}} \tag{20}$$

The quantum yield typically varies between 0 and 1.0. $\Phi > 1$ typically indicates that a chain reaction occurs, e.g., polymerizations can have $\Phi > 10^4$ [110, 111]. Quantum yields can be determined by measuring first the photon flux with chemical actinometry [112] and subsequently carrying out the reaction in the same photochemical setup. The photon flux is defined as follows:

$$\text{photon flux} = \frac{G_\lambda \times \lambda}{hc} \tag{21}$$

where h is the Planck constant and c is the speed of light in vacuum, respectively. Loubiere et al. have reported on the measurement of photon fluxes in photomicroreactors [113]. It is important to note that the energy emitted by the light source is not equal to the photon flux through the reaction medium, i.e., not every photon emitted by the light source will travel through the reactor. The authors compared the photon flux for a microreactor and a batch reactor. The batch reactor received 7.4×10^{-6} einstein/s, while the microreactor acquired a photon flux of

4.07×10^{-6} einstein/s. However, the absorbed photon flux density (Φ/V_r) was much higher for the microreactor: compare 5.02 einstein/(m^3 s) to 0.033 einstein/ (m^3 s) for the batch reactor. This 150-fold higher absorbed photon flux density explains clearly the substantial rate accelerations that are typically observed in microreactors.

The photonic efficiency (ξ) of a reactor can be defined as follows:

$$\xi = \frac{\text{rate of the reaction}}{\text{photon flux}} \tag{22}$$

The photonic efficiency (ξ) in microreactors ($\xi = 0.0262$) [114] is about one order of magnitude higher than those in batch reactors ($\xi = 0.0086$–0.0042) [115]. This value can be further improved by using microscale light sources (e.g., LEDs), which matches the dimensions of the microchannels or the optimization of light propagation with the help of optical fibers or mirrors as light reflectors [116]. By using LEDs and a capillary microreactor, Noel et al. were able to further increase the photonic efficiency to 0.66 representing a 160-fold improvement compared to batch photoreactors [117].

A full description of photon-transport phenomena is quite complex and is beyond the scope of this review [118]. For monochromatic light, photon transport can described according to the following equation:

$$\frac{dI_{\lambda,\underline{\Omega}}(s,t)}{ds} + \underbrace{k_\lambda(s,t)I_{\lambda,\underline{\Omega}}(s,t)}_{\text{Absorption}} + \underbrace{\sigma_\lambda(s,t)I_{\lambda,\underline{\Omega}}(s,t)}_{\text{out-scattering}} = \underbrace{j_\lambda^e(s,t)}_{\text{Emission}} + \frac{\sigma_{\lambda,\underline{\Omega}}(s,t)}{4\pi}$$

$$\times \underbrace{\int_{\underline{\Omega}'=4\pi} p(\underline{\Omega}' \rightarrow \underline{\Omega})I_{\lambda,\underline{\Omega}'}(s,t)d\underline{\Omega}'}_{\text{in-scattering}} \tag{23}$$

This equation describes all relevant phenomena which can be encountered in photochemical processes, including absorption, emission, and scattering effects. Emission effects can be neglected when the reaction is carried out at low reaction temperatures. For homogeneous reaction mixtures, also scattering effects can be minimized, and if the light intensity is kept constant and propagates unidirectional, the equation can be simplified to

$$\frac{dI_{\lambda,\Omega}(s)}{ds} = -k_\lambda(s)I_{\lambda,\Omega}(s) \tag{24}$$

Integration of this equation results into the well-known Bouguer–Lambert–Beer law for photon transport:

Fig. 10 Transmission of incident light as a function of distance in a reaction medium containing Ru (bpy)$_3^{2+}$ as a photocatalyst. The profile is obtained by utilizing the Bouguer–Lambert–Beer law: concentration photocatalyst $c = 0.5$ mM; molar extinction coefficient ε[Ru (bpy)$_3^{2+}$] = 13,000 cm^{-1} M^{-1}; path length l; transmission T
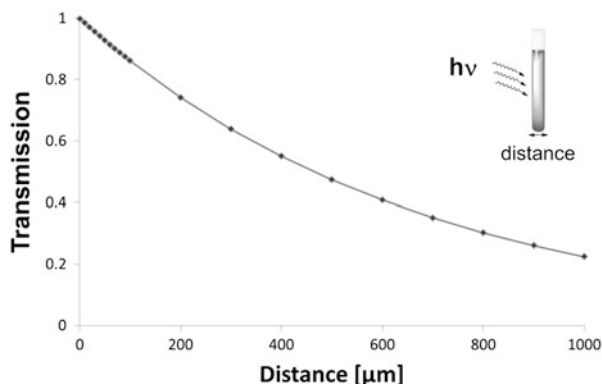
$$A = \log_{10}T = \log_{10}\frac{I_0}{I} = \varepsilon c l \tag{25}$$

This equation displays the dependence of the absorption on the molar extinction coefficient (ε), the concentration of absorbing species (c), and the path length of light propagation (l). The importance of the length scale in photochemistry can be clearly shown by plotting this equation for a relevant photocatalytic reaction using Ru(bpy)$_3^{2+}$ (0.5 mM) as a photocatalyst, as shown in Fig. 10. After 500 μm, already 50% of the light intensity is absorbed by the photocatalyst. It should be noted that in some reactions the catalyst loading and the molar extinction coefficient can be even higher. This clearly demonstrates the importance of using a photomicroreactor to provide sufficiently high-photon fluxes through the entire reaction medium.

6 Determination of Intrinsic Kinetics and Automation of Chemical Processes

For scale-up of a chemical reaction, knowledge of the intrinsic reaction kinetics is crucial. Coupling the obtained kinetics with mass- and heat-transfer phenomena allows one to accurately dimension a large-scale reactor. Elucidation of the kinetics is also important to study the reaction mechanism [119].

The rate law, which links the reaction rate to the concentration of the reactants, can be expressed generally as follows:

$$r = kc_A{}^x c_B{}^y \tag{26}$$

where k is the rate constant, c_A and c_B are the concentrations of the reactants A and B, and the exponents x and y are the reaction orders, which do not need to be an integer and can even be negative values. The sum of the reaction orders is the overall order of the reaction. Table 5 gives an overview of some common reaction

Table 5 Rate laws for some simple reactions

Reaction	Order	Differential form	Integrated form
$A \rightarrow P$	Zeroth	$\frac{d[A]}{dt} = -k$	$[A] = [A]_0 - kt$
$A \rightarrow P$	First	$\frac{d[A]}{dt} = -k[A]$	$\ln[A] = \ln[A]_0 - kt$
$A + A \rightarrow P$	Second	$\frac{1}{2}\frac{d[A]}{dt} = -k[A]^2$	$\frac{1}{[A]} = \frac{1}{[A]_0} + 2kt$
$A + B \rightarrow P$	Second	$\frac{d[A]}{dt} = -k[A][B]$	$kt = \frac{1}{[B]_0 - [A]_0} \ln \frac{[B]_0[A]}{[A]_0[B]}$

orders and the corresponding differential and integrated rate equations. For any reaction, the rate law can be experimentally verified with differential or integral methods. Obtaining reliable kinetic data requires high experimental accuracy and, in addition, transport phenomena can mask the intrinsic reaction kinetics, which further complicates the results gathering [120]. Concentration and temperature gradients can result in misleading information and kinetics obtained under these circumstances still include disturbing transport effects (so-called apparent kinetics). In contrast, intrinsic kinetics are scale independent and can be used to model a reactor accurately, which is required to develop a safe and economical chemical process.

The use of microreactor technology for estimating reaction kinetics has been demonstrated by many authors. Owing to the improved mass- and heat-transfer characteristics, intrinsic kinetic data can be extracted from the experiments. An isothermal operated microreactor is required to determine intrinsic kinetics for highly exothermic or endothermic reactions [121]. The high degree of reproducibility on experimental data in microflow provides better accuracy than obtained in conventional batch reactors. This is especially the case for gas–liquid reactions, where the poorly defined interfacial area in batch increases the error on the kinetic data [122]. In addition, the typical small reactor volumes make that the consumption of chemicals remains small, making the use of microreactors for kinetic studies cost-efficient [123]. Inline spectroscopical detection systems can be combined with microreactor technology and maximizes the information content of each experiment [124]. One of the major advantages of batch kinetics is that it allows to generate a lot of data in a single experiment by collecting several data points over time. Time-series data can be obtained in microflow reactors by using a controlled ramp of the flow rate and inline analysis methods [125, 126].

Obtaining reaction kinetics can be a time-consuming undertaking and, recently, a lot of effort has been devoted to develop completely automated systems [127]. This allows to reduce the manual labor, to increase the efficiency of results collection, and to implement design of experiment (DOE) methods [128]. This approach has been used to optimize the Mizoroki–Heck coupling between 4-chlorobenzotrifluoride and 2,3-dihydrofuran in a microreactor (Fig. 11) [130]. An inline HPLC was used to measure the yield and the selectivity of the reaction. This information was analyzed by a computer and feedback control was delivered with regard to the reagent concentration and residence time. As such, a rapid optimization (19 experiments in total) of the reaction parameters was carried
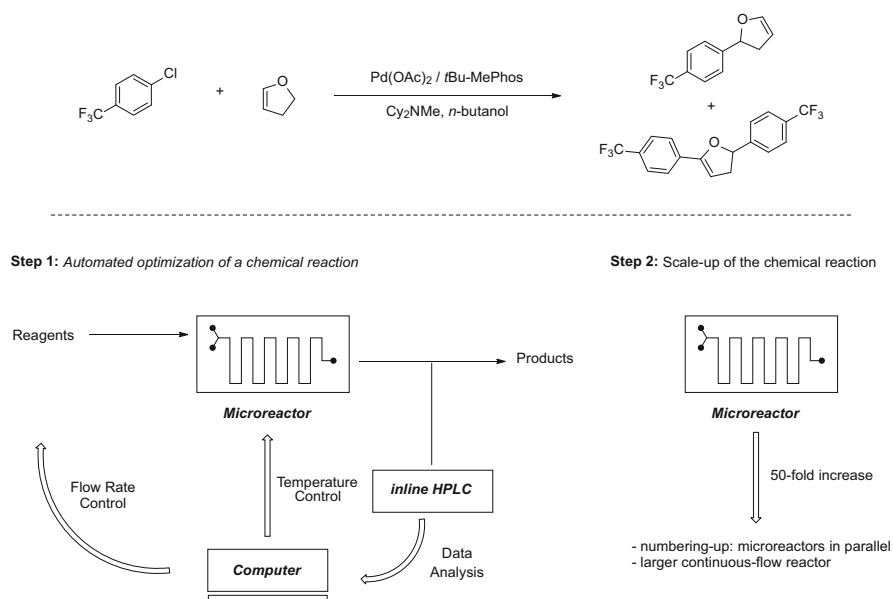
Fig. 11 Schematic representation of a "self-optimizing" microfluidic platform for the Mizoroki–Heck coupling between 4-chlorobenzotrifluoride and 2,3-dihydrofuran in a microreactor. The obtained results could be subsequently scaled up in a mesoscale reactor. Reprinted with permission from [129]. Copyright (2014) Wiley-VCH, Weinheim

out in a time-efficient fashion with no additional manual labor, allowing to mini-mize the total amount of chemical consumption. These reaction conditions were subsequently scaled in a mesoscale reactor requiring no additional optimization. Similar automated approaches were used to determine the reaction kinetics of various chemical reactions [131, 132] and to perform multistep sequences in combination with purification steps [133].

For photochemical reactions, the intrinsic reaction rate strongly depends on the local volumetric rate of energy absorption (LVRPA) and the quantum yield (Φ). For a simplified A→B reaction and under plug flow behavior, the rate equation can be described as follows: [134]

$$r = \Phi_\lambda (LVRPA)_\lambda \tag{27}$$

For the photocatalytic aerobic oxidation of thiols to disulfides [135], Noël et al. have investigated the effect of the photon flux on reaction yield: a clear effect can be seen on the reaction rate constant (Fig. 12) [63, 117]. At low photon fluxes, no difference is noticed between a high and a low catalyst loading (Fig. 12a). This indicates that the reaction occurs under a photon limited regime and the photons are constantly consumed to excite the photocatalyst. Based on the experimental results, a correlation for the reaction rate constant could be derived which demonstrates its dependence on the catalyst loading and photon flux.
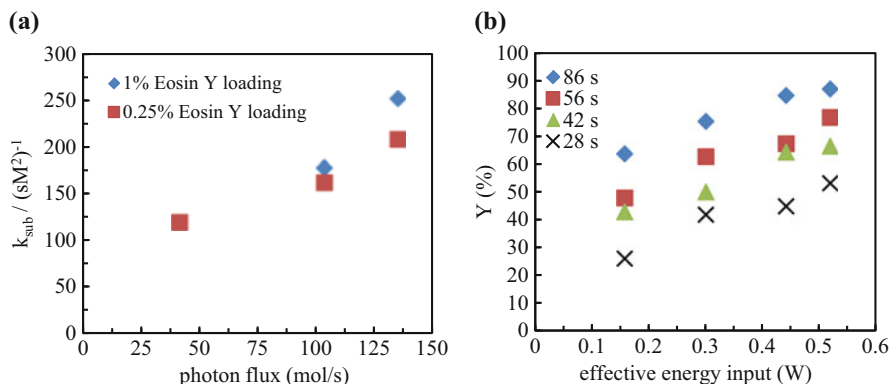
Fig. 12 Photocatalytic aerobic oxidation of thiols to disulfides. (**a**) Dependence of the reaction rate constant on the photon flux. (**b**) Relationship between the yield and the effective energy input at 1% photocatalyst loading. Reprinted with permission from [117]. Copyright (2015) Wiley-VCH, Weinheim

$$k_{\text{sub}} = 228.6 q^{0.56} \varphi^{0.21} \tag{28}$$

At a high catalyst loading, the yield or the reaction rate increased with increasing the effective energy input for a photochemical process (Fig. 12b). The relationship between the yield and the effective energy input was found to be generally linear at various residence times.

7 Safety Aspects

Increased safety of chemical processing is one of the main drivers to implement continuous-flow processing in the industry [136]. The small dimensions of a typical microreactor provide opportunities to process small amounts of hazardous material and, therefore, minimize the risks associated with its handling [76].

The power of an explosion is proportional to the mass of the explosive mixture in the reactor with the power of 1/3. This directly explains why microreactors are inherently safe to use on a laboratory scale and to carry out explosive reaction conditions. However, it is important to note that an explosion can propagate to the mixing chamber or the collection vessels where often the inventory of flammable material is much larger [137, 138]. It has been demonstrated that explosion propagation occurs when the tube diameter is larger than λ/π, where λ represents the detonation cell width and can be calculated from the induction length [139]. This is the so-called $\lambda/3$ rule which has been originally validated for macroscopic tubes. This rule can be used to calculate the diameter of the microreactor in which safe processing of the reaction mixture can be done. For an ethane/oxygen mixture, it was found that the diameter had to be lower than 0.1 mm to avoid explosion
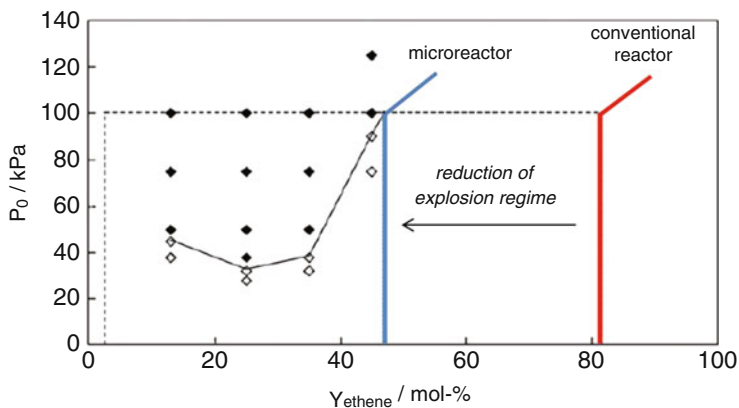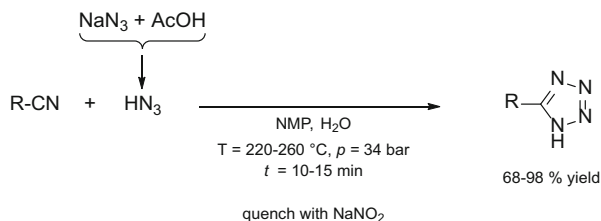
Fig. 13 Explosive behavior of mixtures of ethene with oxygen. A reduction of the explosion regime can be noticed when working in a microreactor. Reprinted with permission from [137]. Copyright (2012) Elsevier

propagation [139]. Although microreactors cannot be regarded as inherently safe, the range of safe operating conditions can be substantially increased as the upper explosion limit is lowered (Fig. 13). The potential of explosion propagation also demonstrates the necessity to quench a reaction adequately upon exiting the reactor. It has been shown by several authors that hazardous intermediates can be generated in situ and subsequently reacted away in a follow-up reaction [140]. Kappe et al. demonstrated elegantly this principle in the synthesis of tetrazoles (Fig. 14) [141]. Hydrazoic acid (HN_3), an extremely toxic compound, was prepared in situ in a microreactor and consumed immediately by reaction with a nitrile to prepare the corresponding tetrazoles. The reaction was subsequently quenched with $NaNO_2$ to decompose any residual hydrazoic acid. This allows to minimize the total inventory of hazardous compounds and thus to reduce the associated risks.

Thermal explosions are caused by an exponential increase of the reaction rate according to the Arrhenius equation with rising temperatures. This leads to a further increase in temperature and eventually to a reaction runaway. The increase in temperature and pressure at runaway conditions can ultimately lead to a reactor rupture and thus explosion. This is called parametric sensitivity; hereby, a small deviation of a parameter can lead to a chain of reaction events where the reaction rate and temperature increase in an incontrollable fashion [142]. Due to the high surface-to-volume ratios, fast heat transfer is possible leading to isothermal conditions in microreactors. Accordingly, for highly exothermic reactions, the conductivity of the reactor material plays an important role. Excellent heat dissipation in combination with high surface-to-volume ratios minimizes the risk of thermal runaways compared to large batch reactions [143]. However, local hot spots can still occur, e.g., in catalyst beds [144], which can serve as an ignition source [145–148].

Fig. 14 Continuous-flow synthesis of tetrazoles by preparing in situ HN_3 and quenching with $NaNO_2$

$$NaN_3 + AcOH$$

$$R\text{-}CN \quad + \quad HN_3 \quad \xrightarrow[\substack{NMP,\ H_2O \\ T = 220\text{-}260\ °C,\ p = 34\ bar \\ t\ = 10\text{-}15\ min}]{}$$

68-98 % yield

quench with $NaNO_2$

Surface effects are also important as they can initiate the decomposition of compounds, e.g., steel reactors can initiate radical formation [149, 150]. Kinetic explosions can take place where radicals are uncontrollably formed. Termination of the radical chain reaction can typically occur at the reactor surface. Consequently, the short length scales encountered in microreactors leads to fast diffusion of the radicals to the reactor walls, tempering efficiently such chain reactions [151].

8 Solids Handling in Flow

The handling of solids remains one of the major obstacles for continuous-flow microreactor technology [16, 152, 153]. Solid materials can aggregate or deposit on the reactor walls, which leads to channel blockage and prevents fluid from flowing. The presence of solids in a reaction stream can have several origins, including solid starting materials and generation of precipitation during the reactions by forming insoluble products or by-products. The nature of the solid and its origin warrant a case-by-case strategy to overcome potential channel blockage.

Essentially two different phenomena can be distinguished which cause clogging, i.e., constriction and bridging (Fig. 15) [154]. Constriction occurs when particles are deposited on the reactor walls. As a consequence of this wall deposition, the diameter gradually reduces and the pressure drop increases until a complete blockage of the microchannel occurs. Bridging is a phenomenon where particles aggregate and form larger particles which eventually span or bridge the entire cross section of the microchannel.

Several strategies have been suggested in the literature to overcome microreactor clogging. Probably the easiest strategy is to use polar solvents which can solubilize highly polar products or inorganic salts. Examples of this strategy are biphasic reaction conditions in which water is added as a second phase to dissolve inorganic salts [48, 51]. Insoluble materials can be transported through the microreactor channels as a slurry [155]. However, this strategy works best when a segmented flow regime is used where intensified mixing patterns in the liquid slugs keep the particles in suspension and avoid interaction with the reactor walls [156]. A popular strategy to deal with insoluble materials, such as heterogeneous catalysts, is immobilization in a packed-bed reactor. This method is often used to avoid extensive downstream purification procedures. Precipitation of highly polar
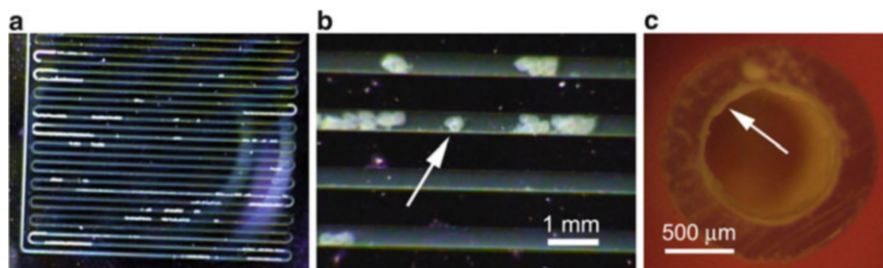
Fig. 15 Precipitation in microreactors leading to microreactor clogging. (**a**) Microreactor clogging occurring predominantly at *sharp bends* and toward the end of the reactor. (**b**) Bridging due to particle growth. (**c**) Wall deposition leading to constriction of the microreactor. Reprinted with permission from [154]. Copyright (2010) American Chemical Society

compounds can be also avoided by heating the reactor above the melting temperature of the solid material [88, 157]. Consequently, the material is processed in its molten state and will not clog the microchannels. Another strategy is to use mechanical energy to keep the solids in suspension. A commercially available agitating cell reactor (Coflore ACR) utilizes this principle to avoid clogging. The reactor consists of a series of continuous stirred tank reactors (CSTR) and was used to prepare N-iodomorpholinium hydroiodide [158]. Finally, ultrasound energy has been increasingly used to facilitate the processing of solid-forming reactions [159]. Acoustic irradiation induces cavitation at the particle surface. Upon implosion of the bubble, high shear forces at the particle surface cause particle breakup. These smaller particles are small enough to be transported through the microchannels. This strategy has been used to avoid clogging in C–N cross coupling [160, 161], Suzuki–Miyaura coupling [162], photodimerization reactions [163], $KMnO_4$ oxidation reactions [164], and other solid-forming reactions [165, 166].

9   Multistep Synthesis

The synthesis of complex organic molecules is a time-consuming and resource-intensive undertaking and represents a formidable challenge for synthetic organic chemists. A typical synthesis of a complex biologically active compound consists of a sequence of different reaction steps and intermediate purification steps. In recent years, many different strategies have been developed to facilitate the preparation of such compounds, including multicomponent reactions, cascade reactions, one-pot syntheses, protecting group free syntheses, and improved catalytic methodologies. These strategies are all focused on improving the efficiency of the chemical transformation itself. However, a change in processing strategy, e.g., from batch to continuous-flow processing, is much less considered by most chemists.

The use of continuous-flow reactors allows to integrate subsequent reaction and purifications steps in one single streamlined and automated process [167]. Several strategies that facilitate multistep reaction sequences have been developed throughout the years [168]. A first strategy includes a telescoping approach in which the individual reaction steps are linked together without intermediate purification steps. This strategy is a convenient approach and resembles the one-pot strategies encountered in batch in which reactants are sequentially and at certain times injected in the flask. However, excess of reagents or by-products needs to be compatible with the downstream reactions. If these reagents or by-products are not compatible, a lower conversion will be obtained than one would anticipate based on the individual reactions with purified starting materials.

A purification of the reaction stream can be carried out to increase the overall efficiency of the continuous-flow protocol. This can be achieved either by using immobilized catalysts, reagents, and scavengers or by incorporating unit operations [169]. The first approach uses packed-bed reactors in which the bed consists of beads with catalysts, reagents, or scavengers. By placing several cartridges in series, subsequent transformations in the preparation of complex biologically active molecules can be carried out in a single-flow operation. "Catch and release" strategies are often employed to execute intermediate purifications or solvent switches or to concentrate the intermediates. The need to periodically replace saturated reagent cartridges is the main drawback of this approach and makes it most suitable for the preparation of small amounts.
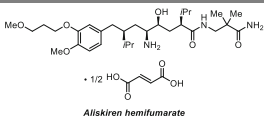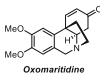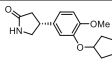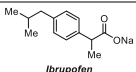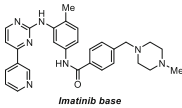
The use of unit operations to carry out separations is a very powerful approach since, in theory, the process can be continuously operated without interruptions. However, the development of such miniaturized unit operations has been challenging due to the fact that interfacial forces dominate over gravitational forces. This is represented by the Bond number:

$$Bo = \frac{\text{gravity force}}{\text{interfacial force}} = \frac{\rho g d_\text{H}^2}{\sigma} \tag{29}$$

where σ denotes the surface tension, g is the gravitational acceleration, ρ is the density, and d_H is the hydraulic diameter. In microchannels, the value of Bo is much lower than 1, which means that one cannot use gravity to establish a phase separation. Alternatively, extractions and distillations can be carried out by employing membrane technology based on the utilization of capillary forces [170, 171]. Consequently, microfluidic extractions [50, 172–177], distillations [178], and even simulated moving beds [179, 180] have been developed and used in combination with microreactors to enable a continuous purification of the reaction stream.

Several interesting multistep syntheses have been carried out in continuous flow; [181] an overview of some notable examples is summarized in Table 6.

Table 6 Notable examples of multistep continuous-flow syntheses

Biologically active compound	Strategy	Highlights	References
Aliskiren hemifumarate	Use of unit operations	Pilot-scale plant	[7]
		Continuous operation for 10 days	
		45 g/h of aliskiren	
		Reduction of number of unit operations from 21 in batch to 14 in flow	
		Reduction total processing time from 300 h in batch to 47 h in flow	
Oxomaritidine	Use of immobilized reagents	40% overall yield	[182]
		Seven separate steps in one continuous process	
		No intermediate purification	
		One of the first examples at this level of complexity	
(R)-Rolipram	Use of immobilized reagents	Immobilization of chiral catalysts to prepare chiral drug structures	[183]
		Chiral catalyst cartridges remain stable for months without decrease in enantioselectivity	
Artemisinin	Telescoping strategy without intermediate purification	Includes a singlet oxygen photochemical step	[184, 185]
		Allows to produce 200 g/day artemisinin	
Ibrupofen	Use of a microfluidic extraction	Three reaction steps + one extraction in only 3 min	[90]
		Contains one solvent-free exothermic step	
		8.09 g/h with an overall yield of 83%	
Imatinib base (Gleevec)	Use of immobilized reagents + evaporator	Inline solvent switch	[186, 187]
		Protocol allows to make several analogues	

10   Scalability

Leading a chemical route from a laboratory scale to a pilot or full production scale is a challenging task for the process engineer. Often, the chemistry developed on a small scale is not compatible with the large-scale processing conditions, which need to take process safety and cost-efficiency into account. Furthermore, the

hydrodynamics and transport properties need to be maintained on each scale complicating the scale-up even more. Microreactor technology has been hauled as a revolutionary technology which can overcome scaling problems by simply putting multiple devices in parallel. However, this statement has been overruled in recent years as it became evident that it was technologically far from easy to achieve this. Several scale-up strategies with continuous-flow reactors can be distinguished: (1) longer operation times + increasing the throughput by using higher flow rates, (2) numbering-up by placing several devices in parallel, and (3) smart scale-out by a dimension-enlarging strategy.

The use of longer operation times is the strategy which is most used on a laboratory scale. Reagents are continuously fed to the microdevice until the desired amount of product is collected. The main advantages of this strategy are the simplicity and the use of the same device for optimization and scale-up. Typically, several milligrams to a few hundreds of grams can be obtained making the strategy ideally suited for the first stages of a drug discovery process. Increasing the flow rate in microreactors is another way to increase the throughput. Longer reactor lengths are used and thus higher flow rates are needed to keep the reaction time constant. High flow rates result into improved transport properties (mixing and heat dissipation), which can result in a reduction of the reaction time. It is important to note that many reactions can already be substantially accelerated in a microreactor due to the excellent transport properties, which allows to increase the throughput in a "natural" way. Examples of reactions that can be substantially accelerated in microflow are gas–liquid reactions, photochemical reactions, transmetallation reactions, electrochemical reactions, and reactions which require extreme reaction conditions (exothermic reactions and reaction at high temperature and concentrations). Furthermore, the processing conditions that are used in such devices can be easily translated to a larger scale process [130].

Numbering-up of microreactors is the most common method to scale the throughput of a single microreactor [188]. Essentially two different methods can be distinguished, i.e., internal and external numbering-up. Internal numbering-up is achieved by placing several microchannels in parallel and using a single pumping and mixing unit. This reduces the overall cost of the numbering-up strategy. The reaction stream is distributed equally over the different microchannels by using a flow distributor. This requires an equal pressure drop over the different parallel channels and is especially difficult to achieve for multiphase reaction streams. Flow maldistribution can lead to great differences in performance between the individual channels [189, 190]. Schouten et al. have developed a barrier-based distributor manifold for gas–liquid flows which allows to achieve a good distribution within ±10% in eight different channels (Fig. 16a) [194]. This manifold was subsequently demonstrated in the numbering-up of a hydrogenation reaction [191]. Noël et al. have developed a cheap and straightforward numbering-up strategy for the photocatalytic aerobic oxidation of thiols to disulfides [195]. The system uses simple T-mixers as the basic flow-splitting units to split up the gas–liquid flow sequentially into eight different photomicroreactors (Fig. 16b). The deviation of the liquid throughput and the yield in the different channels was less than 10%. The
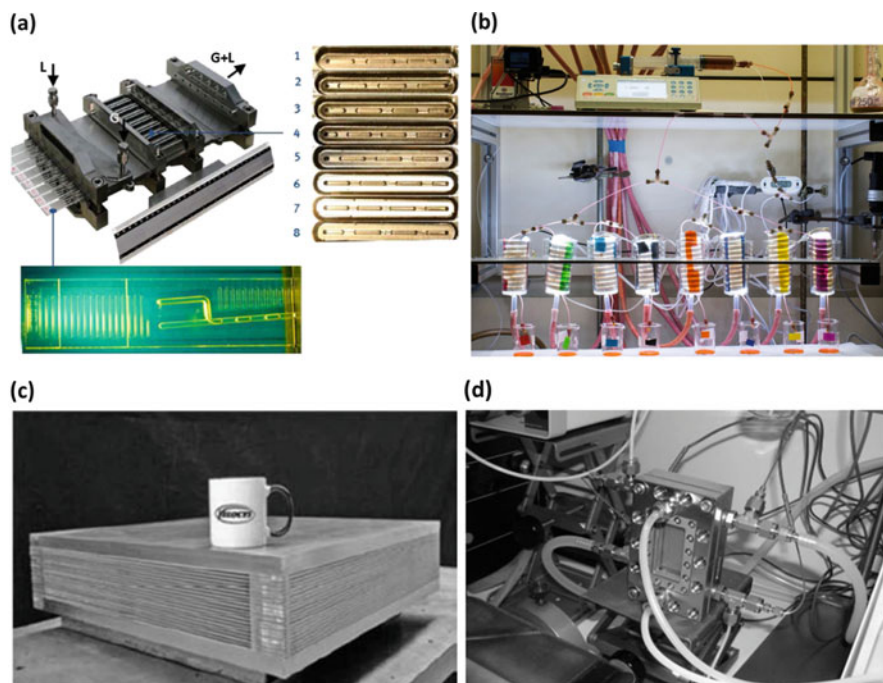
Fig. 16 Examples of internal numbering-up. (**a**) Barrier-based microreactor with a gas–liquid distributor for hydrogenation reactions. Reprinted with permission from [191]. Copyright (2013) American Chemical Society. (**b**) Numbering-up of photocatalytic gas–liquid reactions using cheap PEEK T-mixers as flow-splitting units. (**c**) Velocys manufacturing scale-up device for microflow Fischer–Tropsch. Reprinted with permission from [192]. Copyright (2010) American Chemical Society. (**d**) Falling-film microreactor. Reprinted with permission from [193]. Copyright (2009) American Chemical Society

yield of the target product in the numbered-up system was comparable to those results obtained in a single photomicroreactor. An impressive example of internal numbering-up was realized by researchers from Velocys [192]. A cross-flow heat exchanger configuration was used to carry out a Fischer–Tropsch reaction; the reagents are directed over a heterogeneous particulate catalyst, while boiling water was used to maintain an isothermal operation of the reactor. The intrinsic kinetics of the reaction were studied in a single microchannel. Next, the reaction was further scaled to a manufacturing device (see Fig. 16c). This device ($0.6 \times 0.6 \times 0.15$ m) contained more than 10,000 microchannels and can produce up to 450 t of product per year. The flow distribution was excellent and showed a variability of less than 9%. Other examples of internal numbering-up are the falling film microreactor (Fig. 16d) [196] and multichannel microcapillary films [197].

External numbering-up is a strategy of placing several microreactors in parallel in which each device has its individual pumping system and process control unit. As each device operates autonomously, this strategy ensures that exact the same
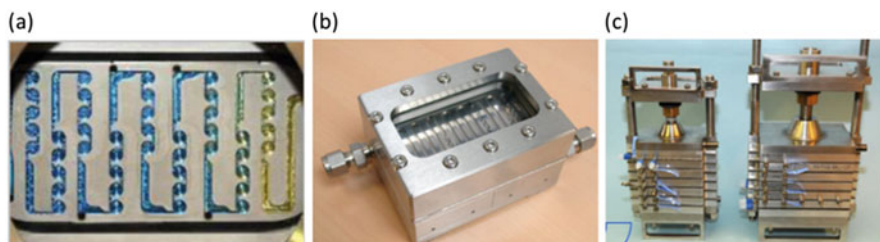
Fig. 17 The Lonza FlowPlate TM concept for a gradual scale-up of continuous-flow reactions. (**a**) Detail of a single reactor plate with tangential mixing elements. (**b**) Reactor plate stacked in an aluminum chuck with a transparent view glass for optical inspection. (**c**) Stack plate reactors to increase the scale gradually. Reprinted with permission from [199]. Copyright (2011) Elsevier

processing conditions are obtained in each individual device. The major drawback of this strategy is the high investment cost since each unit has its own pumps, heating system, flow controllers, etc. and is thus not so much used.

The last method to increase the productivity of microreactors is to use a dimension-enlarging strategy (also called smart scale-out) [136, 198]. Active mixers are used in these millireactors to ensure that the same intensified heat and mass transfer characteristics are obtained as encountered in microreactors. Researchers from Lonza have developed the FlowPlate TM concept, which allows for a reliable scale-up of flow chemistry from lab scale to pilot plant production (Fig. 17) [199]. The flow plate reactor consists of a stack of stainless steel reactor plates, containing tangential mixing elements, and thermal conductive aluminum plates, ensuring an excellent heat dissipation [142]. The hydraulic diameter can be gradually increased by using different reactor plates (from lab plate, A6, A5, to A4 plates). The lab plate is used to study and optimize the reaction conditions and its kinetics and can produce up to a few grams. Next, the reaction can be scaled up to 2,500 kg with the A4 plate.

A similar concept has been developed by researchers from Corning (Fig. 18). The advanced flow reactor allows to scale multiphase reactions and incorporates heart-shaped split-and-recombine mixers to intensify the mixing between the two phases [202]. Overall volumetric mass transfer coefficients (k_La) in this device range between 0.1 and $10 \, \text{s}^{-1}$, which can be compared with those values obtained in a microreactor [203]. This concept has been used to scale oxidation reactions, such as ozonolysis [204] and alcohol oxidations with bleach [200]. For the latter, the oxidation of 1-phenylethanol could be scaled from 0.0064 g/min in a microreactor to a low flow reactor (0.37 g/min) and advanced flow reactor (4.08 g/min). These reactors can be subsequently placed in parallel to reach even higher production scales through the numbering-up strategy [201].
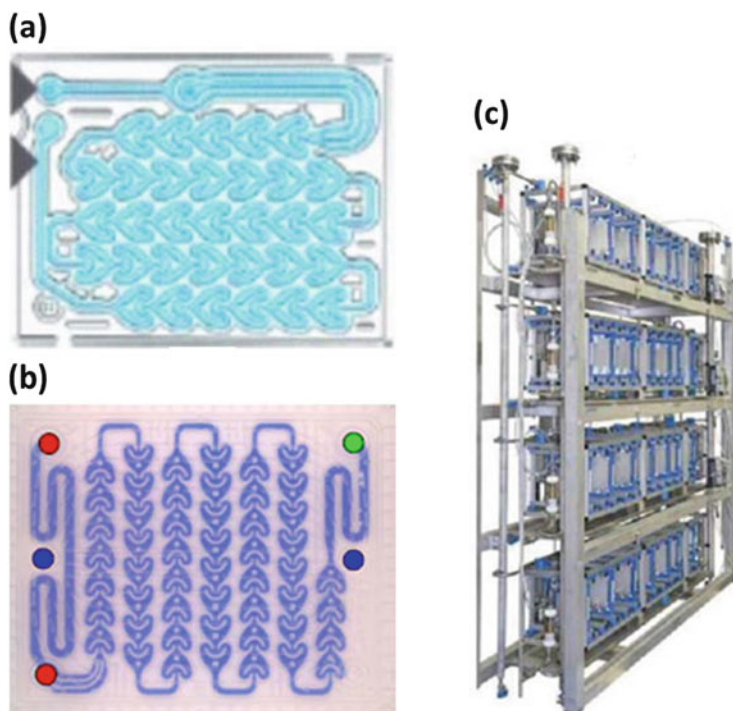
Fig. 18 Corning glass flow reactors: (**a**) Corning low flow reactor (450 μL). (**b**) Corning advanced flow reactor (8.7 mL). Further scale-up by numbering-up. Reprinted with permission from [200]. Copyright (2014) Wiley-VCH. (**c**) Further scale-up by numbering-up. Reprinted with permission from [201]. Copyright (2011) Wiley-VCH

11   Conclusion

In this review, we have focused on giving an overview of the most important engineering principles which are relevant for chemists and chemical engineers to carry out flow chemistry. We have tried to explain these fundamental aspects in a language that is understandable for the synthetic chemist and have provided relevant chemical examples illustrating the importance of these principles. Where relevant, we have directed the reader to more detailed reviews. It is our hope that this review will become a handy tool for flow chemists to recognize where continuous-flow microreactors can actually make a difference and to exploit the full potential of the technology.

Looking back to the last two decades, we have witnessed the transition of microreactor technology from an engineering curiosity to real applications in the chemical and pharmaceutical industry. Commercial available devices exist for both lab and production scales, which makes the technology broadly available. In addition, specialized courses are set up to educate the community about flow

technology. Therefore, it is our firm belief that continuous-flow chemistry will continue to gain ground and become more widespread in industry and academia.

However, further progress is not without a challenge and this will require a combined effort of engineers, chemists, and software developers. From a chemist perspective, many dangerous reagents have been avoided in the past due to safety reasons. However, due to the potential safe processing in a microenviroment, such reagents can be used and give access to novel and previously inaccessible reaction pathways. We anticipate that also increasingly complex molecules will be prepared in a fully automated and continuous fashion. Further, the ability to include automated reaction schemes is one of the most interesting opportunities for synthetic organic chemistry. Would it not be cool to be able to draw your molecule in ChemDraw and subsequently enter the prepare button after which a pure compound comes out of the machine? This seems like science fiction at the moment but examples in this review demonstrate that in fact we have made good progress in making complex natural products in an automated sequence without further manual labor.

From an engineering perspective, more research is necessary to understand all phenomena with regard to fluid dynamics and transport phenomena. Many correlations which have been derived for large-scale systems are not or only limitedly valid on a microscale. For example, entrance effects, surface roughness, and channel geometry are often neglected on a macroscale but can be relevant on a microscale. Furthermore, photon-transport phenomena are quite complex and more research is required to build up models which are broadly applicable. Also the scaling of microreactors to full production scale remains a challenge and more research efforts are required to solve problems associated with flow distribution and reliable process modeling. And last but not least, a holistic process analysis approach, which provides an economical comparison between continuous-flow and batch processing, has not been completely established up to now. Therefore, stepwise and multiscale concepts should be developed when replacing batch reactors with continuous-flow reactors for industrial production.

References

1. Jiménez-González C, Poechlauer P, Broxterman QB, Yang B-S, am Ende D, Baird J, Bertsch C, Hannah RE, Dell'Orco P, Noorman H, Yee S, Reintjens R, Wells A, Massonneau V, Manley J (2011) Org Process Res Dev 15:900–911
2. Poechlauer P, Colberg J, Fisher E, Jansen M, Johnson MD, Koenig SG, Lawler M, Laporte T, Manley J, Martin B, O'Kearney-McMullan A (2013) Org Process Res Dev 17:1472–1478

3. Anderson NG (2012) Org Process Res Dev 16:852–869
4. Poechlauer P, Manley J, Broxterman R, Gregertsen B, Ridemark M (2012) Org Process Res Dev 16:1586–1590
5. Denčić I, Ott D, Kralisch D, Noël T, Meuldijk J, de Croon M, Hessel V, Laribi Y, Perrichon P (2014) Org Process Res Dev 18:1326–1338
6. Hart SL, Cristensen, CM, MIT Sloan Management Review (2002) http://sloanreview.mit.edu/article/the-great-leap-driving-innovation-from-the-base-of-the-pyramid/. Accessed July 2015
7. Mascia S, Heider PL, Zhang H, Lakerveld R, Benyahia B, Barton PI, Braatz RD, Cooney CL, Evans JMB, Jamison TF, Jensen KF, Myerson AS, Trout BL (2013) Angew Chem Int Ed 52:12359–12363
8. Mitic A, Gernaey KV (2015) Chem Eng Technol. doi:10.1002/ceat.201400765
9. Van Gerven T, Stankiewicz A (2009) Ind Eng Chem Res 48:2465–2474
10. Hartman RL, McMullen JP, Jensen KF (2011) Angew Chem Int Ed 50:7502–7519
11. Denčić I, Noël T, Meuldijk J, de Croon M, Hessel V (2013) Eng Life Sci 13:326–343
12. Hessel V, Kralisch D, Kockmann N, Noël T, Wang Q (2013) ChemSusChem 6:746–789
13. Hessel V, Vural Gürsel I, Wang Q, Noël T, Lang J (2012) Chem Eng Technol 35:1184–1204
14. Stouten SC, Noël T, Wang Q, Hessel V (2013) Aust J Chem 66:121–130
15. Roberge DM, Ducry L, Bieler N, Cretton P, Zimmermann B (2005) Chem Eng Technol 28:318–323
16. Hartman RL (2012) Org Process Res Dev 16:870–887
17. Capretto L, Cheng W, Hill M, Zhang X, Zhang X (2011) In: Lin B (ed) Microfluidics, vol 304. Springer, Berlin/Heidelberg, pp 27–68, ch. 150
18. Hessel V, Löwe H, Schönfeld F (2005) Chem Eng Sci 60:2479–2501
19. Kuo JS, Chiu DT (2011) Annu Rev Anal Chem 4:275–296
20. Falk L, Commenge JM (2010) Chem Eng Sci 65:405–411
21. Hessel V, Noël T (2012) Ullmann's encyclopedia of industrial chemistry. Wiley, Weinheim. doi:10.1002/14356007.b16_b37.pub2
22. Suh YK, Kang S (2010) Micromachines 1:82
23. Bourne JR (2003) Org Process Res Dev 7:471–508
24. Yoshida J, Nagaki A, Iwasaki T, Suga S (2005) Chem Eng Technol 28:259–266
25. Nagaki A, Takabayashi N, Tomida Y, Yoshida J-i (2008) Org Lett 10:3937–3940
26. Nagaki A, Togai M, Suga S, Aoki N, Mae K, Yoshida J-i (2005) J Am Chem Soc 127:11666–11675
27. Nagaki A, Tomida Y, Yoshida J-i (2008) Macromolecules 41:6322–6330
28. Jong T, Bradley M (2015) Org Lett 17:422–425
29. Nagy KD, Shen B, Jamison TF, Jensen KF (2012) Org Process Res Dev 16:976–981
30. Fogler HS (2005) Elements of chemical reaction engineering. Prentice Hall, Boston
31. Levenspiel O (1999) Chemical reaction engineering. Wiley, New York
32. Lange H, Carter CF, Hopkin MD, Burke A, Goode JG, Baxendale IR, Ley SV (2011) Chem Sci 2:765–769
33. Hawbaker N, Wittgrove E, Christensen B, Sach N, Blackmond DG (2015) Org Process Res Dev. doi:10.1021/op500360w
34. Kuhn S, Hartman RL, Sultana M, Nagy KD, Marre S, Jensen KF (2011) Langmuir 27:6519–6527
35. Kreutz JE, Shukhaev A, Du W, Druskin S, Daugulis O, Ismagilov RF (2010) J Am Chem Soc 132:3128–3132
36. Song H, Ismagilov RF (2003) J Am Chem Soc 125:14613–14619
37. Zheng B, Tice JD, Roach LS, Ismagilov RF (2004) Angew Chem Int Ed 43:2508–2511
38. Khan SA, Jensen KF (2007) Adv Mater 19:2556–2560
39. Mallia CJ, Baxendale IR (2015) Org Process Res Dev. doi:10.1021/acs.oprd.5b00222
40. Gemoets HPL, Su Y, Shang M, Hessel V, Luque R, Noel T (2015) Chem Soc Rev. doi:10.1039/C5CS00447K

41. Pieber B, Kappe CO (2015) Top Organomet Chem. doi:10.1007/3418_2015_133
42. Jovanović J, Rebrov EV, Nijhuis TA, Hessel V, Schouten JC (2010) Ind Eng Chem Res 49:2681–2687
43. Mellouli S, Bousekkine L, Theberge AB, Huck WTS (2012) Angew Chem Int Ed 51:7981–7984
44. Su Y, Zhao Y, Chen G, Yuan Q (2010) Chem Eng Sci 65:3947–3956
45. Su Y, Zhao Y, Jiao F, Chen G, Yuan Q (2011) AIChE J 57:1409–1418
46. Su Y, Chen G, Yuan Q (2011) Chem Eng Sci 66:2912–2919
47. Pedras MHJ, de Lemos MJS (2001) Int J Heat Mass Transfer 44:1081–1093
48. Naber JR, Buchwald SL (2010) Angew Chem Int Ed 49:9469–9474
49. Li P, Buchwald SL (2011) Angew Chem Int Ed 50:6396–6400
50. Noël T, Kuhn S, Musacchio AJ, Jensen KF, Buchwald SL (2011) Angew Chem Int Ed 50:5943–5946
51. Noël T, Musacchio AJ (2011) Org Lett 13:5180–5183
52. Shang M, Noël T, Wang Q, Hessel V (2013) Chem Eng Technol 36:1001–1009
53. Shang M, Noël T, Wang Q, Su Y, Miyabayashi K, Hessel V, Hasebe S (2015) Chem Eng J 260:454–462
54. Baxendale I, Hayward J, Lanners S, Ley S, Smith C (2008) In: Wirth T (ed) Microreactors in organic synthesis and catalysis. Wiley, Weinheim, pp 84–122
55. Habraken E, Haspeslagh P, Vliegen M, Noël T (2015) J Flow Chem 5:2–5
56. Cantillo D, Kappe CO (2014) ChemCatChem 6:3286–3305
57. Noël T, Maimone TJ, Buchwald SL (2011) Angew Chem Int Ed 50:8900–8903
58. Ceylan S, Friese C, Lammel C, Mazac K, Kirschning A (2008) Angew Chem Int Ed 47:8950–8953
59. Benaskar F, Patil NG, Rebrov EV, Ben-Abdelmoumen A, Meuldijk J, Hulshof LA, Hessel V, Schouten JC (2013) ChemSusChem 6:353–366
60. Sachse A, Galarneau A, Coq B, Fajula F (2011) New J Chem 35:259–264
61. Kirschning A, Solodenko W, Mennecke K (2006) Chem Eur J 12:5972–5990
62. Su Y, Straathof NJW, Hessel V, Noël T (2014) Chem Eur J 20:10562–10589
63. Su Y, Hessel V, Noël T (2015) AIChE J 61:2215–2227
64. Fischer J, Lange T, Boehling R, Rehfinger A, Klemm E (2010) Chem Eng Sci 65:4866–4872
65. Kashid MN, Renken A, Kiwi-Minsker L (2014) Microstructured devices for chemical processing. Wiley, Weinheim, pp 179–230. doi:10.1002/9783527685226.ch5
66. Rebrov EV, Schouten JC, de Croon MHJM (2011) Chem Eng Sci 66:1374–1393
67. Tuckerman DB, Pease RFW (1981) IEEE Electron Device Lett 2:126–129
68. Brandner JJ, Bohn L, Henning T, Schygulla U, Schubert K (2007) Heat Transfer Eng 28:761–771
69. Khan MG, Fartaj A (2011) Int J Energy Res 35:553–582
70. Brandner JJ, Anurjew E, Bohn L, Hansjosten E, Henning T, Schygulla U, Wenka A, Schubert K (2006) Exp Thermal Fluid Sci 30:801–809
71. Brandner JJ (2008) Microreactors in organic synthesis and catalysis. Wiley, Weinheim, pp 1–17. doi:10.1002/9783527622856.ch1
72. Frank T (2008) Microreactors in organic synthesis and catalysis. Wiley, Weinheim, pp 19–41. doi:10.1002/9783527622856.ch2
73. Noel T, Wang X, Hessel V (2013) Chim Oggi 31:10–14
74. Harris C, Despa M, Kelly K (2000) J Microelectromech Syst 9:502–508
75. Newman SG, Gu L, Lesniak C, Victor G, Meschke F, Abahmane L, Jensen KF (2014) Green Chem 16:176–180
76. Gutmann B, Cantillo D, Kappe CO (2015) Angew Chem Int Ed 54:6688–6728
77. Usutani H, Tomida Y, Nagaki A, Okamoto H, Nokami T, Yoshida J-i (2007) J Am Chem Soc 129:3046–3047
78. Haber J, Kashid MN, Renken A, Kiwi-Minsker L (2012) Ind Eng Chem Res 51:1474–1489

79. Roberge DM, Bieler N, Mathier M, Eyholzer M, Zimmermann B, Barthe P, Guermeur C, Lobet O, Moreno M, Woehl P (2008) Chem Eng Technol 31:1155–1161
80. Irfan M, Glasnov TN, Kappe CO (2011) ChemSusChem 4:300–316
81. Kulkarni AA (2014) Beilstein J Org Chem 10:405–424
82. Wang X (2015) J Flow Chem. doi:10.1556/1846.2015.00003
83. Hessel V, Ehrfeld W, Golbig K, Haverkamp V, Löwe H, Storz M, Wille C, Guber AE, Jähnisch K, Baerns M (2000) In: Ehrfeld W (ed) Microreaction technology: industrial prospects. Springer, Berlin/Heidelberg, pp 526–540. doi:10.1007/978-3-642-59738-1_55, ch. 55
84. de Mas N, Günther A, Schmidt MA, Jensen KF (2003) Ind Eng Chem Res 42:698–710
85. Kappe CO, Pieber B, Dallinger D (2013) Angew Chem Int Ed 52:1088–1094
86. Kappe CO (2004) Angew Chem Int Ed 43:6250–6284
87. Glasnov TN, Kappe CO (2011) Chem Eur J 17:11956–11968
88. Borukhova S, Noël T, Metten B, de Vos E, Hessel V (2013) ChemSusChem 6:2220–2225
89. Kobayashi H, Driessen B, van Osch DJGP, Talla A, Ookawara S, Noël T, Hessel V (2013) Tetrahedron 69:2885–2890
90. Snead DR, Jamison TF (2015) Angew Chem Int Ed 54:983–987
91. Bergamelli F, Iannelli M, Marafie JA, Moseley JD (2010) Org Process Res Dev 14:926–930
92. Ceylan S, Coutable L, Wegner J, Kirschning A (2011) Chem Eur J 17:1884–1893
93. Shore G, Yoo W-J, Li C-J, Organ MG (2010) Chem Eur J 16:126–133
94. Patil NG, Hermans AIG, Benaskar F, Meuldijk J, Hulshof LA, Hessel V, Schouten JC, Rebrov EV (2012) AIChE J 58:3144–3155
95. Benaskar F, Patil NG, Engels V, Rebrov EV, Meuldijk J, Hulshof LA, Hessel V, Wheatley AEH, Schouten JC (2012) Chem Eng J 207–208:426–439
96. Stouten SC, Noël T, Wang Q, Hessel V (2014) Chem Eng Process Process Intensif 83:26–32
97. Burguete MI, García-Verdugo E, Luis SV (2011) Beilstein J Org Chem 7:1347–1359
98. Hintermair U, Francio G, Leitner W (2011) Chem Commun 47:3691–3701
99. Bach T, Hehn JP (2011) Angew Chem Int Ed 50:1000–1045
100. Brimioulle R, Lenhart D, Maturi MM, Bach T (2015) Angew Chem Int Ed 54:3872–3890
101. Hoffmann N (2012) ChemSusChem 5:352–371
102. Narayanam JMR, Stephenson CRJ (2011) Chem Soc Rev 40:102–113
103. Tucker JW, Stephenson CRJ (2012) J Org Chem 77:1617–1622
104. Prier CK, Rankic DA, MacMillan DWC (2013) Chem Rev 113:5322–5363
105. Camera Roda G, Santarelli F (2007) Ind Eng Chem Res 46:7637–7644
106. Garlets ZJ, Nguyen JD, Stephenson CRJ (2014) Isr J Chem 54:351–360
107. Gilmore K, Seeberger PH (2014) Chem Rec 14:410–418
108. Knowles JP, Elliott LD, Booker-Milburn KI (2012) Beilstein J Org Chem 8:2025–2052
109. Oelgemoeller M (2012) Chem Eng Technol 35:1144–1152
110. Cismesia M, Yoon T (2015) Chem Sci. doi:10.1039/C5SC02185E
111. Majek M, Filace F, Wangelin AJv (2014) Beilstein J Org Chem 10:981–989
112. Kuhn HJ, Braslavsky SE, Schmidt R (2004) Pure Appl Chem 76:2105–2146
113. Aillet T, Loubiere K, Dechy-Cabaret O, Prat L (2014) Int J Chem React Eng 12:257
114. Gorges R, Meyer S, Kreisel G (2004) J Photochem Photobiol A Chem 167:95–99
115. Jamali A, Vanraes R, Hanselaer P, Van Gerven T (2013) Chem Eng Process Process Intensif 71:43–50
116. Shen B, Bedore MW, Sniady A, Jamison TF (2012) Chem Commun 48:7444–7446
117. Su Y, Talla A, Hessel V, Noël T (2015) Chem Eng Technol. doi:10.1002/ceat.201500376
118. Cassano AE, Martin CA, Brandi RJ, Alfano OM (1995) Ind Eng Chem Res 34:2155–2201
119. Blackmond DG (2005) Angew Chem Int Ed 44:4302–4320
120. Berger RJ, Kapteijn F, Moulijn JA, Marin GB, De Wilde J, Olea M, Chen D, Holmen A, Lietti L, Tronconi E, Schuurman Y (2008) Appl Catal Gen 342:3–28
121. Al-Rifai N, Cao E, Dua V, Gavriilidis A (2013) Curr Opin Chem Eng 2:338–345
122. Noël T, Hessel V (2013) ChemSusChem 6:405–407

123. Zhou X, Medhekar R, Toney MD (2003) Anal Chem 75:3681–3687
124. Yue J, Schouten JC, Nijhuis TA (2012) Ind Eng Chem Res 51:14583–14609
125. Moore JS, Jensen KF (2014) Angew Chem Int Ed 53:470–473
126. Mozharov S, Nordon A, Littlejohn D, Wiles C, Watts P, Dallin P, Girkin JM (2011) J Am Chem Soc 133:3601–3608
127. Ley SV, Fitzpatrick DE, Ingham RJ, Myers RM (2015) Angew Chem Int Ed 54:3449–3464
128. Weissman SA, Anderson NG (2014) Org Process Res Dev. doi:10.1021/op500169m
129. Noël T (2014) Discovering the future of molecular sciences. Wiley, Weinheim, pp 137–164. doi:10.1002/9783527673223.ch6
130. McMullen JP, Stone MT, Buchwald SL, Jensen KF (2010) Angew Chem Int Ed 49:7076–7080
131. McMullen JP, Jensen KF (2011) Org Process Res Dev 15:398–407
132. Reizman BJ, Jensen KF (2012) Org Process Res Dev 16:1770–1782
133. Ingham RJ, Battilocchio C, Fitzpatrick DE, Sliwinski E, Hawkins JM, Ley SV (2015) Angew Chem Int Ed 54:144–148
134. Aillet T, Loubiere K, Dechy-Cabaret O, Prat L (2013) Chem Eng Process Process Intensif 64:38–47
135. Talla A, Driessen B, Straathof NJW, Milroy L-G, Brunsveld L, Hessel V, Noël T (2015) Adv Synth Catal 357:2180–2186
136. Bieringer T, Buchholz S, Kockmann N (2013) Chem Eng Technol 36:900–910
137. Liebner C, Fischer J, Heinrich S, Lange T, Hieronymus H, Klemm E (2012) Process Saf Environ Prot 90:77–82
138. Liebner C, Heinrich S, Edeling F, Hieronymus H, Lange T, Elias K (2013) Chem Eng Trans 31:601–606
139. Fischer J, Liebner C, Hieronymus H, Klemm E (2009) Chem Eng Sci 64:2951–2956
140. Wang X, Cuny GD, Noël T (2013) Angew Chem Int Ed 52:7860–7864
141. Gutmann B, Roduit J-P, Roberge D, Kappe CO (2010) Angew Chem Int Ed 49:7101–7105
142. Kockmann N, Roberge DM (2011) Chem Eng Process Process Intensif 50:1017–1026
143. Di Miceli Raimondi N, Olivier-Maget N, Gabas N, Cabassud M, Gourdon C (2015) Chem Eng Res Des 94:182–193
144. Heinrich S, Edeling F, Liebner C, Hieronymus H, Lange T, Klemm E (2012) Chem Eng Sci 84:540–543
145. Klais O, Westphal F, Benaïssa W, Carson D (2009) Chem Eng Technol 32:1831–1844
146. Klais O, Westphal F, Benaissa W, Carson D (2009) Chem Eng Technol 32:1966–1973
147. Klais O, Westphal F, Benaissa W, Carson D, Albrecht J (2010) Chem Eng Technol 33:444–454
148. Klais O, Albrecht J, Carson D, Kraut M, Lö P, Minnich C, Olschewski F, Reimers C, Simoncelli A, Uerdingen M (2010) Chem Eng Technol 33:1159–1168
149. Theyssen N, Hou Z, Leitner W (2006) Chem Eur J 12:3401–3409
150. Hao J, Cheng H, Wang H, Cai S, Zhao F (2007) J Mol Catal A Chem 271:42–45
151. Veser G (2001) Chem Eng Sci 56:1265–1273
152. Schoenitz M, Grundemann L, Augustin W, Scholl S (2015) Chem Commun 51:8213–8228
153. Flowers BS, Hartman RL (2012) Challenges 3:194
154. Hartman RL, Naber JR, Zaborenko N, Buchwald SL, Jensen KF (2010) Org Process Res Dev 14:1347–1357
155. Liedtke A-K, Scheiff F, Bornette F, Philippe R, Agar DW, de Bellefon C (2015) Ind Eng Chem Res 54:4699–4708
156. Poe SL, Cummings MA, Haaf MP, McQuade DT (2006) Angew Chem Int Ed 45:1544–1548
157. Snead DR, Jamison TF (2013) Chem Sci 4:2822–2827
158. Browne DL, Deadman BJ, Ashe R, Baxendale IR, Ley SV (2011) Org Process Res Dev 15:693–697
159. Hübner S, Kressirer S, Kralisch D, Bludszuweit-Philipp C, Lukow K, Jänich I, Schilling A, Hieronymus H, Liebner C, Jähnisch K (2012) ChemSusChem 5:279–288

160. Noel T, Naber JR, Hartman RL, McMullen JP, Jensen KF, Buchwald SL (2011) Chem Sci 2:287–290
161. Kuhn S, Noel T, Gu L, Heider PL, Jensen KF (2011) Lab Chip 11:2488–2492
162. Shu W, Pellegatti L, Oberli MA, Buchwald SL (2011) Angew Chem Int Ed 50:10665–10669
163. Horie T, Sumino M, Tanaka T, Matsushita Y, Ichimura T, Yoshida J-i (2010) Org Process Res Dev 14:405–410
164. Sedelmeier J, Ley SV, Baxendale IR, Baumann M (2010) Org Lett 12:3618–3621
165. Castro F, Kuhn S, Jensen K, Ferreira A, Rocha F, Vicente A, Teixeira JA (2013) Chem Eng Sci 100:352–359
166. Castro F, Kuhn S, Jensen K, Ferreira A, Rocha F, Vicente A, Teixeira JA (2013) Chem Eng J 215–216:979–987
167. Webb D, Jamison TF (2010) Chem Sci 1:675–680
168. Pastre JC, Browne DL, Ley SV (2013) Chem Soc Rev 42:8849–8869
169. Myers RM, Roper KA, Baxendale IR, Ley SV (2012) Modern tools for the synthesis of complex bioactive molecules. Wiley, Hoboken, pp 359–393. doi:10.1002/9781118342886.ch11
170. Hartman RL, Jensen KF (2009) Lab Chip 9:2495–2507
171. Kenig EY, Su YH, Lautenschleger A, Chasanis P, Grunewald M (2013) Sep Purif Technol 120:245–264
172. Varas AC, Noël T, Wang Q, Hessel V (2012) ChemSusChem 5:1703–1707
173. Vural Gürsel I, Aldiansyah F, Wang Q, Noël T, Hessel V (2015) Chem Eng J 270:468–475
174. Hamlin TA, Lazarus GML, Kelly CB, Leadbeater NE (2014) Org Process Res Dev 18:1253–1258
175. Adamo A, Heider PL, Weeranoppanant N, Jensen KF (2013) Ind Eng Chem Res 52:10802–10808
176. Sahoo HR, Kralj JG, Jensen KF (2007) Angew Chem 119:5806–5810
177. Hu DX, O'Brien M, Ley SV (2012) Org Lett 14:4246–4249
178. Hartman RL, Naber JR, Buchwald SL, Jensen KF (2010) Angew Chem Int Ed 49:899–903
179. O'Brien AG, Horváth Z, Lévesque F, Lee JW, Seidel-Morgenstern A, Seeberger PH (2012) Angew Chem Int Ed 51:7028–7030
180. Horváth Z, Horosanskaia E, Lee JW, Lorenz H, Gilmore K, Seeberger PH, Seidel-Morgenstern A (2015) Org Process Res Dev 19:624–634
181. Baraldi Patricia T, Hessel V (2012) Green Processes Synth 1:149
182. Baxendale IR, Deeley J, Griffiths-Jones CM, Ley SV, Saaby S, Tranmer GK (2006) Chem Commun, pp 2566–2568. doi:10.1039/B600382F
183. Tsubogo T, Oyamada H, Kobayashi S (2015) Nature 520:329–332
184. Lévesque F, Seeberger PH (2012) Angew Chem Int Ed 51:1706–1709
185. Kopetzki D, Lévesque F, Seeberger PH (2013) Chem Eur J 19:5450–5456
186. Hopkin MD, Baxendale IR, Ley SV (2013) Org Biomol Chem 11:1822–1839
187. Hopkin MD, Baxendale IR, Ley SV (2010) Chem Commun 46:2450–2452
188. Kashid MN, Gupta A, Renken A, Kiwi-Minsker L (2010) Chem Eng J 158:233–240
189. Su Y, Chen G, Kenig EY (2015) Lab Chip 15:179–187
190. Tonkovich A, Kuhlmann D, Rogers A, McDaniel J, Fitzgerald S, Arora R, Yuschak T (2005) Chem Eng Res Des 83:634–639
191. Al-Rawashdeh M, Zalucky J, Müller C, Nijhuis TA, Hessel V, Schouten JC (2013) Ind Eng Chem Res 52:11516–11526
192. Tonkovich ALY, Lerou JJ (2010) Novel concepts in catalysis and chemical reactors. Wiley, Weinheim, pp 239–260. doi:10.1002/9783527630882.ch11
193. Hübner S, Bentrup U, Budde U, Lovis K, Dietrich T, Freitag A, Küpper L, Jähnisch K (2009) Org Process Res Dev 13:952–960
194. Al-Rawashdeh M, Yu F, Nijhuis TA, Rebrov EV, Hessel V, Schouten JC (2012) Chem Eng J 207–208:645–655
195. Su Y, kuijpers K, Hessel V, Noël T (2016) React Chem Eng. doi:10.1039/c5re00021a

196. Vankayala Bhanu K, Löb P, Hessel V, Menges G, Hofmann C, Metzke D, Krtschil U, Kost H-J (2007) Int J Chem React Eng 5. doi:10.2202/1542-6580.1463
197. Hornung CH, Hallmark B, Baumann M, Baxendale IR, Ley SV, Hester P, Clayton P, Mackley MR (2010) Ind Eng Chem Res 49:4576–4582
198. Dencic I, Hessel V (2013) Microreactors in organic chemistry and catalysis. Wiley, Weinheim, pp 373–446. doi:10.1002/9783527659722.ch11
199. Kockmann N, Gottsponer M, Roberge DM (2011) Chem Eng J 167:718–726
200. Zhang Y, Born SC, Jensen KF (2014) Org Process Res Dev 18:1476–1481
201. Calabrese GS, Pissavini S (2011) AIChE J 57:828–834
202. Wu K-J, Nappo V, Kuhn S (2015) Ind Eng Chem Res. doi:10.1021/acs.iecr.5b01444
203. Nieves-Remacha MJ, Kulkarni AA, Jensen KF (2015) Ind Eng Chem Res 52:8996–9010
204. Nieves-Remacha MJ, Jensen KF (2015) J Flow Chem 1–6. doi:10.1556/1846.2015.00010

Organic Photoredox Chemistry in Flow

Matthew B. Plutschack, Camille A. Correia, Peter H. Seeberger, and Kerry Gilmore

Abstract The recent movement toward greener, more sustainable chemistry has led to the emergence of photoredox chemistry, capable of catalyzing a wide berth of chemical transformations by channeling the energy of light to reach otherwise unobtainable levels of reactivity and selectivity. A recent parallel development in the field of flow chemistry has led to the enhancement of reactivity and productivity of these photoredox processes, making it a practical method for organic synthesis. This chapter discusses recent advances in the field of organic photoredox chemistry whose reactivity or productivity has been enhanced by flow chemistry.

Keywords Continuous flow · Photocatalytic coupling reactions · Photooxidation · Photoredox catalysis · Photoreduction

Contents

M.B. Plutschack, C.A. Correia, and K. Gilmore (✉)
Department of Biomolecular Systems, Max Planck Institute of Colloids and Interfaces, Am Mühlenberg 1, 14195 Potsdam, Germany
e-mail: Kerry.Gilmore@mpikg.mpg.de

P.H. Seeberger
Department of Biomolecular Systems, Max Planck Institute of Colloids and Interfaces, Am Mühlenberg 1, 14195 Potsdam, Germany

FreieUniversität Berlin, Institute of Chemistry and Biochemistry, Arnimallee 22, 14195 Berlin, Germany

Abbreviations

AIBN	Azobisisobutyronitrile
bpy	2,2′-Bipyridine
dF(CF₃)ppy	2-(2′,4′-Difluorophenyl)-5-trifluoromethylpyridine
dmb	4,4′-Dimethyl-2,2′-dipyridine
DMF	N,N-Dimethylformamide
dmp	2,9-Dimethyl-1,10-phenanthroline
DMSO	Dimethyl sulfoxide
DPEPhos	Bis[(2-diphenylphosphino)phenyl]methane
DSSC	Dye-sensitized solar cell
dtbbpy	di-*tert*-Butylbipyridine
FEP	Fluorinated ethylene propylene
HDF	Hydrodefluorination
IC	Interconversion
ISC	Intersystem crossing
LED	Light-emitting diode
OLED	Organic light-emitting diode
PEEK	Polyetheretherketone
PFA	Polyfluoroalkoxy
ppy	2,2′-Phenylpyridine
SET	Single electron transfer
TFA	Trifluoroacetic acid
THF	Tetrahydrofuran
TMEDA	$N,N,N′,N′$-Tetramethyl-1,2-diaminoethylene
TMS	Trimethylsilyl
TOF	Turnover frequency
UV	Ultraviolet
Xantphos	4,5-Bis(diphenylphosphino)-9,9-dimethylxanthene

1 Introduction

Photoredox catalysis remains one of the cleaner and more sustainable methods to effect a wide variety of transformations, converting the "traceless" energy of photons into oxidative, reductive, or redox neutral processes. Due to the logarithmic

decrease in the transmission of light over distance in a liquid medium (Beer–Lambert law), photochemical processes traditionally suffer from a number of limitations, low irradiation, ineffective irradiation, and over-irradiation, resulting in long reaction times, low selectivity, and by-product formation. Recently, flow chemistry has emerged as a powerful technique for photochemistry [1–5], alleviating many of these previous obstacles due to the significantly narrower path length of the reactor.

This technique has allowed researchers to expand the capabilities of photoredox catalysis, with transformations exhibiting faster reaction times as well as higher yields, selectivities, and productivities. In this chapter, we will discuss the advantages of performing photoredox catalysis in continuous flow, as well as provide a detailed account of the types of transformations (oxidative, reductive, redox neutral) that have been realized thus far.

1.1 Photoredox Catalysis

As a means of activation, light offers a number of distinct advantages. In contrast to thermal activation, light can be completely selective, targeting only those molecules – or sections of molecules – with suitable chromophores. With respect to chemical activation, light produces no waste and does not require quenching, reducing work-up and purification issues. Photocatalysts also offer a variety of options for tuning both reactivity and selectivity. For example, simple substitution of the metal center of organometallic complexes can greatly affect the reactivity, and through ligand manipulations, a broad spectrum of reactivity can be achieved. This versatility is one reason photoredox catalysis has found its niche in a variety of fields, such as renewable energy – in the form of dye-sensitized solar cells (DSSCs) [6] – organic light-emitting diodes (OLEDs) [7, 8], water splitting [9, 10],carbon dioxide reduction [11], polymerizations [12, 13], and photodynamic therapy [14]. Some of the most common catalysts are polypyridyl complexes of ruthenium and iridium [15, 16] and Eosin Y [17] (Fig. 1).

All photocatalysts rely on the ability of the excited catalyst to undergo single electron transfer (SET). Scheme 1 shows a generalized molecular orbital diagram of the catalyst upon irradiation. Absorption of a photon excites an electron from the ground state to an S_1 excited state. Interconversion (IC), followed by intersystem crossing (ISC), produces the T_1 triplet state. Here, the photocatalyst is capable of engaging in SET with organic molecules, acting as an oxidant (D) or reductant (A).

After excitation, two quenching cycles exist, oxidative and reductive (Scheme 2). In the oxidative quenching cycle, the catalyst functions as a reductant, donating an electron to an acceptor (A_o) to produce a +1 catalyst. This species is a good oxidant and can remove an electron from the target molecule (D_o) to reform the ground state catalyst. Common oxidative quenchers (A_o) are viologens, polyhalomethanes, dinitro- and dicyanobenzenes, and aryldiazonium salts. Alternatively, in the reductive quenching cycle, the catalyst acts as an oxidant to D_R (typically a tertiary
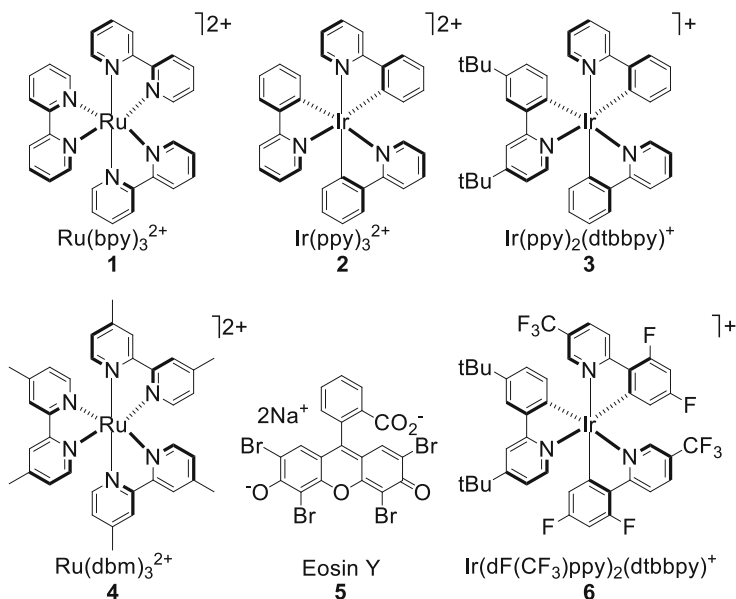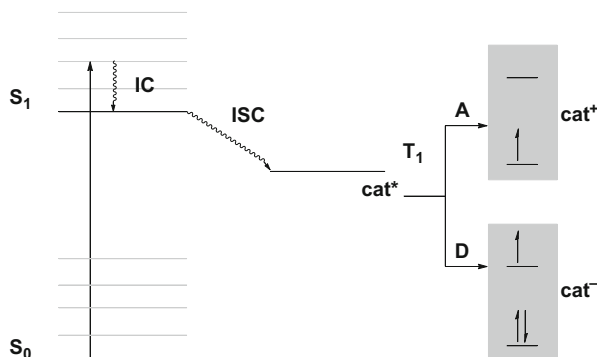
**Fig. 1** Common photoredox catalysts

Scheme 1 Generic energy level diagram of the photocatalyst acting as a reductant to an acceptor (*top pathway*) or an oxidant to a donor (*bottom pathway*)

amine), yielding a −1 catalyst which can then donate an electron into the target molecule (A_R) and reform the catalyst.

1.2 Photochemistry in Flow

The immersion well photoreactor has been the conventional reactor for preparative photochemistry, comparable to the round-bottom flask in organic synthesis. In this
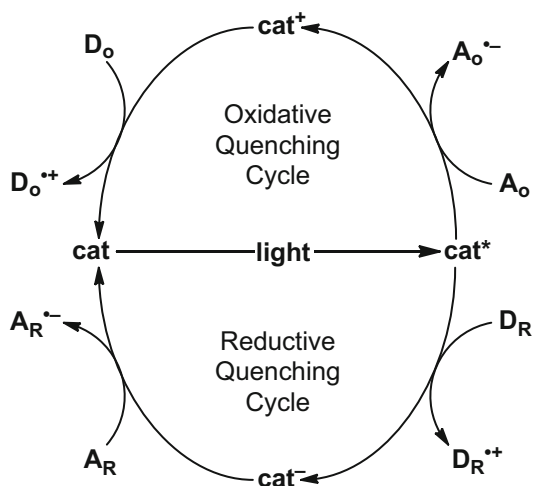
Scheme 2 Oxidative and reductive quenching cycles
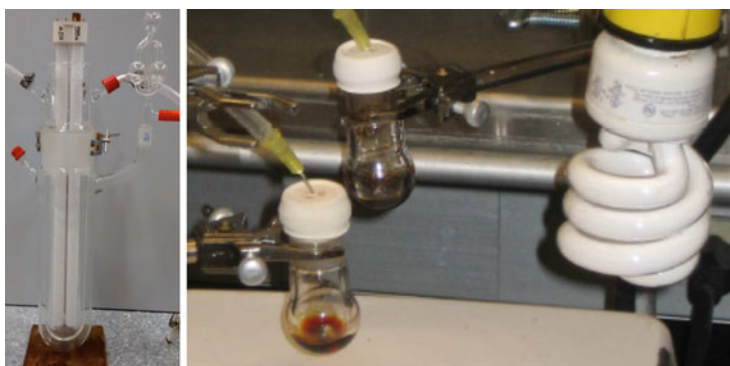
Fig. 2 A typical immersion well reactor (*left*). A common round-bottom flask set up for multiple reactions (*right*). Images reprinted with permission from Elliott et al. [18] (*left*) and Narayanam et al. [19] (*right*)

photoreactor, the lamp is contained in a double-jacketed water-cooled immersion well that can be inserted into a round-bottom flask (Fig. 2, left). This setup is usually enclosed in a shielded cabinet to avoid potentially harmful exposure to intense radiation. Its main drawback is the inability or inefficiency to scale up reactions. For photoredox catalysis, often simpler setups – where round-bottom flasks are irradiated by LED/compact fluorescent light bulbs – are used. However, these setups also face with difficulties or inefficiencies upon scale-up (Fig. 2, right).

The main reason for this scaling problem is the lack of light penetration into the entire solution. This attenuation of light as it passes through the solution is explained by the Beer–Lambert Law (Eq. 1). The absorption of the light by the

solution (A) is directly related to the extinction coefficient (ε), the molar concentration (c), and the path length (l). The transmittance of the solution is expressed as a logarithm of the ratio between the transmitted light (I) and the incident light (I_0). Therefore, the path length required to absorb 90% of the incident light in a 0.05 M benzene solution ($\varepsilon = 200$ M^{-1} cm^{-1}) is just 1 mm. The extinction coefficient for Ru(bpy)$_3$Cl$_2$, for example, is 14,600 m^{-1} cm^{-1} [20]. A 0.05 M concentration of this common photocatalyst would absorb 90% of the incident light at an approximate distance of 0.01 mm:

$$A = \varepsilon c l = -\log_{10}\frac{I}{I_0} \tag{1}$$

In a batch reaction, this means that only a small fraction of the reaction mixture is being irradiated at a given time. A number of homemade photoreactors have been reported that are able to more efficiently capture incident light than the compact fluorescent bulb/round-bottom flask setup (Fig. 3), but they still suffer from inefficient irradiation.

In a flow reactor, a fraction of the reaction mixture is continuously passed through a photoreactor whose path length is generally less than 2 mm. As such, the complete reaction mixture experiences very efficient and uniform irradiation over the course of the reaction. Additionally, since the continuous flow reactor is scale independent, the same reactor which is used to produce a milligram of product could in theory be used to produce gram-scale quantities. This means that once a reaction is optimized on a small scale, scale-up only requires longer operation of the reactor.

There are many commercially available photoreactors and even more homemade photoreactor designs. Three basic designs are usually employed for continuous flow photoredox chemistry: a chip or flat presentation of tubing with irradiation from one or both sides (Fig. 4, left), immersion well-type apparatus

Fig. 3 Homemade visible-light batch reactors with LED strips lining the inside of cylindrical containers. Images reprinted with permission from Weiss et al. [21] (*left*) and Senaweera et al. [22] (*right*)
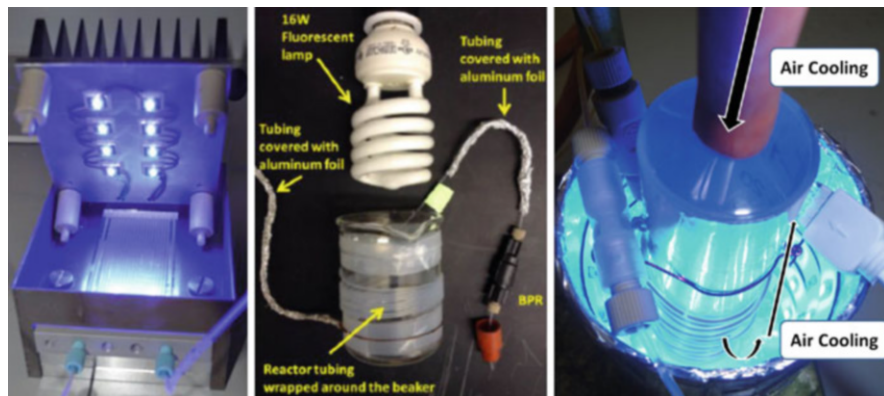
Fig. 4 A flat reactor presentation with blue-light irradiation from the top by eight OSRAM OLSON Black Series LD H9GP LEDs (455 ± 10 nm) (*left*). A homemade immersion well-like flow reactor setup, constructed from PFA tubing wrapped around a beaker with a 16 W compact fluorescent lamp (*middle*). A homemade photoreactor with a blue LED strip coiled around the inside of a beaker surrounding PFA tubing wrapped around the outside of a 50 mL syringe (*right*). Images were reprinted with permission from Rackl et al. [23] (*left*) (this is an Open Access article under the terms of the Creative Commons Attribution License (http://creativecommons.org/licenses/by/2.0)), He et al. [24] (*middle*), and Wang et al. [25] (*right*)

with the tubing coiled around the irradiation source (Fig. 4, middle), and a similar apparatus with the light source coiled around the reactor tubing (Fig. 4, right).

The housing units for the flat planar reactors usually enclose the light source; however, they suffer from one main disadvantage. Light sources, even relatively planar LED strips, emit light in a radial nature. The planar surface of the reactor cannot efficiently capture all the light from the source. The immersion well-like reactors place the reactor tubing around the light source, maximizing the reaction mixtures' ability to capture emitted light. These reactors can be quickly and easily created even by an inexperienced scientist. All that is needed is a syringe pump, tubing, and a lamp. The third type of reactor is also radial in nature. While it may be slightly less efficient than the immersion well reactor at capturing the emitted light, it makes use of cheap and easy-to-use LED strips that come in various colors. One benefit of this reactor setup is that it can easily be converted from a batch photoreactor to a flow reactor.

Combining the two general photoredox processes (oxidation and reduction) with the inherent benefits of flow chemistry has led to a wide variety of efficient chemical transformations including, but not limited to, Mallory-type reactions, amine oxidations, photochemical Heck-type couplings, aryldiazonium coupling, C–X reductions, and heterocyclic alkylation [15–17, 19, 26–31]. For the purpose of this chapter, these chemistries have been categorized as photooxidations or photoreductions and then further divided in terms of the type of transformation. Some reactions involve both a formal oxidation and a reduction and have been organized based on their relevance to other chemistries discussed in the section.

2 Oxidative Quenching

Excitation of the catalyst in the presence of a stoichiometric amount of an oxidative quencher provides access to a powerful oxidant as mentioned previously in Sect. 1.1 (oxidative quenching cycle of Scheme 2). This cycle has been used to perform Vilsmeier–Haack chemistry, Mallory reactions, and to a greater extent the oxidation and functionalization of electron-rich amines. This section will provide an overview of some of the photooxidative reactions which have been carried out in flow reactors.[1]

2.1 Conversion of C–O Bonds to C–X Bonds

In general, the C–O bond is relatively strong. The formation of esters is a common way of increasing reactivity and activating this center for further transformations. Often alcohols are activated and then transformed into alkyl halides that are of intermediate reactivity when compared to the activated species. Commonly used reagents for alkyl halide formation from alcohols include thionyl chloride, phosphorous halides, phenyl methyl iminium salts, benzoxazolium, Viehe's salt, cyclopropenium ions, Appel chemistry, or Vilsmeier–Haack chemistry [33, 34]. While Appel-type chemistry is one of the most ubiquitous methods for converting alcohols into halides, it often uses triphenylphosphine, one of the least atom-economical reducing agents. In addition, the triphenylphosphine oxide produced can be difficult to remove from the reaction mixture.

Stoichiometric amounts of iron and copper in the presence of tetrahalomethanes (CCl_4 and CBr_4) in DMF efficiently convert alcohols to halides via a Vilsmeier–Haack-type intermediate [35]. The Vilsmeier–Haack reaction is a more attractive procedure than Appel-type chemistry since the by-products are CO_2, HBr, and methyl amine. Therefore, it is not only more atom economical, but it also produces by-products that are easily separable from the product mixture. For this reason, Stephenson and co-workers developed a batch photocatalytic Vilsmeier–Haack reaction for the conversion of alcohols to alkyl halides by employing catalyst **1** as a photocatalyst and CBr_4 or CHI_3 as an oxidant (Scheme 3).

The authors hypothesized that the excited Ru^{2+} species acts as a reducing agent, donating an electron to CBr_4, generating a bromide ion and a CBr_3 radical (Scheme 4). This radical reacts with DMF, which subsequently reduces the newly formed Ru^{3+} species and in doing so regenerates $Ru(bpy)_3^{2+}$. Alternatively it can react with another equivalent of CBr_4. Compound **7** can decompose to either form a Vilsmeier–Haack reagent, **8**, and bromophosgene or react directly with the alcohol to form activated intermediate **9**. Both intermediate **9** and the hydrolyzed formate ester can react with bromide to form the alkyl bromide.

---

[1] For an overview of aerobic oxidations in continuous flow, see Pieber and Kappe [32].
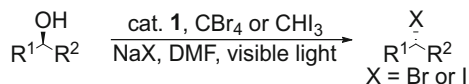
Scheme 3 Photocatalytic Vilsmeier–Haack reaction for the conversion of alcohols into halides
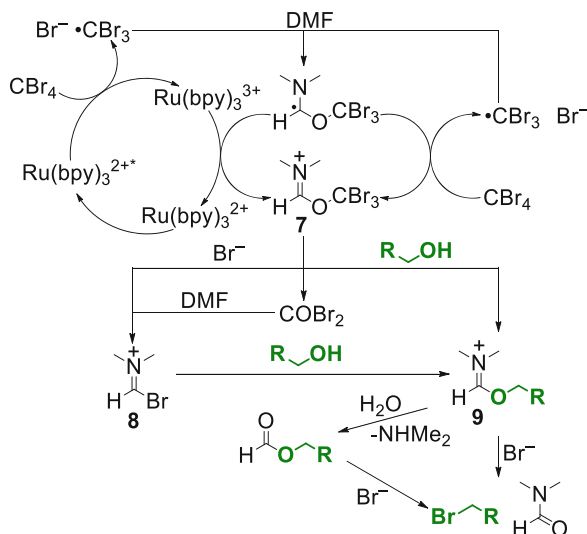
Scheme 4 The proposed mechanistic pathways for the activation and formation of alkyl bromides from alcohols via Vilsmeier–Haack-type intermediates

10a: X = OCHO
10b: X = Br
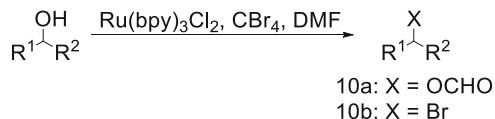
Table 1 Batch versus flow comparison of the photo-Vilsmeier–Haack reaction

Reactor	R^1	R^2	Temp. (°C)	Time	**10a:10b**	% Conv.
Batch	$PhCH_2CH_2$	H	25	8 h	3:2	43
	$PhCH_2CH_2$	H	25	24 h	8:92	100
Flow	$PhCH_2CH_2$	H	25	30 min	92:8	99
	$PhCH_2CH_2$	H	25/100	31 min	0:100	>95
	Bu	Bu	25	30 min	95:5	100
	Bu	Bu	25/100	31 min	0:100	>95

Seeberger and co-workers adapted this reaction to flow and found the reaction to be greatly accelerated in comparison to the corresponding batch process (Table 1) [31]. The photoreactor consisted of FEP tubing wrapped around two metal rods, placed between a pair of 17W white LED lamps. After 8 h in the batch reactor, only

43% conversion was observed, generating a 3:2 mixture of formate ester **10a** to bromide **10b**. After 24 h, full conversion was obtained with an 8:92 ratio of **10a** to **10b**. Under continuous flow conditions, complete activation of the alcohol was achieved after only 30 min. In addition, the flow process demonstrated superior control over the product outcome, where **10a** could be obtained as the major product (92:8 and 95:5 ratios for both 1° and 2° alcohols). To obtain the corresponding alkyl bromide, a second reactor was coupled to the photoreactor, providing full conversion to the desired alkyl bromide after 1 min at 100°C.

Stephenson and co-workers expanded upon this type of chemistry by applying it to the formation of anhydrides [36]. Similar to alcohols, carboxylic acids can be activated for nucleophilic attack by the same photoredox-generated intermediates as in Scheme 4 (compounds **7** or **8**). The activated acid species is trapped by another equivalent of carboxylic acid to form the symmetrical anhydride. The authors demonstrated that this approach was applicable to a variety of carboxylic acids (61–99%); however, amino acids and carboxylic acids bearing aromatic rings with strong electron-withdrawing groups failed to react. By adapting the reaction to flow using an LED-driven homemade reactor, a tenfold increase in productivity and an almost quantitative yield of the desired anhydride was observed (Scheme 5).

In summary, this chemistry offers a new mode of activating C–O bonds, and integration of this chemistry into a flow setup not only increased the productivity and yield but has also allowed chemists to control reactivity in a manner that was not possible in a traditional batch reactor.
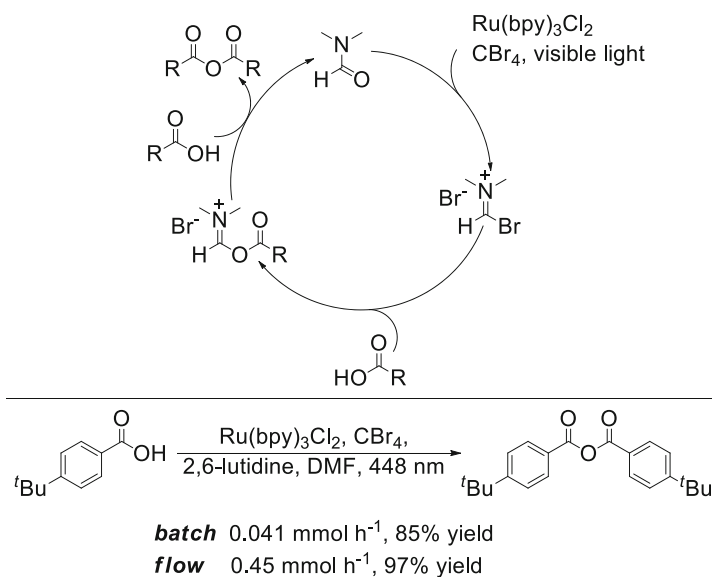
Scheme 5 Synthesis of symmetric anhydrides and the enhanced productivity using a flow reactor

2.2   Cyclization by Photooxidation

Helicenes are 3D polycyclic aromatic systems that have found applications as molecular springs, molecular machines, dyes, and polymers [37]. The batch UV light photocyclization is one of the most important methods for the synthesis of many helicene homologues. This process, however, has several drawbacks. First, UV-mediated chemistry results in poor regiocontrol, forming an undesired regioisomer in 38% yield. Over oxidation of the desired compound is an additional drawback, further reducing the yield of this process. Collins and co-workers addressed these issues, demonstrating that a copper photocatalyst is effective for a visible-light-mediated Mallory reaction, converting a series of stilbenes into [5] helicenes in a flow reactor [38]. Iodine is used as the terminal oxidant, and the photocatalyst is generated in situ from $Cu(MeCN)_4BF_4$, neocuproine (a nitrogen bidentate ligand), and either DPEPhos or Xantphos (bidentate phosphine ligands).

The reaction was initially run in batch, requiring 120 h of reaction time with a 42% yield. The same conditions were tested using the FlowSyn Multi-X reactor from Uniqsis containing an FEP (fluorinated ethylene propylene) microreactor and a household energy-saving light bulb. Upon adaptation to flow, the product could be obtained in 10 h, a 12-fold reduction in time, and in comparable yields, 40% vs. 42% in batch. There was also a significant reduction in the by-products typically observed. This method was also used for the synthesis of pyrene–helicene hybrids, and the flow setup resulted in a similar reduction in time, 18 vs. 120 h, and in significantly higher conversion and yield [39]. Although these flow reactions have a longer than average residence time, the use of flow significantly improved the productivity (Fig. 5).

Similar conditions were applied to the synthesis of carbazoles [40]. Again, an enhancement in the rate of the reaction was observed in flow, 20 h compared to 120 h in batch reactions. A plausible mechanism for the formation of carbazoles is outlined in Scheme 6. The excited copper catalyst undergoes SET with molecular iodine to produce iodide and elemental iodine. Oxidation of the aryl amine reforms the catalyst and produces a radical cation that can cyclize. Deprotonation and oxidation forms the product in 50–95% yield for N-aryl-bearing carbazoles and in 51–79% yield for N-alkyl-bearing carbazoles.

Overall, the new copper photocatalyst outperformed the more common ruthenium and iridium catalysts. Optimization of the photosensitizer's properties was achieved by in situ preparation of the catalyst. In combination with a photoflow reactor, the productivity was greatly increased. This provided access to higher quantities of novel helicenes and a new photocatalytic route to a variety of carbazoles, allowing for additional studies related to the crystal structures of these compounds.

batch 0.55 μmol h⁻¹, 42%
flow 6.0 μmol h⁻¹, 40%

batch 0.19 μmol h⁻¹, 12%
flow 5.5 μmol h⁻¹, 41%

batch 0.17 μmol h⁻¹, 23%
flow 16 μmol h⁻¹, 45%

batch 0.83 μmol h⁻¹, 27%
flow 2.6 μmol h⁻¹, 46%
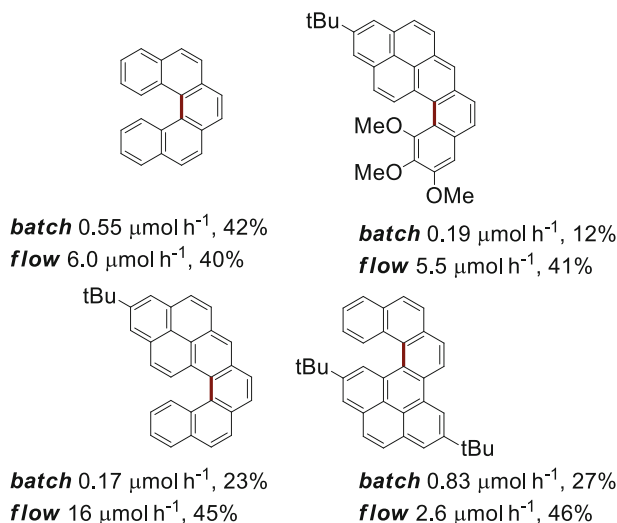
Fig. 5 Batch versus flow productivities calculated from the work of Collins et al. [39]. New bond formed is shown in *red*
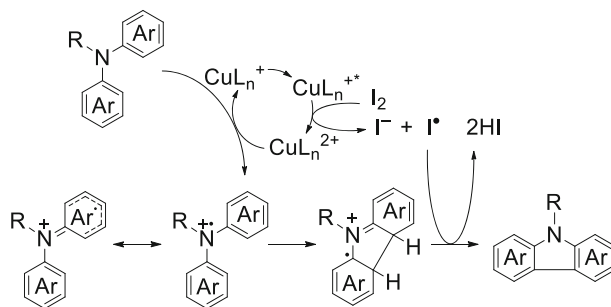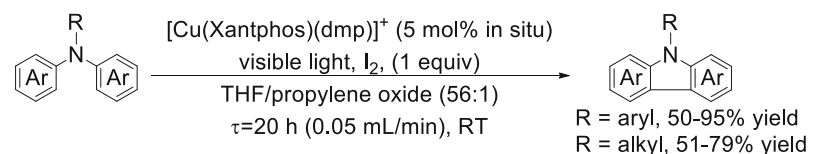

Scheme 6 The synthesis of carbazoles by the photooxidation of arylamines in a flow reactor with the proposed mechanism for oxidation and cyclization

2.3   *Photoredox-Mediated α-Functionalization of Amines*

Oxidation of amines at the alpha position is an attractive method for the selective introduction of functionalities [41]. It is generally achieved either with metal catalysts [42–45], biocatalysts [46], or stoichiometric oxidants [47–51]. While the photosensitized generation of singlet oxygen in both batch [52, 53] and flow

[54, 55] is a promising alternative, it generates by-products capable of further reacting with the desired product [56]. In 2012 Stephenson reported the photooxidation of tetrahydroisoquinoline in a flow reactor consisting of PFA tubing wrapped in a figure-eight pattern around a pair of test tubes [57]. They employed catalyst **1** and BrCCl$_3$ as an oxidant. Upon exiting the reactor, the crude solution was collected in a flask containing 5.0 equivalents of a carbon nucleophile, allowing the authors to quickly generate a variety of α-functionalized amines (Scheme 7). As a representative example, the aza-Henry reaction was run on a 0.24 mmol scale in batch and needed 3 h to reach completion, corresponding to a productivity of 0.081 mmol h^{-1}. In the flow reactor, the reaction reached completion with a residence time of 0.5 min, corresponding to a productivity of 5.75 mmol h^{-1}.

Building on this work, Stephenson and Beatty reported the use of photoredox catalysis as a chemoselective and efficient method for the functionalization of an alkaloid [58, 59]. The authors utilized the amine functionality in the alkaloid for the efficient synthesis of α-amino nitrile **11** via an interesting fragmentation process (Scheme 8).
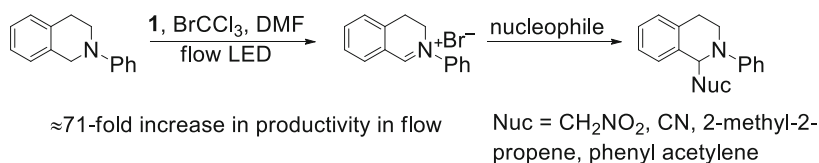
Scheme 7 The photooxidation of tetrahydroisoquinoline in flow, followed by nucleophilic trapping
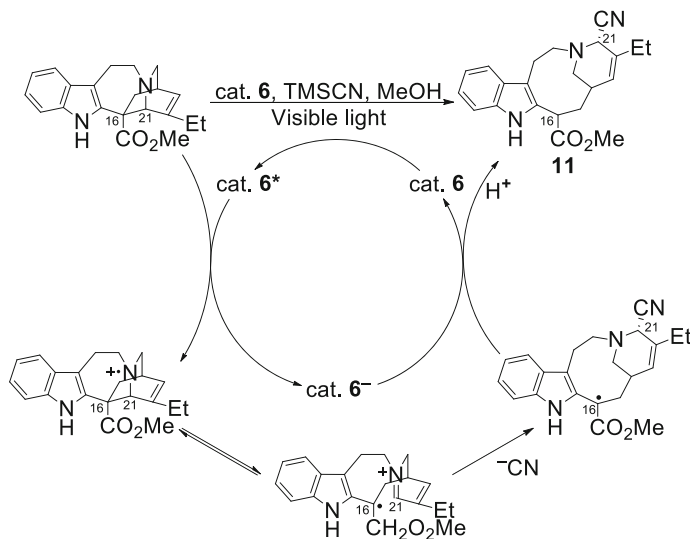
Scheme 8 The proposed mechanism for the oxidation fragmentation and trapping of (+)-catharanthine
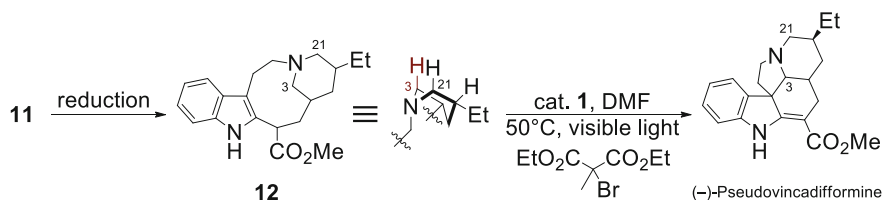
Scheme 9 The synthesis of (−)-pseudovincadifformine via photooxidative iminium formation. The oxidized position (methylene 3) is shown in *red*

When (+)-catharanthine was exposed to blue light in the presence of catalyst **6** and TMSCN in methanol, excellent yields were observed for α-amino nitrile **11**. The authors transferred this reaction to flow, not only to improve the productivity of the process (batch, 0.03 mmol h^{-1}) but also to more safely generate HCN – a poisonous liquid which boils around room temperature. Rewardingly, in flow the yield proved almost quantitative (96%) and the productivity increased by more than 240 times (7.2 mmol h^{-1})!

With the amino nitrile **11** in hand, synthesis of (−)-pseudotabersonine was made possible by refluxing with TFA in toluene and (+)-coronaridine by hydrogenation prior to acid-induced cyclization. However, when the desired iminium isomerization of **11** failed to give (−)-pseudovincadifformine, a second photoredox process was developed. Computational analysis of **12**, formed upon reduction of **11**, revealed that methylene **3** is more accessible than the other two methylene groups (Scheme 9). It was thus envisioned that the desired iminium could be selectively generated with a second photoredox process following reduction to **12**. As such, when **12** was exposed to flow photoredox conditions, using 2-bromo-2-methylmalonate as an oxidant, the desired iminium could be selectively generated and subsequently trapped intramolecularly, providing (−)-pseudovincadifformine in 58% yield (Scheme 9).

In conclusion, amine oxidation using photoredox chemistry is an effective means of selective α-functionalization without the formation of reactive by-products. Two nonsequential continuous flow processes allowed for the synthesis of (−)-pseudovincadifformine. Not only did flow chemistry enhance the productivity and greatly reduce the reaction time, but it also provided the desired intermediate where other chemistries failed.

3   Reductive Quenching

The reduction of functional groups represents an important chemical transformation. Photoredox catalysis is a new avenue being explored to carry out this type of transformation as it generates less waste and maintains milder reaction conditions. Excitation of the catalyst in the presence of a stoichiometric amount of a reductive quencher provides access to a powerful reducing agent cat$^-$ as discussed in

Sect. 1.1 (reductive quenching cycle of Scheme 2). This cycle has been used to perform reductive dehalogenations, C–O deoxygenations, as well as C–X coupling reactions. This section will provide an overview of some of these photoreductions, all of which demonstrate enhanced reactivity in a flow reactor.

3.1   *Photoreduction of sp³ C–X Bonds*

The conversion of C–X bonds to C–H bonds often involves a metal halogen exchange or a hydride source. More commonly, a radical reducing agent is used; however, these reagents are typically toxic (organotin compounds), explosive (AIBN and peroxides), unstable (samarium (II) iodide), or even pyrophoric (trialkyboranes). Recent efforts, particularly in the Stephenson group, have succeeded in replacing these reagents with milder photoredox conditions. The generic reaction covered in this section is shown in Scheme 10 (bottom).

In 2009, Stephenson and co-workers reported a batch, tin-free reductive dehalogenation using photocatalyst **1** and a tertiary amine as a reducing agent (Scheme 11) [19]. They found that the reductive debromination occurred cleanly in DMF following two sets of conditions: (1) $^{i}Pr_2NEt$ and formic acid or (2) $^{i}Pr_2NEt$ and Hantzsch ester. Under either of these conditions, they were able to selectively dehalogenate bromides and chlorides alpha to carbonyls over aryl and alkenyl bromides and iodides.

Seeberger and Bou-Hamdan reported an increase in productivity for this class of transformations when the reaction was converted to flow using a homebuilt, visible-light-driven photoreactor (Scheme 12) [31]. Upon adaptation, they found that the reaction could even be performed in the absence of the Hantzsch ester and on the more challenging alkyl chloride.
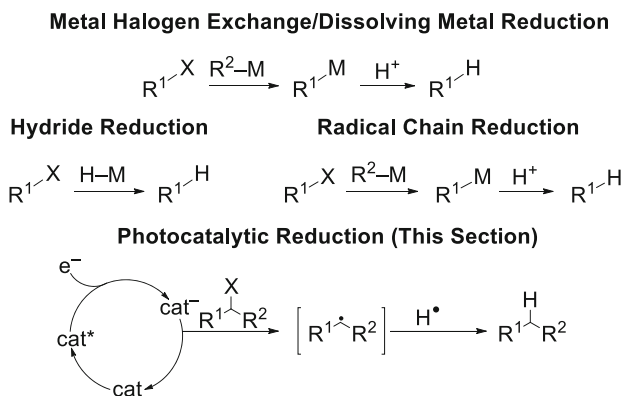
Scheme 10   The generic photocatalytic reduction of sp³ C–X bonds to C–H bonds
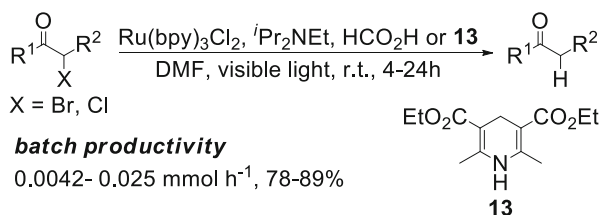
Scheme 11 The photoreduction of α-halocarbonyl compounds in batch. The reaction times range from 4 to 24 h. The productivity range is based on conversion of starting materials
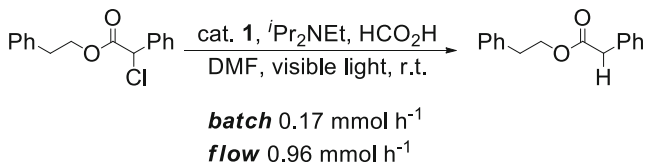
Scheme 12 The photoreduction of a α-chlorocarbonyl compound, with batch versus flow comparison
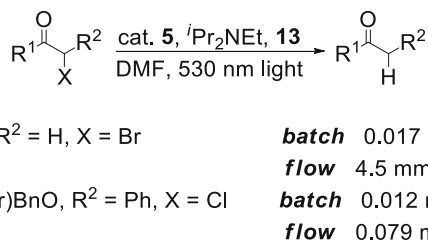
Scheme 13 A batch versus flow comparison for the Eosin Y-mediated photoreduction of α-halo keto compounds

Zeitler and co-workers further demonstrated that this transformation could also be carried out with Eosin Y, catalyst **5**. Additionally, the choice of the reactor design dictated the reaction productivity (Scheme 13) [60]. The batch reactor had comparably low productivities for both the bromo and the chloro compounds (0.017 and 0.012 mmol h^{-1} respectively). The photoredox reactions carried out in flow were performed using a Microflow reactor manufactured by Micronit Microfluidics, operated in a FutureChemistry Holding BV Flowstart B-200 setup with a green (530 nm) LED lamp. With this system, the more easily reduced bromo compound showed over a 250-fold increase in productivity. Conversion of the less activated chloro compound was achieved with complete selectivity (no reaction of the aryl bromide) with a 6.5-fold increase in productivity.

The hydrodeoxygenation reaction is an important transformation in organic synthesis, yet it remains a challenge. One of the most utilized methods is the radical Barton–McCombie deoxygenation [61]. This reaction, along with other common conditions (going through benzoyl ester or phosphite intermediates – similar to

BnO⌒⌒⌒OH $\xrightarrow[\text{\textit{fac}-Ir(ppy)}_3, \ ^i\text{Pr}_2\text{NEt, MeOH}]{\text{PPh}_3, \ \text{I}_2, \ \text{imidazole, MeCN}}$ BnO⌒⌒⌒H
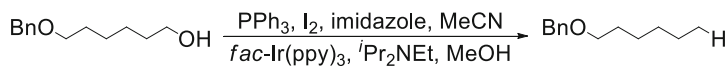
batch 0.0052 mmol h^{-1}, 144 h, 75% conversion
flow 0.64 mmol h^{-1}, τ = 18 min

Scheme 14 Batch versus flow comparison of the "one-pot" Garegg–Samuelsson photoreductive deoxygenation

Sect. 2.1) first activates the C–O bond to allow for a more facile C–O bond cleavage. The Garegg–Samuelsson reaction, which utilizes triphenylphosphine and iodide to activate the alcohol, has exceptional functional group tolerance and can be performed in a variety of solvents, namely, MeCN (the optimal solvent for photocatalytic hydrodeiodination). Stephenson and co-workers initially attempted this reaction in batch, having found Vilsmeier–Haack chemistry not suitable due to a sluggish deiodination in DMF. Even after employing Garegg–Samuelsson/ photoredox deiodination conditions, only 75% conversion was observed after 144 h (Scheme 14).

In order to improve the productivity, they turned to continuous flow. The reactor was constructed from PFA tubing wrapped around three test tubes supported and positioned approximately 2 cm above an LED assembly of seven high-powered Luxeon Rebel LEDs (royal blue, 447.5 nm). Under the optimized conditions, they found that the use of a continuous flow reactor offered over a 120-fold increase in productivity over the batch reactor.

They applied these conditions to a diverse substrate scope and found that this hydrodeoxygenation process had excellent functional group tolerance, leaving benzyl ethers, carbamate esters, cyclopropanes, sulfonamides, acetals, and distal olefins unaffected. Primary alcohols were deoxygenated in 70–88% yield and secondary alcohols in 67–78% yield. Notably, they were able to deoxygenate primary alcohols in the presence of secondary alcohols.

3.2 Photoreduction of sp^2 C–X Bonds

Partially fluorinated arenes make up 20–25% of the compounds in the pharmaceutical pipeline [62]. One attractive approach for their synthesis is the hydrodefluorination (HDF) of polyfluoroarenes. This approach, however, comes with a series of challenges, as it not only necessitates insertion into a strong C–F bond, but upon insertion, another strong bond is formed – between the catalyst and fluorine – which greatly dampens the catalytic cycle and adversely affects the turnover number. Endeavors to establish a dependable catalytic system have predominately resorted to the use of metal hydrido complexes (Rh, Ni, Pd, Au, Al) or pricey Si-hydrides [63–72].

In 2014, Weaver and co-workers reported a photocatalytic approach, where an amine reductant also serves as a trap for fluoride by generating an iminium fluoride salt as a by-product [22]. The proposed mechanism for HDF proceeds via SET between the electron-poor aromatic ring and excited catalyst, producing radical anion **14** (Scheme 15). Decomposition of the radical anion yields fluoride and an aryl radical. In parallel, the +1 photocatalyst is quenched by ^{i}PrNEt, forming an amine-centered radical cation. The aryl radical abstracts a hydrogen atom from the alpha position of the amine, generating the reduced polyfluoroaryl compound as well as the iminium fluoride.

These conditions tolerate a wide range of functional groups; it should be noted amines, alcohols, and thiols all require protection. Certain polyfluorinated aryl compounds can even undergo poly-HDF, with the degree of HDF controlled by the equivalents of amine. As opposed to previous catalytic methods, the described photoredox process can be performed at low catalyst loadings, because no catalyst–F bond is formed in the catalytic cycle. For the HDF of pentafluoropyridine, an unprecedented turnover number of 22,500 was observed [72–74].

With ambitions of scaling this reaction, Weaver and co-workers turned to adapting this reaction to flow. Their reactor design consisted of PFA tubing (1.58 mm ID, 13.6 mL) wrapped around a reflux condenser [75]. An LED strip was placed in the center of the condenser, and a heated mixture (45°C) of water and ethylene glycol was passed through the jacket of the condenser to regulate the temperature (Scheme 16). They found that the use of this reactor significantly increased the productivity for the HDF of pentafluoropyridine (batch 0.004 mmol h^{-1}; flow 0.27 mmol h^{-1}). One of the most sluggish substrates, octafluoronaphthalene, never reached full conversion in either batch or flow; however, the percent conversion, as well as the productivity, was enhanced in the flow reactor (batch 1.4 μmol h^{-1}, 37% conv.; flow 5.1 μmol h^{-1}, 53% conv.).

In summary, photoredox catalysis provides an efficient alternative to perform hydrodefluorinations, a traditionally challenging transformation which utilized
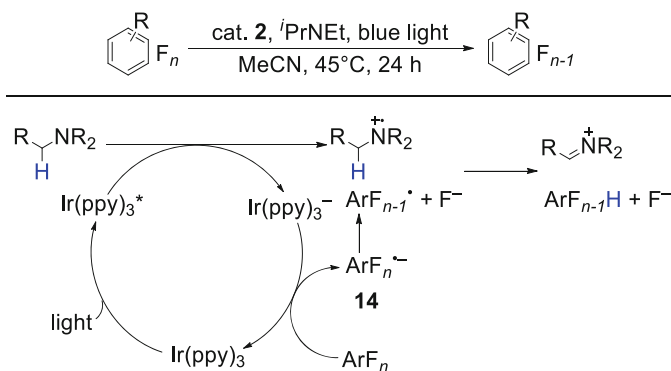
Scheme 15 The proposed mechanism for the hydrodefluorination of polyfluorinated aromatic rings
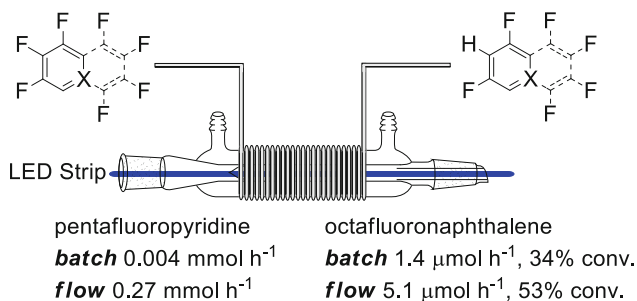
Scheme 16 Photoredox rate acceleration and improved scalability by employing continuous flow conditions for the hydrodefluorination of polyfluoroarenes

dangerous or expensive hydrido species. The developed reaction is widely tolerant of pendent functionalities and uses a tertiary amine as the stoichiometric reductant. As no catalyst–F bonds are formed, the reaction reaches impressively high turnover numbers (22,500). While the productivity of the reaction was poor in batch $(0.004 \text{ mmol h}^{-1})$, in a 13 mL homemade flow reactor, a large jump in productivity ($\times 67$) was observed, making the reaction significantly more applicable to the synthetic community.

3.3 C–O Bond Cleavage via Carbonyl Activation

Selective cleavage of a C–O σ-bond represents a valuable transformation, not only for industrial researchers with its application in the conversion of sugars or biomass to hydrocarbons but also to academic chemists as a valuable tool in synthesis. The movement toward more eco-friendly reactions has led to the development of C–O cleavage via SET redox processes using photocatalysts. Ollivier and co-workers reported a batch photoredox reaction for the activation of α-ketoepoxides and α-ketoaziridines using catalysts **1** and **3** [76]. The mechanism is proposed in Scheme 17. The excited photocatalyst accepts an electron from a Hantzsch ester donor, **13**, producing a strong reducing agent cat$^-$ which activates the α-ketoepoxide via reduction. The α-ketoepoxide radical anion is in equilibrium with the ring-open radical anion **15**, which can be reduced with a proton and hydrogen donor or coupled in the presence of a radical coupling reagent.

Seeberger and Bou-Hamdan reported the same reaction in flow with a moderate improvement to productivity (Scheme 18) [31]. The batch reaction was found to function in the presence of ^{i}Pr$_2$NEt and formic acid without any Hantzsch ester, **13**, reaching complete conversion after 4 h, giving it a productivity of 0.91 mmol h^{-1}. The same reaction was carried out in a flow reactor, and with only 10-min residence time, the reaction reached completion (2.6 mmol h^{-1}). Overall, this method provides quick, easy access to β-hydroxyketones.
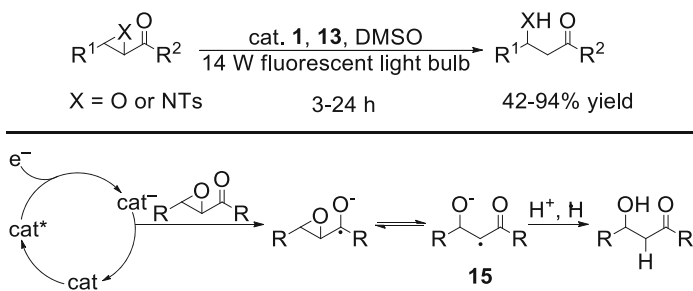
Scheme 17 The photocatalytic reduction of epoxides and aziridines to the corresponding β-keto alcohols and amines (*top*). Proposed mechanism for the reduction of epoxides (*bottom*)
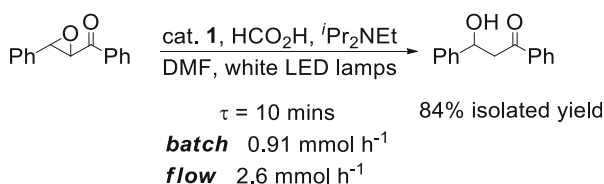
Scheme 18 A comparison of the photocatalytic reduction of epoxides in flow and batch
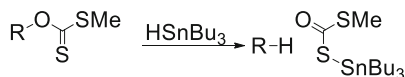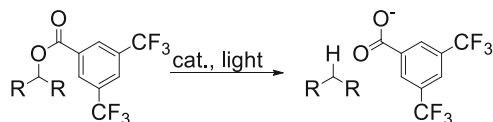
Scheme 19 Comparison of Barton–McCombie deoxygenation with the photocatalytic deoxygenation by Reiser et al. [23]

In 2014, Reiser and co-workers reported a method for the photoredox-catalyzed deoxygenation of alcohols which proceeds via a 3,5-bis(trifluoromethyl)-substituted benzoate (Scheme 19) [23]. This transformation is analogous to the classical Barton–McCombie deoxygenation, but with two notable benefits [61]. In the Barton–McCombie deoxygenation, as well as other electrochemical [77] and photochemical deoxygenations [78–82], the hydroxyl group must be activated, consequently generating a stoichiometric amount of waste. While Reiser's method also produces a stoichiometric amount of 3,5-bis(trifluoromethyl)benzoic acid due to the same requirement for pre-activation, work-up of the reaction mixture resulted in over 90% recovery of the acid, which could be used to regenerate the anhydride needed to activate the alcohol. The second reason this transformation is more

advantageous than classical methods for deoxygenation is that the mode of activation is through a photoredox catalyst as opposed to toxic or explosive radical initiators.

Reiser and co-workers first synthesized different CF$_3$-substituted benzoate esters and investigated their reduction potentials using catalysts **1** and **3**. Out of the three compounds investigated, the 3,5-bis-CF$_3$-substituted benzoate ester was the most promising, in good agreement with the relative reduction potentials of the compounds (it has the highest reduction potential, making it most susceptible to SET).[2] In every case, catalyst **3** outperformed **1**. Under the optimized conditions, they were able to successfully deoxygenate secondary alcohols in 66–95% yield. Deoxygenation of primary alcohols was unsuccessful, most likely due to the unfavorable formation of the primary radical (proposed mechanism, Scheme 20).

Using diphenylmethanol as a model substrate, the reaction was scaled up and additionally done in "one-pot" (activation/deoxygenation). The activation of the alcohol was done in batch, using excess triethylamine. After 18 h, catalyst **3** was added to the reaction mixture, and the solution was pumped through a flat microreactor and irradiated from above with eight LEDs (see Sect. 1.2, Fig. 4, left). The "one-pot" procedure was performed with negligible reduction to productivity or yield (deoxygenation of benzoate ester, 0.2 mmol h^{-1}, 95% yield; "one-pot" deoxygenation, 0.17 mmol h^{-1}, 91% yield). Overall, this method eliminates toxic or explosive activating agents through the use of a photoredox catalyst, has a recoverable activating agent, and is adaptable to flow, which is desirable for large-scale applications in synthesis.

One type of C–O bond that is the focus of a number of large-scale applications is the ether β-O-4 linkage found in Lignin. Lignin is an organic aromatic biopolymer that has a high potential as a sustainable source of low molecular weight aromatic compounds [83]. In industry, lignin is processed to produce materials; however,
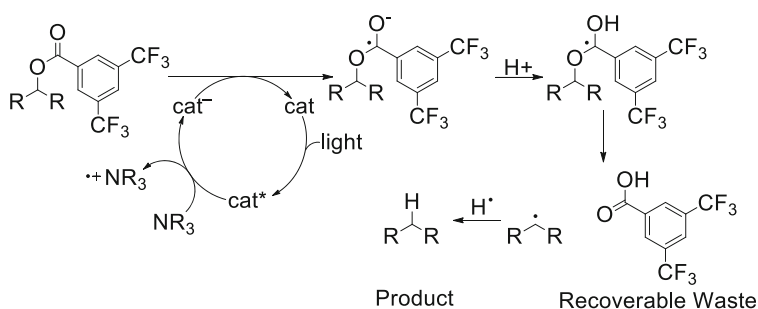
Scheme 20 The proposed mechanism for the photocatalytic deoxygenation of 3,5-bis (trifluoromethyl)benzoates

<hr>

[2] They hypothesized that this was because of the more favorable reduction potential ($E_{red3} = -1.51$ eV vs. $E_{red1} = -1.33$ eV).
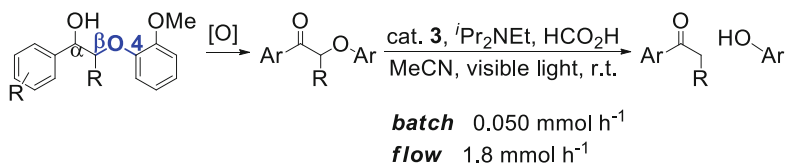
Scheme 21 Two-step redox neutral process for the degradation of lignin at room temperature

due to the energy-intensive degradation, lignin has not found its niche in the production of bulk chemicals [84, 85]. The β-O-4 linkage is the most common type of linkage found in lignocelluloses, comprising over 50% of the linkages [86]. Recently, Stephenson and co-workers have developed a two-step, redox neutral process in flow for the degradation of lignin at room temperature [87]. The first step involves a benzylic oxidation to producing an α-hydroxyketo moiety, which is subsequently cleaved in the second step by the developed photoredox process (Scheme 21). The visible-light-mediated C–O bond cleavage was carried out for a series of α-hydroxyketo model compounds with yields from 70 to 95%.

In order to improve productivity and scalability, this reaction was adapted to flow, where the model substrates exhibited a 36-fold increase in productivity. Lignin, however, presents an additional problem not encountered in the model system. Lignin solutions are often darkly colored due to the presence of lignosulfonate, posing a potential inhibitory problem. Indeed, batch irradiation of the dark brown solution containing one weight equivalent of lignosulfonate resulted in no conversion after 48 h. Impressively, however, when the same reaction was carried out in a flow reactor, complete consumption of the α-hydroxyketo compound was observed (8.9 mmol h^{-1}).

3.4 sp^3 C–X Coupling Reactions

In 2014, Jamison and co-workers reported the synthesis of a series of highly functionalized and diverse polycyclic quinoxaline derivatives [24]. This class of compounds has interesting biological activity and has attracted the attention of the pharmaceutical industry [88]. Despite this interest, there are very few reports for the synthesis of these compounds. Kobayashi and co-workers have reported a room temperature method using iminium salts and aldehydes or ketones; however, the use of strong Lewis acids is necessary [89, 90] – limiting its functional group tolerance. Jamison's method avoids the use of strong Lewis acids. Irradiation of catalyst **2** with a fluorescent light bulb in the presence of phenyliodine dicarboxylates and *ortho*-substituted arylisocyanides provides quinoxalines with excellent functional group tolerance (Scheme 22). Additionally, pyrrole and other nitrogen-rich quinoxalines were produced in fair to very good yields. Alkenes and alkynes, susceptible to attack by carbon radicals, were well tolerated as well.
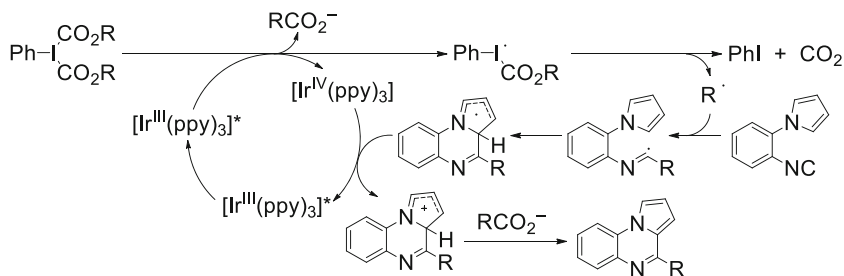
Scheme 22 The proposed mechanism for the photocatalytic redox process for the synthesis of quinoxalines from phenyliodine dicarboxylates and *ortho*-substituted arylisocyanides via carbon-centered radicals

batch 73% yield (1 step)(0.2 mmol h^{-1})
flow 47% yield (3 steps)(0.41 mmol h^{-1})
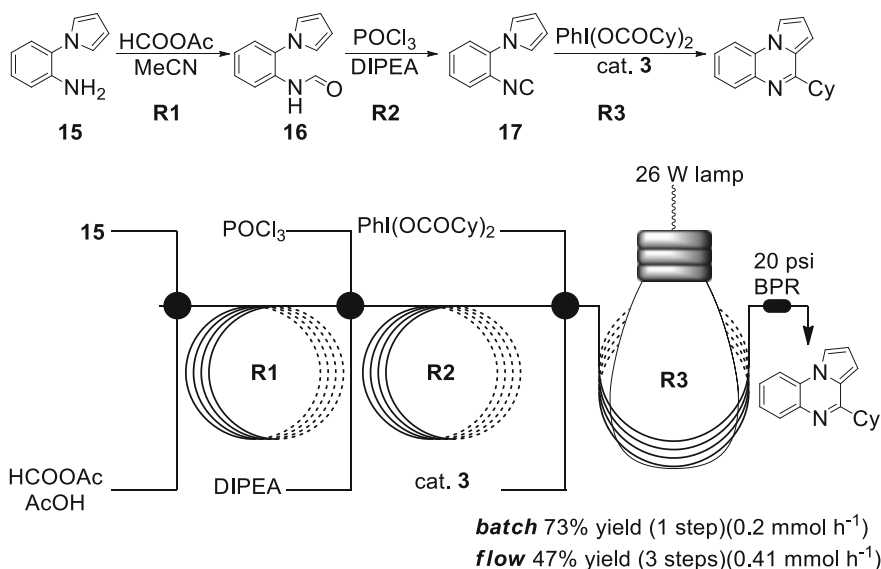
Scheme 23 The continuous flow setup for the conversion of *ortho*-substituted anilines to quinoxalines

In order to demonstrate the practicality of this method for large-scale synthesis, Jamison and co-workers scaled and telescoped this reaction with isocyanide synthesis, starting from substituted anilines using flow chemistry. The entire flow setup consisted of a PEEK T-mixer, two PEEK cross-mixers, and three PFA reactors (Scheme 23). The third reactor was wrapped around a beaker which enclosed a 26W fluorescent light bulb (see Fig. 4, middle). The temperature was regulated with a water-cooling bath. In the first flow reactor, formamide **16** was formed from the substituted aniline and acetic formic anhydride. The resulting stream was mixed with phosphorus oxychloride and diisopropylethylamine to perform the dehydration and form the corresponding isocyanide **17**. Due to solubility reasons,

acetonitrile was used with catalyst **3**. The overall process had a total residence time of 14.6 min with an overall yield of 47% (approx. 78% per step). The throughput was 0.41 mmol h^{-1}, over a twofold improvement compared to the batch reactions (0.2–0.04 mmol h^{-1}).

This visible-light photoredox-catalyzed process for the synthesis of quinoxaline derivatives, utilizing phenyliodine dicarboxylates and *ortho*-substituted arylisocyanides, was high yielding and highly tolerant to various functional groups. The radical precursors, phenyliodine dicarboxylates, are easily accessible and environmentally friendly. In addition, the synthesis of the arylisocyanides from more readily accessible anilines could be performed using flow reactors and telescoped to a modified version of their photoredox reaction. The resulting process was at least twice as productive as the batch reactions.

While the most influential C–C cross-coupling reactions are catalyzed by rare-earth metals [91], photoredox catalysis has garnered recent attention due to its ability to selectively generate carbon-centered radicals that undergo similar types of C–C coupling reactions [92–96]. In 2012, Stephenson and co-workers reported an enhanced reactivity for photoredox-mediated cyclization reactions upon their conversion to flow [31, 57], reducing reaction times of 3–72 h to mere minutes. In particular, the large-scale (2.0 g, 6.2 mmol) intramolecular functionalization of pyrroles using a α-bromoketone moiety failed to go to completion even after 2 days in batch (Scheme 24). The use of a flow reactor resulted in complete conversion in remarkably less time ($\tau = 1.0$ min). Likewise, a continuous flow tandem cyclization/Cope rearrangement reaction with an Ir-based catalyst afforded a 20-fold increase in productivity, transforming a batch reaction's conversion rate of 0.048–0.96 mmol h^{-1}.

At the same time, Stephenson and co-workers reported photoredox intermolecular couplings in flow using catalyst **1** and various tertiary amines as a reductive quenchers [57]. Utilizing flow conditions for this type of coupling proved especially useful in the synthesis of gliocladin C, since the scale-up of this reaction to 10 g required extended reaction times of several days (Scheme 25) [97]. The enhancement of productivity from 0.327 mmol h^{-1} in batch to 0.914 mmol h^{-1} in flow demonstrated a major advantage in this regard.
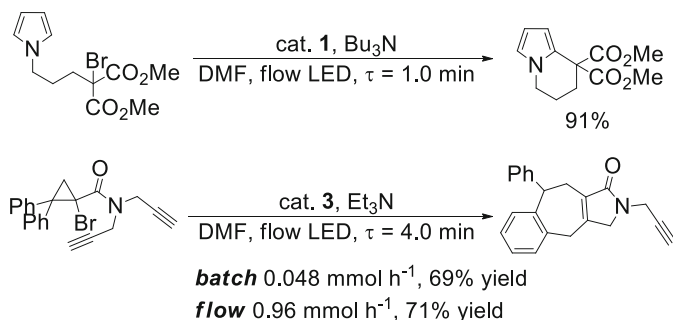
Scheme 24 Intramolecular radical reactions in flow
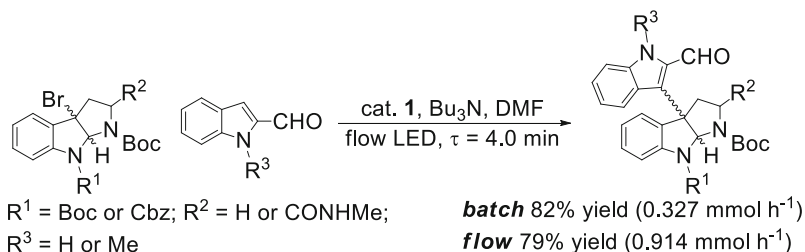
Scheme 25 Key cross-coupling reaction for the synthesis of gliocladin C
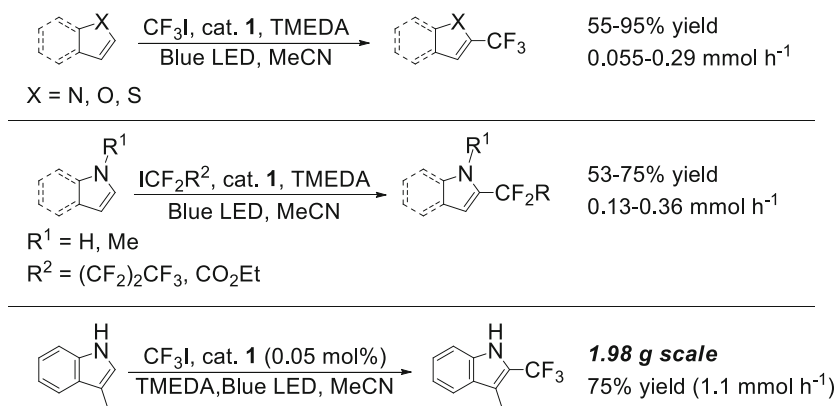

Scheme 26 Trifluoromethylation and perfluoroalkylation of five-membered heterocycles

In 2014, Noël and co-workers published the reductive coupling of perfluorinated alkyl iodides with five-membered heterocycles under similar photoredox conditions as those shown above, using a homemade photoflow reactor (see Sect. 1.2, Fig. 4, right), catalyst **1**, and TMEDA as a reductive quencher [98]. They synthesized trifluoromethylated five-membered heterocycles in 55–95% yield, corresponding to productivities of 0.055–0.29 mmol h^{-1} (Scheme 26). The authors went on to apply this method to additional iodoperfluoroalkyl substrates in 53–75% yield and 0.13–0.36 mmol h^{-1}. Finally, to demonstrate that this methodology and reactor are suitable for the production and scale-up of pharmaceutical and agrochemicals, the authors ran a large-scale reaction (1.98 g, 9.5 mmol) with a low catalyst loading (0.05 mol%). At the same time, the authors demonstrated that Eosin Y was an effective catalyst for perfluoroalkylations in flow [99]. While catalyst **1** was more efficient over a wide range of substrates, Eosin Y, as a metal-free catalyst, offers a method to avoid transition metal contamination of pharmaceuticals.

In 2013, Noël and co-workers reported a one-pot visible-light-mediated Stadler–Ziegler synthesis of arylsulfides [25]. The original process is widely used in industry as it utilizes relatively abundant anilines, which are easily and inexpensively converted into the corresponding diazonium salts. However, there are several

drawbacks of these processes. Often the diazonium salts and thiolates must be isolated prior to coupling, which can be dangerous due to the explosive nature of diazonium salts. Additionally, under the coupling conditions, a diazosulfide inter-mediate forms, which is also explosive, especially when heated [100]. Noël's one-pot, visible-light-mediated Stadler–Ziegler method eliminates the need to isolate diazonium salts, is performed at room temperature (reduces concerns involving explosive intermediates), and exhibits higher yields. Utilizing their optimized photoredox conditions (Scheme 27), they were able to obtain the product in 86% yield, reducing the amount of disulfide by over half when compared to the Cu_2O reaction. Substitution on both the thiophenol and aniline rings were well tolerated. Notably, chloro- and bromo-anilines were not reduced, providing a handle for further functionalization.

Mechanistic studies showed that the diazosulfide intermediate, while potentially explosive, is important. Irradiation in the absence of photocatalyst did not result in degradation of the diazosulfide. However, in the presence of a photoredox catalyst, this decomposition occurs after SET, producing nitrogen, a sulfide, and an aryl radical (Scheme 28) [101]. Coupling of the sulfide and aryl radical, followed by
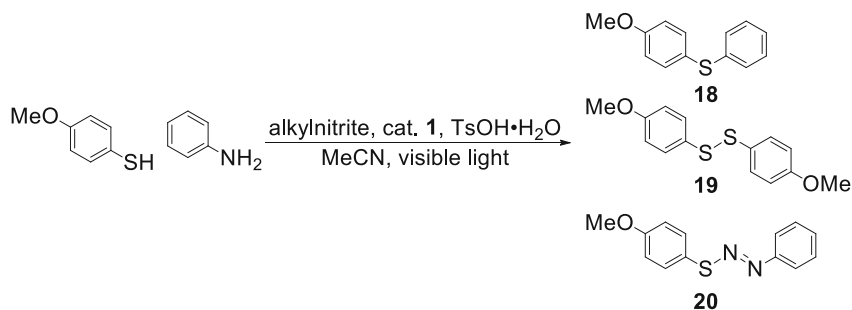
Scheme 27 The photoredox-catalyzed coupling of thiols with diazonium salts
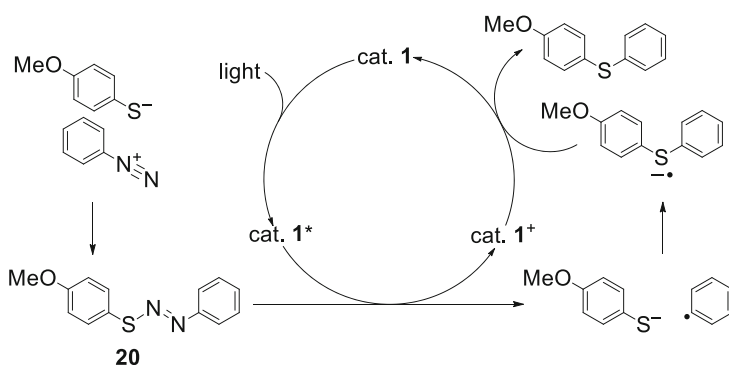
Scheme 28 The proposed mechanism for the photoredox-mediated coupling of thiols with diazonium salts

another SET, regenerates the active photocatalyst and produces the desired thioether.

In order to improve productivity, this reaction was performed in a photoflow reactor, constructed from PFA tubing with an inner diameter of 0.5 mm and a total volume of 0.464 mL. The small dimensions of the reactor, aside from improving the efficiency of irradiation, has the added benefit of addressing safety concerns associated with the explosive nature of some of the intermediates. Three thioethers were synthesized in this reactor with a residence time of 15 s under blue LED irradiation (Fig. 6). The productivities ranged from 13.2 to 14.1 mmol h^{-1}. While the yield was slightly diminished, this productivity corresponds to over a 75-fold increase over the batch setup.

This method of thio functionalization was further expanded in 2014 to trifluoromethylations [102]. The incorporation of a CF_3 moiety in a drug results in an extremely high lipophilicity and increases the stability toward acidic media. Additionally, it provides access to biologically interesting trifluoromethyl sulfoxides and sulfones. Methods have been reported using "CF_3S^+" reagents; however, the shelf-stable reagents are made from the toxic and corrosive gas CF_3SCl [103–105]. To date, construction of these bonds via an ion radical mechanism, employing less expensive CF_3I and CF_3Br, suffer from extended reaction times and harsh conditions or use of UV light [106–112]. Convenient "CF_3+" reagents have been developed, such as Umemoto's reagent and Togni's reagent; however, the cost and multiple-step preparation make them unattractive methods for scaling up [113–115]. Noël's method employs photoredox chemistry and relatively cheap and benign CF_3I to generate CF_3 radicals that couple with thiols to produce a wide scope of trifluoromethylated compounds with excellent yields and functional group compatibility. They utilized photocatalyst **1** with triethylamine in acetonitrile to perform this transformation (Scheme 29). Aryl thiols underwent trifluoromethylation in 67–96% yield. Heteroaromatic compounds were trifluoromethylated slightly less efficiently in 52–91% yields, while aliphatic thiols proved most challenging yielding CF_3 thioethers in 41–55% yield.

To establish better contact between the gaseous CF_3I phase and the liquid reaction mixture, the same reaction was performed in a photoflow reactor consisting of PFA tubing (0.5 mm ID, 2.5 m, 0.5 mL reactor volume) wrapped around a 100 mL disposable syringe. The reactor was connected to a rubber hose supplied with air to maintain a constant temperature. The reactor was irradiated with a coiled LED array (3.12 W, 78 lm, 39 LED (97 cm length), Paulmann Lighting GmbH).
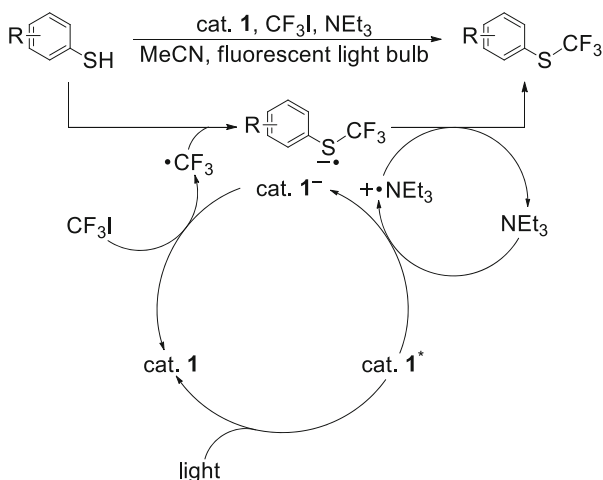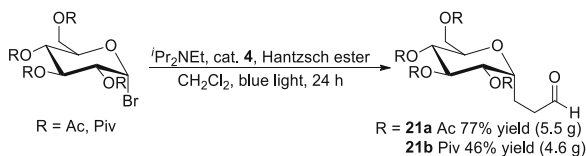

batch 0.17 mmol h^{-1}
flow 13.2 mmol h^{-1} 13.4 mmol h^{-1} 14.1 mmol h^{-1}
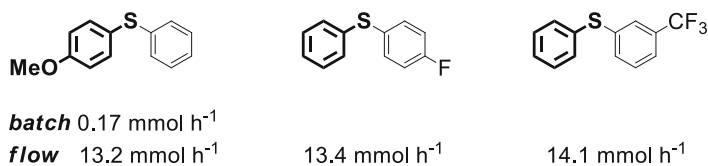
Fig. 6 Continuous flow rate enhancement of diarylsulfide formation. Comparison of batch and flow shows over a 75-fold increase in productivity

Scheme 29 Photoredox-mediated trifluoromethylation of thiols

Scheme 30 Continuous flow production of *C*-glycosides via photoredox-mediated C–C coupling

The reactor was lined with tin foil in order to reflect excess light back to the tubing of the reactor (see Fig. 4 right). In nearly all cases, there was a productivity enhancement in flow (2.3–8.8 mmol h^{-1}) as compared to the batch processes (0.3–1.9 mmol h^{-1}).[3]

Glycolipids represent important targets due to their potential in vaccine therapeutics [116–119]. However, due to the metabolic instability of the *O*-glycosidic linkage, *C*-glycosides are being developed in order to overcome this instability and increase bioavailability [120–125]. In 2012, Gagné and co-workers reported a photoflow reactor for the synthesis of *C*-glycolipids [75]. Their conditions utilized catalyst **4**, and the turnover frequency (TOF) of this catalyst was investigated in a 25 mL flask, a 5 mm NMR tube, and a flow reactor. The TOF for the flask and the NMR tube was 3.5 and 70 h^{-1} respectively. In flow, 1.6 and 0.8 mm inner diameter tubings resulted in 50 and 120 h^{-1} TOFs respectively, demonstrating the importance of photon flux through the entirety of the solution. Despite the lower TOF, the authors chose the thicker tubing, which gave both higher yields and productivities. Under the conditions shown in Scheme 30, they were able to produce *C*-glycoside **21a** in 77% yield (5.46 g, 14.1 mmol, and 0.59 mmol h^{-1}) and *C*-glycoside **21b** in 46% yield (4.62 g, 8.3 mmol, 0. 35 mmol h^{-1}).

---

[3] Two substrates were not accelerated in flow; however, these compounds were also problematic in batch.

   In summary, continuous photoredox conditions offer an attractive alternative for sp^3 reductive coupling reactions. As expected, more efficient transformations are observed, providing scalable access to intermediates for natural product synthesis, interesting new perfluorinated compounds, and even C-glycosides.

4 Conclusions

Photoredox chemistry is a powerful method for organic synthesis, offering numerous advantages when compared to more traditional methods such as the use of ultraviolet light, radical initiators, or highly reactive reducing agents. Inefficiencies associated with irradiation of batch solutions have been overcome by adaptation to flow, and a significant increase in the productivity of these transformations can be observed across the board. These reactions, both oxidative and reductive, exhibit higher yields and selectivities in comparison with the respective batch processes. With the advent of numerous homemade and commercially available flow photoreactors, the incorporation of these clean and efficient processes into a wide breadth of syntheses is currently underway.

References

1. Knowles JP, Elliott LD, Booker-Milburn KI (2012) Flow photochemistry: old light through new windows. Beilstein J Org Chem 8:2025–2052
2. Su Y, Straathof NJ, Hessel V, Noël T (2014) Photochemical transformations accelerated in continuous-flow reactors: basic concepts and applications. Chem Eur J 20:10562–10589
3. Gilmore K, Seeberger PH (2014) Continuous flow photochemistry. Chem Rec 14:410–418
4. Noel T, Wang X, Hessel V (2013) Accelerating photoredox catalysis in continuous microflow. Chim Oggi 31:10
5. Garlets ZJ, Nguyen JD, Stephenson CR (2014) The development of visible-light photoredox catalysis in flow. Isr J Chem 54:351–360
6. Gratzel M, Kalyanasundaram K (1998) Applications of functionalized transition metal complexes in photonic and optoeletronic devices. Coord Chem Rev 77:347–414
7. Lowry MS, Bernhard S (2006) Synthetically tailored excited states: phosphorescent, cyclometalated iridium (III) complexes and their applications. Chem Eur J 12:7970–7977
8. Ulbricht C, Beyer B, Friebe C, Winter A, Schubert US (2009) Recent developments in the application of phosphorescent iridium (III) complex systems. Adv Mater 21:4418
9. Graetzel M (1981) Artificial photosynthesis: water cleavage into hydrogen and oxygen by visible light. Acc Chem Res 14:376–384
10. Meyer TJ (1989) Chemical approaches to artificial photosynthesis. Acc Chem Res 22:163–170
11. Takeda H, Ishitani O (2010) Development of efficient photocatalytic systems for CO2 reduction using mononuclear and multinuclear metal complexes based on mechanistic studies. Coord Chem Rev 254:346–354
12. Lalevée J, Peter M, Dumur F, Gigmes D, Blanchard N, Tehfe MA, Morlet-Savary F, Fouassier JP (2011) Subtle ligand effects in oxidative photocatalysis with iridium complexes: application to photopolymerization. Chem Eur J 17:15027–15031

13. Lalevée J, Blanchard N, Tehfe M-A, Morlet-Savary F, Fouassier JP (2010) Green bulb light source induced epoxy cationic polymerization under air using tris (2, 2′-bipyridine) ruthenium (II) and silyl radicals. Macromolecules 43:10191–10195

14. Howerton BS, Heidary DK, Glazer EC (2012) Strained ruthenium complexes are potent light-activated anticancer agents. J Am Chem Soc 134:8324–8327

15. Koike T, Akita M (2014) Visible-light radical reaction designed by Ru-and Ir-based photoredox catalysis. Inorg Chem Front 1:562–576

16. Prier CK, Rankic DA, MacMillan DW (2013) Visible light photoredox catalysis with transition metal complexes: applications in organic synthesis. Chem Rev 113:5322–5363

17. Hari DP, Konig B (2014) Synthetic applications of Eosin Y in photoredox catalysis. Chem Commun 50:6688–6699

18. Elliott LD, Knowles JP, Koovits PJ, Maskill KG, Ralph MJ, Lejeune G, Edwards LJ, Robinson RI, Clemens IR, Cox B (2014) Batch versus flow photochemistry: a revealing comparison of yield and productivity. Chem Eur J 20:15226–15232

19. Narayanam JM, Tucker JW, Stephenson CR (2009) Electron-transfer photoredox catalysis: development of a tin-free reductive dehalogenation reaction. J Am Chem Soc 131:8756–8757

20. Kalyanasundaram K (1982) Photophysics, photochemistry and solar energy conversion with tris(bipyridyl)ruthenium(II) and its analogues. Coord Chem Rev 46:159–244

21. Weiss ME, Kreis LM, Lauber A, Carreira EM (2011) Cobalt-catalyzed coupling of alkyl iodides with alkenes: deprotonation of hydridocobalt enables turnover. Angew Chem 123:11321–11324

22. Senaweera SM, Singh A, Weaver JD (2014) Photocatalytic hydrodefluorination: facile access to partially fluorinated aromatics. J Am Chem Soc 136:3002–3005

23. Rackl D, Kais V, Kreitmeier P, Reiser O (2014) Visible light photoredox-catalyzed deoxygenation of alcohols. Beilstein J Org Chem 10:2157–2165

24. He Z, Bae M, Wu J, Jamison TF (2014) Synthesis of highly functionalized polycyclic quinoxaline derivatives using visible-light photoredox catalysis. Angew Chem Int Ed 53:14451–14455

25. Wang X, Cuny GD, Noel T (2013) A mild, one-pot Stadler-Ziegler synthesis of arylsulfides facilitated by photoredox catalysis in batch and continuous-flow. Angew Chem Int Ed 52:7860–7864

26. Xuan J, Xiao W-J (2012) Visible-light photoredox catalysis. Angew Chem Int Ed 51:6828–6838

27. Protti S, Fagnoni M, Ravelli D (2015) Photocatalytic C-H activation by hydrogen-atom transfer in synthesis. ChemCatChem 7:1516–1523

28. Xie J, Jin H, Xu P, Zhu C (2014) When C–H bond functionalization meets visible-light photoredox catalysis. Tetrahedron Lett 55:36–48

29. Nguyen JD, D'Amato EM, Narayanam JM, Stephenson CR (2012) Engaging unactivated alkyl, alkenyl and aryl iodides in visible-light-mediated free radical reactions. Nat Chem 4:854–859

30. Nguyen JD, Reiß B, Dai C, Stephenson CR (2013) Batch to flow deoxygenation using visible light photoredox catalysis. Chem Commun 49:4352–4354

31. Bou-Hamdan FR, Seeberger PH (2012) Visible-light-mediated photochemistry: accelerating Ru(bpy)$_3$$^{2+}$-catalyzed reactions in continuous flow. Chem Sci 3:1612–1616

32. Pieber B, Kappe CO (2015) Aerobic oxidations in continuous flow. In: Topics in organometallic chemistry. Springer, Berlin, pp 1–40. doi:10.1007/3418_2015_133

33. Appel R (1975) Tertiary phosphane/tetrachloromethane, a versatile reagent for chlorination, dehydration, and P-N linkage. Angew Chem Int Ed Engl 14:801–811

34. Vilsmeier A, Haack A (1927) Über die Einwirkung von Halogenphosphor auf Alkyl-formanilide. Eine neue Methode zur Darstellung sekundärer und tertiärer p-Alkylamino-benzaldehyde. Ber Dtsch Chem Ges 60:119–122

35. Léonel E, Paugam J, Nédélec J (1997) A new preparative route to organic halides from alcohols via the reduction of polyhalomethanes. J Org Chem 62:7061–7064

36. Konieczynska MD, Dai C, Stephenson CR (2012) Synthesis of symmetric anhydrides using visible light-mediated photoredox catalysis. Org Biomol Chem 10:4509–4511
37. Shen Y, Chen C-F (2011) Helicenes: synthesis and applications. Chem Rev 112:1463–1535
38. Hernandez-Perez AC, Vlassova A, Collins SK (2012) Toward a visible light mediated photocyclization: Cu-based sensitizers for the synthesis of [5] helicene. Org Lett 14: 2988–2991
39. Bédard A-C, Vlassova A, Hernandez-Perez AC, Bessette A, Hanan GS, Heuft MA, Collins SK (2013) Synthesis, crystal structure and photophysical properties of pyrene–helicene hybrids. Chem Eur J 19:16295–16302
40. Hernandez-Perez AC, Collins SK (2013) A visible-light-mediated synthesis of carbazoles. Angew Chem 125:12928–12932
41. Ushakov DB, Plutschack MB, Gilmore K, Seeberger PH (2015) Factors influencing the regioselectivity of the oxidation of asymmetric secondary amines with singlet oxygen. Chem Eur J 21:6528–6534
42. Schümperli MT, Hammond C, Hermans I (2012) Developments in the aerobic oxidation of amines. ACS Catal 2:1108–1117
43. Largeron M (2013) Protocols for the catalytic oxidation of primary amines to imines. Eur J Org Chem 2013:5225–5235
44. Patil RD, Adimurthy S (2013) Catalytic methods for imine synthesis. Asian J Org Chem 2: 726–744
45. Ryland BL, Stahl SS (2014) Practical aerobic oxidations of alcohols and amines with homogeneous copper/TEMPO and related catalyst systems. Angew Chem Int Ed 53:8824–8838
46. Ghislieri D, Green AP, Pontini M, Willies SC, Rowles I, Frank A, Grogan G, Turner NJ (2013) Engineering an enantioselective amine oxidase for the synthesis of pharmaceutical building blocks and alkaloid natural products. J Am Chem Soc 135:10863–10869
47. Yuan Q-L, Zhou X-T, Ji H-B (2010) Efficient oxidative coupling of amines to imines catalyzed by manganese (III) meso-tetraphenylporphyrin chloride under ambient conditions. Catal Commun 12:202–206
48. Chu G, Li C (2010) Convenient and clean synthesis of imines from primary benzylamines. Org Biomol Chem 8:4716–4719
49. Choi H, Doyle MP (2007) Oxidation of secondary amines catalyzed by dirhodium caprolactamate. Chem Commun 745–747
50. Wu X-F, Petrosyan A, Ghochikyan TV, Saghyan AS, Langer P (2013) Metal-free oxidation of benzyl amines to imines. Tetrahedron Lett 54:3158–3159
51. Achar TK, Maiti S, Mal P (2014) IBX works efficiently under solvent free conditions in ball milling. RSC Adv 4:12834–12839
52. Jiang G, Chen J, Huang J-S, Che C-M (2009) Highly efficient oxidation of amines to imines by singlet oxygen and its application in ugi-type reactions. Org Lett 11:4568–4571
53. To WP, Tong GSM, Lu W, Ma C, Liu J, Chow ALF, Che CM (2012) Luminescent organogold (III) complexes with long-lived triplet excited states for light-induced oxidative C-H bond functionalization and hydrogen production. Angew Chem Int Ed 51:2654–2657
54. Ushakov DB, Gilmore K, Kopetzki D, McQuade DT, Seeberger PH (2014) Continuous-flow oxidative cyanation of primary and secondary amines using singlet oxygen. Angew Chem Int Ed 53:557–561
55. Vukelić S, Ushakov DB, Gilmore K, Koksch B, Seeberger PH (2015) Flow synthesis of fluorinated α-amino acids. Eur J Org Chem 2015:3036–3039
56. Ushakov DB, Gilmore K, Seeberger PH (2014) Consecutive oxygen-based oxidations convert amines to α-cyanoepoxides. Chem Commun 50:12649–12651
57. Tucker JW, Zhang Y, Jamison TF, Stephenson CR (2012) Visible-light photoredox catalysis in flow. Angew Chem Int Ed 51:4144–4147
58. Beatty JW, Stephenson CR (2014) Synthesis of (−)-pseudotabersonine,(−)-pseudovincadifformine, and (+)-coronaridine enabled by photoredox catalysis in flow. J Am Chem Soc 136:10270–10273

59. Beatty JW, Stephenson CRJ (2015) Amine functionalization via oxidative photoredox cata-lysis: methodology development and complex molecule synthesis. Acc Chem Res 48: 1474–1484
60. Neumann M, Zeitler K (2012) Application of microflow conditions to visible light photo-redox catalysis. Org Lett 14:2658–2661
61. Barton DH, McCombie SW (1975) A new method for the deoxygenation of secondary alcohols. J Chem Soc Perkin Trans 1:1574–1585
62. Purser S, Moore PR, Swallow S, Gouverneur V (2008) Fluorine in medicinal chemistry. Chem Soc Rev 37:320–330
63. Reade SP, Mahon MF, Whittlesey MK (2009) Catalytic hydrodefluorination of aromatic fluorocarbons by ruthenium N-heterocyclic carbene complexes. J Am Chem Soc 131: 1847–1861
64. Zhan J-H, Lv H, Yu Y, Zhang J-L (2012) Catalytic C-F bond activation of perfluoroarenes by tricoordinated gold(I) complexes. Adv Synth Catal 354:1529–1541
65. Aizenberg M, Milstein D (1994) Catalytic activation of carbon-fluorine bonds by a soluble - transition-metal complex. Science 265:359–361
66. Aizenberg M, Milstein D (1995) Homogeneous metal-catalyzed hydrogenolysis of C-F bonds. J Am Chem Soc 117:8674–8675
67. Archibald SJ, Braun T, Gaunt JA, Hobson JE, Perutz RN (2000) Chemistry of nickel tetra-fluoropyridyl derivatives: their versatile behaviour with Bronsted acids and the Lewis acid BF3. J Chem Soc Dalton Trans 2013–2018
68. Arndt P, Spannenberg A, Baumann W, Burlakov VV, Rosenthal U, Becke S, Weiss T (2004) Reactions of zirconocene 2-vinylpyridine complexes with diisobutylaluminum hydride and fluoride. Organometallics 23:4792–4795
69. Breyer D, Braun T, Klaering P (2012) Synthesis and reactivity of the fluoro complex trans-$[Pd(F)(4-C_5NF_4)(iPr_2PCH_2CH_2OCH_3)_2]$: C-F bond formation and catalytic C-F bond acti-vation reactions. Organometallics 31:1417–1424
70. Edelbach BL, Rahman AKF, Lachicotte RJ, Jones WD (1999) Carbon-fluorine bond cleavage by zirconium metal hydride complexes. Organometallics 18:3170–3177
71. Fischer P, Goetz K, Eichhorn A, Radius U (2012) Decisive steps of the hydrodefluorination of fluoroaromatics using Ni(NHC)(2). Organometallics 31:1374–1383
72. Jaeger-Fiedler U, Klahn M, Arndt P, Baumann W, Spannenberg A, Burlakov VV, Rosenthal U (2007) Room-temperature catalytic hydrodefluorination of pentafluoro-pyridine by zircono-cene fluoro complexes and diisobutylaluminumhydride. J Mol Catal A Chem 261:184–189
73. Kuehnel MF, Lentz D, Braun T (2013) Synthesis of fluorinated building blocks by transition-metal-mediated hydrodefluorination reactions. Angew Chem Int Ed 52:3328–3348
74. Lv H, Cai Y-B, Zhang J-L (2013) Copper-catalyzed hydrodefluorination of fluoroarenes by copper hydride intermediates. Angew Chem Int Ed 52:3203–3207
75. Andrews RS, Becker JJ, Gagné MR (2012) A photoflow reactor for the continuous photo-redox-mediated synthesis of C-glycoamino acids and C-glycolipids. Angew Chem Int Ed 51: 4140–4143
76. Larraufie MH, Pellet R, Fensterbank L, Goddard JP, Lacôte E, Malacria M, Ollivier C (2011) Visible-light-induced photoreductive generation of radicals from epoxides and aziridines. Angew Chem Int Ed 50:4463–4466
77. Lam K, Markó IE (2008) Using toluates as simple and versatile radical precursors. Org Lett 10:2773–2776
78. Saito I, Ikehira H, Kasatani R, Watanabe M, Matsuura T (1986) Photoinduced reactions. 167. Selective deoxygenation of secondary alcohols by photosensitized electron-transfer reaction. A general procedure for deoxygenation of ribonucleosides. J Am Chem Soc 108:3115–3117
79. Prudhomme DR, Wang Z, Rizzo CJ (1997) An improved photosensitizer for the photo-induced electron-transfer deoxygenation of benzoates and m-(trifluoromethyl) benzoates. J Org Chem 62:8257–8260

80. Shen B, Jamison TF (2013) Continuous flow photochemistry for the rapid and selective synthesis of 2′-deoxy and 2′, 3′-dideoxynucleosides. Aust J Chem 66:157–164

81. Bordoni A, de Lederkremer RM, Marino C (2006) Photoinduced electron-transfer α-deoxygenation of aldonolactones. Efficient synthesis of 2-deoxy-d-arabino-hexono-1, 4-lactone. Carbohydr Res 341:1788–1795

82. Bordoni A, de Lederkremer RM, Marino C (2008) 5-Deoxy glycofuranosides by carboxyl group assisted photoinduced electron-transfer deoxygenation. Tetrahedron 64:1703–1710

83. Ragauskas AJ, Williams CK, Davison BH, Britovsek G, Cairney J, Eckert CA, Frederick WJ, Hallett JP, Leak DJ, Liotta CL (2006) The path forward for biofuels and biomaterials. Science 311:484–489

84. Scholze B, Meier D (2001) Characterization of the water-insoluble fraction from pyrolysis oil (pyrolytic lignin). Part I. PY-GC/MS, FTIR, and functional groups. J Anal Appl Pyrolysis 60: 41–54

85. Scholze B, Hanser C, Meier D (2001) Characterization of the water-insoluble fraction from fast pyrolysis liquids (pyrolytic lignin). Part II. GPC, carbonyl groups, and C-13-NMR. J Anal Appl Pyrolysis 58:387–400

86. Zakzeski J, Bruijnincx PCA, Jongerius AL, Weckhuysen BM (2010) The catalytic valorization of lignin for the production of renewable chemicals. Chem Rev 110:3552–3599

87. Nguyen JD, Matsuura BS, Stephenson CR (2014) A photochemical strategy for lignin degradation at room temperature. J Am Chem Soc 136:1218–1221

88. Mamedov V, Kalinin A (2010) Pyrrolo [1, 2-a] quinoxalines based on quinoxalines (Review). Chem Heterocycl Compd 46:641–664

89. Kobayashi K, Irisawa S, Matoba T, Matsumoto T, Yoneda K, Morikawa O, Konishi H (2001) Synthesis of pyrrolo 1,2-a quinoxaline derivatives by Lewis acid-catalyzed reactions of 1-(2-isocyanophenyl)pyrroles. Bull Chem Soc Jpn 74:1109–1114

90. Kobayashi K, Matsumoto T, Irisawa S, Yoneda K, Morikawa O, Konishi H (2001) Synthesis of 4-(1-dialkylaminoalkyl)pyrrolo 1,2-a quinoxalines. Heterocycles 55:973–980

91. Suzuki A, Heck RF, Negishi E-I (2010) The Nobel prize in chemistry 2010. Nobelprize.org. Nobel Media AB 2014. http://www.nobelprize.org/nobel_prizes/chemistry/laureates/2010/. 28 Sept 2015

92. Tucker JW, Stephenson CR (2012) Shining light on photoredox catalysis: theory and synthetic applications. J Org Chem 77:1617–1622

93. Narayanam JMR, Stephenson CRJ (2011) Visible light photoredox catalysis: applications in organic synthesis. Chem Soc Rev 40:102–113

94. Teply F (2011) Photoredox catalysis BY Ru(bpy)$_3^{2+}$ to trigger transformations of organic molecules. Organic synthesis using visible-light photocatalyst and its 20th century roots. Collect Czech Chem Commun 76:859–917

95. Yoon TP, Ischay MA, Du J (2010) Visible light photocatalysis as a greener approach to photochemical synthesis. Nat Chem 2:527–532

96. Zeitler K (2009) Photoredox catalysis with visible light. Angew Chem Int Ed 48:9785–9789

97. Furst L, Narayanam JM, Stephenson CR (2011) Total synthesis of (+)-gliocladin C enabled by visible-light photoredox catalysis. Angew Chem Int Ed 50:9655–9659

98. Straathof NJ, Gemoets HP, Wang X, Schouten JC, Hessel V, Noël T (2014) Rapid trifluoro-methylation and perfluoroalkylation of five-membered heterocycles by photoredox catalysis in continuous flow. ChemSusChem 7:1612–1617

99. Straathof N, Osch D, Schouten A, Wang X, Schouten J, Hessel V, Noël T (2014) Visible light photocatalytic metal-free perfluoroalkylation of heteroarenes in continuous flow. J Flow Chem 4:12–17

100. Laquidara J (2001) 3-Ethoxy(thiocarbonyl)thio quinoline explosion. Chem Eng News 79:6

101. Abeywickrema AN, Beckwith ALJ (1986) Mechanistic and kinetic studies of the thiodedi-azoniation reaction. J Am Chem Soc 108:8227–8229

102. Straathof NJ, Tegelbeckers BJ, Hessel V, Wang X, Noel T (2014) A mild and fast photo-catalytic trifluoromethylation of thiols in batch and continuous-flow. Chem Sci 5:4768–4773

103. Pluta R, Nikolaienko P, Rueping M (2014) Direct catalytic trifluoromethylthiolation of boronic acids and alkynes employing electrophilic shelf-stable N-(trifluoromethylthio) phthalimide. Angew Chem Int Ed 53:1650–1653

104. Alazet S, Zimmer L, Billard T (2013) Base-catalyzed electrophilic trifluoromethylthiolation of terminal alkynes. Angew Chem Int Ed 52:10814–10817

105. Hu F, Shao X, Zhu D, Lu L, Shen Q (2014) Silver-catalyzed decarboxylative trifluoromethylthiolation of aliphatic carboxylic acids in aqueous emulsion. Angew Chem Int Ed 53:6105–6109

106. Billard T, Roques N, Langlois BR (1999) Synthetic uses of thio- and selenoesters of trifluoromethylated acids. 1. Preparation of trifluoromethyl sulfides and selenides. J Org Chem 64: 3813–3820

107. Boiko VN, Shchupak GM, Yagupolskii LM (1977) Reaction of ion-radical perfluoroalkylation. 1. Trifluoromethylation of thiols, initiated by UV-irradiation. Zh Org Khim 13: 1057–1061

108. Boiko VN, Dashevskaya TA, Shchupak GM, Yagupolskii LM (1979) Study on ion-radical perfluoroalkylation reaction. 6. Trifluoromethylation of 2-mercaptopyrimidines. Zh Org Khim 15:396–400

109. Boiko VN, Shchupak GM, Yagupolskii LM (1985) 1-Substituted 3,5-bis(trifluoromethylthio) benzole and 3,5-bis(trifluoromethylsulfonyl)benzole. Zh Org Khim 21:1470–1477

110. Koshechko VG, Kiprianova LA, Fileleeva LI (1992) A new convenient method for the synthesis of perfluoroalkylarylsulfides. Tetrahedron Lett 33:6677–6678

111. Koshechko VG, Kiprianova LA, Fileleeva LI, Rozhkova ZZ (1995) Electrochemical initiation by sulfur-dioxide of radical-chain trifluoromethylation processes of thiophenols with bromotrifluoromethane. J Fluor Chem 70:277–278

112. Koshechko VG, Kiprianova LA, Fileleeva LI, Tsanov KG (1999) Fluoroalkylation of thiophenols with Freons using conjugated electron transfer mediator systems composed of methylviologen-SO2 and I-2-SO2. J Fluor Chem 96:163–166

113. Kieltsch I, Eisenberger P, Togni A (2007) Mild electrophilic trifluoromethylation of carbon- and sulfur-centered nucleophiles by a hypervalent iodine(III)-CF3 reagent. Angew Chem Int Ed 46:754–757

114. Eisenberger P, Gischig S, Togni A (2006) Novel 10-I-3 hypervalent iodine-based compounds for electrophilic trifluoromethylation. Chem Eur J 12:2579–2586

115. Umemoto T, Ishihara S (1993) Power-variable electrophilic trifluoromethylating agents - S-(trifluoromethyl)dibenzothiophenium, Se-(trifluoromethyl)dibenzoselenophenium, and Te-(trifluoromethyl)dibenzotellurophenium salt system. J Am Chem Soc 115:2156–2164

116. Danishefsky SJ, Allen JR (2000) From the laboratory to the clinic: a retrospective on fully synthetic carbohydrate-based anticancer vaccines. Angew Chem Int Ed 39:836–863

117. Doores KJ, Gamblin DP, Davis BG (2006) Exploring and exploiting the therapeutic potential of glycoconjugates. Chem Eur J 12:656–665

118. Hakomori S, Zhang YM (1997) Glycosphingolipid antigens and cancer therapy. Chem Biol 4:97–104

119. Kuberan B, Lindhardt RJ (2000) Carbohydrate based vaccines. Curr Org Chem 4:653–677

120. Sears P, Wong C-H (1999) Carbohydrate mimetics: a new strategy for tackling the problem of carbohydrate-mediated biological recognition. Angew Chem Int Ed 38:2300–2324

121. Lin CH, Lin HC, Yang WB (2005) exo-Glycal chemistry: general aspects and synthetic applications for biochemical use. Curr Top Med Chem 5:1431–1457

122. Marcaurelle LA, Bertozzi CR (1999) New directions in the synthesis of glycopeptide mimetics. Chem Eur J 5:1384–1390

123. Nicotra F (1997) In: Driguez H, Thiem J (eds) Glycoscience synthesis of substrate analogs and mimetics. Springer, Berlin, pp 55–83

124. Yang GL, Schmieg J, Tsuji M, Franck RW (2004) The C-glycoside analogue of the immunostimulant alpha-galactosylceramide (KRN7000): synthesis and striking enhancement of activity. Angew Chem Int Ed 43:3818–3822

125. Zou W (2005) C-glycosides and aza-C-glycosides as potential glycosidase and glycosyltransferase inhibitors. Curr Top Med Chem 5:1363–1391

Organometallic-Catalysed Gas–Liquid Reactions in Continuous Flow Reactors

Paul Watts

Abstract Continuous flow processing significantly enhances gas–liquid mixing. Given that reactive gases are highly valuable reagents for many chemical transformations, flow reactor technology has been extended to enable gas–liquid reactions to be facilitated. This chapter describes how hydrogenation, hydroformylation and trifluoromethylation reactions may be performed exploiting continuous flow technology.

Contents

P. Watts (✉)
InnoVenton: NMMU Institute for Chemical Technology, Nelson Mandela Metropolitan University, PO Box 77 000, Port Elizabeth 6031, South Africa
e-mail: Paul.Watts@nmmu.ac.za

1   The Use of Gaseous Reagents in Flow Reactors

When flow chemistry was first introduced into the scientific community, the vast majority of chemical reactions that were conducted in flow were solution phase chemical processes as these were easier to conduct based on the use of home-made reactors or the commercial equipment available at the time [1–5]. However, reactive gases are highly valuable reagents for many chemical transformations, and as such most vendors have started introducing gas modules in order to allow chemists the ability to perform gas–liquid reactions within the equipment. The flow methodology provides superior gas–liquid contact when compared with batch reactors, which are limited by the rate of gas diffusion into the bulk solvent of the reaction mixture. Flow processing facilitates gas–liquid mixing utilising various technologies such as in-line mixing, as observed in the H-Cube [6, 7], for example, or via the use gas-permeable membranes [8, 9]. This chapter describes how the approach has been used for hydrogenation, hydroformylation, trifluoromethylation and carbonylation reactions; however, readers may also be interested in how similar methodology has been applied for oxidation reactions [10].

2   Hydrogenation

Hydrogenation reactions are undoubtedly the most common reactions conducted under continuous flow using a gas. Until recently the only commercial system was the H-Cube, which is a continuous hydrogenation reactor combining flow chemistry with on-demand hydrogen generation and a heterogeneous catalyst cartridge system. The hydrogen gas used in the reaction is generated in situ by electrolysis of water. The hydrogen and substrate mixture can be heated and pressurised up to 150°C and 100 bar, respectively. The mixture is then passed through a packed heterogeneous catalyst cartridge where the reaction takes place. The advantage of the H-Cube is that the system provides a very safe way of performing hydrogenation reactions in a research laboratory as no gas cylinders or other external hydrogen sources are necessary. In addition, because catalyst is trapped in the cartridge, no catalyst filtration or direct catalyst handling is required, which is highly advantageous when pyrophoric catalysts are being used.

The H-Cube is suitable for a handling a variety of catalysts, many of which are commercially available as pre-packed catalyst cartridges (named CatCarts). Reactions using Pd/C, RANEY Ni and Pt/C [11–13] are the most common; however, a large number of examples are available [6]. More recently, the use of organometallic catalysed reactions have been reported, and this chapter will focus on these examples.

The Ley group [14] pioneered the use of tube-in-tube reactors for facilitating hydrogenation reactions utilising homogeneous catalysts. It should be emphasised that although the methodology is highly efficient from a chemistry perspective,
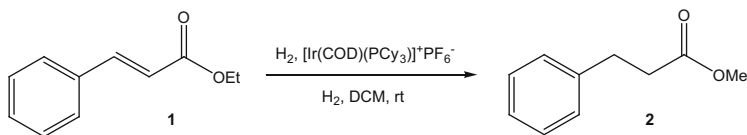
Scheme 1 Hydrogenation using a tube-in-tube reactor using an iridium catalyst

Table 1 Substrate scope for hydrogenation using a tube-in-tube reactor

Substrate	Product	Conversion (%)	Yield (%)
		100	100
		100	100
		100	100
		100	100
		100	100
		100	100
		100	100

these reactions still require a hydrogen gas cylinder to be used. In such systems the hydrogen diffuses into the liquid via a gas-permeable membrane. Using the UniqsisFlowSyn, the substrate ethyl cinnamate **1** (0.5 M in DCM) and Crabtree's catalyst (Iridium based catalyst) (0.0005 M in DCM) were reacted in a tube-in-tube reactor (100 cm long). Using a residence time of 8 s, quantitative hydrogenation of ethyl cinnamate **1** to ester **2** was reported at room temperature at a pressure of 30 bar (Scheme 1). It should be noted that at reduced pressures, lower conversions were observed. Critically the authors demonstrated that the methodology was highly versatile and demonstrated that a variety of substrates could be used in the reaction, giving the product in quantitative conversion and yield (Table 1).

Mercadante et al. [15] have reported the use of the Vapourtec tube-in-tube reactor consisting of a fluoropolymer membrane for the hydrogenation of a variety
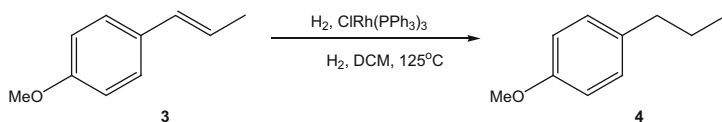
Scheme 2 Hydrogenation using a tube-in-tube reactor using a rhodium catalyst

Table 2 Substrate scope for hydrogenation using a tube-in-tube reactor

Substrate	Product	Yield (%)
		77
		86
		97
		98
		92
		95
		80
		95
		98

of substrates using Wilkinson's catalyst (rhodium-based catalyst). Using anethole **3** as model substrate (5 M in DCM), they demonstrated that 97% conversion to the desired product **4** could be achieved using 1.2 mol% catalyst at 125°C and 250 psi back pressure, obtaining the product in an 89% isolated yield. The authors then extended the optimised conditions to the reduction of other alkene derivatives and obtained all products in high yield (Scheme 2, Table 2).

Asymmetric hydrogenation is a very important transformation, and this has also featured in the literature exploiting flow technology, using both homogeneous and heterogeneous catalysts. Homogeneous catalysis offers the advantage of rapid catalyst screening to determine the optimum catalyst for both high conversion and high enantio- and diastereoselectivity. An early example was reported by de
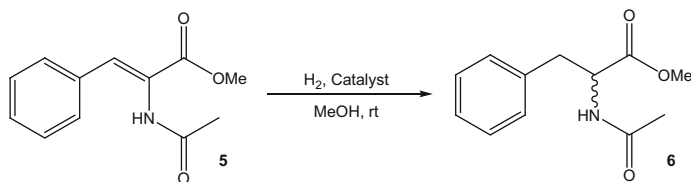
Scheme 3 Asymmetric hydrogenation in a falling film micro-reactor

Table 3 Catalyst screening for the asymmetric hydrogenation in a falling film micro-reactor

Ligand/catalysts	Temperature (°C)	Conversion (%)	ee (%)
S-NMDPP	30.3	<1	13
(R,R)-Et-Duphos	30.1	1.6	>99
(R,R)-Me-Duphos	30.0	26	>99
(R,R)-Et-BPE	31.5	0	–
(R,R)-Me-BPE	31.4	1	84.6
(R,R)-Norphos	31.5	<1	–
(S,S)-Chiraphos	31.5	0	–
(R)-Prophos	31.5	<1	–
(R)-Trost ligand	27.5	0	–
(R)-Quinap	27.4	0	–
(R,R)Diop	33.5	94	63.5
(R,S)Josiphos	33.5	26.5	86.2
(R,S)t-Bu-P-Josiphos	33.5	3	48.6
(R,S)Pcy-Josiphos	33.5	3.7	−7.6
(R,S)cy-cy-Josiphos	33.5	88.1	75.1
(R)-Binap	35	<1	23.7
(R)-[Rh(Binap)COD]BF4	35	<1	–
(S,S)-BPPM	35	22.5	91

Bellefon and co-workers [16] who reported the use of a home-made helicoidal falling film micro-reactor for the asymmetric hydrogenation of methyl-Z-(α)-acetamidocinnamate **5** (Scheme 3). The authors evaluated the use of 18 chiral phosphine catalysts in the reaction (Table 3) showing that (R,R)-Et-Duphos and (R,R)-Me-Duphos gave the product **6** in the highest enantiomeric excess. Although the maximum conversion of starting material was only 26% using this particular catalyst, the starting material could be recycled within the reactor in order to ensure complete conversion was achieved overall. It should be noted that some catalysts gave higher conversion, but the fact that the ee was poor these catalysts were not evaluated further. The authors subsequently demonstrated that the approach could be used with other substrates including methylacetamidoacrylate, dimethyli-taconate, methone and α-pinene.

More recently using the same type of approach, Newton et al. [17] has screened 11 catalysts using the Vapourtec tube-in-tube reactor for the asymmetric
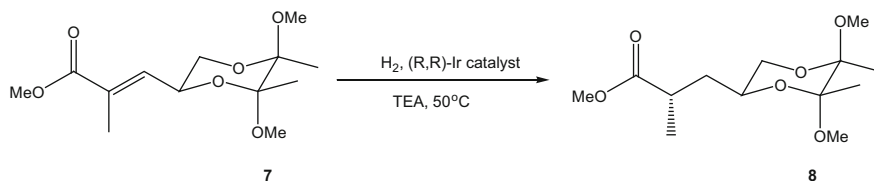
Scheme 4 Asymmetric hydrogenation of acrylates
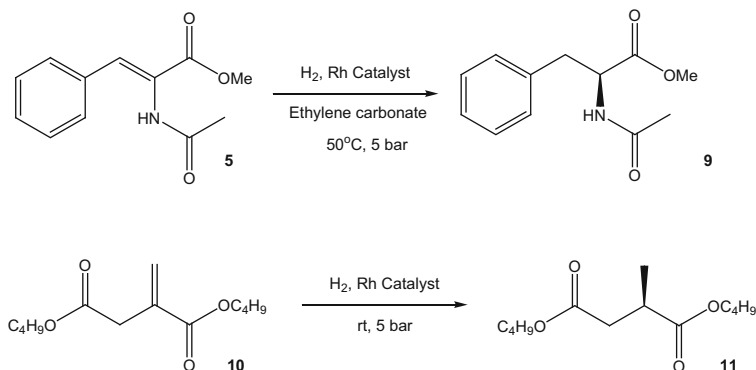
Scheme 5 Asymmetric hydrogenation using heterogeneous Rh catalysts

hydrogenation of acrylate derivative **7** (Scheme 4). The (R,R) derivative of the iridium catalyst was found to yield (S)-**8** in the highest de (77%) in a 75% yield when conducting the reaction at 50°C at a pressure of 20 bar.

Once the optimum catalyst has been identified, heterogeneous catalysis offers the advantage that reaction workup and product purification is far simpler. As such a Rh catalyst was immobilised on mesoporous alumina and packed into a CatCart [18]. Subsequent hydrogenation of **5** generated the product **9** in 99% yield with a 98.8% ee (Scheme 5) when conducting the reaction at 50°C at a pressure of 5 bar. Another example was the hydrogenation of dibutyl itaconate **10**, affording **11** in 99% yield with a 99% ee (Scheme 5) when conducting the reaction at room temperature at a pressure of 5 bar.

Madarasz et al. [19] immobilised [Rh(COD)((S)-monoPhos)$_2$]BF$_4$ in situ within a catalyst cartridge of a H-cube using either Al$_2$O$_3$ or mesoporous Al$_2$O$_3$ as the support matrix. Using the reduction of methyl 2-acetamidoacrylate **12** as a model substrate, they conducted a very detailed study on the effect of substrate concentration, temperature, pressure and flow rate on the formation of product **13** (Scheme 6). Using ethyl acetate as solvent, they found that conversions as high as 99% could be achieved with very high diastereoselectivity (96–97%) when the reactor was operated at 25°C at 1 bar pressure. They also commented that the Al$_2$O$_3$ support with larger surface area showed greater long-term stability under the reaction conditions.
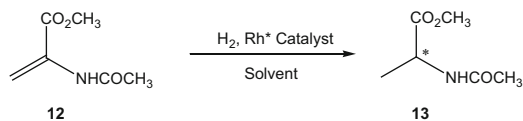
Scheme 6 Asymmetric hydrogenation using heterogeneous Rh catalysts immobilised on mesoporous alumina

Table 4 Substrate screening for the asymmetric hydrogenation using heterogeneous Rh catalysts

Substrate	Solvent	ee (%)
	Propylene carbonate	97.7
	MeOH	97.9
	Propylene carbonate	99.5
	MeOH	98.6
	MeOH	99.5
	MeOH	99.9
	MeOH	99.9
	Propylene carbonate	99.0
	MeOH	96.7
	Propylene carbonate	98.0
	MeOH	97.3

The researchers [20] more recently evaluated the same catalyst for the asymmetric hydrogenation of a range of alkenes (Table 4). All reactions gave high ees in methanol, but the use of the green solvent propylene carbonate also gave excellent results. The catalyst could be used for over 12 h in continuous flow experiments without loss of enantioselectivity.

Along the general theme of hydrogenation, Habraken et al. [21] have applied iridium catalysis for the synthesis of deuterium-labelled compounds. The group firstly made the immobilised catalyst then conducted experimentation in both a continuous stirred tank reactor and a packed-bed micro-reactor. They performed the iridium-catalysed *ortho*-directed hydrogen isotope exchange process by reaction of the substrate **14** with deuterium gas (generated from D_2O in a H-Cube reactor) to produce the labelled derivative **15** (Scheme 7). At room temperature, conversions up to 54% were reported, but this could be further increased to 64% by passing the reaction stream through the reactor for a second cycle.
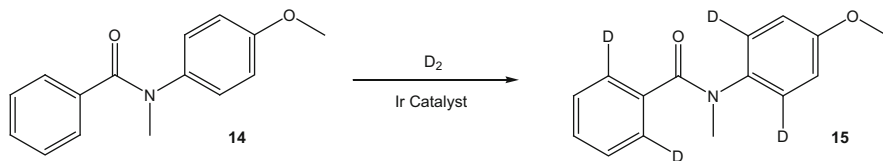
Scheme 7 Deuteration in a flow reactor

3   Hydroformylation

Hydroformylation is an important industrial process for the production of aldehydes from alkenes. It is estimated that in excess of 6 M tonnes of aldehydes are manufactured by this process per annum, for the manufacture of soaps, detergents and plasticizers [22]. Furthermore the aldehydes are easily converted into many products. Hydroformylation is also used in the manufacture of specialty chemicals, relevant to the organic synthesis of fragrances and natural products. The process typically entails treatment of an alkene with high pressures (between 10 and 100 atm) of carbon monoxide and hydrogen at temperatures between 40°C and 200°C. Transition metal catalysts are required [23].

Webb et al. [24] studied the hydroformylation of 1-dodecene **16** to prepare aldehyde **17** (Scheme 8). The rhodium catalyst was dissolved in an ionic liquid, while the substrate **16** and the gaseous reagents (H_2 and CO) that were pumped into the reactor dissolved in supercritical carbon dioxide. As a result of the supercritical conditions, a flow reactor in the simplest sense was not suitable; a home-made continuous flow system was developed comprising of a Hastelloy CSTR reactor (30 ml) fitted with a pressure transducer, a gas inlet, a liquid inlet and an outlet port. The liquid and gas substrates were delivered into the reactor through a check valve at constant flow rates using HPLC pumps. Using [BMIM]PF_6 as the optimised ionic liquid carrier at a temperature of 100°C and pressure of 70 bar, a 99% conversion of the 1-dodecene **16** was observed with the product obtained in up to 84% selectivity. The leaching of rhodium into the product was also found to be as low as 0.012 ppm at the optimum operating conditions. The hydroformylation of propene and 1-octene were also reported.

More recently the research has been extended by Hintermair et al. from the same research group [25] using a supported ionic liquid phase (SILP) catalyst, as well as conducting a more detailed study to determine whether linear or branched products are obtained in the reaction. The hydroformylation of 1-octene **18** to linear nonanal **19** and branched 2-methyloctanal **20** was studied (Scheme 9). The SILP catalyst was prepared from Rh(acac)$_2$ and two different ionic liquids using microporous silica as the support matrix. One of the most important parameters in the reaction was the phase behaviour of the mobile phase, which was studied by varying the reaction pressure. At low pressures the rate of the reaction was low because of poor gas diffusion to the catalytic sites; however, as the pressure was increased, the rate increased. It was also found that catalyst leaching decreased as the pressure increased, to approximately 0.2 ppm under optimal conditions of a temperature of 100°C and
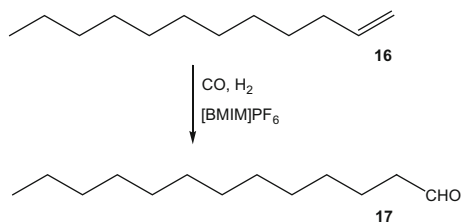
Scheme 8 Hydroformylation of 1-dodecene in a flow reactor
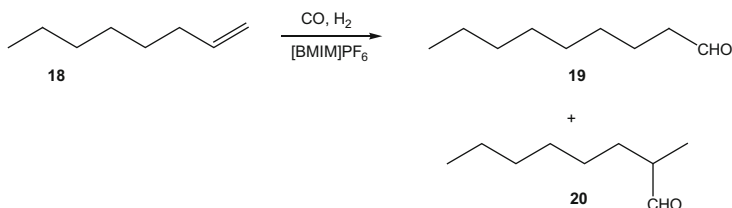
Scheme 9 Hydroformylation of 1-octene in a flow reactor
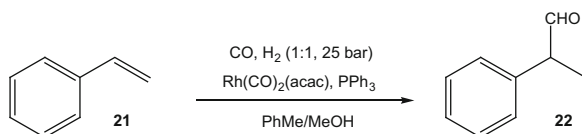
Scheme 10 Hydroformylation of styrene in a tube-in-tube reactor

pressure of 80 bar. The selectivity of the catalyst was not particularly affected and the linear/branched ratios were approximately 3 in all cases. The research has more recently been conducted under solvent-free conditions with similar results [26].

The Ley group [27] have reported flow hydroformylation of styrene derivatives using their tube-in-tube reactor (Scheme 10). Hydroformylation was achieved by enrichment of a solution of substrate **21** and catalyst with syngas, then passage through a heated coil at 65°C to effect the reaction. Optimisation revealed that a Rh catalyst at 25 bar pressure gave high conversions. The chemistry was reported on 11 substrates, and all products were obtained in 69–94% isolated yield. It should also be noted that the group extended the research to develop a telescoped Heck-hydroformylation sequence yielding stilbenes without isolation or the addition of further catalyst [8].

4 Fluorination and Trifluoromethylation

Chambers and Spink [28, 29] have reported the use of micro-reactors for the fluorination and perfluorination of organic compounds using elemental fluorine. A nickel or copper micro-reactor was used for the investigation, and the liquid

Scheme 11 Fluorination in a micro-reactor
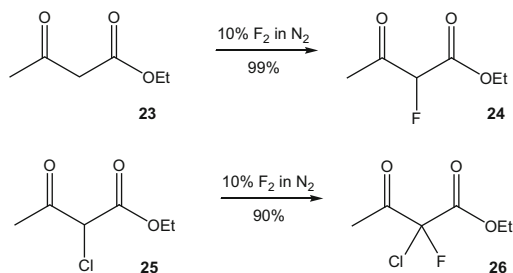
reactants and solvents were introduced into the reaction chamber via a syringe using a syringe pump. Fluorine, in a nitrogen carrier gas, was introduced from a cylinder using a mass flow controller. The liquid–gas mixing proceeded via cylindrical flow, where the liquid forms an outer cylinder coating the reactor surface with the gas flowing through the centre. This flow regime has enormous benefits in that it provides very large surface-to-volume ratios for the liquid phase, producing a very efficient reaction over a short distance. The products were trapped in a tube, which was cooled with either a salt/ice bath (0°C) or an acetone/carbon dioxide bath. The fluorination of β-dicarbonyl compounds proceeded with a high efficiency using 10% fluorine in nitrogen at 5°C and with formic acid as the solvent. Ethyl acetoacetate **23** was fluorinated in 99% conversion to give ethyl 2-fluoroacetoacetate **24,** while ethyl 2-chloroacetoacetate **25** was fluorinated in 90% conversion, yielding ethyl 2-chloro-2-fluoroacetoacetate **26** (Scheme 11). Importantly, under these conditions, no perfluorination of the substrates was observed, with only the monofluorinated derivatives being isolated. The authors report that the bulk fluorination of ethyl 2-chloroacetoacetate **57** gives only a low conversion to **58**, illustrating that the flow system is more efficient. Although it should be noted that no formal catalyst was added to the reaction mixture, the authors postulate that the catalytic effect of the fluorinated metal surface does enhance the rate of the reaction.

The sulphur pentafluoride derivative **28** was prepared in 75% yield by the reaction of the disulphide **26** with 10% fluorine in nitrogen, using acetonitrile as the solvent (Scheme 12) using the same system. Similarly, treatment of the trifluoride **29** with excess fluorine gave the sulphur pentafluoride derivative **30** in 44% yield. The authors have demonstrated that the equipment can be used for a plethora of reactions demonstrating the safe use of fluorine gas.

The trifluoromethyl group appears in a range of pharmaceutical products and as such there is substantial interest in developing efficient methods for incorporating the trifluoromethyl moiety into organic molecules at a preparative scale [30]. Many of the reagents most commonly used for laboratory scale reactions are very expensive and are unobtainable in large quantities, and as such simple protocols suitable for the scale-up of the trifluoromethylation reaction are of utmost importance. One of the most logical reagents to use in the reaction appears to be CF_3I; however, the use of the gas in batch reactions is not trivial.
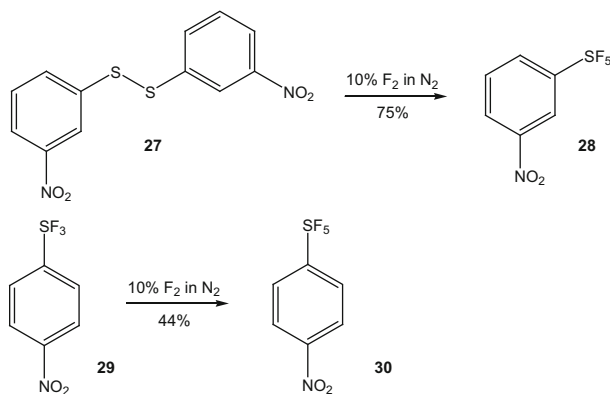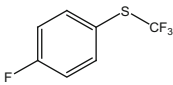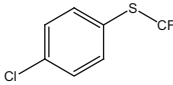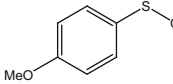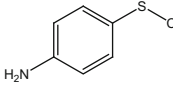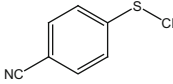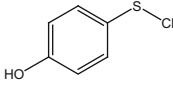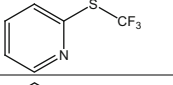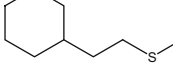
Scheme 12 Sulphur pentafluoride synthesis in a micro-reactor

Given that gases can be more easily and safely handled within continuous flow systems, Straathof et al. [31, 32] developed methodology to effectively trifluoromethylateheteroarenes.

As a model reaction, the authors studied the trifluoromethylation of *N*-methylpyrrole **31** (Scheme 13) using a range of organocatalysts including ruthenium and iridium derivatives [31]. The flow reactor was assembled from a mixer and transparent photoreactor consisting of a transparent PFA tube (750 μm i.d. having a volume of 500 μl) coiled around an LED. Using a residence time of 15 min, the authors reported a 75% yield of product. The authors also studied the effect of pressure on the reaction, but noted that only very slight increases (6%) were observed at 10 psi; consequently it was easier to practically operate the system at atmospheric pressure. The authors also extended the scope of the reaction, reporting a yield of 47% for 2-methylindole and 19% for 3-methylindole; however, it should be pointed out that these yields were significantly higher than the batch yields even after 24-h reaction time. It was also noted that Eosin Y dye was the superior catalyst enabling the first metal-free trifluoromethylation reaction to be reported. Consequently the reaction method facilitates a greener and safer approach to preparing such molecules.

Trifluoromethylation of thiols has been reported in batch using CF_3I and CF_3Br; however, these reactions are reported to have very limited scope. In addition the use of the highly toxic and gaseous trifluoromethylation reagents in batch reactions is complex. As a result Straathof et al. [33] have reported the trifluoromethylation of thiols in continuous flow (Scheme 14). The continuous flow setup consisted of a PFA capillary (2.5 m length, 500 μm i.d. have a volume of 500 μl) and mixer, whereby CF_3I gas from a cylinder controlled by a mass flow controller was mixed with the thiol solution and Ru catalyst to effect the reaction under photochemical conditions. Many of the reactions were reported to be complete in residence times less than 1 min. A range of aromatic, aliphatic and heterocyclic trifluoromethylated

Scheme 13 Trifluoromethylation of *N*-methylpyrrole in a flow reactor
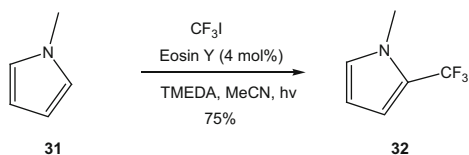
Scheme 14 Trifluoromethylation of thiols in a flow reactor
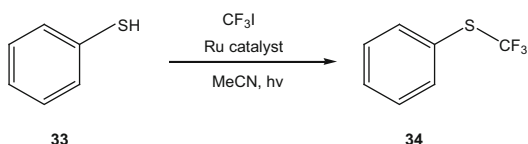
Table 5 Substrate screening for the trifluoromethylation of thiols in a flow reactor

Product	Residence time (min)	Yield (%)
	1	91
	1	96
	1	96
	1	73
	30	47
	3	78
	1	91
	30	59

thiols were produced using the approach in high selectivity and excellent yields obtained (>90%) in most cases (Table 5).

Readers may also be interested in related manuscripts on the continuous α-trifluoromethylation of ketones utilising photo-organocatalysis [34] utilising CF_3SO_2Cl and trifluoromethylation of aromatic and heterocyclic thiols and coumarins utilising CF_3SO_2Na [35, 36]; however, it should be noted that these methods do

not use a gaseous reagent. However it is envisaged that the methodology would be applicable to the use of gaseous CF₃I.

5 Carbonylation
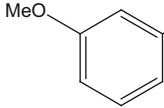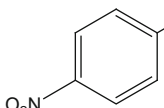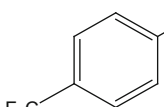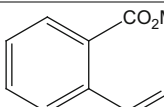
Kelly and co-workers [37] utilised a Vapourtec AF-2400 tube-in-tube gas–liquid reactor for the palladium-catalysed methoxycarbonylation of *m*-iodotoluene **35** (Scheme 15). Operating the reactor using a Pd/ligand ratio of 2.5:3 using a CO pressure of 10 bar was found to be the optimal conditions. Employing a reactor coil with a total volume of 30 ml at 120°C afforded ester **36** in a conversion of 90%.

Subsequently the authors employed the reaction conditions to a range of iodosubstrates to afford a range of aryl, heteroaromatic and vinyl derivatives in excellent overall yields (Table 6). The authors also incorporated a flow-IR into the system, in order to measure the concentration of carbon monoxide dissolved in the solvent.
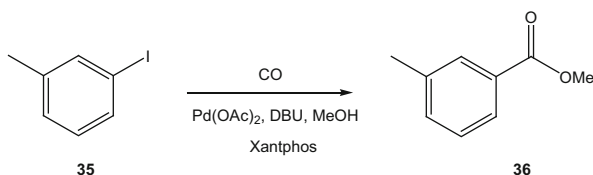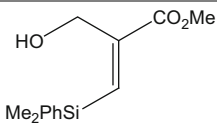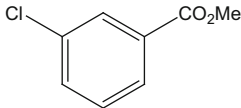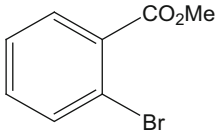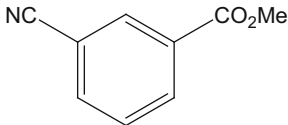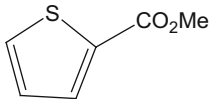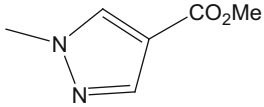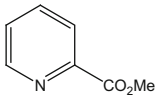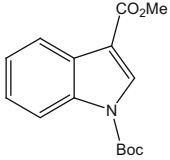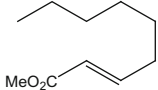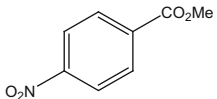
Scheme 15 Methoxycarbonylation in a tube-in-tube reactor

Table 6 Substrate screening for the methoxycarbonylation reaction in a tube-in-tube reactor

Product	Conversion (%)	Yield (%)
	78	63
	95	81
	95	88
	11	–

Table 6 (continued)

Product	Conversion (%)	Yield (%)
HO—, CO$_2$Me, Me$_2$PhSi	100	83
Cl, CO$_2$Me	95	93
CO$_2$Me, Br	77	69
NC, CO$_2$Me	90	72
S, CO$_2$Me	85	71
—N, N, CO$_2$Me	73	65
N, CO$_2$Me	88	62
CO$_2$Me, N, Boc	100	62
MeO$_2$C	100	81
CO$_2$Me, O$_2$N	94	72

Scheme 16
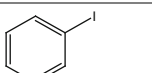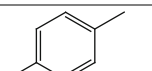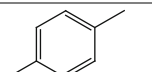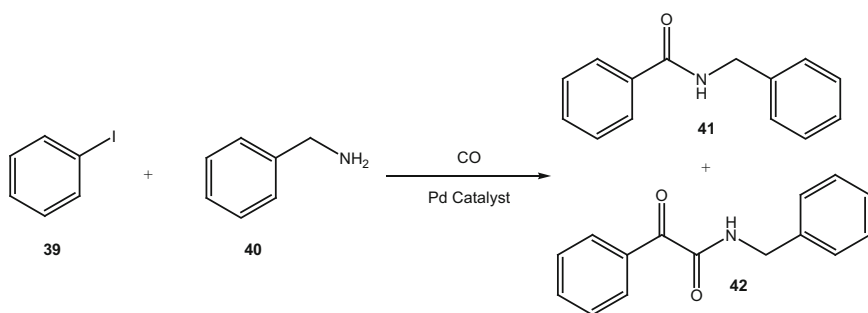Alkoxycarbonylation in a
tube-in-tube reactor
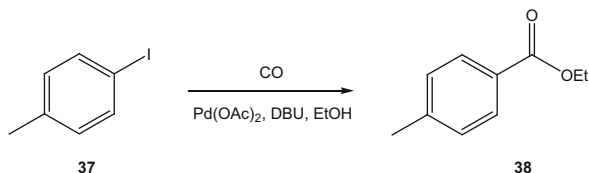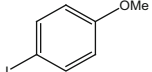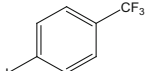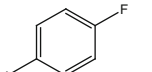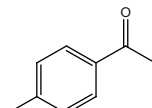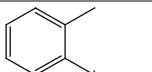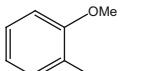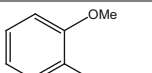
Similarly, Leyand and co-workers [38] utilised a Uniqsis tube-in-tube reactor to conduct a range of alkoxycarbonylation reactions. As a model reaction, they reacted *p*-iodotoluene **37** (Scheme 16) with ethanol to prepare ethyl ester **38**. Operating the reactor using a 0.5% Pd(OAc)$_2$ solution as catalyst using a CO pressure of 180 psi was found to be the optimal condition, employing a residence time of 20 min at 120°C afforded ester **38** in a conversion of 91% and isolated yield of 86%. Subsequently the authors employed the reaction conditions to a range of substrates to afford esters in excellent overall yields (Table 7). In cases where the conversion was low, it was found that this could be increased by passing the reaction solution through the reactor for a second time.

[^{11}C]Carbon monoxide is an important ^{11}C-labelling reagent for radiotracer synthesis as it can provide access to a range of ^{11}C-labelled molecules. Miller et al. [39] demonstrated the continuous synthesis of a series of secondary amides via a carbonylative coupling reaction within a glass micro-reactor (channel dimensions = 200 μm (wide) × 75 μm (deep) × 5 m (length)). Employing a biphasic reaction system, comprising of gaseous carbon monoxide and a solution of iodobenzene **39**, benzylamine **40** and a palladium-phosphine catalyst, the effect of liquid flow rate under a constant gas flow was investigated. Using the synthesis of *N*-benzylbenzamide **41** as a model reaction (Scheme 17), the authors found that annular flow dominated when flow rates of 5.0–20.0 μl min^{-1} were employed. Conducting the micro-reactions for 10 min, an increase in conversion as a function of increased reagent residence time was reported, an observation that the authors attribute to the formation of a stable flow regime within the reactor. Using the optimal flow rate of 5.0 μl min^{-1}, 46% conversion to the respective amide **41** was achieved along with 9% α-ketoamide **42**. The study was extended to use ^{11}CO as the reagent and using the same methodology produced amide **41** in 79% radio-chemicals yield and 96% purity. They extended the study to produce a series of other ^{11}C-labelled derivatives in 45–67% yield.

In a more sophisticated extension, Kealey et al. [40] reported the use of a copper [^{11}C] carbonyl complex (Cu(Tp*)[^{11}C]CO) in a NanoTek reactor, which the authors report as a convenient reagent to handle in solution, which opens up a new radiolabelling techniques. Initially the authors used the same reaction as shown in Scheme 17 to develop the methodology, whereby they report that the amide **41** was produced in a 73% yield at 100–125°C. With the basic methodology in hand, the group used the technique to prepare neuropeptide YY5 receptor antagonist [^{11}C] MK-0233 **44**. Optimisation established that alcohol **43** could be reacted at a temperature of 160°C to afford [^{11}C]MK-0233 **44** in 81% yield in a residence time of just 15 s (Scheme 18).

Table 7 Substrate screening for the alkoxycarbonylation reaction in a tube-in-tube reactor

Aryl iodide	Alcohol	Conversion (%)	Conversion on second pass (%)
	EtOH	85	
	EtOH	88	
	EtOH	71	94
	EtOH	46	
	EtOH	42	84
	EtOH	31	72
	EtOH	55	91
	EtOH	88	
	n-PrOH	88	
	i-PrOH	58	85

Scheme 17 Carbonylative coupling within a glass micro-reactor
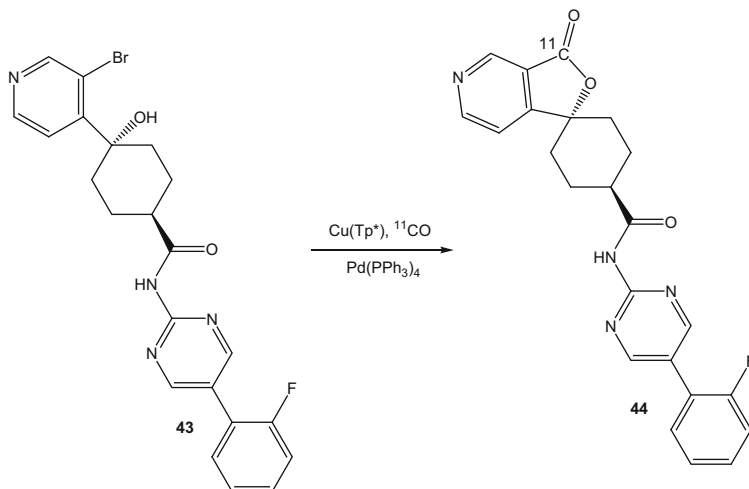
Scheme 18 Synthesis of neuropeptide YY5 receptor antagonist

6 Conclusions

Continuous flow processing significantly enhances gas–liquid mixing. Hydrogenation reactions are undoubtedly the most common reactions performed by synthetic organic chemists using a gaseous reagent. As a result of the better mixing in flow reactors, a range of hydrogenation reactions have been conducted. Importantly the reactions are very efficient, but furthermore the enhanced safety exhibited by the flow technology is a significant driver in the adoption of the technology. Furthermore it has more recently been demonstrated that asymmetric hydrogenation may also be conducted under flow conditions enabling the products to be efficiently prepared in high enantio-/diastereoselectivity. Although less common hydroformylation, trifluoromethylation and carbonylation reactions also give access to a range of useful chemical intermediates. The ease of handling reactive gases in flow opens the possibility of routinely doing such reactions within research and development.

References

1. Hessel V, Renken A, Schouten JC, Yoshida Y (2009) Micro process engineering: a comprehensive handbook volume 2: devices, reactions and applications. Wiley, Germany
2. Wiles C, Watts P (2011) Micro reaction technology in organic synthesis. CRC, London

3. Glasnov TN, Kappe CO (2011) The microwave to flow paradigm. Chem Eur J 17:11956–11968

4. Baumann M, Baxendale IR, Ley SV (2011) The flow synthesis of heterocycles for natural product and medicinal chemistry applications. Mol Divers 15:613–630

5. Wiles C, Watts P (2012) Continuous flow reactors: a green chemistry perspective. Green Chem 14:38–54

6. Jones RV, Godorhazy L, Varga N et al (2006) Continuous-flow high pressure hydrogenation reactor for optimization and high-throughput synthesis. J Comb Chem 8:110–116

7. Cossar PJ, Hizartzidis L, Simone MI (2015) The expanding utility of continuous flow hydrogenation. Org Biomol Chem 13:7119–7130

8. Brzozowski M, O'Brien M, Ley SV et al (2015) Flow chemistry: intelligent processing of gas-liquid transformations using a tube-in-tube reactor. Acc Chem Res 48:349–362

9. Noël T, Hessel V (2013) Membrane microreactors: gas–liquid reactions made easy. Chem SusChem 6:405–407

10. Pieber B, Kappe CO (2015) Aerobic oxidations in continuous flow. Top Organomet Chem. doi:10.1007/3418_2015_133

11. Colombo E, Ratel P, Mounier L et al (2011) Reissert indole synthesis using continuous-flow hydrogenation. J Flow Chem 1:68–73

12. Chen J, Przyuski K, Roemmele R et al (2014) Improved continuous flow processing: benzimidazole ring formation via catalytic hydrogenation of an aromatic nitro compound. Org Process Res Dev 18:1427–1433

13. Bryan MC, Hein CD, Gao H et al (2013) Disubstituted 1-aryl-4-aminopiperidine library synthesis using computational drug design and high-throughput batch and flow technologies. ACS Comb Sci 15:503–511

14. O'Brien M, Taylor N, Polyzos A et al (2011) Hydrogenation in flow: homogeneous and heterogeneous catalysis using Teflon AF-2400 to effect gas-liquid contact at elevated pressure. Chem Sci 2:1250–1257

15. Mercadante MA, Kelly CB, Lee C (2012) Continuous flow hydrogenation using an on-demand gas delivery reactor. Org Process Res Dev 16:1064–1068

16. deBellefon C, Lamouille T, Pestre N et al (2005) Asymmetric catalytic hydrogenations at microliter scale in a helicoidal single channel falling film micro reactor. Catal Today 110:179–187

17. Newton S, Ley SV, Ec A et al (2012) Asymmetric homogeneous hydrogenation in flow using a tube-in-tube reactor. Adv Synth Catal 354:1805–1812

18. Duque R, Pogorzelec PJ, Cole-Hamilton DJ (2013) A single enantiomer (99 %) directly from continuous-flow asymmetric hydrogenation. Angew Chem Int Ed 52:9805–9807

19. Balogh S, Farkas G, Madarasz J et al (2012) Asymmetric hydrogenation of CvC double bonds using Rh-complex under homogeneous, heterogeneous and continuous mode conditions. Green Chem 14:1146–1151

20. Madarasz J, Farkas G, Balogh S et al (2012) A continuous flow system for the asymmetric hydrogenation using supported chiral catalysts. J Flow Chem 1:62–67

21. Habraken ERM, Haspeslagh P, Vliegen M et al (2014) Iridium(I)-catalysed ortho-directed hydrogen isotope exchange in continuous flow reactors. J Flow Chem 5:2–5

22. Webb PB, Sellin MF, Kunene TE et al (2003) Continuous flow hydroformylation of alkenes in supercritical fluid-ionic liquid biphasic systems. J Am Chem Soc 125:15577–15588

23. Wang X (2015) Recent advances in continuous rhodium-catalyzed hydroformylation. J Flow Chem 3:125–132

24. Van Leeuwen PNWM, Claver C (2000) Rhodium catalysed hydroformylation. Kluwer, Dordrecht

25. Hintermair U, Gong Z, Sernanovic A (2010) Continuous flow hydroformylation using supported ionic liquid phase catalysts with carbon dioxide as a carrier. Dalton Trans 39:8501–8510

26. Frisch AC, Webb PB, Guoying G et al (2007) "Solventless" continuous flow homogeneous hydroformylation of 1-octene. Dalton Trans 5531–5538
27. Kasinathan S, Bourne SL, Tolstoy P (2011) Syngas mediated C-C bond formation in flow: selective rhodium-catalysed hydroformylation of styrenes. Synlett 18:2648–2651
28. Chambers RD, Spink RCH (1999) Microreactors for elemental fluorine. J Chem Soc Chem Commun 883–884
29. Chambers RD, Holling D, Spink RCH et al (2001) Elemental fluorine part 13. Gas–liquid thin film microreactors for selective direct fluorination. Lab Chip 1:132–137
30. Beatty JW, Douglas JJ, Cole KP et al (2015) A scalable and operationally simple radical trifluoromethylation. Nat commun 6:7919
31. Straathof NJW, van Osch DJGP, Schouten A et al (2014) Visible light photocatalytic metal-free perfluoroalkylation of heteroarenes in continuous flow. J Flow Chem 4:12–17
32. Straathof NJW, Gemoets HPL, Wang X et al (2014) Rapid trifluoromethylation and perfluoroalkylation of five-membered heterocycles by photoredox catalysis in continuous flow. Chem SusChem 7:1612–1617
33. Straathof NJW, Tegelbeckers HV (2014) A mild and fast photocatalytic trifluoromethylation of thiols in batch and continuous flow. Chem Sci 5:4768–4773
34. Cantillo D, de Frutos O, Rincon JA (2014) Continuous flow a-trifluoromethylation of ketones by metal-free visible light photoredox catalysis. Org Lett 16:896–899
35. Chen M, Buchwald SL (2013) Rapid and efficient trifluoromethylation of aromatic and heteroaromatic compounds using potassium trifluoroacetate enabled by a flow system. Angew Chem Int Ed 52:11628–11631
36. Zhang X, Huang P, Li Y et al (2015) A mild and fast continuous flow trifluoromethylation of coumarins with the CF_3 radical derived from CF_3SO_2Na and TBHP. Org Biomol Chem (in press)
37. Kelly CB, Lee C, Mercadante MA (2011) A continuous flow approach to palladium catalysed alkoxycarbonylation reactions. Org Process Res Dev 15:717–720
38. Koos P, Gross U, Polyzos A (2011) Teflon AF-2400 mediated gas-liquid contact in continuous flow methoxycarbonylations and in-line FTIR measurement of CO concentration. Org Biomol Chem 9:6903–6908
39. Miller PW, Long NJ, de Mello AJ et al (2007) Rapid multiphase carbonylation reactions by using a microtube reactor: applications in positron emission tomography 11C-radiolabeling. Angew Chem Int Ed 46:2875–2878
40. Kealey S, Plisson C, Collier TL (2011) Microfluidic reactions using [11C]carbon monoxide solutions for the synthesis of a positron emission tomography radiotracer. Org Biomol Chem 9:3313–3319

Aerobic Oxidations in Continuous Flow

Bartholomäus Pieber and C.Oliver Kappe

Abstract In recent years, the high demand for sustainable processes resulted in the development of highly attractive oxidation protocols utilizing molecular oxygen or even air instead of more uneconomic and often toxic reagents. The application of these sustainable, gaseous oxidants in conventional batch reactors is often associated with severe safety risks and process challenges especially on larger scales. Continuous flow technology offers the possibility to minimize these safety hazards and concurrently allows working in high-temperature/high-pressure regimes to access highly efficient oxidation protocols. This review article critically discusses recent literature examples of flow methodologies for selective aerobic oxidations of organic compounds. Several technologies and reactor designs for biphasic gas/liquid as well as supercritical reaction media are presented in detail.

Keywords Aerobic oxidation • Continuous flow • Heterogeneous catalysis • Homogeneous catalysis • Oxygen

Contents

B. Pieber and C.O. Kappe (✉)
Institute of Chemistry, University of Graz, NAWI Graz, Heinrichstrasse 28, 8010 Graz, Austria
e-mail: oliver.kappe@uni-graz.at

Abbreviations

Ac	Acetyl
acac	Acetylacetonate
ATR	Attenuated total reflection
bpy	2,2′-Bipyridyl
conv	Conversion
CSTR	Continuous stirred-tank reactor
DBU	1,8-Diazabicyclo[5.4.0]undec-7-ene
DMF	*N,N*-dimethylformamide
DMSO	Dimethylsulfoxide
dr	Diastereomeric ratio
equiv	Equivalent(s)
Et	Ethyl
EXAFS	Extended X-ray absorption fine structure
FDH	Formate dehydrogenase
FEP	Fluorinated ethylene propylene
g	Gram(s)
GC	Gas chromatography
h	Hour(s)
HbpA	2-Hydroxybiphenyl 3-monooxygenase
HPLC	High-performance liquid chromatography
IBX	2-Iodoxybenzoic acid
i-Pr	*iso*-Propyl
IR	Infrared
L	Liter(s)
LED	Light-emitting diode
LOC	Limiting oxygen concentration
m	Meter(s)
M	Molar
Me	Methyl
MFC	Mass flow controller
min	Minute(s)
mol	Mole(s)
MS	Mass spectrometry
NAD	Nicotinamide adenine dinucleotide
NaHMDS	Sodium hexamethyldisilazide
NMI	*N*-Methylimidazole
NMO	*N*-Methylmorpholine *N*-oxide

NMP	*N*-Methyl-2-pyrrolidone
n-Pr	*n*-Propyl
PCC	Pyridiniumchlorochromate
PDC	Pyridinium dichromate
PDMS	Polydimethylsiloxane
PEEK	Polyether ether ketone
PEG	Polyethylene glycol
PFA	Perfluoroalkoxy
Ph	Phenyl
phen	Phenanthroline
PTFE	Polytetrafluoroethylene
quant	Quantitative
rt	Room temperature
s	Second(s)
sc	Supercritical
Sel	Selectivity
SET	Single-electron transfer
SMU	Static mixing unit
t-AmOK	Potassium *tert*-amylate
TBAF	Tetrabutylammonium fluoride
TBR	Trickle-bed reactor
t-bu	*tert*-Butyl
TEM	Transmission electron microscopy
TEMPO	(2,2,6,6-Tetramethylpiperidin-1-yl)oxyl
TEOS	Tetraethoxysilane
Tf	Trifluoromethanesulfonyl
TFA	Trifluoroacetic acid
THF	Tetrahydrofuran
TMEDA	*N*,*N*,*N'*,*N'*-Tetramethyl-1,2-ethylenediamine
TMSCN	Trimethylsilylcyanide
TPAP	Tetrapropylammoniumperuthenate
TPP	*meso*-Tetraphenylporphyrin
U	Unit(s)
UHP	Urea hydrogen peroxide
XAS	X-ray absorption spectroscopy

1 Introduction

The high demand for more sustainable oxidation processes in the synthesis of commodity and fine chemicals necessitates the development of safe and efficient methodologies employing virtually ideal oxidants such as O_2 or even air. The economic and environmental advantages using these cheap and readily available oxidation reagents are apparent. However, applications are often restricted to

substrates capable of undergoing selective autoxidation reactions. For a more widespread use of this sustainable oxidant, a plethora of versatile catalytic methods for aerobic oxidations of complex organic molecules – such as the oxidation of alcohols, oxidative cross coupling reactions, and selective C–H bond oxidations – have been developed in recent years [1–5].

Oxidations using molecular oxygen or air are often associated with severe safety risks and process challenges. Such transformations are generally exothermic and the heat of the reaction can be difficult to dissipate. The consequential non-isothermal conditions potentially reduce reaction selectivity and product quality. Furthermore, aerobic oxidations suitable for fine chemical manufacturing are usually carried out at elevated temperatures and pressures in organic solvents posing severe explosion hazards. To avoid spontaneous ignition of such reactions mixtures, large-scale applications in conventional batch reactors have to be carried out below the limiting oxygen concentration (LOC) [6]. This is typically achieved by mixing the gaseous oxidant with an inert gas as, e.g., N_2, to dilute the oxygen/ solvent vapor. Moreover, nonoptimal temperature and pressure ranges are applied resulting in relatively slow and inefficient processes.

Continuous flow (micro)reactor technology offers the unique possibility to address the abovementioned safety hazards, concurrently working at high-temperature/high-pressure regimes ("novel process windows") feasible for efficient oxidation protocols [7–13]. Exothermic reactions are easily controlled by the excellent mass and heat transfer making this technology an ideal tool to harness hazardous chemical processes [14]. Importantly, the small volumes and channel dimensions minimize the possibility of propagation of an explosion inside the reactor, thereby tremendously broadening the possible operation range [15, 16]. Especially biphasic gas/liquid reactions such as aerobic oxidations can benefit from this enabling technology due to fast mixing characteristics and a dramatically enlarged interfacial area between the liquid and the gaseous phase [17]. Moreover, continuous flow devices allow for rapid screening of process conditions in biphasic gas/liquid reactions compared to pressurized autoclave systems.

A crucial issue for many chemical reactions developed in research laboratories, but especially hazardous reactions involving O_2, is related to a possible large-scale application. Scaling is generally considerably easier for a continuous process than for a batch process, and flow routes developed and optimized in the laboratory can often be scaled to production quantities with minimal re-optimization and/or without major changes in the synthetic path [14]. Numbering up of flow devices or scaling up of the reactor volume increases the throughput, while the performance of the reactor can be largely conserved by keeping certain characteristics of the system constant ("smart dimensioning"). Alternatively, simply running a reactor for extended periods of time to generate the desired quantities of pharmaceutical intermediates or final products is often an acceptable strategy.

In this review we aim to provide a comprehensive overview on recent developments in aerobic oxidation reactions in gas/liquid continuous flow mode. In the first chapter, reactor designs and technologies suitable for such biphasic transformations are introduced. Thereafter, continuous oxidation protocols of small organic

molecules and other reactions involving O_2 as sole oxidant are critically discussed. Finally, the photochemical utilization of molecular oxygen for, for example, the generation of singlet oxygen ($^1O_2$) in organic synthesis will be outlined briefly for selected examples. For reactions involving ozonolysis and gas-phase oxidations, the authors refer to the following references [15, 18–21].

2 Technological Aspects

In general, the majority of gas/liquid reactions in continuous flow such as aerobic oxidations are carried using a gaseous feed and one or more liquid feeds containing the substrate and, if necessary, a homogeneous catalyst or other additives (Scheme 1a). The liquid solution is usually pumped using standard HPLC, syringe,
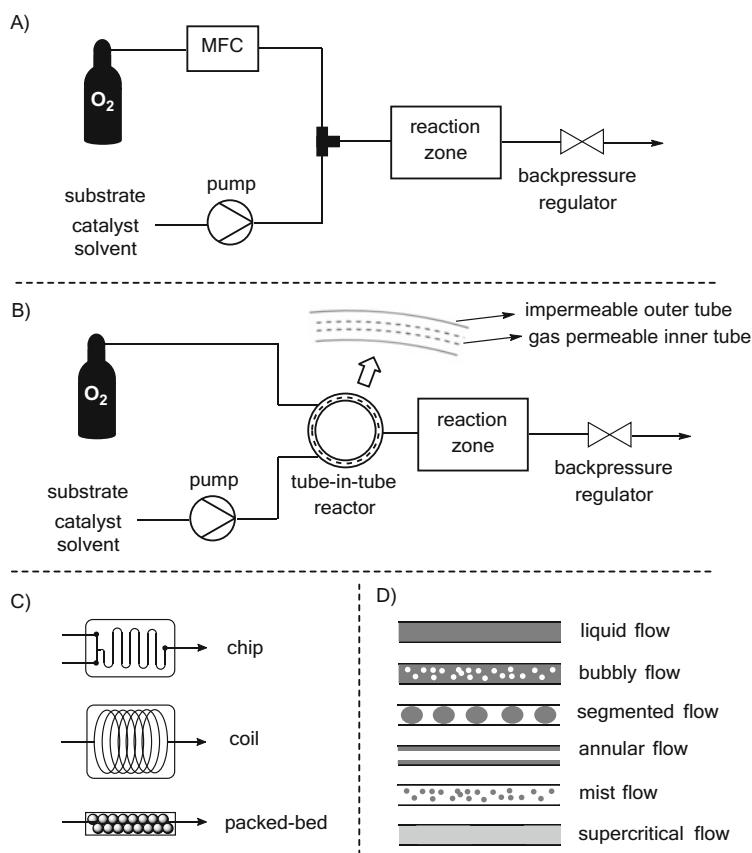
Scheme 1 Typical set ups for aerobic oxidations in continuous flow (**a**, **b**), reactor types (**c**), and common gas/liquid flow regimes (**d**)

or peristaltic pumps, whereas the gaseous phase can be accurately fed using, for example, a mass flow controller (MFC). This dedicated tool enables an easy control of the stoichiometry of the gaseous reagent which can be hardly done in conventional batch processes. Mixing of the streams is carried out in either static or active mixing units before entering the reaction zone where the chemical transformations occurs. A further important feature – in particular for biphasic gas/liquid flow chemistry – is the use of back-pressure regulators (BPR) which allow a precise control of the residence time and straightforward access to elevated pressure regimes. Therefore, a higher solubility of the gaseous oxidant can be conveniently achieved in a safe manner often resulting in intensified protocols.

An alternative approach to feed gaseous reagents in the liquid reaction mixture is the use of membrane reactors (Scheme 1b) [17]. Among those, the so called tube-in-tube reactor developed by Ley and coworkers has gained significant attention since its first application in 2010 [22]. In principal, this device consists of a gas-permeable Teflon AF-2400 membrane tubing (inner tube) that is fixed within larger impermeable tubing (outer tube). These tubes are separated by T-pieces allowing for an independent feed of both channels. Only gaseous reagents can pass the membrane and react with substrates in the liquid phase or simply saturate the solvent for subsequent use. In that respect, Jensen and coworkers recently communicated a quantitative model for predicting gas and substrate concentration profiles in the tube-in-tube reactor unit [23]. The authors concluded that the low gas loading, insufficient radial mixing, and heating characteristics limit the general applicability of this device. It should be further noted that on the one hand an accurate control of the stoichiometry is hardly possible and on the other hand membrane materials are often restricted to relatively low temperature and pressure ranges to avoid damage. Nevertheless, the reactor unit remains a convenient gas-loading tool on laboratory scale for certain applications.

Depending on the application, three different common reactor types (reaction zone) are predominantly used in aerobic oxidations of small molecules (Scheme 1c). Homogeneously catalyzed and catalyst-free oxidations are typically carried out in chip or coil reactors made of glass, simple polymeric materials, ceramics, or metals/alloys. Additionally, the gas-loading unit itself can be simultaneously used as reaction zone by using membrane reactor applications [22]. If a heterogeneous species is used to enhance an oxidation process, packed-bed reactors loaded with a heterogeneous (supported) catalyst are typically employed [24].

The flow pattern of the biphasic mixture represents a very important and controllable parameter in gas/liquid flow reactions which has a significant influence on the interfacial area and the overall flow rate (Scheme 1d). Various flow regimes can be achieved depending on the solubility of the gaseous oxidant in the reaction medium, the reaction temperature, the back pressure, and the flow rates of the liquid as well as the gaseous stream. If the gas is fully dissolved, a homogeneous liquid flow appears which is often the case using membrane reactor applications. Among the biphasic flow patterns, segmented flow (sometimes also referred to as slug, plug, or Taylor flow) and annular flow are most commonly applied in continuous organic synthesis. Single-phase oxidations can be observed in certain cases when

supercritical solvents (sc) like scH$_2$O are used, since both, the substrate and the oxidant, are totally dissolved in the reaction medium [25]. In the latter case, extremely high pressures are usually required which also necessitates special dosing techniques to deliver the gaseous oxidant.

However, an accurate control of gas/liquid reactions such as aerobic oxidations is by no means trivial as a large number of parameters have to be taken into account during the reactor development and design of experiments.

3   Oxidation of Hydrocarbons

Highly efficient methods for the preparation of bulk chemicals by liquid-phase oxidation with O$_2$ have been developed, and several commodity chemicals, such as cyclohexanol/cyclohexanone (KA oil), cumene hydroperoxide, *tert*-butyl hydro-peroxide/*tert*-butyl alcohol, or terephthalic acid, are produced on an enormous scale by aerobic oxidation of petroleum-based compounds. The latter material is an important intermediate in the production of polyester materials. The industrial synthesis (AMOCO Process) is realized by an oxidation of *p*-xylene (**1**) using O$_2$ in acetic acid catalyzed by cobalt and/or manganese salts in presence of a bromide source [26]. In 2002, Poliakoff and coworkers presented an alternative, sustainable methodology for the synthesis of terephthalic acid (**2**) replacing the organic solvent by supercritical water in a continuous process (Scheme 2) [27]. A standard reactor design using compressed air was not feasible since the required amount of oxygen for these experiments was extremely small. Therefore, an aqueous solution of H$_2$O$_2$ was heated at 400°C to in situ generate O$_2$ in the first coil reactor. The oxygen/water mixture was subsequently mixed with a solution of MnBr$_2$ and **1** to initiate the supercritical oxidation process in a Hastelloy C276 coil at 400°C and 280 bar. Afterward, a NaOH solution was fed to prevent the product mixture from precipitation, and the solution was subsequently cooled in an additional coil reactor before passing a back-pressure regulator.
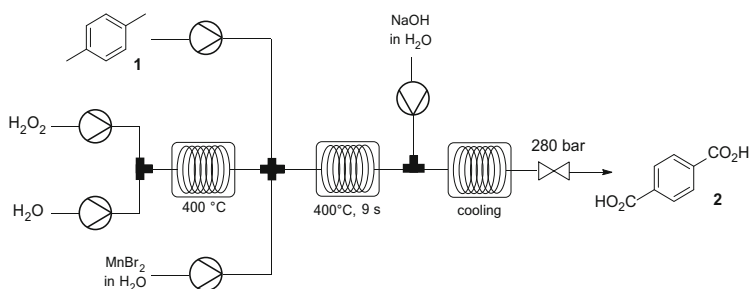
Scheme 2 Continuous synthesis of terephthalic acid (**2**) via aerobic oxidation of *p*-xylene (**1**) in scH$_2$O

Importantly, due to the extreme reaction conditions, a residence time of only 9 s was sufficient to generate **2** in good yields (>79%) and high selectivity (>92%). Problematic impurities such as 4-carboxybenzaldehyde were not observed under optimized conditions, thus offering a potential alternative to common industrial processes. The system could further be applied to other methyl aromatic compounds like *o*- and *m*-xylene, mesitylene, toluene, ethylbenzene, and even heteroaromatic picolines [28, 29]. Despite significant differences in their reactivity, mixed xylenes can be simultaneously oxidized in reasonable yields and good selectivity by carefully tuning the experimental conditions [30]. A main drawback in both the scH$_2$O and the conventional acetic acid process is the hydrolysis of the homogeneous manganese catalyst resulting in insoluble metal oxides [31]. This not only results in a reduced activity and recyclability of the active species but can also lead to reactor clogging in the continuous route. Hence, Poliakoff and coworkers found out that manganese recovery can be significantly improved by the addition of Brønsted acids and by increasing the Br/Mn ratio for the oxidation of *o*-xylene in scH$_2$O [31]. Hydrobromic acid was shown to be the most efficient additive since it provides the required acidity and simultaneously acts as a bromide source.

Detailed mechanistic studies on the continuous oxidation of *o*- and *p*-xylene led to the discovery of another catalytic system using CuBr$_2$ in a selective oxidation process utilizing a similar flow setup [32, 33]. A synergistic effect between copper and other metals, such as cobalt, was found to enhance this reaction as exemplified by utilizing a four-component catalyst system (Cu/Co/NH$_4$/Br). In this case subcritical water gave significantly better results than scH$_2$O which was rationalized by a temperature-dependent equilibrium shift in the ammonium bromide decomposition [33].

In contrast to the synthesis of carboxylic acids discussed above, Kappe and coworkers realized a partial aerobic oxidation of ethylbenzene (**3**) yielding acetophenone (**4**) in a gas/liquid coil reactor (Scheme 3a) [34]. Complete conversion of **3** was obtained within 6 min at 120°C in a PFA coil using catalytic amounts of CoBr$_2$ and Mn(OAc)$_2$ and compressed air as oxygen source. The desired ketone (**4**) was formed in high selectivity (80%) and isolated in 66% yield. Due to the tight control of reaction parameters, over-oxidation to benzoic acid was minimized to a relatively small amount (~10%). This was further demonstrated by processing the same reaction mixture at higher temperatures (150°C) in combination with a longer residence time (16 min) yielding benzoic acid (71%) as a main product.

A similar setup was used for the oxidation of 2-benzylpyridines to the respective ketones in an iron-catalyzed protocol [35]. In this case, standard polar, aprotic solvents like NMP or DMSO as reaction media were prone to decomposition under the harsh reaction conditions (200°C). To overcome these issues, the authors used propylene carbonate, a sustainable, high-boiling solvent with excellent oxidation stability. Good to excellent isolated yields for potential drug precursor molecules were obtained at 200°C within 13 min in a stainless steel coil significantly enhancing the original batch protocol [36].

A silicon nitride-coated halo-etched chip reactor was used by Jensen and coworkers for the metal-free oxidation of picolines (Scheme 3b) [37]. The reaction
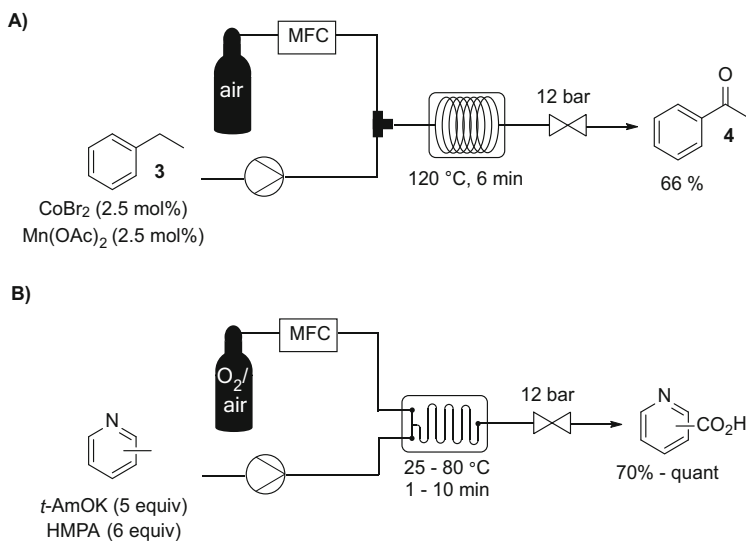
Scheme 3 Aerobic oxidation of ethylbenzene (**a**) and picolines (**b**) in continuous flow

is suggested to proceed via deprotonation of the methyl group in presence of a strong base such as potassium *tert*-amylate (*t*-AmOK) followed by an anionic oxidation step. Notably, different solvent mixtures were necessary for each picoline derivative in order to obtain high conversions. Moreover, the same group recently described the application of a surface-passivated silicon microchip in the solvent-free autoxidation of β-pinene and (+)-valencene gaining insights into reaction kinetics by visual determination of O_2 consumption during the reaction [38].

KA oil, an unrefined mixture of cyclohexanone and cyclohexanol, is an important precursor for the production of ε-caprolactam and adipic acid which are further converted to nylon polymers. Industrial production of KA oil is mainly carried out via the aerobic oxidation of cyclohexane in bubble column reactors within 15–60 min. Typical conversions in these processes are below 6% for obtaining a sufficient selectivity [39]. The group of de Bellefon reported on a segmented flow pattern in a chip-based microreactor by mixing cyclohexanone and O_2 to study this transformation on laboratory scale [40]. At 200°C and 25 bar, 4.3% conversion were obtained maintaining a high selectivity (88%). Under almost identical conditions a significantly lower conversion (1.6%) was observed when oxygen was replaced by compressed air. However, the higher throughput compared to industrial routes applying bubble column reactors or continuous stirred-tank reactors (CSTR) was explained by the intensified conditions and the excellent residence time control.

An intensification study for this industrially relevant oxidation in capillary reactors with inner diameters between 0.5 and 2.15 mm further showed that elevated temperatures (260°C) enable a significant reduction of the reactor volume and thus resulting in a reduction of the power of a potential explosion [41]. The study was conducted by applying a neat cyclohexane stream and air in a segmented

flow pattern (Fig. 1). However, it has to be stressed that the improvement of the gas/liquid mass transfer in the microreactor was shown to be very low compared to standard bubble column reactors.

A more versatile protocol employing homogeneous palladium catalysis was utilized to realize a continuous anti-Markovnikov Wacker oxidation of functionalized styrenes (Scheme 4a) [42]. Initially, an aqueous solution of bis (acetonitrile)dichloropalladium(II) and $CuCl_2$ was mixed with an organic stream containing a styrene derivative. To avoid solvent freezing of t-BuOH – which is necessary to obtain the desired selectivity – toluene was added as a cosolvent. The liquid mixture was subsequently loaded with oxygen as gaseous oxidant in a tube-in-tube membrane reactor. Afterward, the final reaction mixture was fed in a stainless steel coil heated at 60°C to carry out the desired transformation. It could be shown that an accurate control of the oxygen pressure is of crucial importance to

Fig. 1 Gas/liquid segmented flow pattern for the oxidation of cyclohexane with air. Reproduced with permissions from [41]
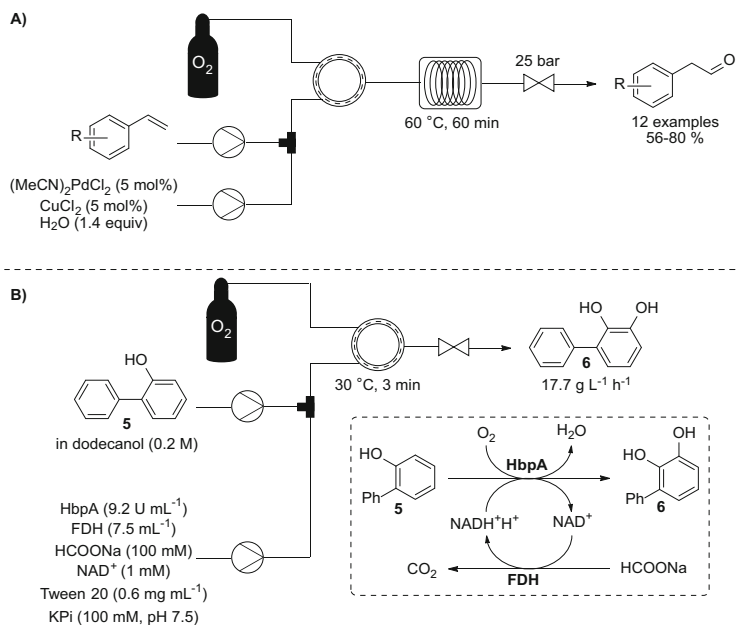
Scheme 4 (**a**) Anti-Markovnikov Wacker oxidation of styrenes using a membrane reactor. (**b**) Biocatalytic catechol synthesis in a tube-in-tube reactor

obtain on the one hand complete conversion and on the other hand to avoid over-oxidation which would generate undesired carboxylic acids. Importantly, a modified system using a second gas addition allowed for higher concentrations and thus an improved throughput, thus accessing a multi-gram scale protocol.

The tube-in-tube reactor was also used in the biocatalytic production of 3-phenylcatechol (**6**) from 2-hydroxybiphenyl (**5**) catalyzed by 2-hydroxybiphenyl 3-monooxygenase (HbpA) (Scheme 4b) [43, 44]. Formate dehydrogenase (FDH) was added for cofactor recycling which converts sodium formate to carbon dioxide. However, high substrate loadings were achieved by using an organic liquid feed containing the substrate and an aqueous stream consisting of both enzymes, the cofactor and sodium formate. Under optimized conditions a productivity of ~18 g L^{-1} h^{-1} of the desired catechol was achieved which is 38 times higher than in conventional batch reactions [43].

Chemists from Bristol–Myers Squibb applied continuous flow technology to develop a scalable, high-yielding route for the hydroxylation of buspirone (**7**) by an enolization/oxidation sequence (Scheme 5) [45]. In the first step, the substrate feed was mixed with the base by slowly reducing the temperature in two sequential static mixing units (SMU) to avoid precipitation of the inorganic base. After complete enolization in a coil-based heat exchanger, the reaction mixture entered a trickle-bed reactor (TBR) packed with Pro-Pak® distillation packing material. The optimized oxidation process was carried out at a reactor temperature of $-36°C$ at atmospheric pressure using a countercurrent O_2 stream and a residence time of 3–4 min. Afterward, the reaction was quenched with 2.5 M HCl in a continuous stirred-tank reactor. Upscaling by a larger reactor volume was not feasible due to a lower cooling efficiency (heat transfer) causing the researchers to use a numbering-up approach. Therefore, the reaction mixture was split into four different streams after enolization and fed into a 4-channel oxidation reactor (quad reactor), to finally result in the potential anxiolytic agent 6-hydroxybuspirone (**8**, Scheme 5). The whole sequence was operated for 72 h using process analytical techniques for in situ
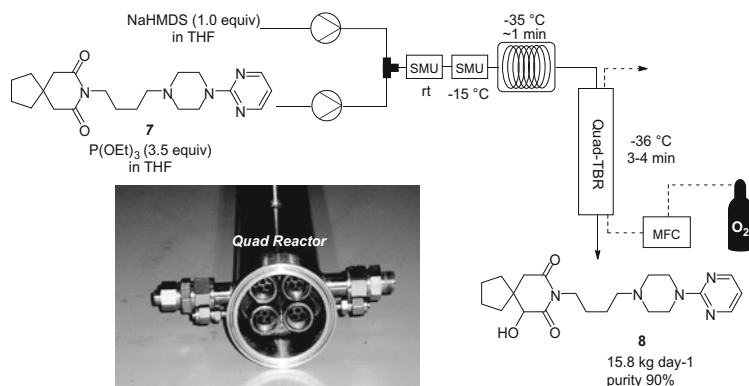
Scheme 5 Continuous enolization and oxidation sequence of Buspirone (**7**). A numbering-up technique is used for the oxidation step (quad reactor). Adapted with permission from [45]

control of its performance. Notably, a constant purity profile was monitored (90%) over time at a high production rate (15 kg d^{-1}).

The last examples clearly demonstrate that aerobic oxidation reactions of hydrocarbons in a continuous manner are not only limited to bulk chemical synthesis. However, applications in fine chemical manufacturing are extremely rare since selective C–H oxidations of more complex organic molecules are by no means trivial due to the lack of selective autoxidation processes. In contrast, oxidations of functional groups, such as alcohols, or catalytic reactions involving an aerobic oxidation of the catalyst potentially allow for a significantly broader scope.

4 Oxidation of Alcohols

The oxidation of primary and secondary alcohols to the corresponding carbonyl compounds is among the most fundamental transformations in organic synthesis. Common strategies involve stoichiometric amounts of special oxidants such as NMO in the presence of TPAP, bleach in combination with TEMPO, permanganates, activated DMSO, toxic chromium(VI) complexes (Collins reagent, PDC, PCC), or hypervalent iodine reagents such as Dess–Martin periodinane and IBX. These relatively expensive reagents generate considerable amounts of often toxic waste and suffer from poor atom economies. In stark contrast, oxidations using air or molecular oxygen theoretically produce water as the only by-product. Therefore, considerable effort has been invested in the development of catalytic protocols to explore the applicability of these environmentally benign alternatives [46–49].

4.1 Heterogeneous Catalysis in Common Solvents

It is not surprising that aerobic alcohol oxidations, especially examples involving heterogeneous catalysis, are often studied in continuous flow reactors since the many advantages of triphasic gas/liquid/solid reactions are quite evident. Early examples applying continuous packed-bed reactors were published already in the late 1980s and early 1990s, marking the beginning of continuous aerobic oxidation studies in research laboratories [50–52].

Various heterogeneous catalysts, especially supported noble metals, are well known to facilitate the aerobic oxidation of primary and secondary alcohols [46, 48]. Among those, ruthenium is probably the most promising and extensively studied material. The pioneering work by Plucinski and coworkers showed the applicability of supported ruthenium catalysts in a multichannel compact reactor for the selective oxidation of benzyl alcohol (**9**) with molecular oxygen (Scheme 6) [53–56]. The reactor elements were fabricated by etching of thin stainless steel plates followed by their assembly applying a diffusion-bonding technique. The liquid and gaseous feeds are combined in a static mixing unit and the resulting
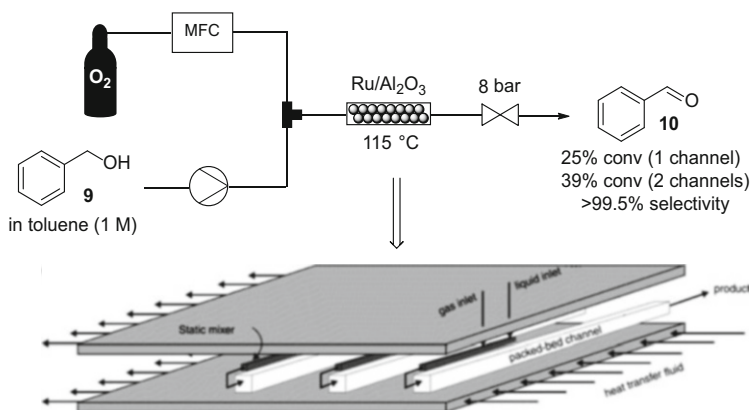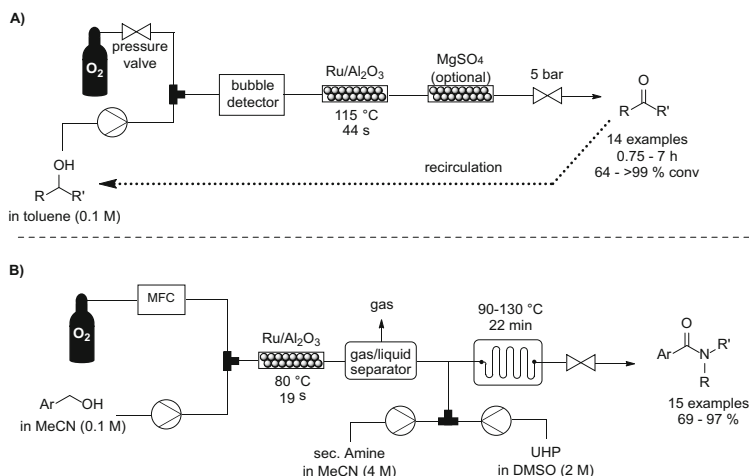
Scheme 6 Aerobic oxidation of benzyl alcohol (**9**) using a multichannel compact reactor. Adapted with permission from [53]

stream is guided into a packed-bed channel. Since the reactor contains five of those units, the length of the catalyst bed can be conveniently varied by connecting two or more channels. This approach also allows for multiple addition of, for example, O_2 by installing another gas feed between two consecutive packed-bed units.

In addition, temperature control can be ensured using glycerol as heat transfer fluid which is circulated toward heat exchange channels. For testing the multichannel reactor, the aerobic oxidation of benzyl alcohol (**9**) to benzaldehyde (**10**) in toluene catalyzed by Ru/Al_2O_3 was chosen as model reaction. Careful optimization of all reaction parameters resulted in 25% and 39% conversion at 115°C by using one or two channels, respectively. In addition, splitting of the oxygen stream by installing a second gas feed after the first packed-bed channel slightly increased the consumption of (**9**) resulting in 46% of the corresponding aldehyde (**10**). Noteworthy, the catalyst activity decreased very slowly during a stability study which is most likely a result of poisoning by over-oxidized benzoic acid. Subsequently, the same reactor design was used to test a ruthenium(III) hydrated oxide catalyst supported on TiO_2 nanotubes for its catalytic activity in the aerobic oxidation of aromatic primary alcohols [54]. The application of this more active ruthenium species improved the single-pass conversions dramatically (75%) maintaining an excellent selectivity for the corresponding aldehyde at similar conditions to the Ru/Al_2O_3 system discussed above.

The versatility of the easily accessible Ru/Al_2O_3 catalyst was further explored on a broader scope by the group of Hii in collaboration with Pfizer using a commercially available reactor system (Scheme 7a) [57]. The oxygen flow was controlled by a pressure valve and the gas/liquid ratio was monitored by a bubble detector unit prior to the packed-bed reactor. Relatively low single-pass conversions for various alcohols at 115°C and 5 bar caused the authors to recirculate the reaction mixture for 45 min to 7 h depending on the reactivity of the respective primary or secondary alcohol. High conversions and selectivities were achieved for

Scheme 7 (**a**) Ru-catalyzed aerobic oxidation of alcohols using a recirculation technique. (**b**) Continuous tow-step amide synthesis toward alcohol oxidation and subsequent amidation

a range of allylic and benzylic primary alcohols including pyridyl and thienyl systems. Even the more challenging aliphatic secondary and primary alcohols could be selectively oxidized in moderate to good conversions under those conditions. It could be shown that catalyst deactivation over time can be circumvented by installing an additional cartridge filled with $MgSO_4$ as desiccant to remove accumulated water. This scavenging technique resulted in improved conversions of 2-hexanol (91% instead of 75%) within a 7 h recirculation experiment. ICP analysis revealed no leaching of the catalytically active material allowing for an almost work-up-free procedure. Given the fact that the reaction mixture exclusively consists of the desired product, the researchers designed a telescoped process by combining the continuous aerobic oxidation with a subsequent Wittig olefination in batch.

More recently, an almost identical experimental setup was utilized to demonstrate the potential of immobilized iron oxide nanoparticles as catalyst for the aerobic oxidation of benzyl alcohol (**9**) [58]. The catalytic material was generated and immobilized by heating $FeCl_2$ together with dispersed aluminum-doped mesoporous silica (Al-SBA15) in ethanol at 150°C for several minutes. The supported catalyst showed promising activities in the presence of TEMPO as a cocatalyst resulting in single-pass conversions of 42% using a *n*-heptane/dioxane mixture as liquid phase. Again recirculation over 1 h was necessary to obtain a selective, almost quantitative oxidation without detectable amounts of iron leaching.

These semicontinuous recirculation protocols are utilized to simulate an extension of the small packed-bed reactors usually applied on laboratory scale. It has to be stressed that after each single pass, a separation of the oxidation agent occurs and fresh oxygen is added for the next cycle. Overall, an enormous excess of the

gaseous reagent is necessary and a continuous monitoring of the conversion over a long time period is required. These circumstances may limit the practical application in the context of an industrial protocol but undoubtedly show the potential of such gas/liquid/solid oxidation procedures in continuous flow.

In contrast to these relatively inconvenient recirculation procedures, Jensen and coworkers could show that high conversions (95%) for aerobic benzyl alcohol oxidations can be achieved in a residence time as low as 19 s at 80°C using the Ru/Al$_2$O$_3$ catalyst [59]. A high excess of oxygen (200 μL min^{-1}) was mixed with the aldehyde precursor in acetonitrile (0.1 M, 5 μL min^{-1}) and the combined mixture entered a silicon–Pyrex microreactor filled with the supported catalyst. Notably, a stable conversion was observed over a period of 24 h. The oxidation procedure was further utilized for a continuous two-step synthesis of amides from various benzylic alcohols and secondary amines (Scheme 7b). Therefore, a membrane separator was installed after the heterogeneously catalyzed oxidation, in order to remove unreacted O$_2$ enabling a better residence time control for the subsequent oxidative amidation using urea hydrogen peroxide (UHP), based on a previous protocol from the same group [60].

More recently, Ru(OH)$_x$/Al$_2$O$_3$ was introduced as an efficient alternative to the classical Ru/Al$_2$O$_3$ catalyst for continuous aerobic oxidations circumventing the necessity for tedious recirculation procedures or high excess of O$_2$ [61]. Careful analysis of the standard benzyl alcohol model oxidation provided insights into the deactivation caused by over-oxidized benzoic acid. Initially, a significant drop in the catalytic activity was observed followed by an almost stable conversion. The resulting catalyst activity profile was the basis for the development of high steady-state single-pass conversions (up to 99%) using the partially deactivated catalyst. The final protocol is characterized by an O$_2$/substrate molar ratio of 2:1, a single-pass residence time of 1 h at 80°C and a back pressure of 11 bar. Noteworthy, the authors used diluted O$_2$ (8% in N$_2$) to work below the LOC of toluene in all experiments, thus showcasing the superior activity of supported Ru(OH)$_x$ compared to metallic ruthenium.

Despite these common heterogeneous catalysts for aerobic oxidation, also TPAP was reported to show activity in the transformation of benzyl alcohol to the corresponding aldehyde [62]. Other common noble metal catalysts such as metallic silver, palladium, or platinum were also mentioned in combination with various supports for the oxidation of alcohols in continuous flow mode [63–68].

Gold-catalyzed oxidation procedures are currently gaining a considerable amount of interest in the continuous flow community [69–78]. Among those, an extremely efficient protocol was communicated by Kobayashi and coworkers (Scheme 8a) [69]. Their reactor unit was fabricated by immobilization of microencapsulated gold on a polysiloxane-coated capillary via cross-linking. Initially, an organic substrate feed was mixed with an aqueous solution containing potassium carbonate and the combined liquid stream was merged with O$_2$ accurately added by a mass flow controller. The multiphasic mixture passed the functionalized heated capillary (50–70°C). Notably, no back pressure is required to convert various secondary alcohols to the corresponding ketones in almost
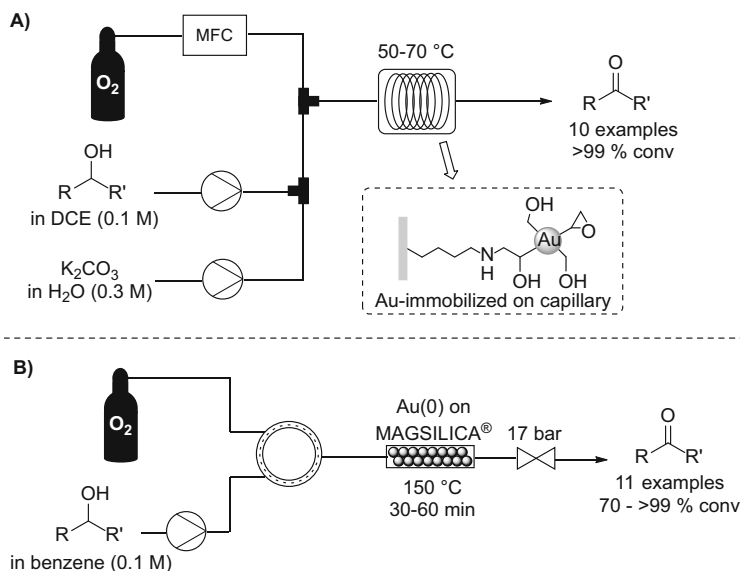
Scheme 8 Gold-catalyzed aerobic oxidation of alcohols using (**a**) microencapsulated Au immobilized on a capillary or (**b**) gold-doped superparamagnetic nanoparticles

perfect isolated yields at temperatures below the boiling point of the solvent mixture. It could be shown that the catalytic activity is completely stable over 4 d and no catalyst leaching could be detected. Unfortunately, low yields were obtained for benzylic and allylic primary alcohols using the Au-functionalized capillary. However, this problem could be solved by using a bimetallic Au/Pd immobilized reactor column instead, resulting in almost quantitative amounts for these less reactive starting materials.

Another strategy was communicated by Kirschning and coworkers in 2014 using an unconventional heating methodology (Scheme 8b) [78]. Catalytically active gold(0) nanocrystals were immobilized on nanostructured particles with a superparamagnetic iron oxide core and a silica shell (MAGSILICA®). The resulting material was filled into a PEEK reactor in order to perform the oxidation of primary and secondary alcohols under continuous flow conditions. By applying an external oscillating electromagnetic field, the particles can be heated inductively. Therefore, the material was not only serving as catalyst but also as heating tool. The starting materials were dissolved in benzene and the organic solution was mixed with oxygen using a tube-in-tube membrane reactor. Inductive heating at 150°C was reported to be necessary to obtain single-pass conversions with residence times of approximately 30 min for simple primary and secondary alcohols. Replacement of benzene by less toxic solvents was not feasible since solvent oxidation or comparably low conversions were observed. Nevertheless, the authors could replace O_2 by compressed air due to the high activity of the nano-catalyst.
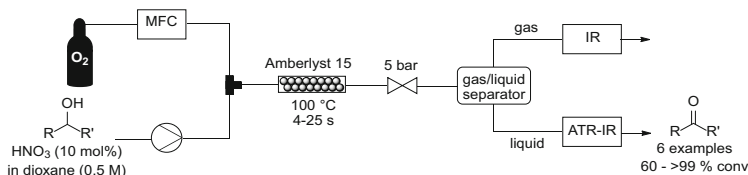
Scheme 9 Metal-free aerobic oxidation of alcohols using a packed-bed reactor

Inspired by HNO_3-based oxidations, Hermans and coworkers recently developed a metal-free batch oxidation protocol using catalytic amounts of HNO_3 as oxygen shuttle in combination with Amberlyst 15. This combination led to an NO_x-propagated chain oxidation using O_2 as terminal oxidant [79]. Subsequently, the group developed an intensified process using continuous flow technology (Scheme 9) [80]. The ion-exchange resin was placed into a packed-bed reactor as heterogeneous catalyst. Oxygen was mixed with a liquid feed containing the alcohol and 10 mol% HNO_3. At a reaction temperature of 100°C, 4–25 s were sufficient to synthesize several aldehydes and ketones in excellent yields and selectivity. Online monitoring of gas-phase N_2O and of the oxidation efficiency was realized by using a gas/liquid separator in combination with different infrared spectroscopic techniques. In addition, a milder protocol (55°C) using TEMPO on silica instead of Amberlyst 15 was developed [81].

4.2 Heterogeneous Catalysis in Supercritical CO_2

Supercritical CO_2 (scCO_2) is an extremely attractive medium for reactions involving molecular oxygen due to its inert environment which minimizes safety concerns compared to common organic solvents [82–84]. Although the advantages connected with this green solvent are quite obvious, the necessity of high-pressure equipment such as autoclaves has limited its application in organic synthesis. Continuous flow processing offers a comparably convenient access to such process windows especially in academic research laboratories. As already discussed in the oxidation of xylenes in scH_2O, the reactor design usually differs from common gas/liquid-phase flow setups. The relatively harsh temperature and pressure conditions often necessitate special materials compared to liquid-phase oxidations for safety reasons. In case of scCO_2, the substrate is usually fed into the flow system in a separate stream and mixed with the supercritical solvent in the reactor system.

At the turn of the millennium, Baiker and colleagues started an intensive research period on heterogeneous noble metal-catalyzed aerobic oxidations using this nonexplosive and nonflammable "solvent" under continuous flow conditions (Scheme 10) [85–97]. In general, their setup consisted of a liquid CO_2 feed controlled by a compressor unit which was in a first step mixed with O_2. Control of the gaseous oxidant supply was carried out using a 6-way valve, dosing 50 μL
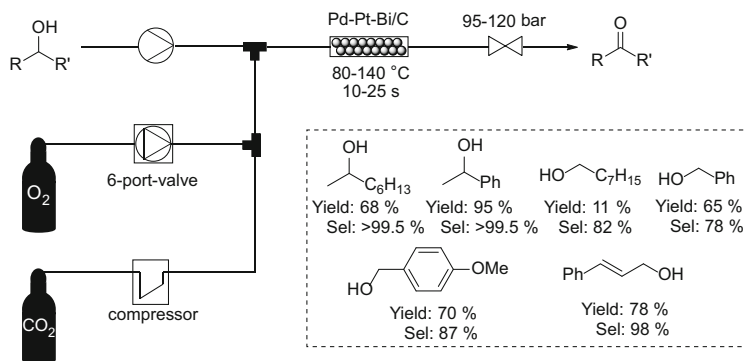
Scheme 10 Aerobic oxidation of alcohols in scCO$_2$

pulses at high pressure and constant frequency. Afterward, the CO$_2$/O$_2$ stream was combined with a liquid stream of the substrate (neat or with butanone as cosolvent) and the mixture was heated in a fixed-bed reactor filled with a precious metal catalyst (e.g., 4% Pd, 1% Pt, 5% Bi/C) at a back pressure of 95–120 bar. Several secondary alcohols could be oxidized to the corresponding ketones in good yields and selectivities within less than 30 s. The oxidation of primary alcohols required an internal stabilization by an aromatic system or unsaturated carbon–carbon bonds in order to give satisfactory results. Furthermore, accurate control of the oxygen concentration was crucial to avoid over-oxidation of the catalyst which could cause a dramatic reduction in activity. Under optimized conditions, neither catalyst deactivation nor metal leaching was observed.

A detailed investigation of all reaction parameters using 1- and 2-octanol as model substrates in the presence of Pd/Al$_2$O$_3$ using the same reactor showed that the oxidation of unstabilized primary alcohols is generally troublesome, while ketone synthesis from the corresponding secondary alcohols is straightforward and conversions up to 46% can be obtained at 140°C [86]. Good selectivity values for 1-octanol could be achieved at low conversion rates avoiding a subsequent hydration of the aldehyde which would result in a geminal diol which itself is prone to oxidative dehydration resulting in the corresponding carboxylic acid.

More recently, the group of Poliakoff reported an improved protocol using a supported platinum and bismuth catalyst [98]. Initial problems of catalyst over-oxidation due to inhomogeneous O$_2$ concentrations and formation of "hot spots" in the exothermic reaction were solved by dosing smaller volumes of O$_2$ via the 6-port valve and improving the CO$_2$/O$_2$ mixing prior to addition of the substrate. This strategy resulted in 75% conversion of 2-octanol without evidence for catalyst deactivation over 5 h at 150°C. A higher mass balance could be obtained using a catalyst-filled T-piece instead of a standard packed-bed reactor unit. Utilizing the final experimental design, several simple secondary alcohols were converted to the corresponding ketones in reasonable yields. Furthermore, the challenging oxidation of 1-octanol leading to the corresponding aldehyde in >70% yield could be realized by carefully optimizing temperature and equivalents of O$_2$ [98].

Notably, supported palladium was shown to be far more active than Pt or Ru in the selective oxidation of benzyl alcohol (**9**) [87]. In order to obtain *operando* structural analysis by X-ray absorption spectroscopy (XAS), the standard reactor design of the Baiker group (Scheme 10) was adapted for analytical applications (Fig. 2a) [88, 89, 96].

Miniaturization of the fixed-bed reactor and installation of two X-ray transparent beryllium windows on both sites of the catalyst compartment facilitated in situ measurements of the solid catalyst during aerobic oxidation of (**9**) in $scCO_2$. The continuous experiments indicated that palladium was mainly present in the metallic state during the overall process. As anticipated, the catalytic activity increased with the O_2 concentration since removal of adsorbed hydrogen (H_{ad}) originating from alcohol dehydration is accelerated (Fig. 2b). The reaction rate reaches a maximum and subsequently drops at higher oxygen concentrations. This was rationalized by the inhibiting effect of surface PdO_x species resulting from catalyst over-oxidation as analyzed by XAS.

A similar analytical reactor was further used for in situ EXAFS studies of aerobic benzyl alcohol and cinnamyl alcohol oxidations in O_2-saturated organic solvents, demonstrating that metallic palladium exhibits a higher activity for alcohol oxidation than the palladium oxide species [99–101].

In 2005, Leitner and colleagues realized that the palladium cluster $[Pd_{561}phen_{60}(OAc)_{180}]$ displays an active catalyst in the aerobic oxidation of alcohols in $scCO_2$ when embedded in a PEG-1000 matrix [102]. The active material was identified as highly dispersed Pd nanoparticles stabilized by the organic matrix. A similar catalyst could be also obtained by simply heating $Pd(acac)_2$ in PEG-1000 in the presence of a commercial surfactant. Benzyl alcohol (**9**) was chosen as model substrate for the development of a continuous process in a CSTR. It was shown that the aldehyde precursor and O_2 can be transported through the catalytic PEG phase without extrusion of the nanoparticles or the matrix material using $scCO_2$. With both Pd nanoparticle precursors, ~15% single-pass conversion with excellent
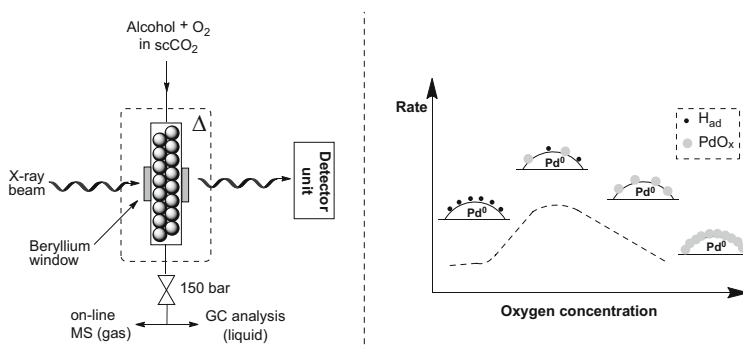
Fig. 2 (**a**) Packed-bed reactor for in situ XAS measurements of aerobic oxidation in $scCO_2$. (**b**) Simplified model for structure–activity relationship in Pd-catalyzed oxidation of benzyl alcohol (**9**)

selectivity was obtained at 80°C and 155 bar back pressure after isolating the product mixture in a cold trap. Notably, a steady increase in activity was observed during continuous operation over 40 h. Transmission electron microscopy (TEM) studies of the catalytic material formed from the Pd cluster indicated that the dispersion of the nanoparticles is significantly improved after a batch oxidation process explaining the increasing activity in the continuous long-run experiment (Fig. 3). However, reduction of the system pressure to 132 bar resulted in a twofold higher activity due to a shift of the partition coefficient of the substrate in the biphasic medium. This rationalization could be supported by the fact that the solubility of (**9**) became insufficient in $scCO_2$ when the back pressure is further decreased to 110 bar [102].

Based on these results the authors developed a well-defined Pd nanoparticle catalyst on a solid, inorganic matrix using PEG-modified silica surfaces for the application in a continuous packed-bed reactor [103]. Initially, a covalently anchored PEG phase (**12**) was synthesized by reacting 3-chloropropyltriethoxysilane (**11**) with polyethylene glycol 750 monomethyl ether in the presence of NaH (Scheme 11a). Copolymerization with tetraethoxysilane (TEOS) afforded the PEG-modified silica support (**13**) which was subsequently impregnated with a solution of $[Pd_{561}phen_{60}(OAc)_{180}]$ yielding the final catalytic material (**14**). The supported nanoparticles were shown to efficiently catalyze the aerobic oxidation of several secondary alcohols as well as benzylic and allylic primary alcohols to the corresponding ketones and aldehydes using $scCO_2$ in batch mode. A stainless steel packed-bed reactor was used for the translation to a continuous process, and good single-pass conversions (50–60% with a selectivity of >98%) were obtained for the benzyl alcohol oxidation within an estimated residence time of 1.2 h at 80°C and 150 bar. Importantly, a stable catalytic activity was observed during a 30 h experiment with a total turnover number of 1750. TEM analysis confirmed that the particles were effectively prevented from agglomeration by the covalently bound PEG chains.

In an alternative approach, 2,2′-dipyridylamine (**16**) was installed as a linker unit instead of PEG to immobilize and simultaneously stabilize the Pd nanoparticles on mesoporous silica for a catalytic aerobic oxidation in $scCO_2$ [104]. Similar to the

Fig. 3 TEM images of the catalytically active material formed from $[Pd_{531}phen_{60}(OAc)_{180}]$ and PEG-1000 before (**a**) and after (**b**) the aerobic oxidation. Reproduced with permission from [102]
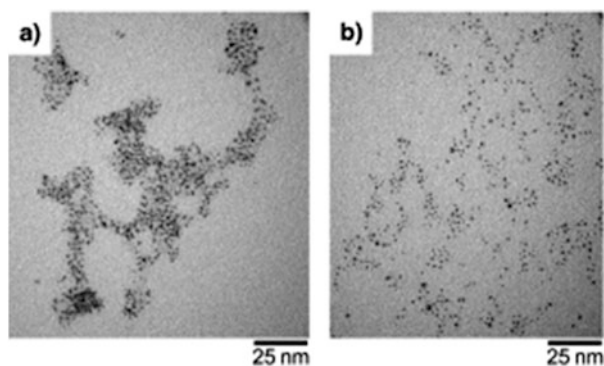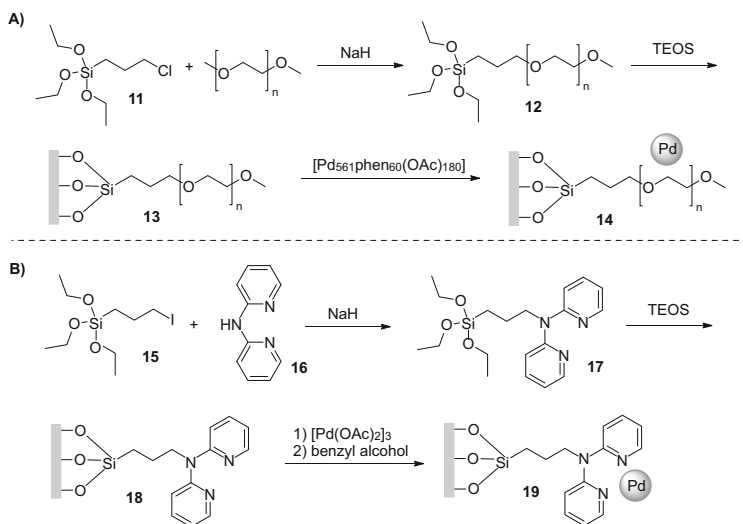
Scheme 11 Catalyst preparation using a PEG (**a**) and a 2,2′-dipyridylamine (**b**) unit for immobilization of Pd nanoparticles

immobilization technique discussed above, coupling of a trialkoxysilyl derivative (**15**) with (**16**) followed by addition of TEOS led to a functionalized mesoporous material (**18**) (Scheme 11b). Treatment with palladium acetate and subsequent reduction with benzyl alcohol under reflux yields the catalytically active supported nanoparticles (**19**). It has to be noted that significant amounts of unreduced Pd (II) were still present on the surface. An alternative reduction using molecular hydrogen on the one hand provided a higher degree of Pd(II) reduction but on the other hand resulted in a significantly decreased catalytic activity for the aerobic oxidation of benzyl alcohol in $scCO_2$. This could be explained by generation of small primary crystallites in case of the benzyl alcohol reduction leading to a large number of high-indexed planes in small-volume units. However, catalyst (**19**) showed good single-pass conversions (41% at a selectivity >98%) at temperatures as low as 60°C and remained constant over >28 h. Although at higher temperatures an increased activity was achieved, a significantly lower selectivity (90%) and leaching of catalytic material did not allow for further intensification.

4.3 Homogeneous Catalysis

Homogeneous catalysts are often superior compared to heterogeneous materials regarding their activity and selectivity. Furthermore, the possibility for fine-tuning of the active material by, for example, ligands often accesses a broader scope compared to metallic species or salts used in heterogeneous catalysis. Over the past years a plethora of effective aerobic oxidation protocols utilizing homogeneous

palladium or copper catalysis have been developed [49, 105, 106]. These contributions are almost exclusively small-scale laboratory reactions predominantly carried out in a flask equipped with an O_2-filled balloon. Apparently, the oxygen concentration in the liquid solution is relatively low and mixing of the different phases is rather poor. This is especially problematic for homogeneous palladium catalysis as the catalyst stability is highly sensitive to the dissolved oxygen concentration. Even temporary periods of poor gas/liquid mixing can lead to catalyst decomposition via agglomeration of homogeneous Pd(0) complexes forming metallic palladium [107].

In order to tackle these mechanistic challenges and simultaneously providing a scalable aerobic oxidation protocol, a continuous approach was developed by the Stahl group together with chemists from Eli Lilly (Scheme 12) [108]. Translation of the batch protocol using catalytic amounts of Pd(OAc)$_2$ and pyridine was realized toward a three-feed methodology. To avoid the abovementioned reduction or decomposition of the catalyst, a solution of Pd(OAc)$_2$ was initially mixed with oxygen. Subsequently, the substrate as well as pyridine enter the flow system via a second mixing unit before the central coil reactor. A residence time of 2.5 h was necessary to oxidize several secondary and benzylic primary alcohols to the corresponding carbonyl compounds on a multi-gram scale using diluted oxygen (8% in N_2). Furthermore, the synthesis of benzaldehyde (6) was carried out on a kilogram scale using a 7 L stainless steel coil as residence time unit highlighting the reliability of the flow reactor for large-scale applications.

However, all alcohol oxidations discussed so far were limited to secondary alcohols or stabilized primary alcohols due to over-oxidation of unstabilized derivatives to the corresponding carboxylic acid. This limitation can be elegantly circumvented by the well-established homogeneous copper-catalyzed aerobic oxidation protocol developed by Stahl using a catalytic mixture of Cu(OTf)$_2$, 2,2′-bipyridine, TEMPO, and NMI [49]. Similar reactor concepts as for the Pd-catalyzed protocol were used in order to test the feasibility of the copper-based system for continuous purposes [109, 110]. Importantly, a stainless steel syringe pump and storage unit for the catalyst mixture caused severe problems since a significant drop in catalytic activity was observed [109]. This was attributed to a reaction of the catalyst material with stainless steel. Thus, the authors modified the experimental setup by replacing steel units by, for example, PTFE-based
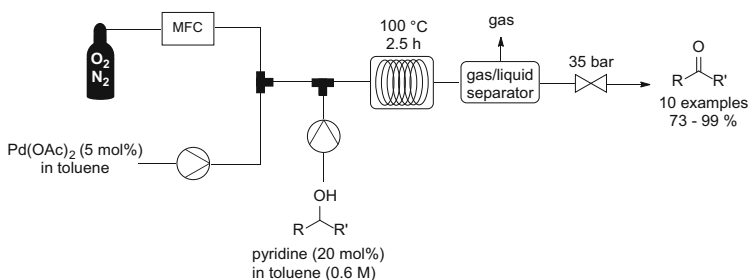
Scheme 12 Aerobic oxidation of alcohols using homogeneous Pd catalysis in flow

equipment. A range of aliphatic alcohols could be almost quantitatively converted into the corresponding aldehydes at 60°C within 30–45 min (Table 1). Moreover, stabilized alcohols were selectively oxidized within only 5 min at 100°C showing the tremendous activity of the Cu(I)/TEMPO strategy compared to palladium catalysis.

Root and colleagues used this copper-catalyzed protocol to test an inexpensive variant of the tube-in-tube reactor by utilizing simple PTFE instead of the costly Teflon AF-2400 as gas-permeable membrane material [111]. Their reactor design consisted of a PTFE tubing coiled into a stainless steel shell (tube in shell, Scheme 13). An oxygen bottle was connected to the "shell" and the whole reactor unit was heated. Under elevated conditions (100°C), the oxygen permeability of the PTFE tubing was high enough to convert a 0.2 M solution of primary or secondary alcohols within only 1 min residence time. The scalability was also demonstrated in a multi-tube membrane reactor by mounting 13 PTFE tubes in a pressure vessel. This numbering-up approach could be used to oxidize 10 g of benzyl alcohol within

Table 1 Scope of the Cu(I)/TEMPO catalyzed aerobic oxidation in flow
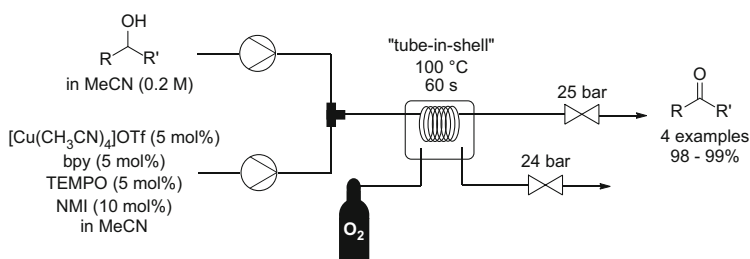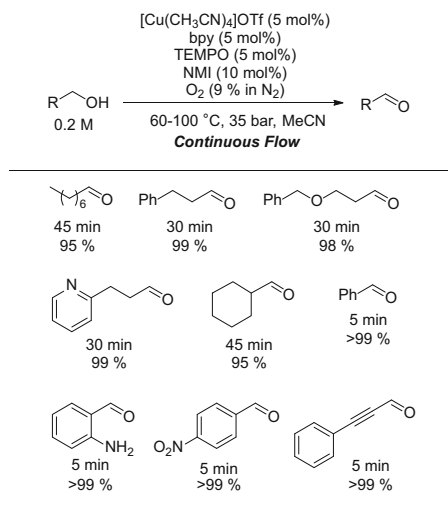
Scheme 13 Cu(I)/TEMPO catalyzed aerobic oxidation of alcohols using in a tube-in-shell reactor

a total processing time of 45 min instead of 21 h in the single-tube reactor. Furthermore, the authors used the prototype tube-in-shell reactor as gas-loading unit prior to a packed-bed reactor filled with $RuOH_x/Al_2O_3$ in a heterogeneously catalyzed oxidation of benzyl alcohol to highlight its versatility for multiple applications.

Albeit this method exemplifies a potential alternative to expensive gas-permeable membrane materials such as Teflon AF-2400, the utilization of PTFE, PFA, or other common tubing materials is presumably limited to applications at relatively harsh conditions since the gas permeability of these material strongly depends on the temperature. Thus, reactions at room temperature or below might not be feasible or would require extremely diluted conditions to maintain a proper stoichiometry.

5   Oxidation of Aldehydes

Aldehydes are produced on an enormous scale typically from olefins and syngas (CO/H_2) via hydroformylation (oxo process) [112]. These valuable compounds are further used in the synthesis of several bulk chemicals such as alcohols, amines, or carboxylic acids (and their corresponding esters). The latter are usually obtained via liquid-phase aerobic oxidation processes either in presence of a metal catalyst or following catalyst-free strategies [113]. Catalytic oxidations of aldehydes are interesting model reactions for gas/liquid microreactors since the transformations generally are quite fast and selective [114, 115]. As an example, Hessel and coworkers used the oxidation of butyraldehyde to test the reliability of a mathematical reactor model for predicting conversions in a microbubble column based on hydrodynamic information and transport modeling [114].

A heterogeneously catalyzed oxidation of 4-isopropoxybenzaldehyde using Pt/Al_2O_3 in a single-channel silicon–Pyrex reactor was carried out by Jensen and colleagues (Fig. 4) [115]. An initial temperature screening showed an optimum temperature of 90°C. The molar ratio of O_2 to the substrate was optimized by varying the liquid flow at constant flow rate of the gaseous oxidant. An O_2/substrate

Fig. 4 (a) Single-channel packed-bed reactor for heterogeneously catalyzed aldehyde oxidations. (b) Front view showing the catalyst bed. Reproduced with permission from [115]
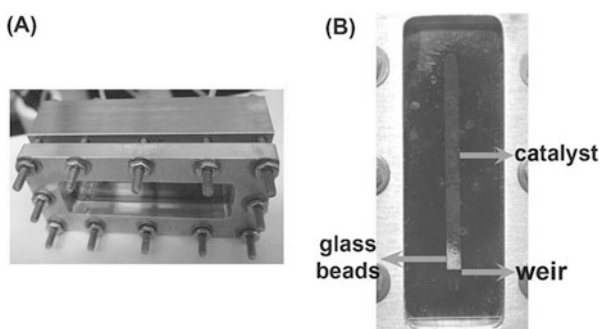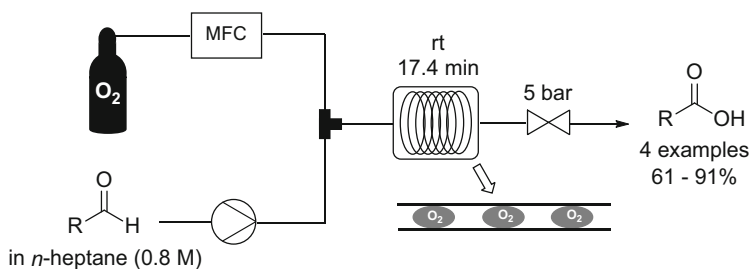
Scheme 14 Catalyst-free aerobic oxidation of aldehydes at room temperature

ratio of 1.5 was sufficient to obtain 95% conversion to the corresponding carboxylic acid within less than 6 s. Replacement of O_2 by compressed air at the same O_2/substrate ratio gave a conversion of only 76% since the gas flow had to be increased resulting in a shorter contact time (~1 s). In order to obtain a higher residence time and a better conversion, the liquid flow had to be decreased. This increased the amount of O_2 by a factor of ~5 compared to the substrate.

The group of Favre-Réguillon could show that the aerobic oxidation of reactive aliphatic aldehydes can be carried out in a segmented flow pattern without the need of adding any catalytically active material at room temperature (Scheme 14) [116]. To maintain mild conditions, catalytic amounts of a Mn(II) salt (100 ppm) were added in the oxidation of less reactive substrates. More recently, these authors established a synergistic effect of Mn(II) catalyst and a large range of salts as additives improving both the reaction rate and selectivity for the oxidation of aldehydes [117].

6 Oxidative Carbon–Carbon Coupling Reactions

Metal-catalyzed coupling reactions are undoubtedly among the most widely used reactions to construct carbon–carbon or carbon–heteroatom bond. Among those, palladium-catalyzed cross coupling reactions have a significant impact on the synthesis of pharmaceuticals, agrochemicals, and natural products due to their high selectivity and functional group tolerance [118]. Over the past years, a plethora of examples were translated from conventional batch regimes into flow approaches allowing for continuous manufacturing [119, 120].

The oxidative Heck reaction (Fujiwara–Moritana reaction) is of special interest since it does not require an electrophilic (pseudo)halide. This avoids the formation of stoichiometric amounts of the corresponding salts which typically cause extensive environmental pollution [121, 122]. From a mechanistic point of view, these transformations involve catalytic amounts of a Pd(II) species which initially undergoes an oxidative addition of the nucleophile followed by coordination of an alkene, β-hydride elimination, and reductive elimination of the desired product.

To close the catalytic cycle, the resulting Pd(0) species has to be reoxidized by, for example, molecular oxygen [121, 122]. It is therefore not surprising that several researchers have recognized the potential of continuous gas/liquid processing for this versatile coupling strategy.

In their seminal contribution, Park and Kim established a membrane-based dual-channel microreactor for the oxidative Heck reaction of arylboronic acids and alkenes under continuous flow conditions (Scheme 15a) [123]. In a typical dual-channel setup, one of the channels carries the liquid feed containing the substrates and the catalyst, while the other channel is fed with O_2. The oxidant diffuses through a permeable poly(dimethylsiloxane) (PDMS) membrane separating the two channels thus providing a continuous supply of the gaseous reagent. PDMS is reasonably stable in polar organic solvents such as DMF, DMSO, or acetonitrile, but many common nonpolar solvents diffuse into the PDMS polymer and cause the material to swell. However, the authors demonstrated that good conversions can be obtained within 30 min at room temperature using their experimental setup. A comparison of the results of oxidative couplings in the dual-channel reactor with a simple single-channel reactor using a segmented flow showed slightly better conversions as well as higher selectivity for the desired product using the membrane concept.

In a related approach Park and coworkers applied the tube-in-tube reactor for an oxidative Heck coupling of arylboronic acids with cyclohex-2-enone and its subsequent oxidative dehydrogenation to the corresponding phenol [124]. Excellent yields were observed at 70°C for various arylboronic acids at residence times of just
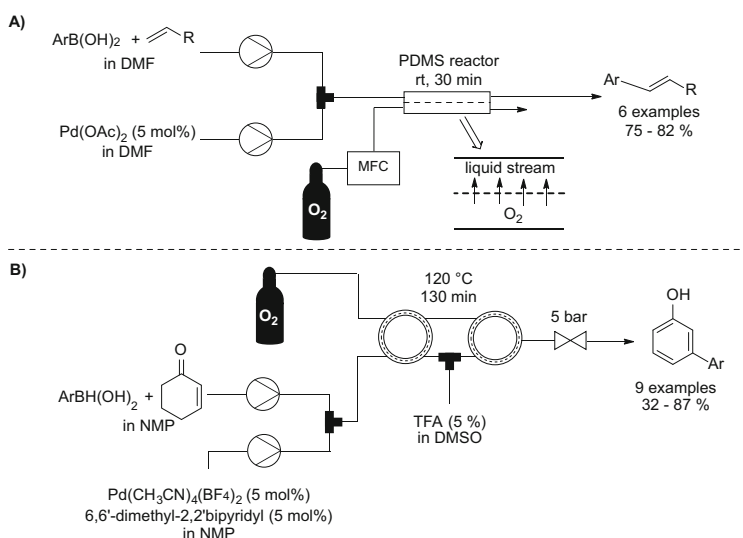
Scheme 15 (**a**) Dual-channel reactor for oxidative Heck reactions in continuous flow. (**b**) Oxidative Heck reaction followed by oxidative dehydrogenation in a sequence of tube-in-tube reactors

20 min. A comparison of the oxidative coupling of 4-methxyphenylboronic acid and cyclohex-2-enone under identical conditions (20 min, 70°C) gave excellent isolated yields for the continuous approach (92%) in contrast to a classical batch reaction (20%) clearly showing the benefits of continuous gas/liquid processing. The authors put great efforts into the development of an oxidative dehydrogenation protocol for the transformation of the coupling product to the corresponding phenol. Long reaction times (120 min) were required in order to obtain sufficient conversions at 120° and a back pressure of 5 bar in presence of TFA. Gratifyingly, after further optimization studies a combination of both steps using a sequence of tube-in-tube reactors was applicable resulting in a single continuous process at 120°C with two consecutive reactions involving O_2 (Scheme 15b).

It is worth noting that the oxidative Heck coupling is not only limited to arylboronic acids as nucleophilic reagent. As an alternative strategy, Leadbeater et al. optimized the reaction conditions for the decarboxylative Heck reaction of 2,6-dimethoxycinnamic acid (**20**) and methyl acrylate (**21**) utilizing microwave irradiation in batch [125]. A direct translation of the optimized protocol (140°C, 30 min) was not feasible using the tube-in-tube technique. After a reevaluation in flow, a residence time of 2 h at 140°C was found to be necessary to obtain satisfying yields of the coupling product (**22**) (Scheme 16a). However, the process suffers from some limitations as other alkenes such as styrene or acrylonitrile were prone to decomposition. This resulted in the formation of large amounts of undesired by-products under the relatively harsh reaction conditions.

The continuous cross dehydrogenative Heck reaction of olefins and indoles has recently been described by Noel and coworkers using a coil reactor setup (Scheme 16b) [126]. A solution of the indole and TFA was first mixed with the alkene in a mixing unit. Afterward, oxygen was added using a mass flow controller
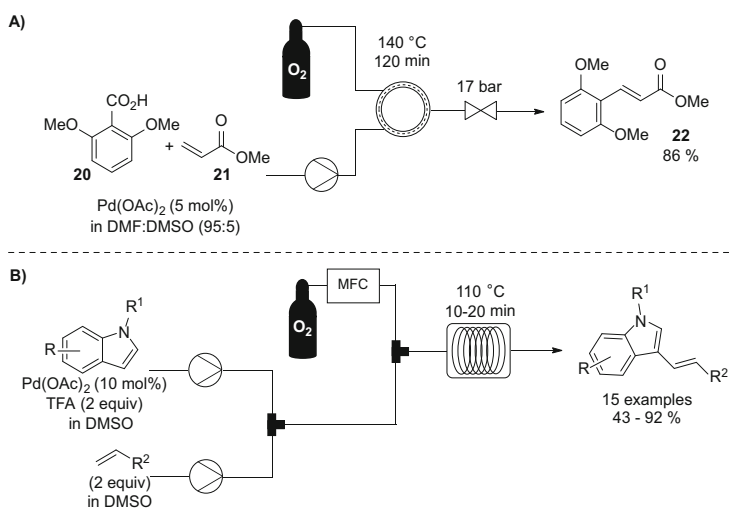
Scheme 16 (**a**) Decarboxylative oxidative Heck-type coupling in a tube-in-tube reactor. (**b**) Cross dehydrogenative coupling of indoles and olefins using molecular oxygen

and another static T-mixer. The utilization of high-boiling DMSO allowed for a continuous process without the need of a back-pressure controlling unit. A short residence time of 10–20 min was demonstrated to be sufficient to generate a broad range of coupling products at 110°C using a segmented flow pattern, while higher temperatures caused decomposition of the catalytically active material. Importantly, control experiments in batch showed that very long reaction times (4 h) were necessary to obtain full conversion of the starting materials. Moreover, significantly lower yields were obtained in batch mode presumably due to indole decomposition as a result of the long reaction times.

In addition to the Pd-catalyzed cross coupling protocols discussed above, the Ley group demonstrated the applicability of their tube-in-tube membrane reactor for copper-catalyzed Glaser–Hay acetylene homocouplings (Scheme 17a) [127]. An oxygenated solvent stream was merged with a pre-combined solution of the terminal alkyne and catalytic amounts of $CuOTf(MeCN)_4$ and TMEDA. The combined mixture then entered a coil reactor heated at 100°C. Several aromatic alkynes resulted in good to excellent yields after 17 min reaction time. In case of aliphatic derivatives, 25 mol% of DBU had to be added in order to obtain satisfying results. Scavenger cartridges were used for in-line purification of the generated 1,3-butadienes. Immobilized thiourea was packed into a cartridge to remove the copper catalyst and polymer-supported sulfonic acid neutralized remaining TMEDA to avoid purification by column chromatography.

In 2015, a combination of a tube-in-tube membrane reactor followed by a residence time coil was utilized in an iron-catalyzed aerobic nitro-Mannich reaction via a radical pathway by the group of Polyzos (Scheme 17b)[128]. A process intensification study resulted in a 2 h protocol using 10 mol% of $FeCl_2$ as catalyst, while the original batch protocol required 5–7 days for similar results [129].
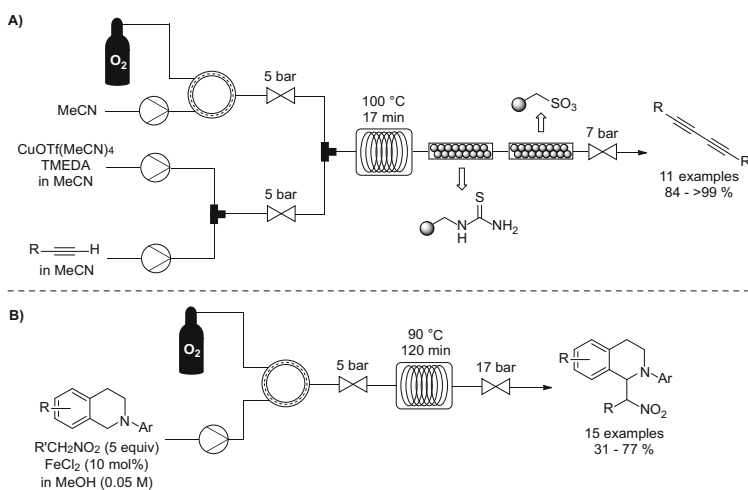
Scheme 17 Tube-in-tube-based continuous flow setups for (**a**) a Glaser–Hay coupling for the synthesis of symmetric 1,3-butadiynes and (**b**) the iron-catalyzed aerobic nitro-Mannich reaction

7 Miscellaneous

The fact that alkyl Grignard reagents can be oxidized by O_2 to produce the corresponding alcohols has been known for more than a hundred years [130]. Aerobic oxidation of the analogous aryl Grignard compounds often results in complex reaction mixtures resulting from poor selectivity for the desired phenols due to the low reactivity of the aryl radicals intermediates toward O_2 [131, 132].

In 2014, Jamison and coworkers hypothesized that the high surface-to-volume ratio of a continuous flow reaction in combination with the faster heat and mass transfer may enhance the reactivity and thus provide a general strategy for the synthesis of valuable phenols [133]. A simple two-feed flow reactor was assembled to evaluate this theory (Scheme 18a). Under optimized conditions ($-25°C$, 17 bar, 3.4 min) several electron-rich or electron-deficient aryl magnesium bromides and even heteroaryl magnesium reagents could be successfully converted into the corresponding phenols in good yields using pressurized air as oxygen source. Noteworthy, oxidation-sensitive functional groups such as alkenes, anilines, tertiary amines, and thiol ethers were tolerated illustrating the broad applicability of this methodology. Furthermore, the authors were able to expand their continuous system by generating *ortho*-substituted aryl magnesium compounds prior to the oxidation (Scheme 18b).
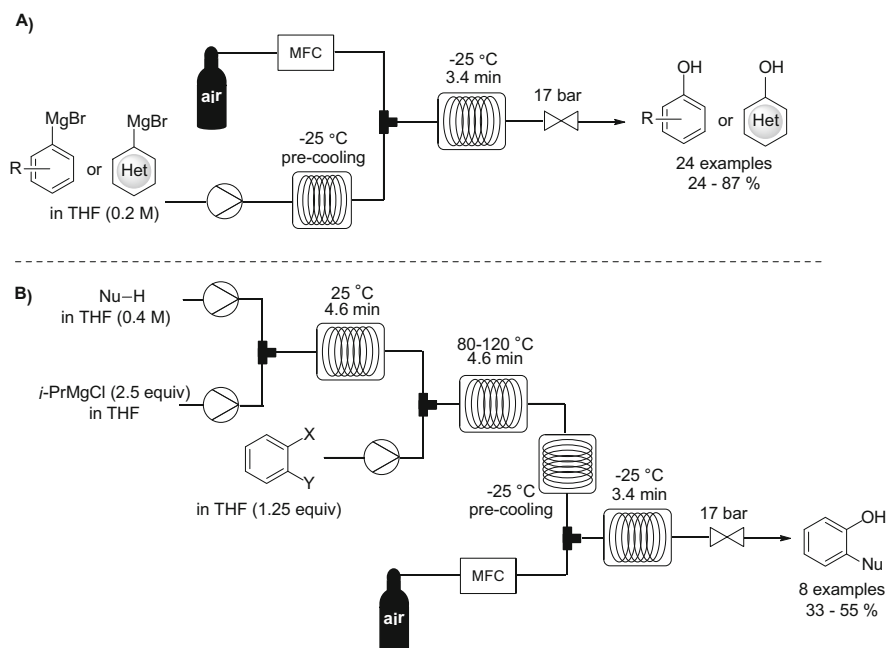
Scheme 18 Aerobic oxidation of aryl Grignard reagents in single-step flow procedure (**a**) and in a telescoped three-step process (**b**)

The aromatic hydroxyl group synthesized via this oxidation strategy is undoubtedly an important structural motif in several relevant compounds. Among them, the simplest molecule, phenol, is produced on an enormous scale via several industrial routes starting from cumene, chlorobenzene, benzene, or toluene [134]. In case of the latter raw material, aerobic oxidation generates benzoic acid which is further oxidized to phenol (Dow phenol process). The second step was studied by Poliakoff using heterogeneous catalysis in water under high-temperature/high-pressure continuous flow conditions [135]. The general setup involving hydrogen peroxide decomposition to in situ generate oxygen was already thoroughly discussed in Sect. 3 (Scheme 2). The main difference to their earlier contributions is that the heated coil was replaced by a packed-bed reactor to evaluate various heterogeneous materials for their applicability in this industrially relevant process. Among the tested catalysts, Carulite® showed promising activity and high robustness at 350°C and 200 bar for the selective formation of phenol in this proof-of-concept study.

The researchers additionally used this setup in studies on the oxidative dehydrogenation of 4-vinylcyclohexene to yield ethylbenzene catalyzed by Pd/Al$_2$O$_3$[136]. Unfortunately, total oxidation to CO$_2$ was to a large extent observed at 420°C and 90 bar. This could be rationalized by periodic temperature spikes at the catalyst bed indicating flame propagation due to the extremely harsh conditions.

Oxygen is not exclusively applied for the oxidation of hydrocarbons and specific functionalities or to reoxidize a catalyst but also in the generation of the highly reactive species diimide (N$_2$H$_2$) from hydrazine, which subsequently acts as selective reducing agent for unpolarized carbon–carbon double bonds [137, 138]. Since the initial oxidation step is rather slow under laboratory batch conditions, catalysts are usually added in order to provide a feasible experimental protocol. Kappe and coworkers could show that a continuous flow protocol in a high-temperature/high-pressure regime significantly enhances this process and thus eliminates the need for a catalyst [139, 140]. In the original procedure, an organic stream consisting of an olefin and hydrazine hydrate in n-propanol was mixed with oxygen resulting in a segmented flow pattern which is heated in a residence time unit to 100–120°C at a back pressure of 20 bar [139]. Reaction times of 10–30 min were sufficient to selectively reduce various terminal and internal carbon–carbon double bonds. Since nitrogen gas and water were the only by-products, most saturated compounds could be isolated simply by evaporation of the solvent.

By studying the hydrazine oxidation in more detail, the authors developed a strategy for more challenging substrates such as artemisinic acid (**23**) to obtain the direct precursor molecule (**24**) of the anti-malaria drug artemisinin (Scheme 19) [140].

Key to the success was the multiple additions of small portions of hydrazine hydrate to reduce the disproportionation of the reactive intermediated diimide and circumvent its complete over-oxidation in a single coil. In addition, the temperature could be reduced to 60°C in order to obtain high selectivity and diastereomeric ratio. Notably, a comparison with the catalyst-free batch reduction of the same compound at 40°C demonstrated significantly longer reaction times (11 h) in order to obtain similar values for isolated yield and product purity [141].
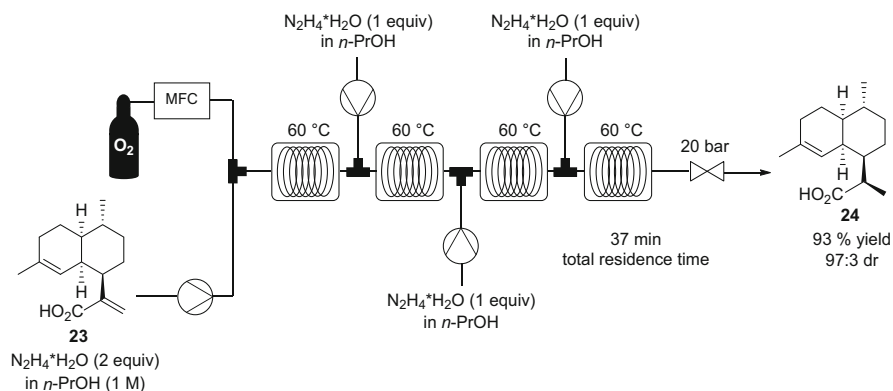
Scheme 19 Selective reduction of artemisinic acid (**23**) by in situ generated diimide

8 Photochemical Reactions Involving Molecular Oxygen

A serious issue coming along with photochemical transformations – especially on larger scales – is arising from the logarithmic decrease with path length of the transmission of light through a liquid medium (Lambert−Beer law) resulting in inefficient irradiation of the entire reaction mixture. This severe limitation in conventional batch processes can be addressed using continuous flow processing [142, 143]. The large surface-to-volume ratio which is typically present using this enabling technology ensures a highly increased irradiation efficiency of the entire solution often resulting in significantly intensified protocols. Apparently, such a process using oxygen as reagent is well suited for continuous flow processing since it offers advantages in both gas/liquid processing and photochemistry.

Noël and coworkers used oxygen in a photocatalytic oxidation of thiols to generate the corresponding symmetric disulfides [144, 145]. Initial batch experiments revealed that a combination of eosin Y as catalyst and stoichiometric amounts of TMEDA can facilitate this oxidation in the presence of oxygen [144]. Mechanistically, the photosensitizer is excited by visible light and subsequently activates the thiol by generating a thiyl radical. This key step is proposed to be facilitated by the base as demonstrated in kinetic experiments. Oxygen is used to reoxidize [eosin Y]$^-$ via single-electron transfer (SET) in order to close the catalytic cycle. The continuous strategy is based on a simple two-feed setup using a mass flow controller to control the O$_2$ stream. The resulting segmented flow pattern entered a PFA capillary which was irradiated by white LED light for 20 min to convert various simple thiols to the corresponding disulfidein excellent yield (87–99%). Furthermore, the authors put great effort in demonstrating the versatility of their strategy in an intramolecular peptide coupling affording the hormone oxytocin in a short residence time of 200 s (Scheme 20).

The single-electron transfer from a reduced photocatalyst and oxygen is not only interesting for the reoxidation of the catalytic species but also for generating a
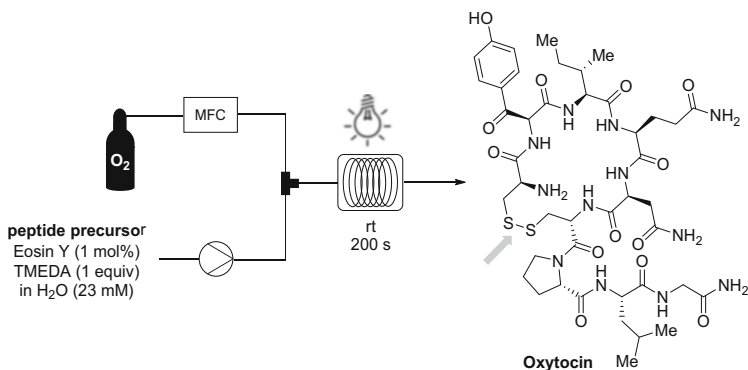
Scheme 20 Continuous photochemical disulfide formation to produce oxytocin

superoxide radical ($O_2^{.-}$). This reactive oxygen species is able to react with aryl boronic acids selectively generating the corresponding phenols [146]. Safety concerns and long reaction times in batch forced George and coworkers to intensify this process under flow conditions using air as oxygen source [147]. The gaseous oxidant was mixed with the liquid feed and irradiated with white LEDs in a tubular sapphire photo reactor filled with glass beads to promote gas/liquid mixing. With the aid of continuous processing under high-pressure regimes, the original catalyst $[Ru(bpy)_3Cl_2] \cdot 6H_2O$ could be replaced by the inexpensive organic dye Rose Bengal and the solvent (DMF) was substituted by a more sustainable ethanol–water mixture. Notably, a continuous reaction at 20 bar gave a quantitative reaction with a 90-fold higher productivity than the batch control experiment.

Another versatile reactive dioxygen species is singlet oxygen ($^1O_2$) which can be generated either through chemical processes or, more commonly, by photoexcitation of molecular oxygen in the presence of a photosensitizer [148]. Even though singlet oxygen is rather widely used in contemporary organic synthesis, its application in the pharmaceutical industry on a large scale has not yet proven to be feasible. In 2002, de Mellow and coworkers demonstrated that microreactor technology is a promising tool to tackle this limitation [149]. In their pioneering work, a solution of Rose Bengal and terpinene (**25**) in methanol was mixed with oxygen in a glass chip reactor irradiated by a tungsten lamp (Scheme 21). Both, the gaseous and the liquid stream were controlled by using gas-tight syringe pumps resulting in residence times of approximately 5 s. Within this short residence time, 85% conversion to ascaridole (**26**) was observed.

Prompted by these encouraging results, a multitude of reactor designs – including microfluidic chip reactors [150], falling-film reactors [151], dual- and triple-channel microreactors [152, 153], coil-based devices [154, 155], gas-permeable micro-capillary films [156], and tube-in-tube membrane devices [157] – were subsequently applied for the generation and subsequent utilization of $^1O_2$ in gas/liquid continuous flow regimes using well-known photosensitizers such as Rose Bengal, methylene blue, and porphyrins. Furthermore, it was shown that
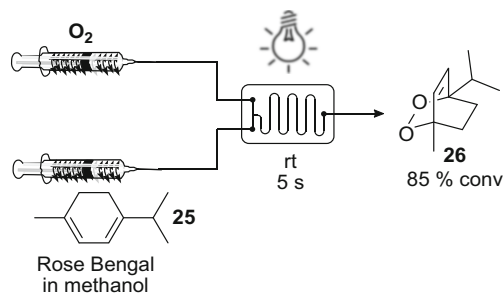
Scheme 21 Generation of singlet oxygen for the synthesis of ascaridole (**26**) from α-terpinene (**25**)
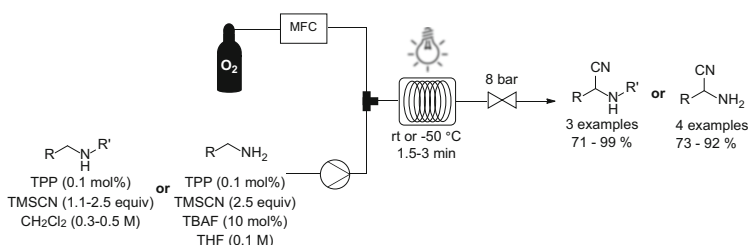
Scheme 22 Oxidation of amines to imines with singlet oxygen in continuous flow and subsequent trapping to yield α-aminonitriles

porphyrins can be immobilized on the channel wall of a glass microreactor to heterogeneously catalyze the formation of the reactive oxygen species [158].

In this context Seeberger and coworkers developed a procedure for the oxidation of primary and secondary amines to the corresponding imines in continuous flow using singlet oxygen which was generated using low amounts of *meso*-tetraphenylporphyrin (TPP) [159–162]. The imines generated from secondary amines immediately resulted in the corresponding α-aminonitriles in good to excellent isolated yields at room temperature using CH_2Cl_2 as solvent in the presence of trimethylsilyl cyanide as trapping agent (Scheme 22) [159].

When primary amines were subjected to these conditions, an oxidative homo-coupling resulting in the corresponding N-substituted imines was observed. The authors found that primary amines could be converted to α-aminonitriles in a selective manner by switching from CH_2Cl_2 to THF as solvent at significantly lower temperatures (−50°C) adding sub-stoichiometric amounts of TBAF to activate the TMSCN. The concept was further expanded for the synthesis of α-cyanoepoxides and fluorinated α-amino acids [160, 162].

Oxygen, and especially singlet oxygen, plays an important role in the (semi-) synthesis of the anti-malaria drug artemisinin. In the previous chapter, the reduction of artemisinic acid (**23**) to dihydroartemisinic acid (**24**) utilizing O_2 and hydrazine was already discussed [140]. The reduced compound (**24**) forms an allylic hydroperoxide in the presence of $^1O_2$ which subsequently undergoes an acid-promoted Hock cleavage and oxidation by O_2. This triggers a spontaneous cascade of

condensation reactions generating artemisinin (**27**). Seeberger and coworkers performed the whole reaction sequence as a single, fully continuous process using a sequence of coil reactors (Scheme 23) [163, 164]. Under optimized conditions, a mixture of (**24**), TFA, and catalytic amounts of 9,10-dicyanoanthracene in toluene were mixed with pure O_2 and passed through the photoreactor at $-20°C$ [164]. The reactor unit consisted of FEP tubing wrapped around a glass plate which was immersed in a cooling bath. A LED module was mounted at a fixed distance in front of the reactor to efficiently irradiate the solution. Afterward, the mixture was slowly heated in to consecutive coils to accomplish the acid-catalyzed Hock cleavage, the oxidation and the condensation cascade resulting in (**27**) in good selectivity. Extraction and recrystallization gave 46% of the final anti-malarial drug. The continuous protocol was subsequently expanded to a modular multistep approach to access various pharmaceutically active derivatives of (**27**) [165].

George and coworkers thoroughly studied the applicability of $scCO_2$ as solvent for the continuous generation and utilization of $^1O_2$ in a tubular sapphire reactor using homogeneous and immobilized photosensitizers [166–171]. Their findings recently led to a more sustainable strategy for the continuous synthesis of artemisinin (**27**) using liquid CO_2 and a solid catalyst (Scheme 24) [172]. Thus,
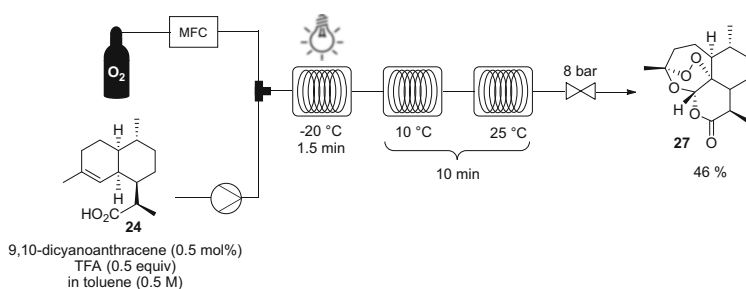
Scheme 23 Synthesis of artemisinin (**27**) from dihydroartemisinic acid (**24**) in continuous flow
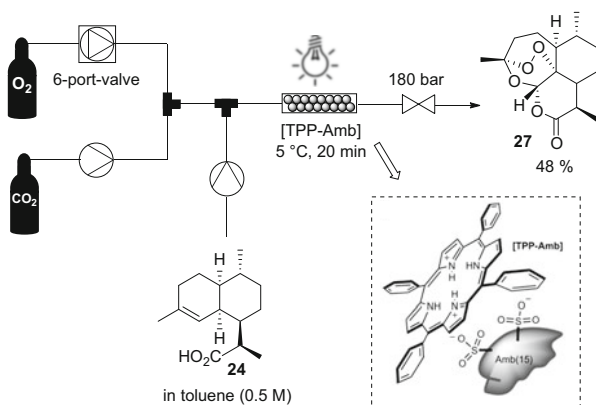
Scheme 24 Synthesis of artemisinin (**27**) in liquid CO_2 using a dual-function solid catalyst. Adapted with permission from [172]

meso-tetraphenylporphyrin was anchored onto the ion-exchange resin Amberlyst 15 resulting in [TPP-Amb]. This elegant dual catalyst system combines the ability to facilitate the generation of singlet oxygen as well as the Brønsted-acid mediated Hock cleavage to generate **27**. In the final continuous protocol, O_2 was mixed with CO_2 using a dosing technique (see Sect. 4.2). Afterward a solution of (**24**) in toluene was added via a second mixing unit at a back pressure of 180 bar. The final reaction mixture was passed through the tubular sapphire tube reactor containing the dual-function solid catalyst at 5°C. The whole reactor unit is subjected to irradiation by light in the visible region using an array of LEDs. A residence time of 20 min was sufficient to fully convert dihydroartemisinic acid (**24**) and obtain similar yields to the homogeneously catalyzed process discussed above.

In addition, the authors presented a second sustainable continuous strategy utilizing aqueous solvent mixtures to obtain up to 66% of artemisinin (**27**) by using [Ru(bpy)$_3$]Cl$_2$ as catalyst in the presence of TFA in THF:H_2O (6:4) [172].

9   Concluding Remarks

The utilization of oxygen in continuous flow environments offers several advantages compared to conventional batch techniques and a broad range of oxidation reactions have been studied using this enabling technology. The main drivers are on the one hand that safety concerns can be significantly reduced when working with a continuous flow (micro-)reactor. Exothermic reactions are easily controlled by the excellent mass and heat transfer and the small volumes and channel dimensions minimize the possibility for propagation of an explosion inside the reactor even under extreme conditions. On the other hand, working at elevated temperatures and, more importantly, at high pressures can be easily achieved often resulting in improved and highly intensified oxidation protocols. Thus, especially aerobic oxidation protocols using supercritical solvents are predominantly studied in continuous environments.

Several technologies and reactor designs have been developed in the past to perform reactions involving oxygen in order to meet these demands. Liquid-phase oxidations are typically carried out by using a mass flow controlling unit or membrane reactors to deliver the gaseous reagent. In case of supercritical solvents, dosing techniques are often applied due to the high system pressures. However, a universal reactor design does not exist and all reaction parameters have to be taken into account for developing a suitable continuous flow reactor. Thus, strong collaborations between chemists and process engineers are of utmost importance for this rapidly growing area.

The application of continuous flow has already reached widespread use for the aerobic oxidation of specific functional groups such as alcohols in order to replace expensive and often toxic reagents thus providing more sustainable alternatives. Furthermore, in recent years a clear trend to other applications such as oxidative coupling reactions or photochemical applications can be observed. Since

continuous processing is gaining increasing attention by synthetic chemists, it is apparent that entirely new synthetic routes will be developed on a more routine basis by using this enabling technology. Therefore, flow chemistry can potentially help to access more selective strategies and better (catalytic) systems which are hardly feasible in traditional batch equipment. Flow chemistry on laboratory scale is not only used to enhance aerobic oxidations developed in batch but also to get deeper insights into industrial processes and reaction mechanisms of well-known transformations.

References

1. Allen SE, Walvoord RR, Padilla-Salinas R, Kozlowski MC (2013) Chem Rev 113:6234
2. Campbell AN, Stahl SS (2012) Acc Chem Res 45:851
3. Cao Q, Dornan LM, Rogan L, Hughes NL, Muldoon MJ (2014) Chem Commun 50:4524
4. Davis SE, Ide MS, Davis RJ (2013) Green Chem 15:17
5. Wendlandt AE, Suess AM, Stahl SS (2011) Angew Chem Int Ed 50:11062
6. Osterberg PM, Niemeier JK, Welch CJ, Hawkins JM, Martinelli JR, Johnson TE, Root TW, Stahl SS (2015) Org Process Res Dev. doi:10.1021/op500328f
7. Hessel V, Kralisch D, Kockmann N, Noel T, Wang Q (2013) ChemSusChem 6:746
8. Wiles C, Watts P (2014) Green Chem 16:55
9. Vaccaro L, Lanari D, Marrocchi A, Strappaveccia G (2014) Green Chem 16:3680
10. Jensen KF, Reizman BJ, Newman SG (2014) Lab Chip 14:3206
11. Pastre JC, Browne DL, Ley SV (2013) Chem Soc Rev 42:8849
12. McQuade DT, Seeberger PH (2013) J Org Chem 78:6384
13. Baxendale IR, Brocken L, Mallia CJ (2013) Green Process Synth 2:211
14. Gutmann B, Cantillo D, Kappe CO (2015) Angew Chem Int Ed 54:6688
15. Jahnisch K, Hessel V, Lowe H, Baerns M (2004) Angew Chem Int Ed 43:406
16. Inoue T, Schmidt MA, Jensen KF (2007) Ind Eng Chem Res 46:1153
17. Noel T, Hessel V (2013) ChemSusChem 6:405
18. Kolb G, Hessel V, Cominos V, Hofmann C, Lowe H, Nikolaidis G, Zapf R, Ziogas A, Delsman ER, de Croon MHJM, Schouten JC, de la Iglesia O, Mallada R, Santamaria J (2007) Catal Today 120:2
19. Roydhouse MD, Ghaini A, Constantinou A, Cantu-Perez A, Motherwell WB, Gavriilidis A (2011) Org Process Res Dev 15:989
20. Nobis M, Roberge DM (2011) Chim Oggi 29:56
21. Irfan M, Glasnov TN, Kappe CO (2011) Org Lett 13:984
22. Brzozowski M, O'Brien M, Ley SV, Polyzos A (2015) Acc Chem Res 48:349
23. Yang L, Jensen KF (2013) Org Process Res Dev 17:927
24. Munirathinam R, Huskens J, Verboom W (2015) Adv Synth Catal 357:1093
25. Schmieder H, Abeln J (1999) Chem Eng Technol 22:903
26. Tomas RAF, Bordado JCM, Gomes JFP (2013) Chem Rev 113:7421
27. Hamley PA, Ilkenhans T, Webster JM, Garcia-Verdugo E, Venardou E, Clarke MJ, Auerbach R, Thomas WB, Whiston K, Poliakoff M (2002) Green Chem 4:235

28. Garcia-Verdugo E, Venardou E, Thomas WB, Whiston K, Partenheimer W, Hamley PA, Poliakoff M (2004) Adv Synth Catal 346:307
29. Fraga-Dubreuil J, Garcia-Verdugo E, Hamley PA, Vaquero EM, Dudd LM, Pearson I, Housley D, Partenheimer W, Thomas WB, Whiston K, Poliakoff M (2007) Green Chem 9:1238
30. Garcia-Verdugo E, Fraga-Dubreuil J, Hamley PA, Thomas WB, Whiston K, Poliakoff M (2005) Green Chem 7:294
31. Fraga-Dubreuil J, Garcia-Verdugo E, Hamley PA, Perez E, Pearson I, Thomas WB, Housley D, Partenheimer W, Poliakoff M (2009) Adv Synth Catal 351:1866
32. Perez E, Fraga-Dubreuil J, Garcia-Verdugo E, Hamley PA, Thomas WB, Housley D, Partenheimer W, Poliakoff M (2011) Green Chem 13:2389
33. Perez E, Fraga-Dubreuil J, Garcia-Verdugo E, Hamley PA, Thomas ML, Yan C, Thomas WB, Housley D, Partenheimer W, Poliakoff M (2011) Green Chem 13:2397
34. Gutmann B, Elsner P, Roberge D, Kappe CO (2013) ACS Catal 3:2669
35. Pieber B, Kappe CO (2013) Green Chem 15:320
36. De Houwer J, Tehrani KA, Maes BUW (2012) Angew Chem Int Ed 51:2745
37. Hamano M, Nagy KD, Jensen KF (2012) Chem Commun 48:2086
38. Neuenschwander U, Jensen KF (2014) Ind Eng Chem Res 53:601
39. Musser MT (2000) Cyclohexanol and cyclohexanone Ullmann's encyclopedia of industrial chemistry. Wiley-VCH, Weinheim, Germany
40. Leclerc A, Alame M, Schweich D, Pouteau P, Delattre C, de Bellefon C (2008) Lab Chip 8:814
41. Fischer J, Lange T, Boehling R, Rehfinger A, Klemm E (2010) Chem Eng Sci 65:4866
42. Bourne SL, Ley SV (2013) Adv Synth Catal 355:1905
43. Tomaszewski B, Lloyd RC, Warr AJ, Buehler K, Schmid A (2014) ChemCatChem 6:2567
44. Tomaszewski B, Schmid A, Buehler K (2014) Org Process Res Dev 18:1516
45. LaPorte TL, Hamedi M, DePue JS, Shen LF, Watson D, Hsieh D (2008) Org Process Res Dev 12:956
46. Zhan BZ, Thompson A (2004) Tetrahedron 60:2917
47. Schultz MJ, Sigman MS (2006) Tetrahedron 62:8227
48. Parmeggiani C, Cardona F (2012) Green Chem 14:547
49. Ryland BL, Stahl SS (2014) Angew Chem Int Ed 53:8824
50. Felthouse TR (1987) J Am Chem Soc 109:7566
51. Felthouse TR, Fraundorf PB, Friedman RM, Schosser CL (1991) J Catal 127:393
52. Kimura H (1993) Appl Catal A-Gen 105:147
53. Bavykin DV, Lapkin AA, Kolaczkowski ST, Plucinski PK (2005) Appl Catal A-Gen 288:175
54. Bavykin DV, Lapkin AA, Plucinski PK, Friedrich JM, Walsh FC (2005) J Catal 235:10
55. Plucinski PK, Bavykin DV, Kolaczkowski ST, Lapkin AA (2005) Ind Eng Chem Res 44:9683
56. Plucinski PK, Bavykin DV, Kolaczkowski ST, Lapkin AA (2005) Catal Today 105:479
57. Zotova N, Hellgardt K, Kelsall GH, Jessiman AS, Hii KK (2010) Green Chem 12:2157
58. Obermayer D, Balu AM, Romero AA, Goessler W, Luque R, Kappe CO (2013) Green Chem 15:1530
59. Liu XY, Jensen KF (2013) Green Chem 15:1538
60. Liu XY, Jensen KF (2012) Green Chem 14:1471
61. Mannel DS, Stahl SS, Root TW (2014) Org Process Res Dev 18:1503
62. Cao EH, Motherwell WB, Gavriilidis A (2006) Chem Eng Technol 29:1372
63. Cao E, Gavriilidis A, Motherwell WB (2004) Chem Eng Sci 59:4803
64. Muzen A, Fraguio MS, Cassanello MC, Ayude MA, Haure PM, Martinez OM (2005) Ind Eng Chem Res 44:5275
65. Tarasov AL, Kustov LM, Bogolyubov AA, Kiselyov AS, Semenov VV (2009) Appl Catal A-Gen 366:227
66. Brandner A, Lehnert K, Bienholz A, Lucas M, Claus P (2009) Top Catal 52:278

67. Al Badran F, Awdry S, Kolaczkowski ST (2013) Catal Today 216:229
68. Osako T, Torii K, Uozumi Y (2015) RSC Adv 5:2647
69. Wang NW, Matsumoto T, Ueno M, Miyamura H, Kobayashi S (2009) Angew Chem Int Ed 48:4744
70. Kaizuka K, Lee KY, Miyamura H, Kobayashi S (2012) J Flow Chem 2:1
71. Zope BN, Davis RJ (2009) Top Catal 52:269
72. Zope BN, Davis SE, Davis RJ (2012) Top Catal 55:24
73. Pollington SD, Enache DI, Landon P, Meenakshisundaram S, Dimitratos N, Wagland A, Hutchings GJ, Stitt EH (2009) Catal Today 145:169
74. Cao EH, Sankar M, Firth S, Lam KF, Bethell D, Knight DK, Hutchings GJ, McMillan PF, Gavriilidis A (2011) Chem Eng J 167:734
75. Asao N, Hatakeyama N, Menggenbateer, Minato T, Ito E, Hara M, Kim Y, Yamamoto Y, Chen MW, Zhang W, Inouei A (2012) Chem Commun 48:4540
76. Heidkamp K, Aytemir M, Vorlop KD, Prusse U (2013) Catal Sci Technol 3:2984
77. Wu GW, Constantinou A, Cao EH, Kuhn S, Morad M, Sankar M, Bethell D, Hutchings GJ, Gavriilidis A (2015) Ind Eng Chem Res 54:4183
78. Chaudhuri SR, Hartwig J, Kupracz L, Kodanek T, Wegner J, Kirschning A (2014) Adv Synth Catal 356:3530
79. Aellig C, Girard C, Hermans I (2011) Angew Chem Int Ed 50:12355
80. Aellig C, Scholz D, Hermans I (2012) ChemSusChem 5:1732
81. Aellig C, Scholz D, Conrad S, Hermans I (2013) Green Chem 15:1975
82. Leitner W (2002) Acc Chem Res 35:746
83. Rayner CM (2007) Org Process Res Dev 11:121
84. Han X, Poliakoff M (2012) Chem Soc Rev 41:1428
85. Jenzer G, Sueur D, Mallat T, Baiker A (2000) Chem Commun 2000:2247
86. Jenzer G, Schneider MS, Wandeler R, Mallat T, Baiker A (2001) J Catal 199:141
87. Jenzer G, Mallat T, Baiker A (2001) Catal Lett 73:5
88. Grunwaldt JD, Caravati M, Ramin M, Baiker A (2003) Catal Lett 90:221
89. Caravati M, Grunwaldt JD, Baiker A (2004) Catal Today 91–2:1
90. Caravati M, Grunwaldt JD, Baiker A (2005) Phys Chem Chem Phys 7:278
91. Burgener M, Tyszewski T, Ferri D, Mallat T, Baiker A (2006) Appl Catal A-Gen 299:66
92. Caravati M, Grunwaldt JD, Baiker A (2006) Appl Catal A-Gen 298:50
93. Grunwaldt JD, Baiker A (2005) Phys Chem Chem Phys 7:3526
94. Caravati M, Meier DM, Grunwaldt JD, Baiker A (2006) J Catal 240:126
95. Caravati M, Grunwaldt JD, Baliker A (2007) Catal Today 126:27
96. Grunwaldt JD, Caravati M, Baiker A (2006) J Phys Chem B 110:9916
97. Beier MJ, Grunwaldt JD, Tsivintzelis I, Jensen AD, Kontogeorgis GM, Baiker A (2012) J Supercrit Fluid 63:199
98. Chapman AO, Akien GR, Arrowsmith NJ, Licence P, Poliakoff M (2010) Green Chem 12:310
99. Keresszegi C, Grunwaldt JD, Mallat T, Baiker A (2003) Chem Commun 2304
100. Grunwaldt JD, Keresszegi C, Mallat T, Baiker A (2003) J Catal 213:291
101. Grunwaldt JD, Caravati M, Baiker A (2006) J Phys Chem B 110:25586
102. Hou Z, Theyssen N, Brinkmann A, Leitner W (2005) Angew Chem Int Ed 44:1346
103. Hou ZS, Theyssen N, Leitner W (2007) Green Chem 9:127
104. Hou Z, Theyssen N, Brinkmann A, Klementiev KV, Grunert W, Buhl M, Schmidt W, Spliethoff B, Tesche B, Weidenthaler C, Leitner W (2008) J Catal 258:315
105. Stahl SS (2005) Science 309:1824
106. Stahl SS (2004) Angew Chem Int Ed 43:3400
107. Steinhoff BA, Stahl SS (2006) J Am Chem Soc 128:4348
108. Ye XA, Johnson MD, Diao TN, Yates MH, Stahl SS (2010) Green Chem 12:1180
109. Greene JF, Hoover JM, Mannel DS, Root TW, Stahl SS (2013) Org Process Res Dev 17:1247
110. Vanoye L, Pablos M, de Bellefon C, Favre-Reguillon A (2015) Adv Synth Catal 357:739

111. Greene JF, Preger Y, Stahl SS, Root TW (2015) Org Process Res Dev doi:10.1021/acs.oprd.5b00125
112. Franke R, Selent D, Borner A (2012) Chem Rev 112:5675
113. Röhrscheid F (2000) Carboxylic acids, aromatic Ullmann's encyclopedia of industrial chemistry. Wiley-VCH, Weinheim, Germany
114. Haverkamp V, Hessel V, Liauw MA, Lowe H, Menges MG (2007) Ind Eng Chem Res 46:8558
115. Liu XY, Unal B, Jensen KF (2012) Catal Sci Technol 2:2134
116. Vanoye L, Aloui A, Pablos M, Philippe R, Percheron A, Favre-Reguillon A, de Bellefont C (2013) Org Lett 15:5978
117. Vanoye L, Pablos M, Smith N, de Bellefon C, Favre-Reguillon A (2014) RSC Adv 4:57159
118. Seechurn CCCJ, Kitching MO, Colacot TJ, Snieckus V (2012) Angew Chem Int Ed 51:5062
119. Cantillo D, Kappe CO (2014) ChemCatChem 6:3286
120. Noel T, Buchwald SL (2011) Chem Soc Rev 40:5010
121. Karimi B, Behzadnia H, Elhamifar D, Akhavan PF, Esfahani FK, Zamani A (2010) Synthesis 2010:1399
122. Gligorich KM, Sigman MS (2009) Chem Commun 3854
123. Park CP, Kim DP (2010) J Am Chem Soc 132:10102
124. Park JH, Park CY, Kim MJ, Kim MU, Kim YJ, Kim GH, Park CP (2015) Org Process Res Dev. doi:10.1021/acs.oprd.5b00077
125. Rudzinski DM, Leadbeater NE (2013) Green Process Synth 2:323
126. Gemoets HPL, Hessel V, Noel T (2014) Org Lett 16:5800
127. Petersen TP, Polyzos A, O'Brien M, Ulven T, Baxendale IR, Ley SV (2012) ChemSusChem 5:274
128. Brzozowski M, Forni JA, Savage GP, Polyzos A (2015) Chem Commun 51:334
129. Ratnikov MO, Xu XF, Doyle MP (2013) J Am Chem Soc 135:9475
130. Goebel MT, Marvel CS (1933) J Am Chem Soc 55:1693
131. Porter CW, Steel C (1920) J Am Chem Soc 42:2650
132. Russell GA, Bridger RF (1963) J Am Chem Soc 85:3765
133. He Z, Jamison TF (2014) Angew Chem Int Ed 53:3353
134. Schmidt RJ (2005) Appl Catal A-Gen 280:89
135. Fraga-Dubreuil J, Garcia-Serna J, Garcia-Verdugo E, Dudd LM, Aird GR, Thomas WB, Poliakoff M (2006) J Supercrit Fluid 39:220
136. Thomas ML, Fraga-Dubreuil J, Coote AS, Poliakoff M (2008) Green Chem 10:197
137. Hunig S, Muller HR, Thier W (1965) Angew Chem Int Ed 4:271
138. Pasto DJ, Taylor RT (1991) Org React 40:91
139. Pieber B, Martinez ST, Cantillo D, Kappe CO (2013) Angew Chem Int Ed 52:10241
140. Pieber B, Glasnov T, Kappe CO (2015) Chem Eur J 21:4368
141. Feth MP, Rossen K, Burgard A (2013) Org Process Res Dev 17:282
142. Gilmore K, Seeberger PH (2014) Chem Rec 14:410
143. Su YH, Straathof NJW, Hessel V, Noel T (2014) Chem Eur J 20:10562
144. Talla A, Driessen B, Straathof NJW, Milroy L-G, Brunsveld L, Hessel V, Noël T (2015) Adv Synth Catal. doi:10.1002/adsc.201401010
145. Su Y, Hessel V, Noël T (2015) AIChE 61:2215
146. Zou YQ, Chen JR, Liu XP, Lu LQ, Davis RL, Jorgensen KA, Xiao WJ (2012) Angew Chem Int Ed 51:784
147. Penders IGTM, Amara Z, Horvath R, Rossen K, Poliakoff M, George MW (2015) RSC Adv 5:6501
148. Ogilby PR (2010) Chem Soc Rev 39:3181
149. Wootton RCR, Fortt R, de Mello AJ (2002) Org Process Res Dev 6:187
150. Loponov KN, Lopes J, Barlog M, Astrova EV, Malkov AV, Lapkin AA (2014) Org Process Res Dev 18:1443
151. Jahnisch K, Dingerdissen U (2005) Chem Eng Technol 28:426

152. Park CP, Maurya RA, Lee JH, Kim DP (2011) Lab Chip 11:1941
153. Maurya RA, Park CP, Kim DP (2011) Beilstein J Org Chem 7:1158
154. Levesque F, Seeberger PH (2011) Org Lett 13:5008
155. Heugebaert TSA, Stevens CV, Kappe CO (2015) ChemSusChem 8:1648
156. Elvira KS, Wootton RCR, Reis NM, Mackley MR, DeMello AJ (2013) ACS Sustain Chem Eng 1:209
157. Park CY, Kim YJ, Lim HJ, Park JH, Kim MJ, Seo SW, Park CP (2015) RSC Adv 5:4233
158. Lumley EK, Dyer CE, Pamme N, Boyle RW (2012) Org Lett 14:5724
159. Ushakov DB, Gilmore K, Kopetzki D, McQuade DT, Seeberger PH (2014) Angew Chem Int Ed 53:557
160. Ushakov DB, Gilmore K, Seeberger PH (2014) Chem Commun 50:12649
161. Ushakov DB, Plutschack MB, Gilmore K, Seeberger PH (2015) Chem Eur J 21:6528
162. Vukelic S, Ushakov DB, Gilmore K, Koksch B, Seeberger PH (2015) Eur J Org Chem 2015:3036
163. Levesque F, Seeberger PH (2012) Angew Chem Int Ed 51:1706
164. Kopetzki D, Levesque F, Seeberger PH (2013) Chem Eur J 19:5450
165. Gilmore K, Kopetzki D, Lee JW, Horvath Z, McQuade DT, Seidel-Morgenstern A, Seeberger PH (2014) Chem Commun 50:12652
166. Bourne RA, Han X, Chapman AO, Arrowsmith NJ, Kawanami H, Poliakoff M, George MW (2008) Chem Commun 2008:4457
167. Bourne RA, Han X, Poliakoff M, George MW (2009) Angew Chem Int Ed 48:5322
168. Han X, Bourne RA, Poliakoff M, George MW (2009) Green Chem 11:1787
169. Han X, Bourne RA, Poliakoff M, George MW (2011) Chem Sci 2:1059
170. Hall JFB, Han X, Poliakoff M, Bourne RA, George MW (2012) Chem Commun 48:3073
171. Hall JFB, Bourne RA, Han X, Earley JH, Poliakoff M, George MW (2013) Green Chem 15:177
172. Amara Z, Bellamy JFB, Horvath R, Miller SJ, Beeby A, Burgard A, Rossen K, Poliakoff M, George MW (2015) Nat Chem 7:489

Preparation and Use of Organolithium and Organomagnesium Species in Flow

Aiichiro Nagaki and Jun-Ichi Yoshida

Abstract This chapter presents a brief overview regarding the use of flow micro-reactors for the preparation and reactions of organometallic species, with special emphasis on the synthetic transformations using highly reactive species such as organolithiums and organomagnesiums that are difficult or impossible to achieve using conventional batch reactors.

Contents

A. Nagaki and J.-I. Yoshida (✉)
Department of Synthetic Chemistry and Biological Chemistry, Graduate School of Engineering, Kyoto University, Nishikyo-ku, Kyoto 615-8510, Japan
e-mail: anagaki@sbchem.kyoto-u.ac.jp; yoshida@sbchem.kyoto-u.ac.jp

1   Introduction

Organometallic species, which have carbon–metal bonds, are vital in organic synthesis because they serve as carbanion equivalents which can be used for carbon–carbon formation to make carbon skeletons of organic compounds. The properties of organometallic species are highly dictated by the nature of the metal. In general, as the difference in electronegativity between metal and carbon is larger, the degree of polarization is larger. Accordingly, the reactivity of the organometallic species increases with an increase in the difference in electronegativity. Table 1 shows the differences in electronegativity between carbon and metals which are commonly used as organometallic reagents in organic synthesis.

Organolithium species are the most reactive and organomagnesium species are the second most reactive among those in the Table 1. In fact, organolithium and organomagnesium species are highly reactive toward various electrophiles including carbonyl compounds such as aldehydes, ketones, and esters. However, high reactivity of such organometallic species often causes the difficulty in controlling the reactions, especially in the case of large-scale industrial productions. Therefore, this chapter focuses on the use of flow microreactors [1–4] for performing the preparation and use of such highly reactive organometallic species in a controlled way. Catalytic reactions with organometallic species are not included in this chapter, because such reactions are discussed in a separate chapter.

2   Organolithium Species

Organolithium species are the most reactive among the organometallic species which are commonly used in organic synthesis. However, high reactivity of organolithium species limits their applications and inorganic syntheses because of the following reasons. First, they must be synthesized at very low temperatures due to

Table 1   The difference in electronegativity between metal and carbon

Metal	Li	Mg	Zn	Sn	B
The difference in electronegativity	1.53	1.27	0.84	0.78	0.49
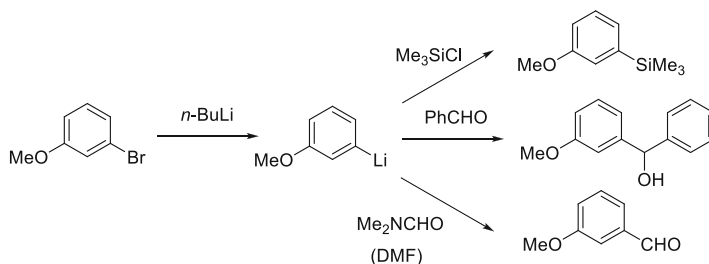
Fig. 1 Br–Li exchange to generate aryllithium species followed by the reactions with electrophiles

their low stabilities. In addition, reactions involving such species are often extremely fast and highly exothermic, making the reactions difficult or even impossible to control in conventional batch reactors [5]. Extremely low temperatures ($< -78°C$) are often required to avoid decomposition of highly unstable organolithiums. Therefore, the industrial applications of organolithium species are quite limited. These characteristics suggest that flow microreactors can be applied to solve such problems in organolithium chemistry. In the following sections, we will discuss how organolithium species are generated and reacted with electrophiles in flow microreactors in a controlled way.

2.1 Aryllithium and Heteroaryllithium Species

The halogen–lithium exchange is often used to generate aryllithium and heteroaryllithium species, although hydrogen–lithium exchange (deprotonation) and carbolithiation can also serve as powerful methods for generating organolithium species.

In 2003, it was reported that flow microreactors enable Br–Li exchange of bromobenzene derivatives with *n*-butyllithium at 0°C, which is much higher than the temperatures required for batch reactions (Fig. 1) [6]. Fast heat exchange and short residence times in flow microreactors seem to be responsible. The resulting aryllithium species react with various electrophiles including chlorotrimethylsilane, benzaldehyde, and DMF (dimethylformamide). The use of flow microreactors is also effective for halogen–lithium exchange reactions of heteroaryl halides.

An independent research on similar reactions in a flow microreactor revealed that a throughput of 59 g/h can be achieved for approximately 24 h under nearly isothermal conditions in the two-stage microreaction system consisting of the Br–Li exchange of 3-bromoanisole followed by the reaction with DMF [7]. Similar reactions are also extensively studied in connection with the synthesis of tramadol [8].

The Br–Li exchange of *m*- and *p*-dibromobenzenes with *n*-BuLi followed by reaction with an electrophile, such as iodomethane, chlorotrimethylsilane, chlorotributylstannane, benzaldehyde, and acetophenone, can be conducted at 20°C ($t^{R1} = 0.39$ s) in a flow microreactor (Fig. 2), though a much lower reaction temperatures such as −48°C is required for batch reaction [9]. An assembled

Fig. 2 Flow microreactor for Br–Li exchange of dibromobenzenes. M1 and M2 represent micromixers; R1 and R2 represent microtube reactors

m- and p-dibromobenzene $T = 20\ ^{\circ}C$, $t^{R1} = 0.39$ s
o-dibromobenzene $T = -78\ ^{\circ}C$, $t^{R1} = 0.82$ s
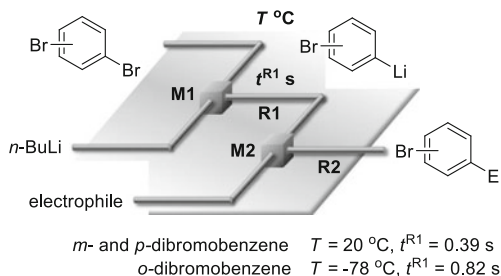
Fig. 3 Effects of temperature and residence time on bromobenzene yield in Br–Li exchange of o-dibromobenzene followed by reaction with methanol. Contour plots with scatter overlay of yields (%) against temperature ($^{\circ}C$) and logarithm of residence time (s)
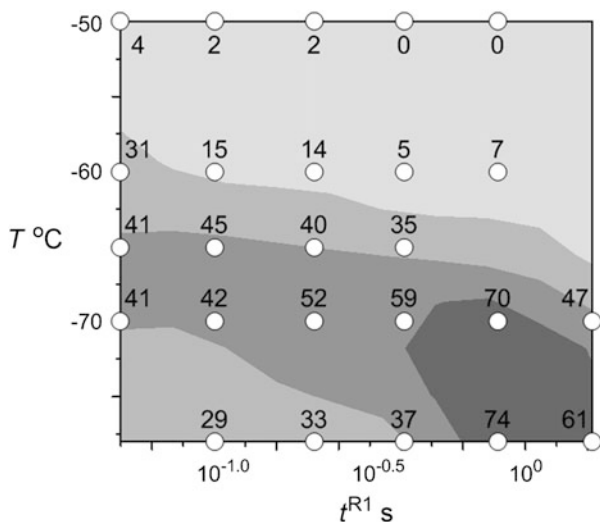
reactor consisting of mixing, residence time, and heat exchange units was developed and applied to generation and reactions of p-bromophenyllithium [10].

In addition, the Br–Li exchange of o-dibromobenzene can be conducted at $-78^{\circ}C$ using a flow microreactor [11]. This particular reaction must be performed below $-110^{\circ}C$ in a batch reactor because LiBris rapidly eliminated to form benzyne even at $-78^{\circ}C$ [12]. Figure 3 shows a mapping of product yield against temperature and residence time. This type of temperature–residence time map is effective in revealing the stability of reactive intermediates and optimizing reaction conditions. In fact, the desired products can be obtained in high yields by appropriately adjusting the residence time ($t^{R1} = 0.82$ s) and temperature ($-78^{\circ}C$). The resulting o-bromophenyllithium reacts with various electrophiles, such as methyl triflate, trimethylsilyl triflate, chlorotributylstannane, benzaldehyde, or acetophenone to give the desired products. Furthermore, under the optimized conditions, sequential introduction of two electrophiles has been achieved using integrated flow microreactor systems consisting of four micromixers and four microtube reactors to synthesize a variety of p-, m-, and o-disubstituted benzenes in good yields (53–93%).
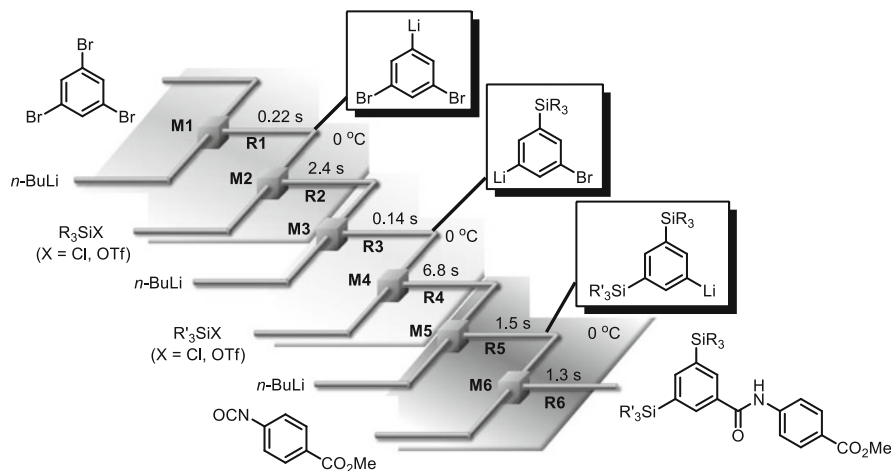
Fig. 4 Flow syntheses of TAC-101 and its analogs. M1, M2, M3, M4, M5, and M6 represent micromixers; R1, R2, R3, R4, R5, and R6 represent microtube reactors

Many other examples of preparation and use of aryllithium and hetero-aryllithium species in flow microreactors have been reported in the literature, some of which are shown below.

TAC-101 (4-[3,5-bis(trimethylsilyl)benzamido]benzoic acid) is a synthetic retinoid having differentiation-inducing activity on human promyelocytic leukemia cells HL-60. The following syntheses of TAC-101 and its analogs demonstrate the utility of reaction integration using flow microreactors. Three sets of Br–Li exchange reactions followed by reaction with an electrophile were integrated in space using 1,3,5-tribromobenzene as the starting material. To achieve such integration, an integrated flow microreactor system composed of six micromixers and six microtube reactors was used, as shown in Fig. 4. By adjusting the residence time in each reactor, sequential introduction of two silyl groups followed by introduction of an amide functionality was accomplished at 0°C in one flow to give various TAC-101 methyl ester analogs having two different silyl groups in good yields [13]. Notably, the total residence time was 12.2 s, and the productivity ranged from 132 to 194 mg/min depending on the nature of the silyl groups.

The Br–Li exchange of bromonaphthalenes followed by reaction with 9,10-anthraquinone at −20°C using a flow microreactor system involving caterpillar split–recombine micromixers provided the naphthyl-substituted anthracene in 85% conversion (9,10-anthraquinone) and 97% purity (Fig. 5) [14].

The generation and reaction of pyridyllithiums through Br–Li exchange of bromopyridines is a powerful method for the introduction of substituents into pyridine rings. Flow microreactors enable such reactions at higher temperatures, such as −28°C (pyridyllithiums) and 0°C (bromopyridyllithiums), than those required for conventional batch reactions (Fig. 6) [15, 16]. In the case of dibromo-pyridines, sequential introduction of two electrophiles can be achieved using
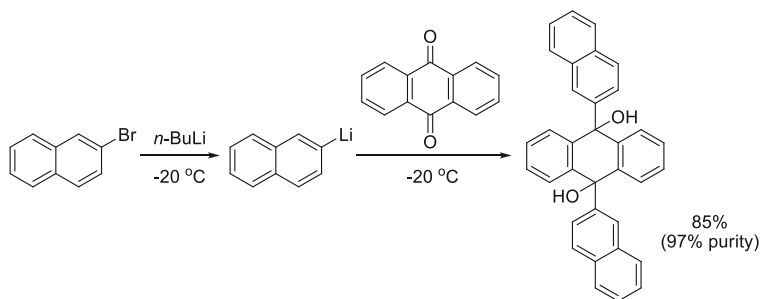
Fig. 5 Br–Li exchange of 2-bromonaphthalene followed by reaction with 9,10-anthraquinone using flow microreactor
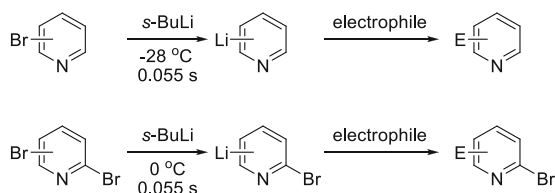
Fig. 6 Br–Li exchange of bromopyridines and dibromopyridines followed by reaction with electrophile using flow microreactor
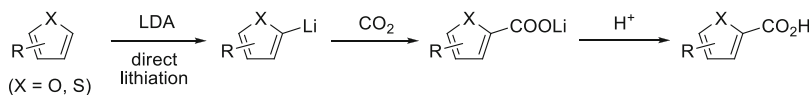
Fig. 7 Generation of heteroaryllithium species followed by the reaction with CO_2

integrated flow microreactors. The Br–Li exchange of bromopyridines and their reactions with ketones can be also conducted at 0°C under in situ quenching conditions using a flow microreactor [17].

Various electrophiles can be used for aryllithium and heteroaryllithium species generated in flow. For example, reactions with electrophilic fluorinating reagents, such as N-fluorobenzenesulfonimide and N-fluorosultams, give the corresponding aryl fluorides [18].

Gaseous CO_2 can also be used as an electrophile in flow. For example, the reactions of heteroaryllithiums generated by deprotonation with gaseous CO_2 can be accomplished to obtain the corresponding carboxylic acids after protonation (Fig. 7) [19].

Furthermore, the synthesis of ketones from aryllithium species, alkyllithium or aryllithium species, and CO_2 has also been developed [20], which exhibits significant advantages over conventional batch conditions in terms of suppressing undesirable symmetric ketones and tertiary alcohol by-products. Although excess CO_2 causes

$$ArLi \xrightarrow{CO_2} ArCOOLi \xrightarrow{RLi} \underset{Ar \quad R}{\overset{LiO \quad OLi}{\diagup}} \longrightarrow \underset{Ar \quad R}{\overset{O}{\diagup}}$$

$$\downarrow CO_2$$
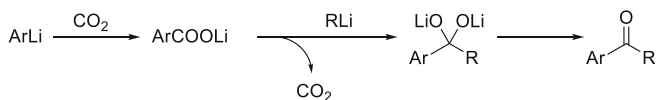
Fig. 8 Synthesis of ketones from aryllithium species, alkyllithium or aryllithium species, and CO_2

negative effects on the downstream reaction, it can easily be removed by integration of a mini-vacuum degasser (Fig. 8).

2.2 Functional Aryllithium Species

Chemical conversions using organometallic species bearing unprotected functional groups, in particular electrophilic functional groups, serve as atom and step economical methods to construct organic molecules [21–23]. Functional organolithium species are among the most difficult to generate and use for subsequent reactions with intentionally added electrophiles due to their high reactivities toward the functional groups attached to themselves. However, flow microreactors often enable such transformations without protecting the functional groups.

Compounds having a nitro group are useful intermediates in organic synthesis because of high potential of the nitro group for driving and directing reactions. Also, nitro compounds also serve as useful precursors of amino compounds. However, the use of nitro compounds in organometallic syntheses has been very limited in conventional batch reactors, presumably because of their incompatibility with organometallic reagents. For example, the generation of aryllithium and aryl-magnesium species bearing nitro groups in their *ortho* positions can be achieved only at very low temperatures. Moreover, the generation of *m*- or *p*-nitro-substituted aryllithium and arylmagnesium species has been reported to be impossible using conventional batch methods [24]. In contrast, flow microreactors enable generation and use of *o*-, *m*-, and *p*-nitro-substituted aryllithium species without protecting their nitro groups, which can be accomplished by choosing an appropriate temperature (0 or $-28°C$) and short residence time (0.01 s) (Fig. 9) [25]. Moreover, aryllithium species bearing highly reactive alkoxycarbonyl groups, such as ethoxy-carbonyl or methoxycarbonyl groups, and cyano groups can also be generated and reacted with various electrophiles [26–28]. The precise temperature control and short residence time (0.01 s) achievable using flow microreactors are responsible for the success of such transformations.

Flow microreactors also enable organolithium reactions without protection of ketone carbonyl groups [29]. By significantly reducing the residence time (to 0.003 s or less) in an integrated microreactor, in which two micromixers and one microtube reactor are integrated in a single device, aryllithium species bearing ketone carbonyl groups are generated by I–Li exchange of the corresponding aryl iodides with mesityllithium. The resulting aryllithium species can then be reacted with various electrophiles without affecting the ketone carbonyl groups. In

FG	batch macro reactor			flow microreactor		
	o-	*m-*	*p-*	*o-*	*m-*	*p-*
CO$_2^t$Bu	-100 °C	-100 °C	-100 °C	T = 0 °C	T = 0 °C	T = 0 °C
CO$_2^i$Pr	-100 °C	impossible	impossible	T = -28 °C	T = -48 °C	T = -48 °C
CO$_2$Et	impossible	impossible	impossible	T = -48 °C	T = -58 °C	T = -58 °C
CO$_2$Me	impossible	impossible	impossible	T = -48 °C	T = -58 °C	T = -78 °C
NO$_2$	-100 °C	impossible	impossible	T = 0 °C	T = -28 °C	T = -28 °C
CN	-100 °C	-100 °C	-100 °C	T = 0 °C	T = -28 °C	T = -28 °C
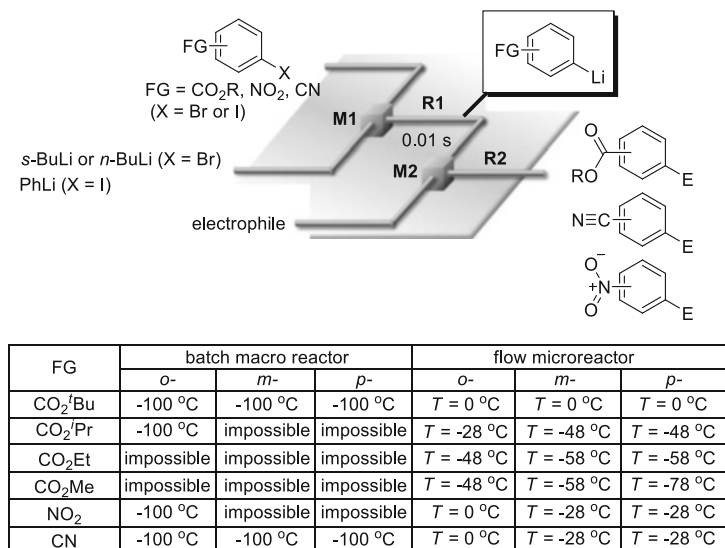
Fig. 9 Generation and reaction of aryllithium species bearing electrophilic functional groups. M1 and M2 represent micromixers; R1 and R2 represent microtube reactors
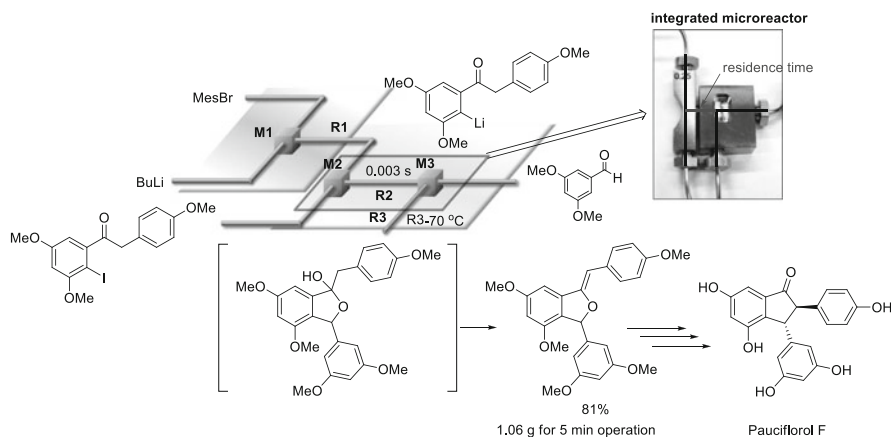
Fig. 10 Formal total synthesis of pauciflorol F based on generation and reaction of aryllithium species bearing ketone carbonyl groups in flow. M1, M2, and M3 represent micromixers; R1, R2, and R3 represent microtube reactors

addition, the present method was successfully applied to the formal synthesis of pauciflorol F, a natural product isolated from stem bark (Fig. 10). The I–Li exchange of iodoketone with mesityllithium generated in flow followed by reaction with 3,5-dimethoxybenzaldehyde was conducted using a flow microreactor consisting of the integrated device (residence time: 0.003 s) to give the desired product in 81% isolated yield. Notably, the productivity of the present method is
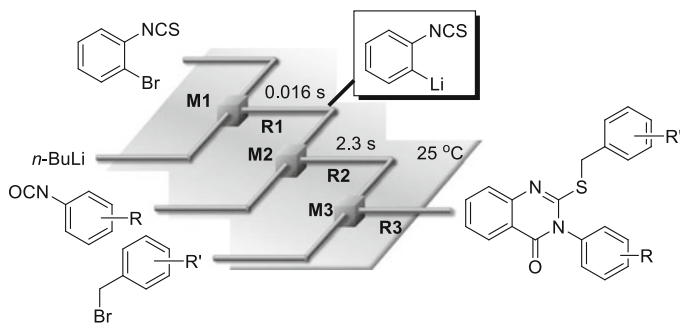
Fig. 11 Synthesis of S-benzylic thioquinazolinones via Br–Li exchange of *o*-bromophenyl isothiocyanate followed by sequential reactions with two electrophiles. M1, M2, and M3 represent micromixers; R1, R2, and R3 represent microtube reactors
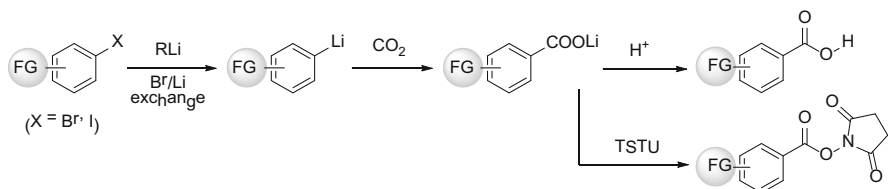
Fig. 12 Synthesis of functional benzoic acids and active esters via generation of functional aryllithiums followed by the reaction with CO_2

relatively high (1.06 g for 5 min operation) indicating that the flow micro reaction system provides an efficient method for producing useful pharmaceutical compounds in sufficient amounts for screening and clinical studies.

Thioquinazolinones are important heterocyclic compounds used as new types of bioactive chemical structures with antiplatelet activity. The generation of *o*-lithiophenyl isothiocyanate followed by reaction with isocyanates was accomplished at room temperature (Fig. 11) [30]. However, it is important to maintain a residence time of 16 s in this process because *o*-lithiophenyl isothiocyanate is unstable. The resulting lithium thiolate intermediates were reacted with benzyl bromides to produce thioquinazolinones.

Functional aryllithium species generated by Br–Li exchange can be reacted with CO_2 without affecting the functional groups to afford functional benzoic acids (Fig. 12) [31]. Active esters can also be directly synthesized because the products exist as lithium salts of carboxylic acids prior to protonation.

Arylboronic acids and esters have found widespread applications in transition-metal-catalyzed reactions, as represented by the Suzuki–Miyaura coupling reaction. The most commonly utilized method to prepare these boron compounds is the reaction of Grignard or organolithium reagents with trialkyl borates [32]. Although this traditional approach is still widely used, it is difficult or impossible to apply the method to substrates bearing electrophilic functional groups that are incompatible
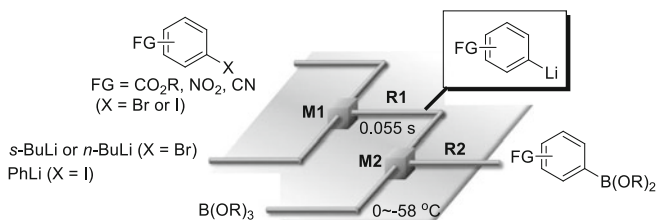
Fig. 13 Synthesis of functional arylboronic esters via halogen–lithium exchange followed by borylation using a flow microreactor system. M1 and M2 represent micromixers; R1 and R2 represent microtube reactors

with organometallic species, such as alkoxycarbonyl, cyano, and nitro groups [21]. Alternatively, arylboronic esters can be prepared from aryl halides or aryl triflates via palladium-catalyzed coupling reactions with tetraalkoxydiborane or dialkoxyborane [33], which tolerate a wide range of functional groups. The borylation of arylamines has also been developed [34]. However, these methods are not suitable for large-scale syntheses because borylation reagents, such as tetraalkoxydiborane and dialkoxyborane, are very expensive. Therefore, synthesis of arylboronic esters bearing electrophilic functional groups through the use of trialkyl borates should be considered.

The synthesis of various arylboronic esters via metalation followed by borylation can be performed using a flow microreactor [35–37]. For example, aryllithium species, generated by halogen–lithium exchange, react with isopropoxyboronic acid pinacol ester in a flow microreactor to afford the corresponding arylboronic acid pinacol esters in reasonable yields (Fig. 13) [38]. Notably, aryllithium species bearing electrophilic functional groups can be rapidly generated and used in the borylation reaction prior to decomposition in the flow microreactor due to the extremely short residence time. Therefore, alkoxycarbonyl, cyano, and nitro groups tolerate the individually optimized conditions, whereas such functional groups readily undergo decomposition in conventional batch reactions. It is also noteworthy that simple phenylboronic acid pinacol ester can be obtained at higher temperatures, such as at 24°C.

The borylation reactions can be integrated with Pd-catalyzed Suzuki–Miyaura coupling using flow microreactors (vide infra) [37, 38].

2.3 Alkenyllithium and Allenyllithium Species

Alkenyllithium species have a wide range of applications in organic synthesis. Through the use of a flow microreactor, alkenyllithium species can be effectively generated by Br–Li exchange reactions of alkenyl bromides with one equivalent of s-BuLi at 0 or 20°C, whereas two equivalents of t-BuLi and much lower temperatures are required for conventional batch reactions (Fig. 14) [39, 40]. The resulting
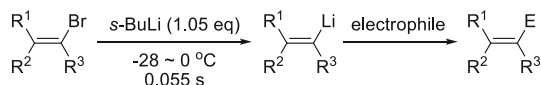
Fig. 14 Br–Li exchange of alkenyl bromides with one equivalent of s-BuLi followed by reaction with electrophiles using a flow microreactor
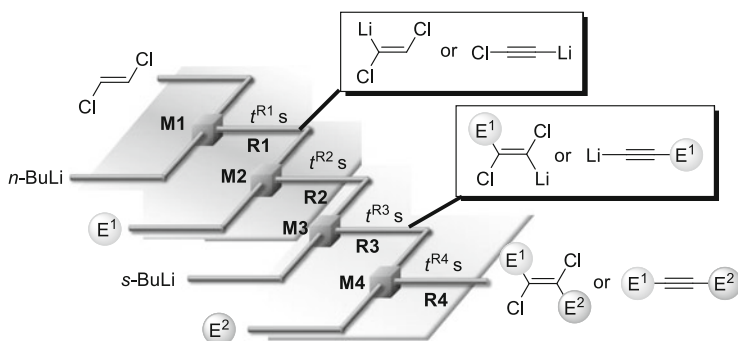
Fig. 15 Synthesis of alkenes and alkynes from *trans*-1,2-dichloroethene based on precise residence time control using a flow microreactor system. M1, M2, M3, and M4 represent micromixers; R1, R2, R3, and R4 represent microtube reactors

alkenyllithium species are then allowed to react with various electrophiles to provide the desired products.

The following transformations demonstrate the power of precise residence time control [41]. By choosing the appropriate residence time, switching of the reaction pathways of 1,2-dichlorovinyllithium species generated by deprotonation of 1,2-dichloroethene with *n*-BuLi can be achieved (Fig. 15). With short residence times 1,2-dichlorovinyllithium species can be reacted with an electrophile to give the corresponding substituted 1,2-dichloroethene. The second deprotonation with *s*-BuLi followed by the reaction with a second electrophile gives 1,2-disubstituted 1,2-dichloroethene. With longer residence time, 1,2-dichlorovinyllithium eliminates LiCl and the resulting chloroacetylene undergoes deprotonation if we use an excess amount of *s*-BuLi. The resulting 2-chloroethynyllithium species react with an electrophile to afford the corresponding substituted chloroacetylene. The Cl–Li exchange with *s*-BuLi followed by the reaction with a second electrophile affords the corresponding 1,2-disubstituted acetylene. Thus, alkenes and alkynes are selectively produced at will. A similar transformation can also be achieved via trichlorovinyllithium species generated from trichloroethene, which is much less expensive than *trans*-1,2-dichloroethene [42].

α-(Trifluoromethyl)vinyllithium serves as a powerful building block for constructing CF_3-containing molecules. However, when using conventional batch reactors, it must be both generated and reacted at extremely low temperatures such as −100°C due to the rapid elimination of LiF to give 1,1-difluoroallene, which occurs at higher temperatures [43, 44]. Through the use of a flow microreactor, efficient generation of α-(trifluoromethyl)vinyllithium followed by reaction with an electrophile can be performed at −78°C (Fig. 16) [45].
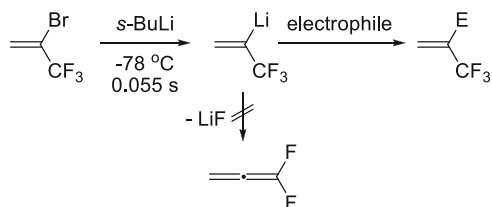
Fig. 16 Br–Li exchange of 2-bromo-3,3,3-trifluoropropene with *s*-BuLi followed by reaction with an electrophile using a flow microreactor
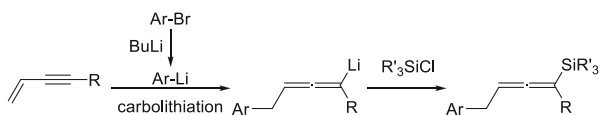
Fig. 17 Carbolithiation of enynes. Generation of allenyllithium species
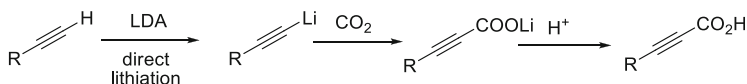
Fig. 18 Generation of alkynyllithium species and their reactions with CO_2

Carbolithiation of unsaturated compounds, such as alkenes, alkynes, and enynes, is an attractive method for carbon–carbon bond formation because it leads to the production of a second organolithium intermediate, which can be utilized for subsequent reactions with various electrophiles. Using an integrated flow microreactor, carbolithiation of conjugated enynes with aryllithium species followed by reaction of the resulting allenyllithium species with chlorosilanes can be achieved to obtain various allenylsilanes in high yields (Fig. 17) [46].

2.4 Alkynyllithium Species

Treatment of terminal alkynes with lithium diisopropylamide leads to the formation of alkynyllithium species because acetylenic C–H is sufficiently acidic (Fig. 18). This process can be performed using a flow reactor [19]. The resulting alkynyllithium species have been successfully reacted with CO_2 in flow to give the corresponding carboxylic acids.

2.5 Benzyllithium and Allyllithium Species

Benzyllithium species can be prepared by reductive lithiation using lithium naphthalenide (LiNp). However, this process suffers from the problem of Wurtz-type homocoupling to give bibenzyls in conventional batch reactors [47]. However,
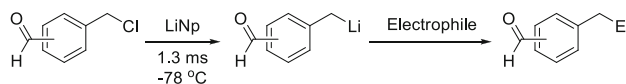
Fig. 19 Generation and reaction of aldehyde-functionalized benzyllithium
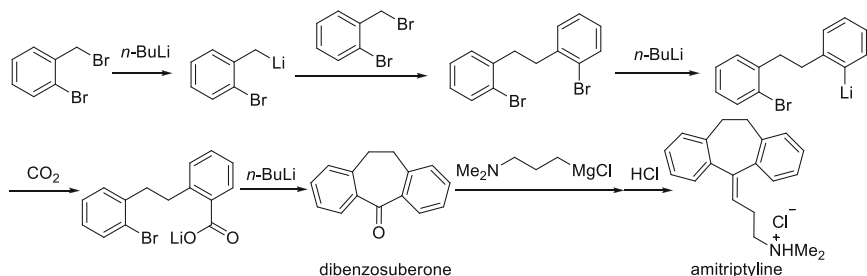
Fig. 20 Synthesis of amitriptyline in flow
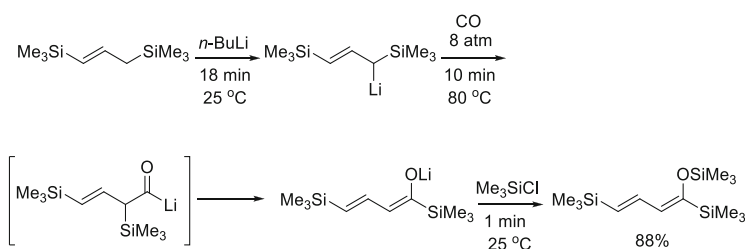
Fig. 21 Generation and carbonylation of 1-silyl-substituted organolithiums followed by reaction with electrophile

extremely fast mixing using a micromixer solves the problem. Thus, the lithiation of benzyl chloride using LiNp followed by the reaction with electrophiles can be performed to give the desired products in high yields.

Remarkably, the generation of benzyllithium species bearing aldehyde carbonyl group (formyl group) and their use in subsequent reactions with various electrophiles have been successfully accomplished without affecting the aldehyde as a result of short residence times in the flow microreactor (Fig. 19) [48]. In general, aldehydes are more reactive than ketones, making their use in protecting-group-free reactions much more difficult. The conditions that allowed for the preservation of the aldehyde were a 1.3 ms residence time and a temperature of $-78°C$.

The following transformation using a flow reactor system is interesting. The Br–Li exchange of 1-bromo-2-(bromomethyl)benzene with *n*-BuLi gives *o*-bromo-benzyllithium which reacts with the unchanged starting material to give 1,2-di (2-bromophenethyl)ethane. The second Br–Li exchange gives [2-(2-bromophenethyl)phenyl]lithium. The reaction with CO_2 followed by the third Br–Li exchange takes place to afford dibenzosuberone, a tricyclic antidepressant which can be used as a synthetic precursor for amitriptyline (Fig. 20) [49]. In

order to remove excess carbon dioxide, either a tube-in-tube reactor or gas remover was used. The reaction of dibenzosuberone with [3-(dimethylamino)propyl] magnesium chloride and subsequent hydrolysis was then conducted to give amsitriptyline.

The flow method is also effective for generation of allyllithium species. For example, the treatment of 1,3-bis(trimethylsilyl)propene with n-BuLi in flow led to deprotonation and the resulting allyllithium species was reacted with CO, which was kept under slightly pressurized conditions through the use of a backpressure regulator (Fig. 21) [50]. When combined with heating, these conditions were quite effective for accelerating the CO trapping reaction.

2.6   Alkyllithium Species

Perfluoroalkyllithium species readily undergo rapid elimination of LiF to form perfluoroalkenes [51]. Thus, flow microreactors can provide an efficient method for generating and using perfluoroalkyllithium species [7, 52]. Two methods are generally used for the reactions of perfluoroalkyllithiums with electrophiles. The more popular method is based on in situ trapping with an electrophile. Flow microreactors are effective for this in situ trapping method, enabling for the reactions to be conducted at much higher temperatures (e.g., $0°C$) than those required for conventional batch reactors ($-78°C$). In the second method, perfluoroalkyllithium is first generated in the absence of an electrophile, with the electrophile being subsequently added. This method can also be successfully achieved using a flow microreactor, because elimination of LiF is avoided by using a short residence time and efficient temperature control (Fig. 22). This method is quite effective for highly reactive electrophiles, such as chlorotributylstannane, trimethylsilyltriflate, and isocyanates, which are not compatible with the lithiation process.

Carbolithiation of alkenes is a useful method for generating alkyllithium species. For example, sequential carbolithiation of octafluorocyclopentene with heteroaryl-lithiums (generated via a Br–Li exchange reaction), each with subsequent LiF elimination, can be conducted to obtain photochromic diarylethenes without the use of cryogenic conditions, because of effective temperature and residence time control in integrated flow microreactors. In contrast, much lower temperatures ($<-78°C$) are needed when using conventional batch reactors (Fig. 23) [53, 54].

Halomethyllithium species are regularly employed for homologation-type reactions of various carbonyl derivatives. In general, the generation of halomethyl-lithiums is conducted using a halogen–lithium exchange reaction under cryogenic conditions (typically below $-78°C$) in the presence of an electrophile. This is due to α-elimination, which occurs at high temperatures to form carbene-like species. However, by controlling the residence time (0.18 s), highly reactive

Fig. 22 X–Li exchange of perfluoroalkyl iodides with MeLi followed by reaction with electrophiles using a flow microreactors

Fig. 23 Sequential carbolithiation of octafluorocyclopentene with heteroaryllithium species. Syntheses of photochromic diarylethenes in flow

Fig. 24 I–Li exchange of chloroiodomethane with MeLi followed by reaction with electrophiles using a flow microreactor

chloromethyllithium species can be generated and reacted with various electrophiles at much higher temperatures (e.g., −40°C) than those used in batch reactors and without internal quenching (Fig. 24) [55].

2.7 Oxiranyllithium and Aziridinyllithium Species

Deprotonation of epoxides and aziridines to generate oxiranyllithium and aziridinyllithium species followed by trapping with an electrophile serves as powerful methods for synthesizing epoxides and aziridines with various substituents [56, 57]. The flow microreactor method provides a powerful approach for generation and reaction of unstable oxiranyllithium and aziridinyllithium species without decomposition by virtue of short residence times (Fig. 25). For example, α-aryloxiranyllithium species can be generated through the deprotonation of styrene oxides with s-BuLi at −78°C using a flow microreactor, whereas much lower temperatures (<−100°C) are needed for conventional batch reactions [58]. The flow microreactor method can also be applied to the generation and reaction of

Fig. 25 Generation and reaction of oxiranyllithiums and aziridinyllithiums
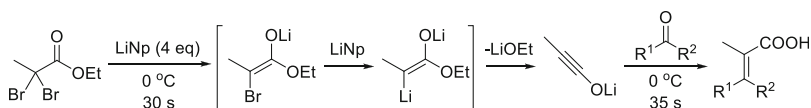
Fig. 26 Reductive lithiation of α,α-dibromoesters with LiNp followed by reaction with ketones using a flow microreactor

α-triphenylsilyloxiranyllithium and aziridinyllithium species [59–62]. Efficient and highly reproducible syntheses of functionalized aziridines and 1,2,3,4-tetrahydro-isoquinolines have also been developed using a flow microreactor [63].

2.8 Lithium Ynolates

Ynolates participate in a variety of reactions and have been prepared via elimination of lithium alkoxide from ester dianions generated by double lithiation of α,α-dibromo esters. However, batch processes generally require low temperature control. In addition, the exothermic nature of the reaction is difficult to control when scaling up the batch reaction. In contrast, the generation of ynolates via double lithiation of α,α-dibromo esters through reductive lithiation followed by reaction with benzophenone can be achieved at 0°C using a flow microreactor to obtain the desired product in 75% yield (1.18 g) (Fig. 26) [64, 65].

2.9 Control of Isomerization of Organolithium Species

In some cases organolithium species isomerize to give isomeric organolithium species. In such cases, the reaction pathways can be controlled at will based on residence time and temperature control in flow microreactors.

The following example shows that either the non-isomerized and isomerized aryllithium species can be selectively formed and used for reactions with electrophiles by changing the residence time. The Br–Li exchange of 1-bromo-2,5-dimethoxy-3-nitrobenzene with a residence time of 0.06 s at −48°C resulted in
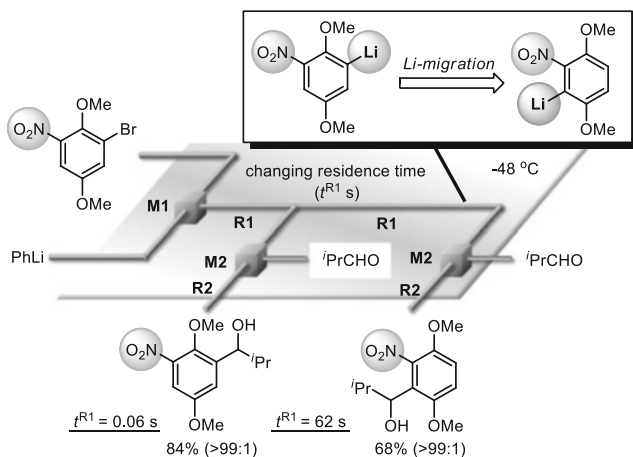
Fig. 27 Control of reaction pathways by the residence time control. M1 and M2 represent micromixers; R1 and R2 represent microtube reactors
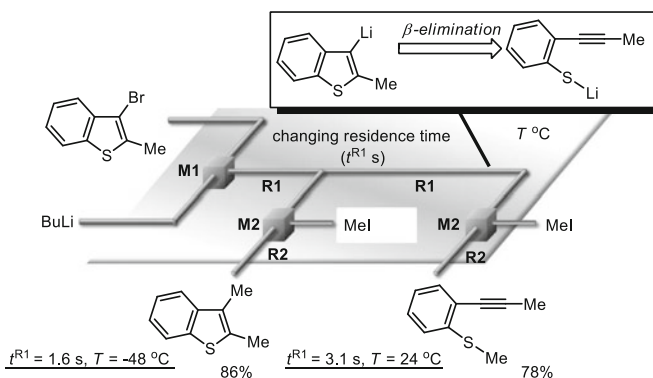
Fig. 28 Br–Li exchange reaction of 3-bromo-2-methylbenzothiophene with *n*-BuLi followed by reaction with iodomethane. Switching the reaction pathways by the residence time and temperature control. M1 and M2 represent micromixers; R1 and R2 represent microtube reactors

selective formation of the aryllithium species and subsequent trapping with an aldehyde afforded the corresponding product in 84% yield (Fig. 27). In contrast, an increase in residence time (62 s) led to the migration of lithium to give the isomeric aryllithium species. The reaction with the aldehyde afforded the isomeric product (68% yield).

Precise control of the residence time and temperature in a flow microreactor also enables switching of the reaction pathways of heteroaryllithium species, such as benzo[*b*]thiophen-3-yllithium and benzo[*b*]furan-3-yllithium [66]. Reaction with an electrophile prior to and following ring-opening can be switched at will (Fig. 28).
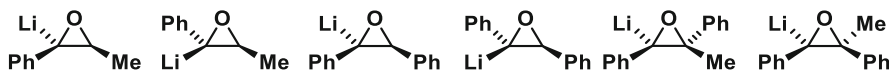
Fig. 29 Generation and reaction of configurationally unstable α-aryloxiranyllithiums
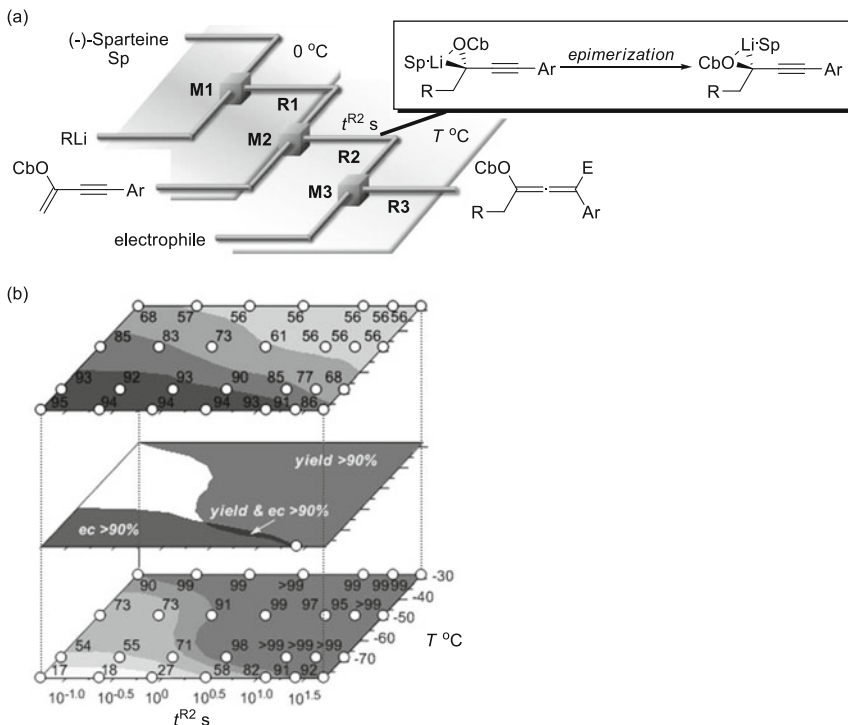
Fig. 30 Enantioselective carbolithiation followed by reaction with electrophile. (**a**) Flow microreactor system. M1, M2, and M3 represent micromixers; R1, R2, and R3 represent microtube reactors. (**b**) Temperature–residence time map (electrophile = MeOH, R = Bu, Ar = C_6H_5). (*Upper*) Contour map with scatter overlay of enantiomeric composition (ec) of product, (*lower*) contour plot with scatter overlay of the yield of product, and (*middle*) domain that generated highest yield (>90%) and highest ec (where enantiomeric ratio normalizes to percent, as proposed by Kagan [68]) (>90%)

Flow microreactors enable the rapid generation of configurationally unstable organolithiums and allow for reaction with various electrophiles prior to epimerization by taking advantage of the short residence time. For example, configurationally unstable α-aryloxiranyllithium species are generated by the deprotonation of disubstituted epoxides and trisubstituted epoxides, and they are then reacted with various electrophiles while avoiding isomerization and decomposition (Fig. 29). Moreover, by repeating the sequence of deprotonation and reaction with an electrophile using an integrated flow microreactor system, diastereoselective synthesis of tetrasubstituted epoxides has been achieved.

Flow microreactors also enable generation of configurationally unstable enantiomerically enriched organolithiums. They can be reacted with various electrophiles prior to epimerization by virtue of precise residence time and temperature control [67]. For example, enantioselective carbolithiation of conjugated enynes followed by reaction with various electrophiles can be performed to obtain enantiomerically enriched allenes through fine tuning of the reaction conditions with the aid of the temperature–residence time map (Fig. 30).

2.10 Selectivity Control of Organolithium Reactions by Micromixing

The selectivity of chemical reactions is often determined by kinetics. However, for extremely fast reactions conducted in conventional batch reactors, such as flasks, kinetics often cannot be used due to the lack of a homogeneous reaction environment after addition of one reaction component to the other reaction component. Therefore, such reactions cannot be controlled using conventional batch reactors. In such cases, the product selectivity is determined based on mixing (disguised chemical selectivity) [69]. To obtain predictable selectivity based on the kinetics, extremely fast mixing is necessary, which can be provided by micromixing based on short diffusion paths [70–74].

Halogen–lithium exchange reactions of dihalobiaryls in conventional batch reactors have generally afford mixtures of mono- and dilithiated species, even when only one equivalent of butyllithium is used [75, 76]. This is because the reaction takes place before homogeneity of the solution is achieved.

Selective monolithiation of dibromobiaryls, such as 2,2′-dibromobiphenyl, 4,4′-dibromobiphenyl, 2,7-dibromo-9,9-dioctylfluorene, 2,2′-dibromo-1,1′-binaphthyl, and 5,5′-dibromo-2,2′-bithiophene, can be achieved by extremely fast 1:1 micromixing of a solution of a dibromobiaryl and that of *n*-butyllithium (Fig. 31) [77, 78]. The selectivity increases upon decreasing the diameter of micromixer and increasing the flow rate, presumably because faster mixing can be achieved using a smaller-diameter mixer and a faster flow rate. Moreover, sequential introduction of two different electrophiles using an integrated flow microreactor affords unsymmetrically substituted biaryls, which are useful synthetic intermediates of functional materials such as electrochromic compounds [79–81].

Micromixing serves as a powerful method for selectivity control of various competitive consecutive reactions. For example, fast micromixing enables reactions of functionalized aryllithiums with dialkyl oxalates in order to obtain α-keto esters with high selectivity [82]. However, reactions of organometallic species with dialkyl oxalates or oxalyl chloride often suffer from low yields because the initial products react with other molecules of the organometallic species, producing by-products such as alcohols and diketones even when only one equivalent of the organometallic species is used.
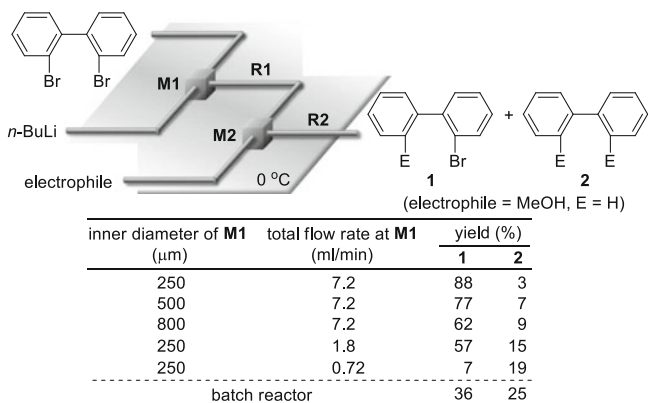
Fig. 31 Selective monolithiation of dibromobiaryls followed by reaction with electrophiles using a flow microreactor system. M1 and M2 represent micromixers; R1 and R2 represent microtube reactors
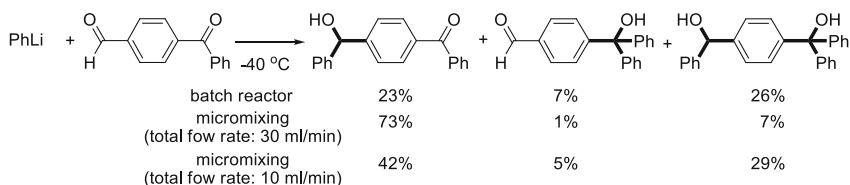
Fig. 32 Chemoselective reaction of 4-benzoylbenzaldehyde with PhLi using either conventional macro batch reactor or flow microreactor

Micromixing also allows for highly chemoselective reactions [83]. One of the central issues in organic synthesis is chemoselectivity, which refers to the preferential reaction of a chemical reagent or reactive species with one of two or more different functional groups. In general, chemoselective nucleophilic reactions of difunctional electrophiles are simple if the reactivity of one functional group is higher than that of the other. However, this is not true if the reaction is very fast. In fact, the reaction of 4-benzoylbenzaldehyde with one equivalent of phenyllithium in a batch reactor leads to the formation of a mixture of three products, even though aldehydes are generally more reactive than ketones (Fig. 32). Conversely, remarkable chemoselectivity has been achieved using fast micromixing, affording the desired compound with high selectivity at high flow rates. Moreover, the flow microreactor method can also be applied to chemoselective three-component couplings. For example, the reaction with *p*-cyanophenyllithium at the aldehyde carbonyl group followed by reaction with *p*-nitrophenyllithium at the ketone carbonyl group successfully afforded the desired product in 61% yield (Fig. 33).
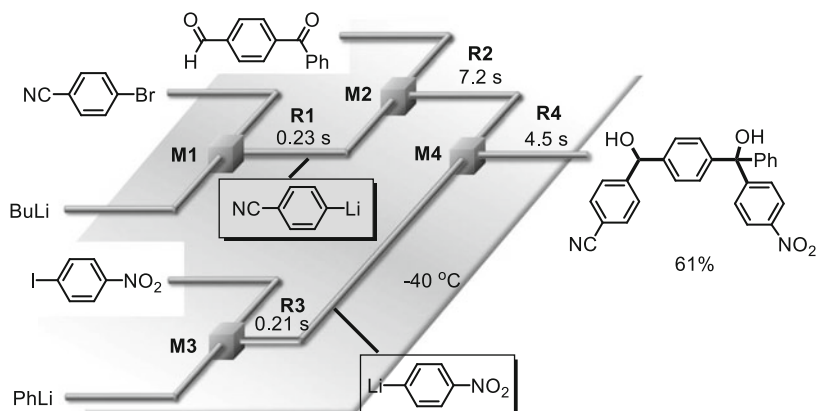
Fig. 33 Chemoselective three-component coupling using integrated flow microreactor system. M1, M2, M3, and M4 represent micromixers; R1, R2, R3, and R4 represent microtube reactors

2.11 Integration of Organolithium Reactions

Generally, complex molecules are synthesized via stepwise formation of individual bonds in the target molecule (multistep synthesis). Intermediate products are often separated and purified before being used as substrates for the next step, making the overall synthesis labor-intensive and time-consuming. To meet demands for synthesis of variety of compounds of desired functions, the speed and efficiency of multistep chemical syntheses need to be greatly enhanced through integration of several chemical reactions, that is, by forming several bonds in a single sequence in one pot (time integration) or one flow (space integration) without isolating intermediates [84, 85].

Carbolithiation of benzyne with functionalized aryllithium species followed by reaction with various electrophiles serves as a good example of reaction integration using a flow microreactor system [86]. 2-Bromophenyllithium and a functional aryllithium are generated from 1-bromo-2-iodobenzene and the corresponding aryl halide, respectively in flow, and then are mixed at −70°C. In the subsequent reactor, 2-bromophenyllithium decomposes at −30°C to generate benzyne without affecting the functional aryllithium. This process is followed by spontaneous carbolithiation of benzyne with the aryllithium. The resulting functional biaryllithium is then reacted with an electrophile in the subsequent reactor to yield the corresponding three-component coupling product. The precise optimization of the reaction conditions using temperature–residence time mapping is responsible for the success of this three-component coupling. The method has been successfully applied to the synthesis of Boscalid (Fig. 34).

The direct use of aryllithiums generated by halogen–lithium exchange for metal-catalyzed coupling reactions, such as Pd-catalyzed Murahashi coupling [87] with aryl halides, expands the scope of flow microreactor syntheses using organolithium species (Fig. 35). However, the formation of BuBr in Br–Li exchange is a major
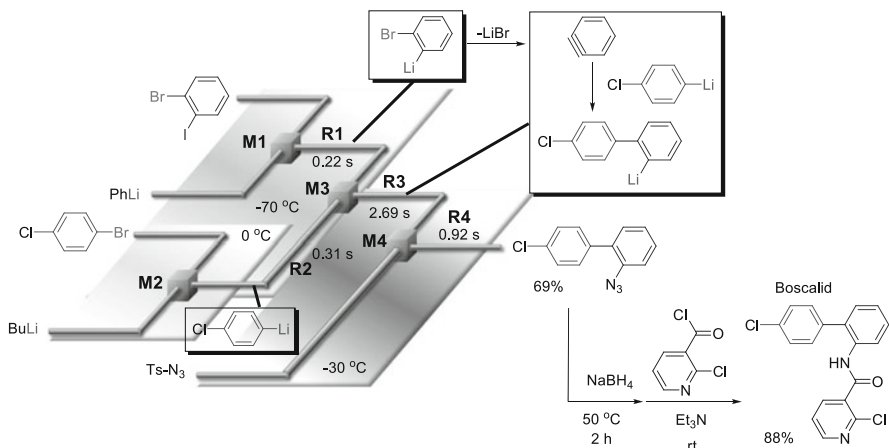
Fig. 34 Synthesis of Boscalid via the three-component coupling of benzyne, a functional aryllithium, and a tosyl azide. M1, M2, M3, and M4 represent micromixers; R1, R2, R3, and R4 represent microtube reactors
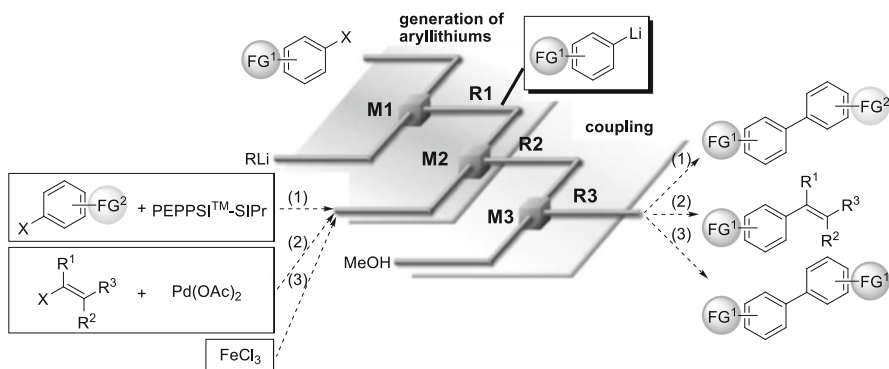
Fig. 35 Space integration of X–Li exchange and (*1*) Murahashi coupling with aryl halides, (*2*) Murahashi coupling with vinyl halides, and (*3*) oxidative homocoupling. M1, M2, and M3 represent micromixers; R1, R2, and R3 represent microtube reactors

problem for this integration, because BuBr causes serious side reactions if the subsequent Pd-catalyzed coupling with aryl halides, which is the so-called Murahashi coupling, is slow. However, PEPPSI-SIPr ([1,3-bis(2,6-diisopropyl-phenyl)imidazolidene](3-chloropyridyl)palladium(II) dichloride) serves as an effective catalyst for this purpose. Thus, halogen–lithium exchange followed by Murahashi coupling provides a straightforward method for coupling of two different aryl and heteroaryl bromides to afford the corresponding biaryls and biheteroaryls [88]. Moreover, this method can be applied to coupling with vinyl halides [89]. The oxidative homocoupling of aryllithium species can also be accomplished by using a stoichiometric amount of FeCl$_3$ [90]. Organolithium reagents are also

used for various metal-catalyzed reactions such as Rh-catalyzed 1,4-addition [91] under continuous flow conditions.

3   Organomagnesium Species

Organomagnesium species or Grignard reagents have played important roles in organic and organometallic chemistry since their Nobel-Prize-winning discovery by Grignard. Many organomagnesium reagents are commercially available and have found various applications in industrial processes because of their excellent reactivities toward various electrophiles. However, reactions involving organomagnesium reagents often need to be controlled by operating at low temperatures; therefore, flow microreactors can be used.

3.1   Arylmagnesium Halides and Heteroarylmagnesium Halides

Organomagnesium halides are often prepared by the reaction of organic halides with magnesium metal. Halogen–magnesium exchange reactions can also be used for preparing organomagnesium halides that are difficult to prepare by the method using magnesium metal. Sometimes halogen–magnesium exchange reactions are, however, very fast and highly exothermic and therefore are difficult to control, especially in large-scale syntheses. In such cases slow addition is used to avoid rapid temperature increase. Thus, flow microreactors are quite effective for performing such halogen–magnesium exchange reactions.

For example, continuous operation of the Br–Mg exchange reaction of ethylmagnesium bromide and bromopentafluorobenzene (BPFB) has been achieved at 20°C for 24 h using a system involving a micromixer connected to a shell and tube microheat exchanger to produce pentafluorobenzene (PFB) after protonation (Fig. 36) [92].

Flow microreactors also proved effective for LiCl-mediated halogen–magnesium exchange reactions. The preparation of functional arylmagnesium species followed by reaction with various electrophiles has been accomplished at room temperature using a flow system (Fig. 37) [93]. Inline IR spectroscopy is very useful to ensure the quality of the organomagnesium halides in solution and to quickly optimize the reaction conditions.

Magnesiation of heteroaromatic compounds containing electron-withdrawing substituents should be performed at cryogenic temperatures such as −78°C to avoid dimerization through nucleophilic addition reactions to the heterocyclic ring. However, magnesiation of functional pyridines using TMPMgCl·LiCl (TMP = 2,2,6,6-tetramethylpiperidyl) can be conducted using a continuous flow
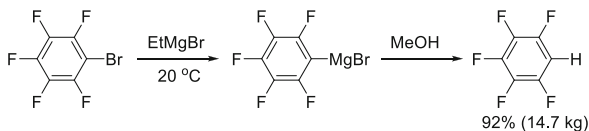
Fig. 36 Br–Mg exchange reaction of ethylmagnesium bromide (EtMgBr) and bromopentafluorobenzene (BPFB) followed by reaction with methanol
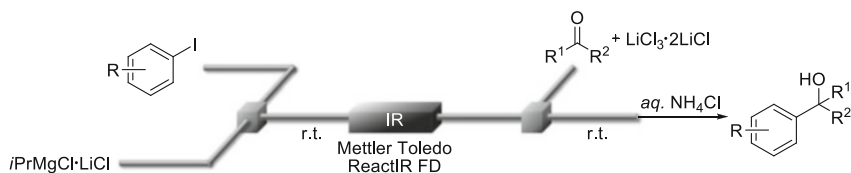
Fig. 37 Generation of functional arylmagnesiums followed by reaction with electrophiles in flow
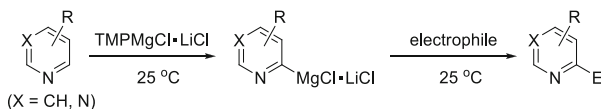
Fig. 38 Metalation of functional pyridines followed by reaction with electrophile using continuous flow reactor
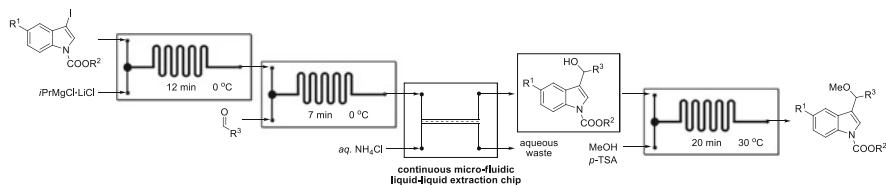
Fig. 39 Metalation of functional pyridines followed by reaction with electrophile using continuous flow reactor

system at 25°C [94], allowing for avoidance of the cryogenic conditions (Fig. 38). TMPMgClLiCl is a highly THF-soluble base that can magnesiate a wide range of substrates. Moreover, the present method can be applied to the magnesiation of other heteroaromatic compounds, such as pyrimidines, thiophenes, and thiazoles, bearing electron-withdrawing substituents.

The iodine–magnesium exchange of 3-iodoindoles was used for the continuous flow multistep synthesis of compounds containing the 3-indolylmethyl motif. Transformations, including iodo–magnesium exchanges, trapping reactions with aldehydes, and acid-catalyzed nucleophilic substitutions, were performed to obtain 36 indole derivatives in an automated sequential fashion (Fig. 39) [95].
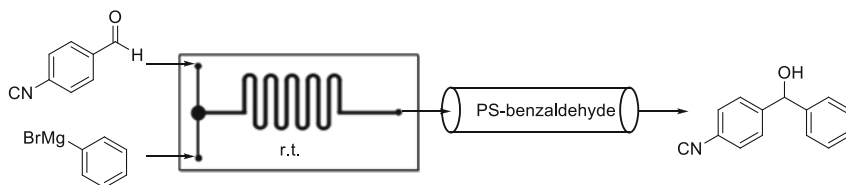
Fig. 40 Reactions of organomagnesium halides with aldehyde in flow
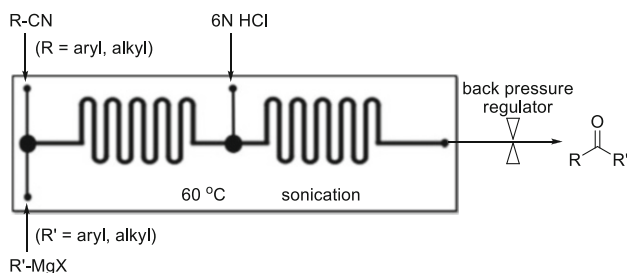
Fig. 41 Synthesis of ketones by the addition of organomagnesium halides to nitriles in flow

The use of flow microreactors is also effective for controlling reactions of organomagnesium halides that are prepared in batch. For example, reactions of carbonyl compounds with phenylmagnesium bromide were performed in an efficient and safe manner at room temperature using a flow reactor connected to a glass column packed with PS-benzaldehyde to trap excess Grignard reagent (Fig. 40) [96]. This method afforded secondary and tertiary alcohols in excellent yields and could also be applied to the preparation of tramadol. Moreover, selective addition of Grignard reagents to aldehydes and ketones in the presence of a nitrile group was achieved.

Continuous flow reactors can be applied for the synthesis of ketones through nucleophilic addition of Grignard reagents to nitriles and subsequent hydrolysis (Fig. 41) [97]. This method provides a safe and reproducible procedure, resulting in gram-scale preparations, whereas inverse addition of the reaction mixture over 6N HCl and longer reaction times are required for batch reactions. Reactions of organomagnesium halides with other electrophiles can also be formed using flow microreactors [98–100].

The use of flow microreactors is also effective for Grignard reactions with gaseous reagents. The introduction of gases into flow streams can be achieved through various methods such as plug-flow techniques and mechanical mixing of gas–liquid phases. The use of gas-permeable membrane tubing (Teflon AF-2400) is a particularly effective method of delivering gas to liquid flow streams in a controlled manner, and it has been developed and applied for the carboxylation of Grignard reagents (Fig. 42) [101]. Teflon AF-2400 is a chemically inert copolymer of tetrafluoroethylene (TFE) and 2,2-bis(trifluoromethyl)-4,5-difluoro-1,3-dioxole with high gas permeability. Thus, Teflon AF-2400 tubing was placed within a 1/8″
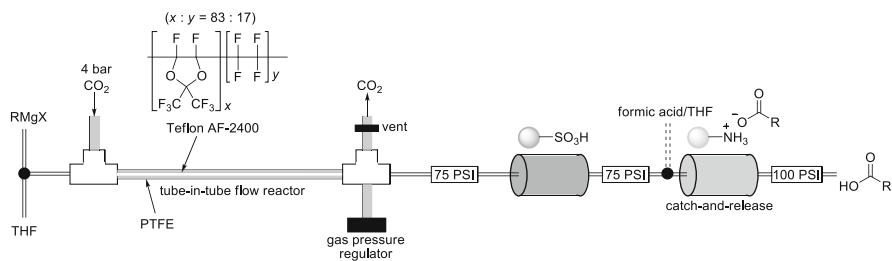
Fig. 42 Carboxylation of organomagnesium halides in flow
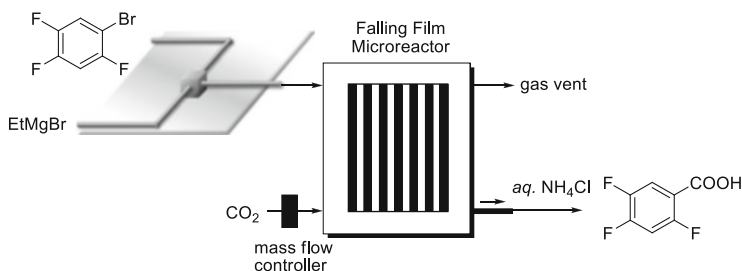
Fig. 43 Synthesis of 2,4,5-trifluorobenzoic acid in flow

(outer diameter) PTFE tube. The PTFE outer tubing was filled with CO_2, which was then transferred into the Grignard reagent stream through diffusion. The gas pressure regulator was set to depressurize the reactor upon exceeding the 10 bar limit. The Grignard reagent stream was diluted with THF to preclude blocking of the reactor through precipitation of magnesium salts formed during the carboxylation step. In addition, the resulting solutions were purified through a glass cartridge packed with polymer supported sulfonic acid (QP-SA) to effectively remove the magnesium salts and simultaneously protonate the carboxylate to form the corresponding acid in a catch-and-release manner. In addition to arylmagnesium halides, alkyl and alkynyl magnesium halides can be used for the carboxylation reactions.

A continuous flow microreactor system was successfully applied to the preparation of 2,4,5-trifluorobenzoic acid via a two-step reaction involving halogen–magnesium exchange and carboxylation (Fig. 43) [102]. 2,4,5-Trifluorobenzoic acid is a valuable synthetic intermediate with important applications in the pharmaceutical industry and materials science. The halogen–magnesium exchange reaction was conducted in a simple T-microreactor, generating the 2,4,5-trifluorophenylmagnesium bromide in nearly quantitative yields from 2,4,5-trifluorobromobenzene and EtMgBr. Commercially available falling film microreactor (FFMR) was then used to facilitate the gas–liquid carboxylation reaction. The use of a FFMR enabled the highly efficient gas–liquid reaction of the resultant Grignard reagent with CO_2 under atmospheric pressure. This procedure is simple,

Fig. 44 Aerobic oxidation
of arylmagnesium halides to
give phenols in flow
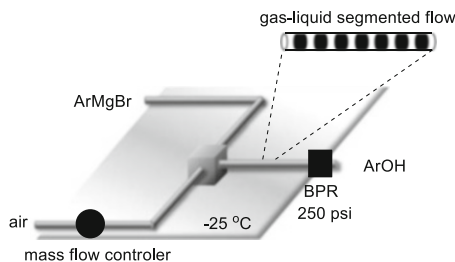
convenient, and efficient, affording the desired product in high yield and high purity
after a simple extraction.

Phenol synthesis via direct aerobic oxidation of arylmagnesium halides with
compressed air can be performed in a continuous gas–liquid segmented flow system
consisting of a precooling PFA tubing coil and a backpressure regulator (Fig. 44)
[103]. A gas–liquid segmented flow is generated in the tubing reactor coil after
combination of the liquid and gas streams in the mixer. The outcome of the reaction
significantly depends on temperature and pressure. Higher yields are obtained under
pressures greater than 200 psi at −25°C. A wide range of substituted phenols can be
synthesized using the method. In addition, by incorporating inline generation of
functionalized arylmagnesium halides from benzyne intermediates before the aero-
bic oxidation process, a facile three-step one-flow preparation of *ortho*-
functionalized phenols has been accomplished in a modular fashion.

Arylmagnesium halides have also been used for metal-catalyzed coupling reac-
tions such as the Kumada coupling under continuous flow conditions [104, 105].

Arylboronic acids can be synthesized by the reaction of arylmagnesium halides
with borate esters. For example, the reaction of phenylmagnesium bromide with
trimethylborate leads to the formation of phenyldimethoxyborane, which is hydro-
lyzed to give phenylboronic acid. However, a batch reaction gives a significant
amount of a boron compound having two phenyl groups presumably because of the
disguised chemical selectivity. The use of a flow microreactor system involving a
micromixer solves the problem [106]. Phenylboronic acid can be obtained in high
selectivity by virtue of extremely fast mixing.

3.2   Alkynylmagnesium Halides

Alkynylmagnesium halides, such as ethynylmagnesium bromide, for the introduc-
tion of acetylenic functionality are fundamental in organic synthesis; however, they
are generally prepared via a highly exothermic gas–liquid reaction of acetylene
with an alkyl–Grignard reagent. Therefore, development of an efficient method for
generation of ethynyl–Grignard reagents from acetylene is highly needed. The
preparation of ethynylmagnesium bromide in a batch reactor generally involves
the slow addition of EtMgBr into a THF solution followed by a strong flow of
acetylene with vigorous stirring, producing large amounts of precipitates. In
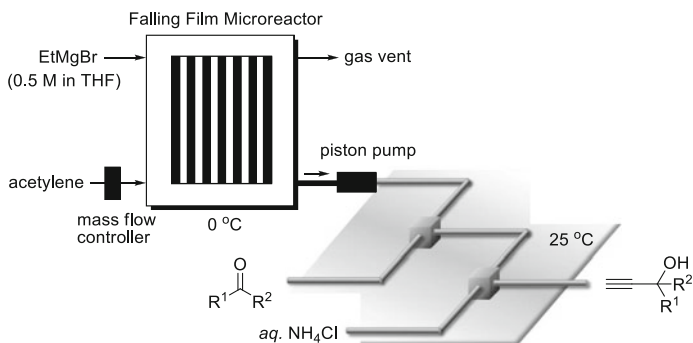
Fig. 45 Synthesis of propargylic alcohols from EtMgBr, acetylene, and carbonyl compounds in flow
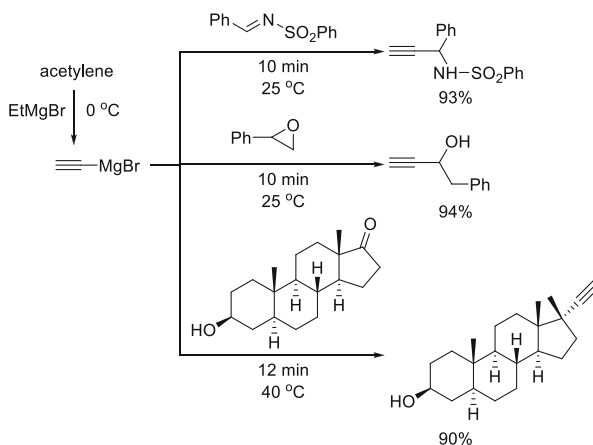
Fig. 46 Syntheses of acetylenic compounds using ethynylmagnesium bromide generated by the reaction of ethylmagnesium bromide and acetylene using the gas–liquid microflow protocol

addition, excess reagents (e.g., alkyl–Grignard reagents) and possible by-products such as bis(halidomagnesium)acetylene can also negatively affect the downstream reactions, resulting in poor yields and selectivity. Conversely, the use of a commercially available FFMR composed of 64 vertically positioned microchannels (300 μm width and 100 μm depth) enabled the efficient and consistent gas–liquid contact reaction of acetylene gas at atmospheric pressure and EtMgBr to generate thin liquid layers in the microchannels (Fig. 45) [107]. After reaction with carbonyl compounds, various propargylic alcohols were obtained in high yields. Decreasing the acetylene flow rate was crucial for increasing the yields of the desired products as the gas flows in a large chamber above the microchannels, thereby facilitating gas–liquid contact and diffusion. Moreover, this gas–liquid microflow protocol could be readily extended to the synthesis of various important acetylenic compounds such as propargylic amides (Fig. 46).
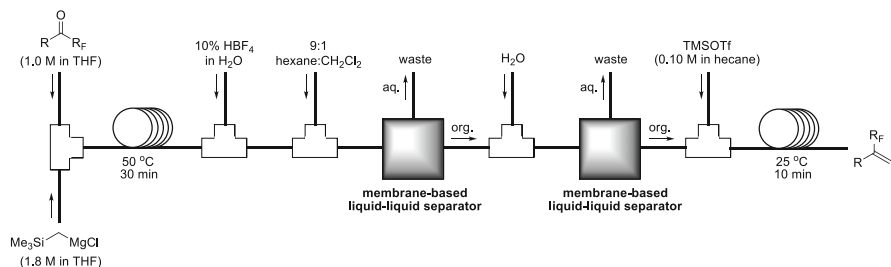
Fig. 47 Methylenation of trifluoromethyl ketones using (trimethylsilyl)methylmagnesium chloride in flow

The reaction of ethynylmagnesium bromide with 2-adamantanone in a reactor affords 2-ethynyl-2-adamantanol in 80% isolated yield on a 0.30 mol scale after standard aqueous extraction [108].

3.3   Alkylmagnesium Halides

Alkylmagnesium halides can also be used in continuous flow reactions. For example, (trimethylsilyl)methylmagnesium chloride reacts with trifluoromethyl ketones to give 3,3,3-trifluoromethylpropenes in flow; Grignard addition followed by dehydrative desilylation with trimethylsilyl trifluoromethanesulfonate takes place (Fig. 47) [109]. Although the first step should be performed in a Lewis basic solvent such as THF, these solvents have severely detrimental effects on the dehydrative desilylation step. Therefore, an inline aqueous/organic extraction and concomitant solvent switch are essential for the success of this methodology. For this purpose, a membrane-based liquid–liquid separator is used to remove the water-soluble magnesium salts and switch THF for hexane/dichloromethane. This two-step reaction sequence avoids the isolation of the intermediate, α-trifluoromethyl-β-hydroxysilyl alcohols.

4   Anionic Polymerization

Anionic polymerization has received significant attention since their first report by Michael Szwarc in 1956 [110] and serves as an important and powerful method in macromolecular synthesis. Organolithium species are often used as initiators for anionic polymerizations of vinyl monomers such as styrenes, alkyl methacrylates, and alkyl acrylates. Therefore, anionic polymerization reactions can be regarded as organolithium reactions. A major drawback of conventional anionic polymerizations performed in polar solvents in batch reactors is that they require very low temperatures (e.g., −78°C), severely limiting their industrial applications.

Through the use of nonpolar solvents, these polymerizations can be conducted at higher temperatures, but much longer reaction times are required for completion. The use of flow microreactors enables anionic polymerization at higher temperatures than those required for batch polymerization.

4.1 Anionic Polymerization of Styrenes

Anionic polymerization of styrene derivatives having silyl, methoxy, alkynyl, and alkylthio groups on the benzene ring can be conducted at 0–24°C in tetrahydrofuran (THF) to obtain the corresponding polystyrenes with narrow molecular weight distributions (e.g., styrene: number average molecular weight (M_n) = 1,200–20,000, M_w/M_n = 1.09–1.13) (Fig. 48) [111, 112]. Moreover, the molecular weight can be easily controlled by changing the ratio of monomer and initiator solution flow rates. It should be noted that complete dryness of the apparatus and high vacuum techniques are required for classical batch methods; however, such experimental efforts can be significantly reduced by using flow microreactors. Residual impurities and moisture can be removed by purging the reactor with small amounts of monomer and initiator solutions prior to collection of the desired polymer product from the outlet of the flow microreactor. The flow microreactor method also enables living anionic polymerization of 2-vinylpyridine without additives [113]. This polymerization in a batch system requires the addition of inorganic salts such as LiCl due to the occurrence of an undesired side reaction between the carbanionic active chain ends and the electron-poor pyridine ring. In contrast, controlled polymerization can be achieved without the addition of LiCl using flow microreactors to obtain polymers with narrow molecular weight distributions. It is important to note that a tangential four-way jet mixing device produced a turbulent mixing pattern that enabled the formation of high-molecular-weight polymers.

Because the carbanionic polymer ends are living, structurally well-defined polymers, such as end-functionalized polymers and block copolymers, can be synthesized using integrated flow microreactor systems consisting of two micromixers and two microtube reactors, for example, functionalization of a living polymer end with chlorosilanes, such as chlorotrimethylsilane and chlorodimethylvinylsilane to obtain silyl-functionalized polystyrenes. Block copolymerization can also be effectively achieved using an integrated flow microreactor system at 24°C to obtain copolymers composed of two different styrenes in quantitative yields (Fig. 49).

End functionalization of carbanionic polymer ends with epoxides is also popular. Styrene polymerization followed by end functionalization with various glycidyl ethers having acetal structures, such as ethoxy ethyl glycidyl ether, 1,2-isopropylidene glyceryl glycidyl ether, and *trans*-2-phenyl-1,3-dioxane glycidyl ether, was accomplished using an integrated flow microreactor system
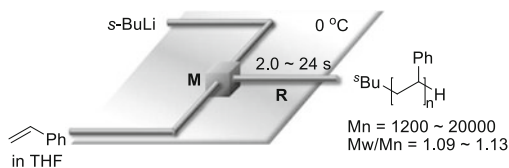
Fig. 48 Anionic polymerization of styrene in THF initiated by *s*-BuLi using a flow microreactor. M represents a micromixer; R represents a microtube reactor
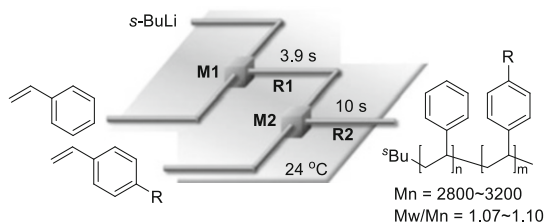
Fig. 49 Anionic block copolymerization of styrenes in THF using an integrated flow microreactor system. M1 and M2 represent micromixers; R1 and R2 represent microtube reactors
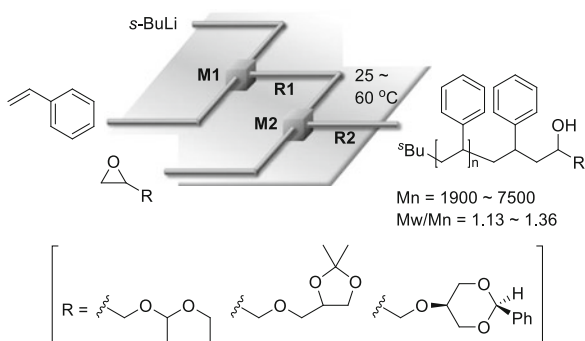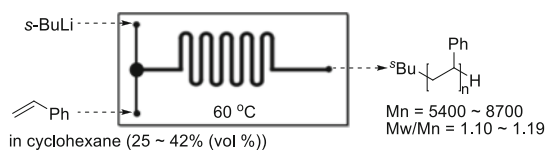

Fig. 50 Anionic polymerization of styrene in THF initiated by *s*-BuLi and subsequent functionalization with epoxides using an integrated flow microreactor system. M1 and M2 represent micromixers; R1 and R2 represent microtube reactors

(Fig. 50) [114]. The acetal and ketal protecting groups in glycidyl ethers are stable toward highly reactive carbanionic polymer ends but can easily be cleaved under acidic conditions to afford multihydroxyl end-functionalized polymers.

Syntheses of various branched polymers with complex architectures, such as star polymers and dendrimer-like, star-branched polymers, using living anionic polymerization have been extensively studied. Block copolymers having different polymer chains on a single core are especially interesting. To synthesize such a structure, an initial selective 1:1 reaction of a living polymer chain and a polyfunctional core molecule are essential. In a conventional batch reactor, an excess amount of the polyfunctional core should be used to suppress formation of the 1:2 adduct. However, this is problematic because an excess amount of the functional
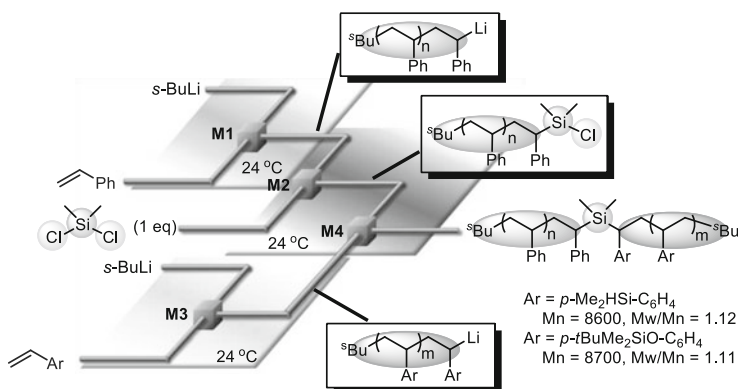
Fig. 51 Synthesis of block copolymers having two different polymer chains on single silicon core using an integrated flow microreactor system. M1, M2, M3, and M4 represent micromixers; R1, R2, R3, and R4 represent microtube reactors

Fig. 52 Anionic polymerization of styrene initiated by s-BuLi in cyclohexane at 60°C at high monomer concentrations using aluminum–polyimide microfluidic device

core should remain unchanged in the first step; therefore, it should be removed before proceeding to the second step. This problem can be solved by micromixing because of the problem of disguised chemical selectivity can be avoided [70–72, 115, 116]. As shown in Fig. 51, end functionalization with one equivalent of dichlorodimethylsilane leads to selective formation of a product having a single polymer chain on silicon ($M_n = 1,400$, $M_w/M_n = 1.13$). Extremely fast 1:1 micromixing of the living polymer chain and dichlorodimethylsilane enables selective formation of the 1:1 adduct. Therefore, the subsequent reaction with another living polymer chain using an integrated flow microreactor system affords block copolymers having two different polymer chains on a single silicon core. Chlorosilane having a single polymer chain can also be used for the subsequent reaction with alcohols and Grignard reagents.

Flow microreactors are also effective for anionic polymerization of styrenes in nonpolar solvents. It is important to note that batch polymerizations should be conducted with <20% v/v styrene, because those with >20% v/v may result in rapid increase of the reaction temperature, causing potential danger. This problem can be solved by the use of a flow microreactor. In fact, controlled anionic polymerization of styrene initiated by s-BuLi in cyclohexane as a nonpolar solvent can be conducted at 80°C using a flow microreactor to obtain polystyrenes in quantitative yields within 1–5 min (Fig. 52). Controlled polymerization of styrene in

cyclohexane at high monomer concentrations (25–42% v/v styrene) at 60°C can be achieved using an aluminum–polyimide microfluidic device [117]. The molecular weight distribution of the polymers is influenced by the channel patterns (i.e., straight, periodically pinched, obtuse zigzag, and acute zigzag channels).

4.2   Anionic Polymerization of Alkyl Methacrylates

Synthesis of poly(alkyl methacrylate)s with well-defined structures is very important from a viewpoint of materials chemistry. However, anionic polymerization of alkyl methacrylates using a conventional batch reactor must be conducted at low temperatures (e.g., −78°C) to obtain polymers with narrow molecular weight distributions. In contrast, anionic polymerization using flow microreactors affords the corresponding poly(alkyl methacrylate)s with a high level of molecular weight control at easily accessible temperatures (e.g., −28°C for methyl methacrylate (MMA) ($M_w/M_n = 1.16$), 0°C for butyl methacrylate (BuMA) ($M_w/M_n = 1.24$), and 24°C for *tert*-butyl methacrylate (*t*-BuMA) ($M_w/M_n = 1.12$)) [118]. Precise control of the reaction temperature and fast mixing of the monomer and initiator in a flow microreactor system seem to be responsible for better controllability (Fig. 53). In these cases, 1,1-diphenylhexyllithium is used as an initiator.

Whether the polymer end is living in a flow microreactor can be verified by changing the residence time (Fig. 54). To perform this verification, alkyl methacrylate and 1,1-diphenylhexyllithium solutions are mixed in the first micromixer (M1) and polymerization is conducted in the first microtube reactor (R1). A solution of the same monomer is then introduced in the second micromixer (M2), which is connected to the second microtube reactor (R2), where the sequential polymerization occurs. By changing the length of R1 with a fixed flow rate, the effect of residence time there can be examined. M_n increases upon addition of the second monomer solution; however, increasing the residence time causes an increase in M_w/M_n, presumably due to decomposition of the polymer end before addition of the second monomer solution (Fig. 54). By choosing an appropriate residence time in R1 (2.95 s for MMA; 0.825 s for BuMA), sequential polymerization can be successfully conducted without significant decomposition of the living polymer end, leading to the formation of a polymer having a narrow molecular weight distribution [119].

Living anionic polymerization of perfluoroalkyl methacrylates initiated by 1,1-diphenylhexyllithium can also be formed in a flow microreactor system [120]. High degree of molecular weight distribution control is achieved for the polymerization of 2-(nonafluorobutyl)ethyl and 2-(tridecafluorohexyl)ethyl methacrylates without the addition of LiCl at 0°C, whereas very low temperatures (e.g., −78°C) and four equivalents of LiCl are required to prevent side reactions in batch reactors.
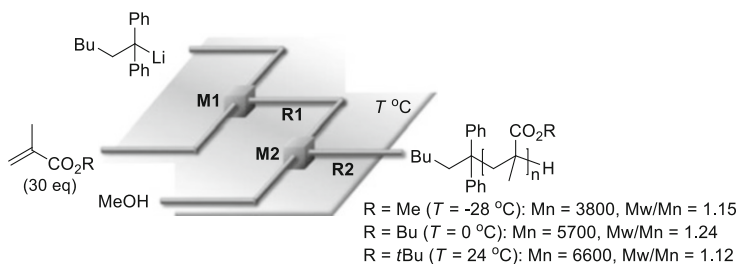
Fig. 53 Anionic polymerization of alkyl methacrylates initiated by 1,1-diphenylhexyllithium using a flow microreactor system. M1 and M2 represent micromixers; R1 and R2 represent microtube reactors
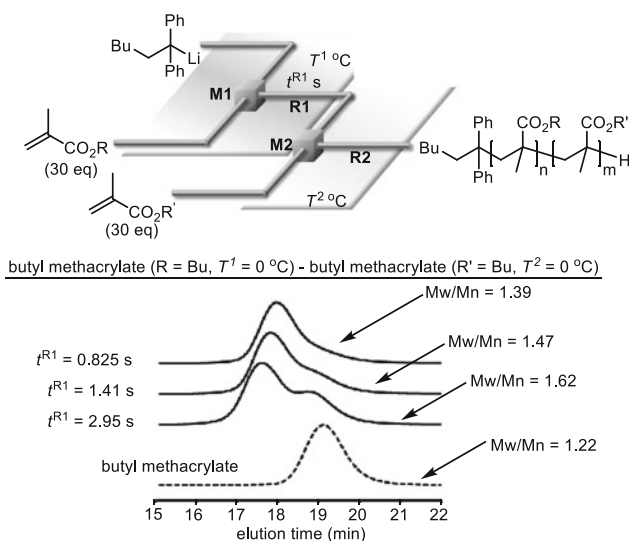
Fig. 54 Sequential anionic polymerization of alkyl methacrylates initiated by 1,1-diphenylhexyllithium using a flow microreactor system

The subsequent reaction of a reactive polymer chain end leads to the formation of fluorine-containing block copolymers with narrow molecular weight distribution.

4.3 Anionic Polymerization of Alkyl Acrylates

The anionic polymerization of acrylates is more problematic than that of styrenes or alkyl methacrylates in terms of polymer yield, molecular weight, and molecular weight distribution. This increased difficulty is due to inherent side reactions such as nucleophilic attack of the initiator and/or the enolate anion propagating
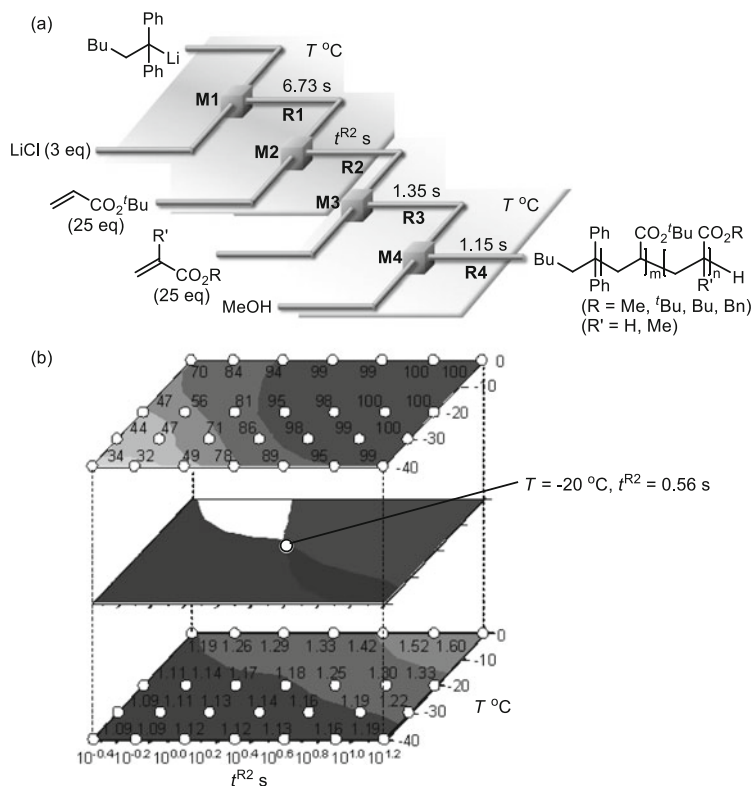
Fig. 55 Sequential polymerization of *tert*-butyl acrylate with *tert*-butyl acrylate or alkyl methacrylates initiated by 1,1-diphenylhexyllithium. (**a**) An integrated flow microreactor system. M1, M2, M3 and M4 represent micromixers; R1, R2, R3 and R4 represent microtube reactors. (**b**) Temperature–residence time (in R1) map. (*Upper*) Contour map with scatter overlay of conversion for the first polymerization of *tert*-butyl acrylate, indicated by *numbered circles*; (*lower*) contour map with scatter overlay of M_w/M_n of the final polymer, indicated by *numbered circles*; and (*middle*) domain that yielded highest conversion (>95%) and narrowest molecular weight distribution ($M_w/M_n < 1.2$)

polymer chain end on the ester carbonyl group in the polymer chain, as well as abstraction of an acidic hydrogen attached to the carbon alpha to the ester carbonyl group. Significant amounts of additives such as LiCl are often used to suppress such side reactions; however, the use of flow microreactors enables the anionic polymerization of *tert*-butyl acrylate at $-20°C$ with a significantly reduced amount of LiCl while maintaining a narrow molecular weight distribution [121]. Moreover, block copolymerization reactions of a reactive polymer chain end with *tert*-butyl acrylate or an alkyl methacrylate can be achieved using an integrated flow microreactor system to obtain block copolymers with a narrow molecular weight distribution. In an example shown in Fig. 55, narrow molecular weight distribution ($M_w/M_n < 1.2$) with quantitative conversion in the first polymerization (>95%) was obtained using the appropriate residence time and temperature ($T = -20°C$, $t^{R2} = 0.56$ s).
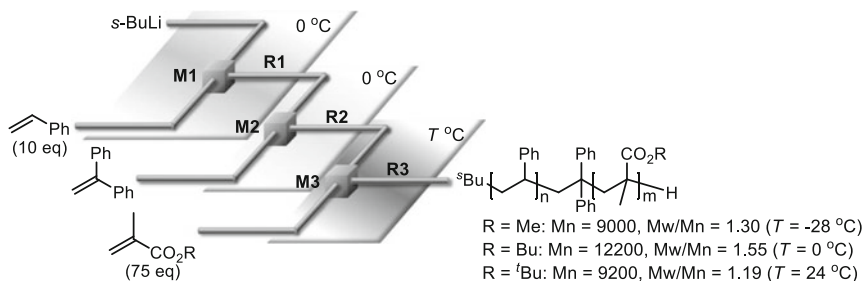
Fig. 56 Anionic block copolymerization of styrene and alkyl methacrylates initiated by *s*-BuLi using an integrated flow microreactor system. M1, M2, and M3 represent micromixers; R1, R2, and R3 represent microtube reactors

4.4 Anionic Block Copolymerization of Styrenes and Alkyl Methacrylates

As mentioned above, flow microreactors are effective at controlling the anionic polymerizations of styrenes and alkyl methacrylates. One advantage of flow microreactor-controlled polymerization is the easy modulation of flow microreactors to integrate polymerization reactions. In fact, through the use of integrated flow microreactors, the polystyrene living polymer end, which is produced by *s*-BuLi-initiated anionic polymerization of styrene, can be effectively trapped with 1,1-diphenylethylene, and the resulting organolithium species can be used as a macroinitiator for the anionic polymerization of alkyl methacrylates. Therefore, styrene-alkyl methacrylate diblock copolymers can be synthesized with a high level of molecular weight distribution control at easily accessible temperatures, such as between 24°C and −28°C (Fig. 56) [122]. Moreover, triblock copolymers can be synthesized in a similar manner by sequential introduction of styrene and two different alkyl methacrylates (styrene–*t*-BuMA–MMA triblock copolymer, $M_n = 8{,}800$, $M_w/M_n = 1.23$; styrene–*t*-BuMA–BuMA triblock copolymer, $M_n = 9{,}000$, $M_w/M_n = 1.35$).

5 Conclusions

As demonstrated by the examples discussed in this chapter, organometallic reactions that are difficult to perform via batch processes can be accomplished through the use of flow microreactors. The characteristic features of flow microreactors, such as short residence time and precise residence time control, are responsible for the control of various organometallic reactions. Thus, it is expected that continuous flow microreactor systems will become an indispensable technology for organic synthesis in laboratory research and industrial production involving organometallic species.

References

1. Hessel V, Hardt S, Löwe H (2004) Chemical micro process engineering. Wiley-VCH, Weinheim
2. Wirth T (2008) Microreactors in organic synthesis and catalysis. Wiley-VCH, Weinheim
3. Hessel V, Renken A, Schouten JC, Yoshida J (2009) Micro process engineering. Wiley-VCH, Weinheim
4. Watts P, Wiles C (2011) Micro reaction technology in organic synthesis. CRC, New York
5. Baldwin JE, Williams RM (2002) Organolithiums: selectivity for synthesis. Pregamon, Amsterdam
6. Hikage S, Yoshida J. JP 2003-337787, JP 4639042
7. Schwalbe T, Autze V, Hohmann M, Stirner W (2004) Org Process Res Dev 8:440
8. Zhang X, Stefanick S, Villani FJ (2004) Org Process Res Dev 8:455
9. Nagaki A, Tomida Y, Usutani H, Kim H, Takabayashi N, Nokami T, Okamoto H, Yoshida J (2007) Chem Asian J 2:1513
10. Aoki N, Kitajima R, Itoh C, Mae K (2008) Chem Eng Technol 31:1140–1145
11. Usutani H, Tomida Y, Nagaki A, Okamoto H, Nokami T, Yoshida J (2007) J Am Chem Soc 129:3046
12. Chen LS, Chen GJ, Tamborski C (1980) J Organomet Chem 193:283
13. Nagaki A, Imai K, Kim H, Yoshida J (2011) RSC Adv 1:758
14. Choe J, Seo JH, Kwon Y, Song KH (2008) Chem Eng J 135S:S17
15. Nagaki A, Yamada S, Doi M, Tomida Y, Takabayashi N, Yoshida J (2011) Green Chem 13:1110
16. Nagaki A, Yamada D, Yamada S, Doi M, Tomida Y, Takabayashi N, Yoshida J (2013) Aust J Chem 66:199
17. Goto S, Velder J, Sheikh SE, Sakamoto Y, Mitani M, Elmas S, Adler A, Becker A, Neudörfl JM, Lex J, Schmalz HG (2008) Synlett 9:1361
18. Nagaki A, Uesugi Y, Kim H, Yoshida J (2013) Chem Asian J 8:705
19. Pieber B, Glasnov T, Kappe CO (2014) RSC Adv 4:13430–13433
20. Wu J, Yang X, He Z, Mao X, Hatton TA, Jamison TF (2014) Angew Chem Int Ed 53:8416–8420
21. Knochel P (2005) Handbook of functionalized organometallics. Wiley-VCH, Weinheim
22. Parham WE, Bradsher CK (1982) Acc Chem Res 15:300
23. Sapountzis I, Knochel P (2002) Angew Chem Int Ed 41:1610
24. Sapountzis I, Dube H, Lewis R, Gommermann N, Knochel P (2005) J Org Chem 70:2445
25. Nagaki A, Kim H, Yoshida J (2009) Angew Chem Int Ed 48:8063
26. Nagaki A, Kim H, Yoshida J (2008) Angew Chem Int Ed 47:7833
27. Nagaki A, Kim H, Moriwaki Y, Matsuo C, Yoshida J (2010) Chem Eur J 16:11167
28. Nagaki A, Kim H, Matsuo C, Yoshida J (2010) Org Biomol Chem 8:1212
29. Kim H, Nagaki A, Yoshida J (2011) Nat Commun 2:264
30. Kim H, Lee H, Kim D (2015) Angew Chem Int Ed 54:1877
31. Nagaki A, Takahashi Y, Yoshida J (2014) Chem Eur J 20:7931–7934
32. Brown HC, Cole TE (1983) Organometallics 2:1316
33. Ishiyama T, Miyaura N (2000) J Organomet Chem 611:392
34. Mo F, Jiang Y, Qiu D, Zhang Y, Wang J (2010) Angew Chem Int Ed 49:1846
35. Browne DL, Baumann M, Harji BH, Baxendale IR, Ley SV (2011) Org Lett 13:3312
36. Newby JA, Huck L, Blaylock DW, Witt PM, Ley SV, Browne DJ (2014) Chem Eur J 20:263–271
37. Shu W, Pellegatti L, Oberli MA, Buchwald SL (2011) Angew Chem Int Ed 50:10665
38. Nagaki A, Moriwaki Y, Yoshida J (2012) Chem Commun 48:11211
39. Neumann H, Seebach D (1976) Tetrahedron Lett 17:4839
40. Nagaki A, Takahashi Y, Yamada S, Matsuo C, Haraki S, Moriwaki Y, Kim S, Yoshida J (2012) J Flow Chem 2:70

41. Nagaki A, Matsuo C, Kim S, Saito K, Miyazaki A, Yoshida J (2012) Angew Chem Int Ed 51:3245
42. Nagaki A, Takahashi Y, Henseler A, Matsuo C, Yoshida J (2015) Chem Lett 44:214–216
43. Drakesmith FG, Stewart OJ, Tarrant P (1968) J Org Chem 33:280
44. Nadano R, Fuchibe K, Ikeda M, Takahashi H, Ichikawa J (2010) Chem Asian J 5:1875
45. Nagaki A, Tokuoka S, Yoshida J (2014) Chem Commun 50:15079
46. Tomida Y, Nagaki A, Yoshida J (2009) Org Lett 11:3614
47. Chinkov N, Chechik H, Majumdar S, Liard A, Marek I (2002) Synthesis 2473
48. Nagaki A, Tsuchihashi Y, Haraki S, Yoshida J (2015) Org Biomol Chem 13:7140–7145
49. Kupracz L, Kirschning A (2013) Adv Synth Catal 355:3375–3380
50. Fukuyama T, Totoki T, Ryu I (2014) Org Lett 16:5632–5635
51. Uneyama K, Katagiri T, Amii H (2008) Acc Chem Res 41:817
52. Nagaki A, Tokuoka S, Yamada S, Tomida Y, Oshiro K, Amii H, Yoshida J (2011) Org Biomol Chem 9:7559
53. Ushiogi Y, Hase T, Iinuma Y, Takata A, Yoshida J (2007) Chem Commun 2947
54. Asai T, Takata A, Nagaki A, Yoshida J (2012) ChemSusChem 5:339
55. Degennaro L, Fanelli F, Giovine A, Luisi R (2015) Adv Synth Catal 357:21–27
56. Satoh T (1996) Chem Rev 96:3303
57. Capriati V, Florio S, Luisi R (2008) Chem Rev 108:1918
58. Nagaki A, Takizawa E, Yoshida J (2009) J Am Chem Soc 131:1654
59. Nagaki A, Takizawa E, Yoshida J (2009) Chem Lett 38:486
60. Nagaki A, Takizawa E, Yoshida J (2010) Chem Eur J 16:14149
61. Nagaki A, Takizawa E, Yoshida J (2009) Chem Lett 38:1060
62. Takizawa E, Nagaki A, Yoshida J (2012) Tetrahedron Lett 53:1397
63. Giovine A, Musio B, Degennaro L, Falcicchio A, Nagaki A, Yoshida J, Luisi R (2013) Chem Eur J 19:1872
64. Umezu S, Yoshiiwa T, Tokeshi M, Shindo M (2014) Tetrahedron Lett 55:1822–1825
65. Yoshiiwa T, Umezu S, Tokeshi M, Baba Y, Shindo M (2014) J Flow Chem 4:180–184
66. Asai T, Takata A, Ushiogi Y, Iinuma Y, Nagaki A, Yoshida J (2011) Chem Lett 40:393
67. Tomida Y, Nagaki A, Yoshida J (2011) J Am Chem Soc 133:3744
68. Kagan HB (1995) Recl Travl Chim Pays-Bas 114:203
69. Rys P (1976) Acc Chem Res 9:345
70. Suga S, Nagaki A, Yoshida J (2003) Chem Commun 354
71. Nagaki A, Togai M, Suga S, Aoki N, Mae K, Yoshida J (2005) J Am Chem Soc 127:11666
72. Suga S, Nagaki A, Tsutsui Y, Yoshida J (2003) Org Lett 5:945
73. Suga S, Tsutsui Y, Nagaki A, Yoshida J (2005) Bull Chem Soc Jpn 78:1206
74. Yoshida J, Nagaki A, Iwasaki T, Suga S (2005) Chem Eng Technol 28:259
75. Beak P, Liu C (1994) Tetrahedron Lett 20:5999
76. Klis T, Servatowski J (2007) Tetrahedron Lett 48:1169
77. Nagaki A, Takabayashi N, Tomida Y, Yoshida J (2008) Org Lett 10:3937
78. Nagaki A, Takabayashi N, Tomida Y, Yoshida J (2009) Beilstein J Org Chem 5(16)
79. Ishigaki Y, Suzuki T, Nishida J, Nagaki A, Takabayashi N, Kawai H, Fujiwara K, Yoshida J (2011) Materials 4:1906
80. Suzuki T, Uchimura Y, Ishigaki Y, Takeda T, Katoono R, Kawai H, Fujiwara K, Nagaki A, Yoshida J (2012) Chem Lett 41:541
81. Suzuki T, Uchimura Y, Nagasawa F, Takeda T, Kawai H, Katoono R, Fujiwara K, Murakoshi K, Fukushima T, Nagaki A, Yoshida J (2014) Chem Lett 43:86–88
82. Nagaki A, Ichinari D, Yoshida J (2013) Chem Commun 49:3242–3244
83. Nagaki A, Imai K, Ishiuchi S, Yoshida J (2015) Angew Chem Int Ed 54:1914–1918
84. Yoshida J, Saito K, Nokami T, Nagaki A (2011) Synlett 1189
85. Suga S, Yamada D, Yoshida J (2010) Chem Lett 404
86. Nagaki A, Ichinari D, Yoshida J (2014) J Am Chem Soc 136:12245–12248
87. Murahashi SI, Yamamura M, Yanagisawa K, Mita N, Kondo K (1979) J Org Chem 44:2408

88. Nagaki A, Kenmoku A, Moriwaki Y, Hayashi A, Yoshida J (2010) Angew Chem Int Ed 49:7543
89. Nagaki A, Moriwaki Y, Haraki S, Kenmoku A, Hayashi A, Yoshida J (2012) Chem Asian J 7:1061
90. Nagaki A, Uesugi Y, Tomida Y, Yoshida J (2011) Beilstein J Org Chem 7:1064
91. Shu W, Buchwald SL (2012) Angew Chem Int Ed 51:5355
92. Wakami H, Yoshida J (2005) Org Process Res Dev 9:787–791
93. Brodmann T, Koos P, Metzger A, Knochel P, Ley SV (2012) Org Process Res Dev 16:1102–1113
94. Petersen TP, Becker MR, Knochel P (2014) Angew Chem Int Ed 53:7933–7937
95. Tricotet T, O'Shea DF (2010) Chem Eur J 16:6678–6686
96. Riva E, Gagliardi S, Martinelli M, Passarella D, Vigo D, Rencurosi A (2010) Tetrahedron 66:3242–3247
97. Mateos C, Rincon JA, Villanueva J (2013) Tetrahedron Lett 54:2226–2230
98. Taghavi-Moghadam S, Kleemann A, Golbig KG (2001) Org Process Res Dev 5:652–658
99. Golbis K, Hohmann M, Kursawe A, Schwalbe T (2004) Chem Ing Tech 76(5):598–603
100. Roberge DM, Bieler N, Mathier M, Eyholzer M, Zimmermann B, Barthe P, Guermeur C, Lobet O, Moreno M, Woehl P (2008) Chem Eng Technol 31:1155–1161
101. Polyzos A, O'Brien M, Petersen TP, Baxendale IR, Ley SV (2011) Angew Chem Int Ed 50:1190–1193
102. Deng Q, Shen R, Zhao Z, Yan M, Zhang L (2015) Chem Eng J 262:1168–1174
103. He Z, Jamison TF (2014) Angew Chem Int Ed 53:3353–3357
104. Seyler H, Subbiah J, Jones DJ, Holmes AB, Wong WWH (2013) Beilstein J Org Chem 9:1492–1500
105. Styring P, Parracho AIR (2009) Beilstein J Org Chem 5(29):1–10
106. Hessel V, Hofmann C, Löwe H, Meudt A, Scherer S, Schönfeld F, Werner B (2004) Org Process Res Dev 8:511–523
107. Deng Q, Shen R, Ding R, Zhang L (2014) Adv Synth Catal 356:2931–2936
108. Battilocchio C, Baxendale IR, Biava M, Kitching MO, Ley SV (2012) Org Process Res Dev 16:798–810
109. Hamlin TA, Lazarus GML, Kelly CB, Leadbeater NE (2014) Org Process Res Dev 18:1253–1258
110. Szwarc M (1956) Nature 178:1168
111. Nagaki A, Tomida Y, Yoshida J (2008) Macromolecules 41:6322
112. Wurm F, Wilms D, Klos J, Löwe H, Frey H (2008) Macromol Chem Phys 209:1106
113. Natalello A, Morsbach J, Friedel A, Alkan A, Tonhauser C, Müller AHE, Frey H (2014) Org Process Res Dev 18:1408–1412
114. Tonhauser C, Wilms D, Wurm F, Berger-Nicoletti E, Maskos M, Löwe H, Frey H (2010) Macromolecules 43:5582
115. Nagaki A, Kawamura K, Suga S, Ando T, Sawamoto M, Yoshida J (2005) J Am Chem Soc 126:14703
116. Yoshida J, Nagaki A, Iwasaki T, Suga S (2005) Chem Eng Technol 3:259
117. Iida K, Chastek TQ, Beers KL, Cavicchi KA, Chun J, Fasolka MJ (2009) Lab Chip 9:339
118. Nagaki A, Tomida Y, Miyazaki A, Yoshida J (2009) Macromolecules 42:4384
119. Nagaki A, Miyazaki A, Tomida Y, Yoshida J (2011) Chem Eng J 167:548
120. Nagaki A, Akahori K, Takahashi Y, Yoshida J (2014) J Flow Chem 4:168–172
121. Nagaki A, Takahashi S, Akahori K, Yoshida J (2012) Macromol React Eng 6:467
122. Nagaki A, Miyazaki A, Yoshida J (2010) Macromolecules 43:8424

Preparation of Nanomaterials in Flow at Supercritical Conditions from Coordination Complexes

Samuel Marre and Cyril Aymonier

Abstract The development of nanosciences and nanotechnologies in the twenty-first century is linked to the progresses made with the nanomaterial synthesis approaches. Control, reproducibility, scalability, and sustainability are the key issues for the design of advanced nanostructured materials. Among the synthesis methods, the supercritical fluid-based flow process presents an efficient alternative for the continuous, controlled, scalable, and sustainable synthesis of nanomaterials, especially from coordination complexes, which is the main topic of this book chapter. First, the supercritical fluids are defined and their specific properties introduced with the possibility to adjust them playing with pressure, temperature, and composition for mixtures. The case of water is also described underlining the remarkable evolution from a polar solvent in normal conditions of pressure and temperature to a nonpolar one at supercritical conditions. After, the typical supercritical flow processes of nanomaterials are technically described in details with the different elements, namely injection, mixers, reactors, and pressure regulators. This allows introducing the main operating parameters giving access to a continuous and control synthesis of nanomaterials by mastering thermodynamics, hydrodynamics, and chemistry. Coupling chemistry of coordination complexes and chemical engineering in supercritical fluids leads to the design of high-quality and unique nanostructures. This is in particular illustrated with the synthesis of nanooxides from flow supercritical sol–gel syntheses. The access to highly crystallized oxides with controlled compositions is discussed with the synthesis of $BaTiO_3$-based materials. The supercritical route is also a versatile method. Beyond the continuous production of nanooxides, it is also possible to prepare in flow nitrides, sulfides, selenides, phosphides, ..., nanocrystals (GaN, CdS, CdSe, InP, ...). Adding surfactants in situ or ex situ playing with the process offers the possibility to design

S. Marre (✉) and C. Aymonier
Supercritical Fluids Group, CNRS, Univ. Bordeaux, ICMCB, UPR9048, 33600 Pessac, France
e-mail: samuel.marre@icmcb.cnrs.fr

hybrid organic/inorganic nanoparticles with a control of the strength of the bond at the interface between the inorganic core and the organic shell. This chapter is ended with the description of supercritical coflow reactors, which allow a high level of control of the synthesis operating conditions. All the bricks are now available from a chemical engineering and coordination complex chemistry point of view to go towards multisteps and one pot processes for the continuous and sustainable design of advanced and multifunctional nanomaterials.

Keywords Continuous processes • Microfluidics • Nanomaterial synthesis • Supercritical fluids

Contents

1 Introduction

Nanomaterials and nanostructures are generally used as the active elements and/or building blocks in many applications, including photovoltaic, energy, displays [1], catalysis, imaging [2], and sensing [3–5]. Most of these applications require high-quality materials in terms of characteristics (size, size distribution, crystallinity, composition, surface functionalities, etc.), for ensuring optimal properties and ease in their final implementation. It is therefore highly important to develop nanomaterial synthesis processes exhibiting average to high production rates, being highly reproducible and potentially integrated with in situ probes for instant quality checking.

Most of the current synthesis approaches considered batch modes, which provide simple ways to demonstrate proof of concept and to synthesize non-negligible quantities of products. However, batch synthesis approaches generally display limitations in reproducibility, in particular considering size, size distribution, and quality of the nanomaterials. Such problems are mostly due to lack of control of the operating parameters. Additionally, process optimization is time consuming given

that products and reaction rates cannot be analyzed in real time due to the fact that the implementation of in situ characterization techniques is complicated.

In this view, continuous processes turn out to be solutions of choice, although this evolution from batch to flow reactor design is not always straightforward or even accepted [6], as it can lead to disruptive technology. Nevertheless, continuous nanostructure synthesis approaches have demonstrated unrivaled capacities to improve reproducibility, being able to access precise control over temperature, reagents concentration, mixing, and residence time, which are key parameters to control accurately the characteristics of the synthesized nanomaterials [7, 8]. Additionally, such processes can partly address the scaling-up limitations, by producing high-quality nanomaterials in sufficient quantities, without reducing the quality of the obtained materials [9, 10].

As a matter of fact, most of the continuous nanostructure synthesis processes are directly adapted from batch mode approaches, using liquid as the main solvents. However, these liquid characteristics have sometimes to fulfill drastic specifications in terms of physicochemical properties. The particular case of coordination complex reagents often requires high temperatures for the thermal decomposition and further nucleation/growth of nanostructures. This implies that the solvents need to remain liquid in a wide range of temperatures (from the injection at room temperature to the process temperature), which characteristics can be obtained with high-boiling-point viscous solvents. This requirement limits the number of solvents available for some synthesis (which should remain liquid – or at least dense enough – over a wide range of temperatures) and could lead to choose costly and/or toxic solvent systems, which cannot be foreseen to be used in a high production scale in a view of sustainability.

Therefore, applying pressure to the system could help using a wider range of conditions, by being able to maintain the solvents in their liquid state or also by attaining the supercritical domain [11, 12]. In this context, the particular case of materials synthesis at supercritical conditions has gained increasing interest over the past 20 years [13]. First motivated by the ability to use nontoxic solvent systems (CO_2, water, etc.), their particular tuneable properties intermediate between gases and liquids have later driven their use in this field, but also in chemistry [14].

In this chapter, we first describe the general properties of supercritical fluids and the conventional strategies/setups that have been developed to continuously synthesize materials in such fluids from coordination complex reagents. A particular emphasis will be placed on chemical engineering considerations highlighting the interest of supercritical fluids flow processes for continuous nanomaterial production. Eventually, several examples of continuous synthesis of nanomaterials in supercritical fluids are presented as an illustration.
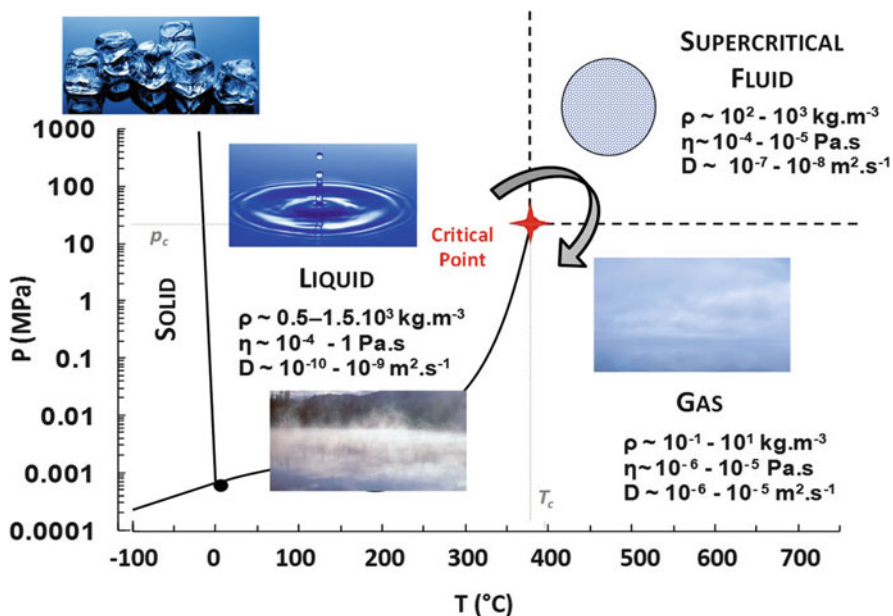
Fig. 1 p, T phase diagram of pure water

2 Supercritical Fluids and Their Associated Properties

Whatever compound can be supercritical. Indeed, as there exist three states of matter (solid, gas, liquid), a fluid is said "supercritical" when the temperature and pressure conditions exceed its critical coordinates in a p, T diagram (critical temperature: T_c and pressure: p_c, see Fig. 1 in the particular case of water) [15, 16].

The critical point is located at the very end of the gas–liquid equilibrium curve, where the densities of the gas and liquid phases become equal, meaning that the gas–liquid interface disappears. This equilibration of densities occurs via multiple fluctuations of the density of the medium at small scales (hundreds of nanometers = visible light wavelengths), which turns cloudy because of light scattering (this phenomenon is called the critical opalescence [17, 18]).

Although fluids put in close conditions to their critical points undergo mechanical and thermal instabilities leading in particular to an infinite compressibility ($\beta = -\frac{1}{V}\left(\frac{\partial V}{\partial p}\right)_T$), as $\left(\frac{\partial P}{\partial V}\right)_T = 0$ and $\left(\frac{\partial^2 P}{\partial V^2}\right)_T = 0$ where V is the molar volume), this trend is not true anymore in the conventional conditions in which supercritical fluids are used (typically $T_c < T < 2\,T_c$ and $p_c < p < 3\,p_c$), but β values remain important anyway.

Table 1 displays the critical coordinates of commonly used supercritical fluids. It can be seen that supercritical water exhibits the most difficult conditions to reach as a technological point of view to be used in its supercritical domain, while

Table 1 Critical coordinates and densities of some conventionally used supercritical fluids

Compounds	T_c (°C)	p_c (MPa)	ρ_c (kg m^{-3})
CO_2	31	7.4	468
H_2O	374	22.1	322
NH_3	132.3	11.3	235
CH_3CH_3	32.2	4.9	207
$CH_3(CH_2)_4CH_3$	234.7	3.0	233
CH_3CH_2OH	241	6.3	276
CH_3COCH_3	235	4.76	278

supercritical CO_2 has somewhat milder critical coordinates, which have driven its use in most of the supercritical fluid applications.

Depending on the targeted application, supercritical mixtures can also be considered, either to adjust the critical temperature to the practical operating conditions or to benefit from synergy effect between components to control the chemical reaction, the nucleation/growth process, or the surface functionalization of the synthesized nanomaterials.

Interestingly, the evolution of the critical coordinates of fluid mixtures is not straightforward and a particular attention has to be paid to their determination. Considering complex fluid mixtures, these data are generally difficult to find in the literature. Therefore, one can choose among either an analytical determination using conventional equations of state such as Peng–Robinson (PR) or Soave–Redlich–Kwong (SRK) [19], or an experimental determination using high-pressure optical cells. It has to be mentioned that these latters are time consuming, which has led researchers to recently develop fast and efficient microfluidic approaches in this purpose [20].

To illustrate this, Fig. 2 shows the evolution of the critical pressures and temperatures for the water/ethanol mixture.

One of the most interesting aspects of fluids exploited in their supercritical domain is definitely the possibility to switch from liquid to gas state (or opposite) without crossing the gas–liquid equilibrium curve (see arrow in Fig. 1), and therefore without experiencing any phase transition. The supercritical fluids
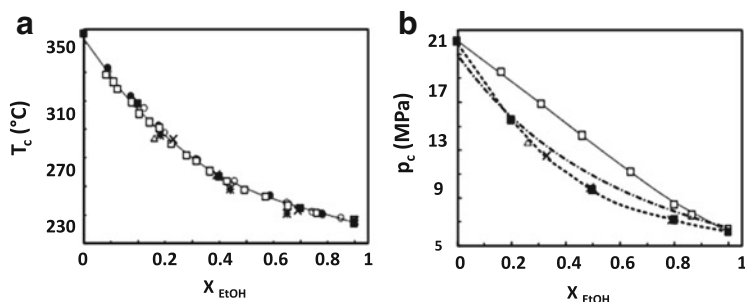
Fig. 2 Evolution of the critical coordinates of ethanol/water mixtures as a function of the molar fraction of ethanol (adapted from [21]). (**a**) Critical temperature and (**b**) critical pressure

therefore have "hybrid" physicochemical properties, intermediate between liquids and gases, which are continuously adjustable with small variations of pressure and temperature (see inserts in Fig. 1).

As seen, the first observation is that supercritical fluids exhibit liquid-like densities. Figure 3a displays the variation of the density of hexane as a function of the temperature for different pressures. It can be noticed that beyond the critical temperature (T_c), the density drops pretty fast before reaching a plateau. This phenomenon is even more pronounced when the operating pressure is getting close to the critical pressure of hexane (P_c(hexane) = 30.34 bar). However, the variation is more linear when higher pressures are considered. Overall, the density of supercritical fluids is typically in the range of 20–80% of their value in the liquid state. This means that these fluids are dense enough to be used as solvents to
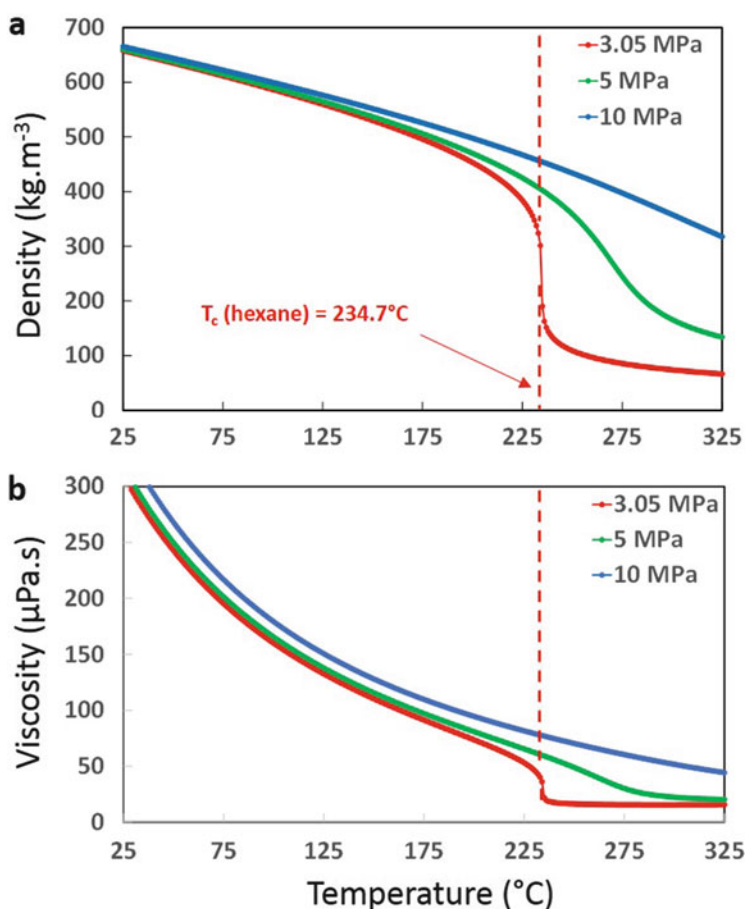
Fig. 3 Variation of the density (**a**) and the viscosity (**b**) of hexane as a function of temperature for different pressures

dissolve many molecules, such as coordination complex precursors in non-negligible concentration for processing nanomaterials [13]. Indeed, at the macroscopic scale, it is possible to correlate the solvation power of a solvent as a function of its density through the following empirical equation [22]:

$$C = \rho^k \exp\left(\frac{a}{T} + b\right)$$

where ρ is the density of the media (kg m^{-3}), while a and b can be obtained through the following relations:

$$a = \frac{\Delta H_{\text{solvation}} + \Delta H_{\text{vaporisation}}}{R}$$
$$b = \ln(M_{\text{A}} + k \cdot M_{\text{B}}) + q - k \cdot \ln M_{\text{B}}$$

With M_{A} and M_{B} being the solute and the solvent molar mass, respectively, and q a constant. k is an adjustable value determined experimentally. Therefore, there is a direct relation between the solubility of a molecule (C) and the density of the solvent (ρ). By considering a liquid solution of coordination complex reagents injected inside a high-temperature/high-pressure reactor, it is possible to finely tune the solubility of the reagents by small changes of pressure and/or temperature, gaining an additional operating parameter for controlling the nucleation processes and mastering the final nanostructure characteristics.

In addition to density, SCFs exhibit gas-like viscosities, which are of particular interest in small-scale continuous processes such as micro- and millifluidic, reducing drastically the pressure drops along the reactor (see Sect. 3). Figure 2b presents the variation of the hexane viscosity as a function of temperature for different pressures. Similarly to density, viscosity is decreasing with temperature reaching almost gas-like values when the solvent is supercritical. For viscosity, the typical values are in the range of 5–10% of their liquid-state values. This leads to a dramatic increase of the diffusion coefficient of molecules in SCFs (see Table 2), compared to liquid solvents, thus providing better mixing of reagents in continuous processes and allowing overcoming mass transfer limitation generally occurring in liquid-phase processes.

Furthermore, SCFs exhibit no surface tension, which turns out to be an undeniable advantage for processes involving surface and interface chemistries [23, 24].

As above mentioned, fluid properties undergo dramatic changes when reaching the supercritical area. However, these can be finely controlled by small variations of the pressure and temperature. The particular case of water is worth to be mentioned as no other solvent exhibits properties, which change more strongly as a function of pressure and temperature (near or above the critical point) than water. In particular, the relative static permittivity evolution of pure water (Fig. 4) shows that water becomes a good organic solvent in the supercritical region. Under ambient conditions, liquid water has a high dielectric constant (78.5 at $T = 298$ K and $p = 0.1$ MPa), which arises from dipoles of individual molecules and association

Table 2 Comparison of Reynolds numbers considering liquid or supercritical flows at various scales

	Density (kg m^{-3})	Viscosity (μPa s)	Fluid velocity (m s^{-1})	d_h (mm)	Re
Liquid millifluidics (1/8" tubing) (liquid hexane, 25°C – 0.1 MPa)	655	297	10^{-2}–1	1.6	35–3,500
Sc-millifluidics (1/8" tubing) (sc-Hexane, 300°C – 10 MPa)	358	52	10^{-2}–1	1.6	100–10,000
Liquid microfluidics (liquid hexane, 25°C – 0.1 MPa)	655	297	10^{-3}–10^{-1}	0.1	0.2–20
Sc-microfluidics (sc-Hexane, 300°C – 10 MPa)	358	52	10^{-3}–1	0.1	0.7–700

Fig. 4 Variation of the dielectric constant of water as a function of temperature for different pressures. Comparison with the relative dielectric constants of conventional solvents used in the normal conditions of pressure and temperature
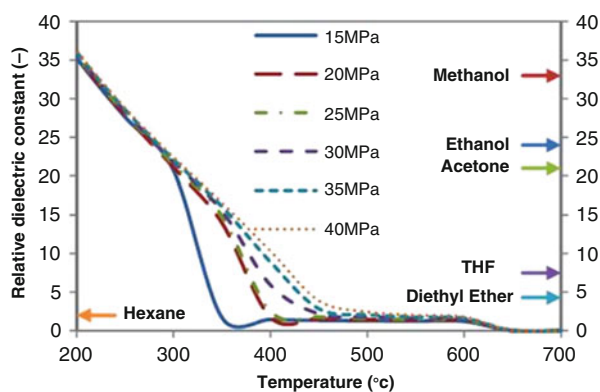
of molecules due to hydrogen bonding. Under supercritical conditions, much of these intermolecular associations break down [25] causing the dielectric constant falling down to a value of about 6 at the critical point. One of the consequences is the high solubility of organic compounds and gases in scH$_2$O. On the contrary, salt solubility falls down by some orders of magnitude, at the origin of the supercritical hydrothermal synthesis of nanomaterials.

In brief, water turns from a polar solvent at ambient pressure and temperature to a nonpolar one at supercritical conditions ($T_\mathrm{c} > 374$°C, $p_\mathrm{c} > 22.1$ MPa).

Thanks to these unique properties, SCFs have been extensively used for more than 20 years in the field of materials science. Their use is closely linked to the rise of nanosciences and nanotechnologies associated with the development of sustainable chemistry and engineering [13, 15, 26, 27]. Indeed, the environmental interest of SCFs such as scCO$_2$ or scH$_2$O brings opportunities for replacing some more

harmful solvent systems [23, 24], being nonflammable and exhibiting no or low toxicity. However, the poor solvent power of CO_2 and the polar nature of water at room pressure and temperature do not provide means for considering a wide range of precursors. Therefore, other SCFs have been later used for nanomaterial synthesis, such as ammonia (NH_3) [28], various alkanes or hydrocarbons (pentane, hexane, toluene, . . .), and alcohols (methanol, ethanol, isopropanol). Although much less attractive for their environmental interest, hydrocarbons are advantageous when considering oxygen- or water-sensitive coordination complex reagents and to solubilize hydrophobic precursors.

Overall, continuous flow synthesis of nanomaterials at supercritical conditions brings additional advantages compared to conventional liquid- or liquid–gas-phase approaches: (1) there are no mass-transfer limitation due to liquid–gas-phase boundary, (2) thermal and diffusion processes are fast, (3) reaction rates of few seconds to few minutes are used, and (4) SCF processes can be seen to some extent as green and sustainable processes depending on the considered solvent [29, 30].

3 Supercritical Fluid Flow Processes and Strategies Towards Continuous Nanomaterial Synthesis

Continuous supercritical fluid approaches for nanomaterial synthesis are generally carried out in coiled reactors, whose size can range from micro- up to millifluidic at lab scale, taking benefit of the fluid thermodynamic properties and of the chemical reaction kinetics with or without surfactants or templates in short times (from seconds to minutes). Nevertheless, these technologies are not anymore confined in laboratories since the easy scalability of these processes has been recently demonstrated with the realization of the first commercial plant (1,000 tons/year – Hanwha Chemical in Republic of Korea) for the continuous supercritical hydrothermal synthesis of $LiFePO_4$. The following paragraph gives a brief overview of the general setup conventionally considered for implementing such reaction processes and some of the latest developments using microfluidics systems.

3.1 Flow Supercritical Setups

Flow supercritical setups are very similar to conventional continuous flow chemical setups using liquids or gases. The main difference stands in the use of higher pressures and temperatures, leading to some adaptations of the technology.

Figure 5 shows a schematic representation of a continuous facility of nanomaterial processing in supercritical fluids. It is constituted of four main components: injection system for the precursor's solution, mixers, a reactor, and
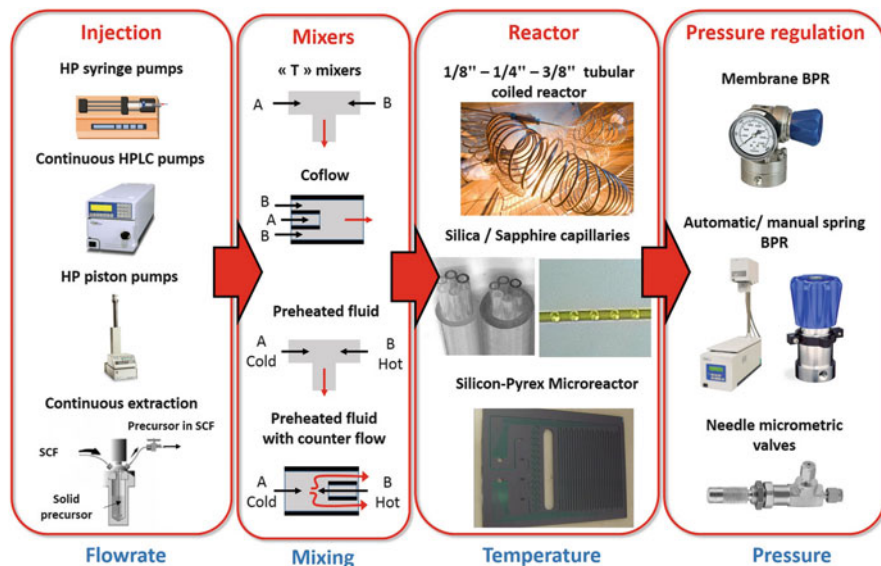
Fig. 5 Flow sheet of a continuous process of nanomaterial synthesis using supercritical fluids

a back pressure regulator downstream [13, 31], the nanostructures being recovered either as dry powders (using an online filter) or in solution upon depressurization.

The various experimental parts mentioned in Fig. 5 are used to control the operating synthesis parameters such as (1) *pressure*, using an appropriated back pressure regulator and pump(s); (2) *temperature* in the reactor, using preheaters, and reactor heating system; (3) *residence time* in the reactor by controlling the flow rates (Q), the reactor volume (tubing type), the temperature, and the pressure (related with the fluid density); and (4) the *concentrations of reagents* of the feed solutions [26]. We describe hereafter some of the elements required to build a supercritical setup to synthesize nanomaterials at high pressures and temperatures.

3.1.1 Injection

When considering supercritical processes for nanomaterial synthesis, the injection of precursors within the reactor could be of two main kinds. The first strategy consists in injecting liquid solution at room temperature and high pressure, which will later be brought to the supercritical region by increasing the temperature within the reactor, leading to a transcritical flow from liquid to supercritical. The requirements for high-pressure pumps somewhat limit the choice of available equipments. Depending on the considered size of the setup (and therefore the considered flow rate range) and the nature of the fluids to inject, one can choose among (Fig. 5 – left) (1) high-pressure syringe pump (low flow rates, low volumes) available from KD scientific, Harvard Apparatus, or Cetoni; (2) continuous HPLC pump (various flow

rates, unlimited volumes) from all the chromatography equipment suppliers; and (3) high-pressure piston pumps (various flow rates, average volumes, and equipped with temperature-controlled jacket for liquefying solvents such as CO_2 or ammonia before their injection) from Teledyne ISCO. The second strategy (continuous extraction) was employed with processes using supercritical CO_2 or ammonia as the main solvent. The principle is similar to what is done in chemical vapor deposition processes, aiming at using a supercritical fluid – SCF – as a "carrier solvent/reagent." It passes through a high-pressure cell where a solid precursor is located. The precursor therefore is continuously solubilized in the SCF and is later transported to the reactor with the SCF flow. Thanks to the ability to change the solubility of the precursor with little variations of pressure and/or temperature, the concentration of the precursor can be finely tuned [32].

3.1.2 Mixers

As in every processes, the introduction of several precursors/ligands or solvent solutions requires appropriate mixing/contacting/heating of the flows. The general reported approaches for supercritical continuous processes use either (1) a mixing at room temperature followed by a temperature increase within the reactor or (2) a rapid heating by mixing a hot preheated solution with a room-temperature flow. In the first family, basic T mixers or coflows [33, 34] are employed. In the second family, T mixer types [35] or counterflow mixing [36, 37] have been reported for efficiently reaching the reaction temperature.

3.1.3 Back Pressure Regulators

Controlling pressure continuously required some elements allowing to select downstream the operating pressure within the reactor. Although outlet capillaries can be used to generate a pressure drop when working at constant flow rate in chemical synthesis [38], this strategy cannot be applied in nanomaterial synthesis due to the potential clogging induced by nanoparticle bridging or capillary constriction. Therefore, a constant back pressure can be applied by pressurizing an outlet chamber containing recovery vials with an inert gas such as argon or nitrogen. The main advantage of this option stands in the perfect control of the back pressure, preventing from any fluctuation of the residence time within the reactor. Despite its advantage, such type of process still requires to be stopped to collect sample upon depressurization of the outlet chamber. Ways towards fully continuous processes require valves. Several technologies can be considered for these back pressure regulators (Fig. 5, right):(1) membranes (from Equilibar), (2) springs (from Idex, Swagelok, or Tescom), (3) needle valves (from Swagelok, autoclave engineers, etc.), or a combination of these (automatic BPR from Jasco). Such equipment can provide efficient ways to control downstream pressure up to 50 MPa at various flow

rates (down to 10 µL min^{-1} depending on the chosen technology) while allowing a fully continuous recovery of nanomaterials.

3.1.4 Reactor

As in every process, the heart is the reactor (Fig. 5, center right). The choice of the reactor depends on (1) the required hydrodynamics linked to the expected characteristics of the nanomaterials and (2) the desired production rates. Millifluidic-scale reactors typically use 1/8" stainless steel tubing (1–2 mm internal diameter) or even higher 1/4", 3/8" . . .. They provide flexible approaches for synthesizing appreciable amount of materials (up to gram scale) for developing proof of concept for future device fabrication. The general concept to control the reaction temperature consists in rolling the tubular reactor around a heating element (heating cartridge or heating block made of aluminum), which temperature is controlled via a temperature controller. Another approach consists in putting the reactor within an oven.

Despite their advantages, these processes exhibit two main limitations: (1) first, they are generally blind, preventing from implementing in situ characterization techniques for performing real-time optimization, and (2) it is difficult to fully control the hydrodynamics at these intermediate scales, which could dramatically change the final nanomaterial characteristics.

In this view, it is convenient to first consider optically transparent materials, which can withstand high-pressure and high-temperature conditions such as sapphire tubing or fused silica capillaries, generally used for chromatography applications. Meanwhile, going to microscale (microfluidics) provides additional advantages. Indeed, microreactors offer a solution to feedback control of temperature, feed streams, reproducibility, in situ reaction monitoring [39] using sensor integration, rapid screening of parameters [40], fast mass and heat transfer [41], and low reagent consumption during optimization. The development of high-pressure/high-temperature microreactors able to withstand supercritical conditions [42–44] has allowed to combine the advantage of size reduction provided by microsystems to the unique properties of SCFs. There are three main motivations to develop the synthesis of advanced nanocrystals in supercritical microreactors: (1) a better understanding of what is going on for a better control through in situ characterization opportunities; (2) an exploitation of microfluidics advantages – hydrodynamics control, enhancement of mass and heat transfers, reproducibility, rapid screening of parameters, and low reagent consumption during optimization – for the design and synthesis of high-quality nanocrystals; and (3) the ability to do process intensification for the development of cheaper, safer, and greener synthesis technologies.

The construction materials have to be carefully chosen for such on-chip high-pressure/high-temperature applications since commonly used microfluidic systems made of polymers, such as polydimethyl siloxane (PDMS), cannot be employed for SCF-based processes, given their poor temperature and pressure resistance. Therefore, it is possible to choose among either metal [45–47] – although limiting the integration of characterization techniques – glass [31, 38, 48, 49], or silicon-Pyrex

[42, 50–53], providing an easy optical access. In particular the latter presents a good compromise between metal and glass microreactors. Additionally, glass and silicon-based microfluidic reactors offer the opportunity to modify the wettability properties of the channels, thanks to silane chemistry for surface modifications [54–56].

3.2 Continuous Nanomaterial Synthesis at Supercritical Conditions: Chemical Engineering Considerations

As a matter of fact, running continuously a chemical reaction at supercritical conditions for the synthesis of nanomaterials will induce variations of several parameters that are conventionally used by chemical engineers to design their process (flow regime, mixing time, residence time distribution, etc.), given the specific properties of the fluids in such conditions. It is therefore interesting to have a closer look at what could be expected from a supercritical fluid process compared to a conventional liquid-phase process.

3.2.1 Reynolds Number/Turbulence

Reaching supercritical conditions in continuous synthesis reactors offers substantial advantages over liquid-phase processes. As above mentioned, the potential useful characteristics of supercritical fluids (SCFs) include high diffusivity (typically one to two orders of magnitude higher than in liquid phases), gas-like viscosity (in the order of few tens of μPa s), and the liquid-like density (typically 200–800 kg m^{-1} [3]). These properties induce some variations of the flow regime, which can be characterized using the Reynolds number. The Reynolds number is defined as $Re = \rho v d_h / \eta$, with ρ being the fluid density (kg m^{-3}), v the average fluid velocity (m s^{-1}), d_h the hydrodynamic radius of the flow (m), and η the fluid viscosity (Pa s). Therefore, depending on the flow rate considered in a 1/8 inch tubing (internal diameter ~1.6 mm), it is possible to work either in the laminar or in the turbulent regime, as reported in Table 2. Switching to the microscale, much smaller Reynolds numbers are conventionally obtained when considering liquid flows in microreactors (Re < 10), restricting fluids flows to the laminar regime. However, thanks to the intrinsic properties of SCFs, the Reynolds numbers for supercritical microflows can be easily tuned from laminar to almost turbulent (0.7 < Re < 700), playing on the pressure and temperature conditions. In particular, higher flow rates can typically be accessed thanks to the low pressure drop (see next section). The ability to confine SCF flows in the laminar regime allows for creating stable hydrodynamic structures such as droplet-based flows, which can be further used for continuous minireactor synthesis of nanomaterials [57] or interface chemistry
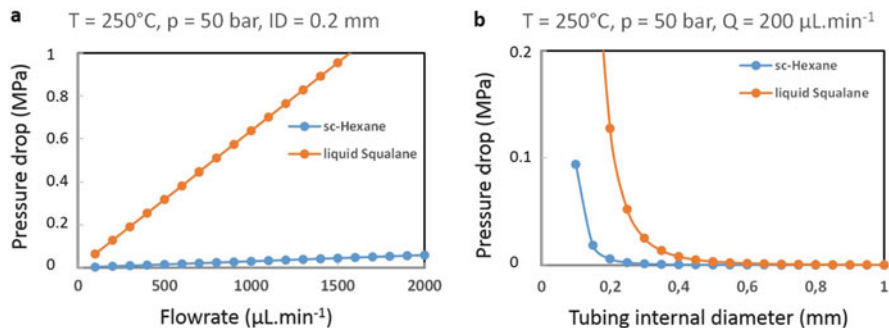
Fig. 6 Evolution of the pressure drop within a 3 m long tubing depending on (**a**) the flow rate at constant tubing internal diameter and (**b**) tubing internal diameter at constant flow rate for both liquid squalane (high-boiling-point solvent) and supercritical hexane in the same pressure and temperature conditions

applications. Oppositely, accessing turbulent flows provides means for fast mixing of reagents, which is of primary interest in particular at microscale [58].

3.2.2 Low Pressure Drop

The low viscosities of SCFs are particularly interesting for continuous flow processes where pressure drop can reach high values (i.e., small scales or high flow rates). For instance, considering cylindrical geometries (pipe), the pressure drop can be expressed as:

$$\Delta P = \frac{8\eta L}{\pi R^4} Q$$

with η being the fluid viscosity (Pa s), L the reactor length (m), R the tubing radius (m), and Q the volumetric flow rate (m^3 s^{-1}). Therefore, there is a linear relationship between ΔP and η resulting in much lower pressure drop for SCFs than liquids, displaying 1–2 orders of magnitude lower viscosity than liquid. This is exemplified in Fig. 6 where the pressure drop induced by flowing either high-boiling-point liquid squalane or supercritical hexane is compared. As seen, this advantage can be really beneficial when considering either small-scale flow (typically below 200–300 μm ID tubing, see Fig. 6a) or considering high flow rate processes ($Q > 200$ μL min^{-1}, see Fig. 6b) for keeping the pressure drop at a low value (<1 bar).

Low viscosities also induce high diffusivities, typically encountered in gas phases, which greatly contribute to enhanced mixing and to address limitation of mass transfer-limited processes (see next paragraph).

3.2.3   Mixing/Diffusivity

As mentioned earlier, most continuous liquid or liquid–gas continuous processes are restricted to the laminar regime, which can significantly reduce the mixing efficiency, leading to small Damköhler numbers[1] (Da_{II} and Da_{III}), which can limit the process efficiency when considering fast reactions. The absence of turbulence or recirculation makes mixing primarily dependent upon diffusion between fluids. This is the reason why many researches have been carried out to design properly continuous reactor in order to overcome the mixing challenge, by creating passive [59, 60] or active [61] micromixers, which, however, add complexity in the system, making it more difficult to be characterized and understood. Back to a simple single-phase laminar flow in a straight capillary, one can estimate the mixing time as $t_{mixing} = \frac{<x>^2}{D}$, with x being the typical flow width and D being the diffusion coefficient expressed from the Stokes–Einstein equation by $D = \frac{kT}{6\pi\eta a}$, where k is the Boltzmann constant (J K^{-1}), T is the temperature (K), η is the fluid viscosity (Pa s), and a is the hydrodynamic diameter of the considered molecules or nanoparticles in the fluid (m).

Considering a 1 nm large nanoparticle flowing in ethanol at 25 MPa, the diffusion coefficient will be equal to 1.45×10^{-10} m^{-2} at 25°C (liquid ethanol) and 1.1×10^{-8} m^{-2} at 250°C (supercritical ethanol), resulting in a two orders of magnitude higher diffusivity at supercritical conditions compared to liquid phase. This will therefore lead to greatly enhanced mixing. For instance, the mixing time by pure diffusion in a 100 μm tubing will decrease from ~100 s to ~1 s going from liquid to supercritical conditions. More importantly, these short mixing times can be achieved without the use of any mixing part.

To highlight this effect, a microsystem was realized by inserting two capillaries into each other. A solution of rhodamine in ethanol is injected in the inner flow, while pure ethanol is injected in the outer flow, in order to access information about the diffusion process. The pressure was set at 25 MPa and the internal/external flow velocities were kept constant ($v_{int} = 1$ mm s^{-1} and $v_{ext} = 2$ mm s^{-1}). By comparing the diffusion and hydrodynamic behavior at two different temperatures: 25°C, where EtOH is liquid and 250°C, where EtOH is supercritical (for EtOH: $T_c = 241$°C and $p_c = 6.1$ MPa), we can see that in both cases, the coaxial injection first results in a flow focusing effect on the inner flow (Fig. 7). In a second step, the width of the created jet starts increasing thanks to the diffusion of rhodamine molecules from the inner flow to the outer pure ethanol flow. It can be noticed that this effect is much more pronounced when scEtOH is compared to liquid

---

[1] The Damköhler numbers (Da_{II} and Da_{III}) represent the ratio between the reaction kinetic and the mass or heat transfer, respectively. They are defined as $Da_{II} = \frac{k \times Ca^{n-1} \times L_c^{2}}{D}$ and $Da_{III} = \frac{k \times Ca^{n} - \Delta_r H \times L_c}{\rho \times C_p \times T \times v}$ with k, Ca, L_c, and D being the kinetics constant, the concentration, the characteristic length, and the diffusion coefficient, respectively, for Da_{II} and $\Delta_r H$, ρ, C_p, T, and v being the reaction enthalpy, the fluid density, the fluid heat capacity, the temperature, and the fluid velocity, respectively, for Da_{III}.
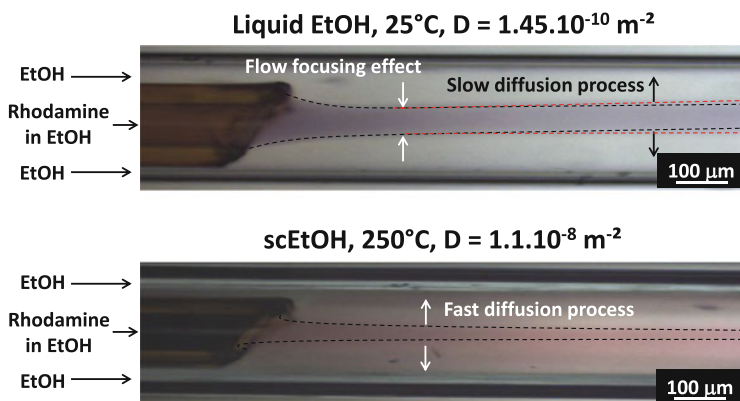
Fig. 7 Optical microscopy picture obtained from the coaxial injection of a rhodamine in EtOH solution within a pure EtOH flow at 25 MPa, at either liquid (25°C) or supercritical (250°C) conditions (adapted from [12])

ethanol, which is in good agreement with the large difference in the diffusion coefficients.

3.2.4 Residence Time Distribution

The mean residence time in non-compressible liquid processes can be easily calculated by dividing the total volumetric flow rate by the volume of the reactor. However, in continuous nanomaterial synthesis at supercritical conditions, it is important to take into account the fluid density variation. Indeed, depending on the variation of the temperature conditions inside the reactor, the fluid might expand or contract. For conventional constant flow processes, the pump delivers a constant volumetric/mass flow rate. The fluid getting out of the pump is therefore at defined pressure and temperature conditions (T_{init}, p_{init}, exhibiting a fixed density - ρ_{init}). However, when reaching the reacting zone in the reactor, the fluid characteristics might be somewhat different from the fluid exiting the pump (e.g., $T_{reac}, p_{reac}, \rho_{reac}$). In order to maintain a constant mass flow rate, the fluid velocity is changing within the reactor. The actual mean residence time will therefore vary and can be estimated by:

$$R_t = \frac{Q_{tot}}{V} \times \frac{\rho_{init}}{\rho_{reac}}$$

where Q_{tot} is the total volumetric flow rate (m^3 s^{-1}), V is the reactor volume (m^3), and ρ_{init} and ρ_{reac} are the fluid density at the pump exit and in the reactor, respectively.

Another important point to keep in mind when designing continuous nanomaterial process is the residence time distribution. Indeed, at laminar
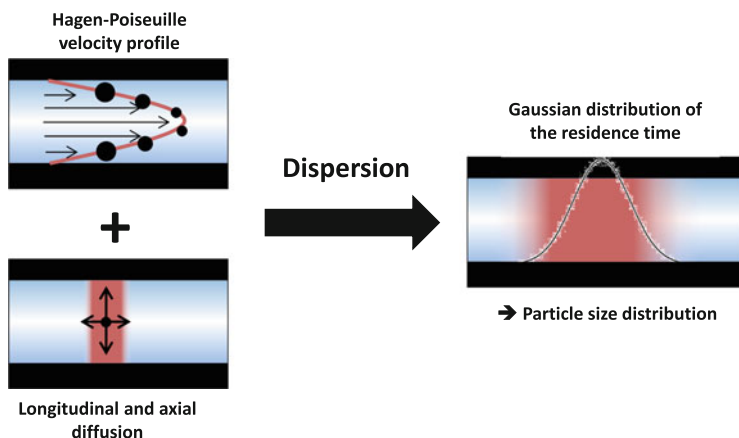
Fig. 8 Details of the dispersion mechanism encountered within a laminar fluid flowing inside a pipe and leading to residence time distribution at the reactor outlet

conditions for a single phase flow, the fluid undergoes a velocity profile when flowing inside a pipe or a channel (Hagen–Poiseuille equation), meaning the fluid velocity is not constant radially, being faster in the center and equal to zero at the walls. Although longitudinal and axial diffusion processes occur, molecule or particle can hardly move from one stream line to another in poorly diffusive fluid (liquids), being confined during the process to one particular velocity. The combined effects lead to a dispersion process (therefore a residence time distribution). This means that all the particles nucleating and growing will not spend the same time inside the reactor. The velocity profile therefore induces a particle size distribution at the reactor outlet (Fig. 8).

The residence time distribution curve (also called E curve) can be estimated thanks to the Taylor dispersion model [62]:

$$E_\theta(L) = \frac{1}{\sqrt{4\theta\pi\left(\frac{D^*}{vL}\right)}} \exp\left[-\frac{(1-\theta)}{4\theta\left(\frac{D^*}{vL}\right)}\right]$$

With θ being defined as $\theta = Rt/Rt_{\mathrm{mean}}$ (Rt and Rt_{mean} being the actual residence time and the mean residence time, respectively) and L the length of the capillary tubing or microchannel. D^* is called the dispersion coefficient and can be expressed for cylindrical tubing and for Peclet number flows ($Pe = vd_\mathrm{h}/D$) > 100 as:

$$D^* = \frac{v^2 d_h^2}{196D}$$

D^* is therefore inversely proportional to the diffusion coefficient. Since the E curve is highly dependent on the D^*/vL value (the smaller the narrower RTD), narrow

Fig. 9 Evolution of the RTD curve as a function of the viscosity considering a fluid at 50 °C flowing at a velocity of 0.05 m s^{-1} in a 1 mm ID tubing
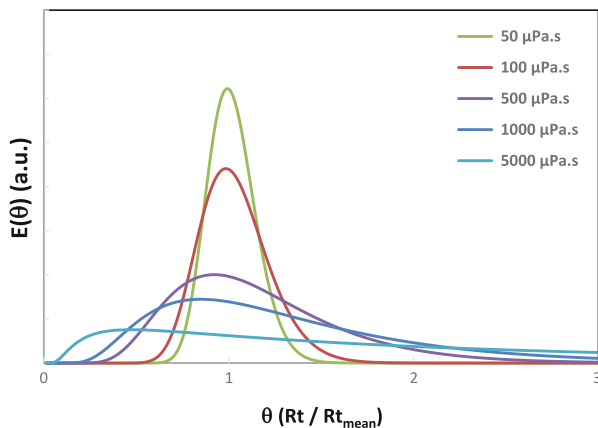
RTDs can be obtained when considering fluids with high diffusivity. In this context, working with supercritical fluids for nanomaterial synthesis leads to narrow residence time distributions (RTD), thanks to low viscosities and high diffusivities. As seen in Fig. 9, the solvent viscosity plays an important role in the RTD wideness going from wide RTD for highly viscous solvents to almost plug flow for nonviscous ones.

Working with SCFs can therefore dramatically reduce the dispersion along the reactor, and provides an useful option for efficiently narrowing the size distributions of nanomaterials during synthesis or to obtain better control over reaction yields. This was in particular demonstrated for the synthesis of narrow-size distributed CdSe and InP quantum dots in supercritical hexane and octane [63–65].

In brief, continuous supercritical synthesis of nanomaterials exhibits several advantages compared to liquids ones, in particular:

 (i) Tunable Reynolds number flows from laminar to almost turbulent ones
 (ii) Low pressure drop at high flow rate or small scales
(iii) Fast mixing/heat and mass transfers
(iv) Narrow residence time distributions

These characteristics make continuous supercritical reactors ideal tools for performing nanostructure synthesis in controlled environments.

4 Nanomaterial Flow Synthesis in Supercritical Fluids from Coordination Complexes

The design of inorganic nanomaterials from coordination complex precursors using supercritical fluids processes can be achieved continuously through chemical reactions mostly adapted from solution chemistry, among which are (1) supercritical hydrothermal reactions [27], (2) thermal decomposition [32], (3) Red/Ox reactions

(with hydrogen, for instance) [66], or (4) sol/gel reactions in or assisted by a SCF [67]. These approaches are particularly well suited for the control of the nucleation and growth of inorganic and hybrid organic/inorganic nanostructures, based on the abovementioned advantages of such processes compared to liquid-based ones.

In most of these approaches, the supercritical media are used either only as solvents or as solvent/reagents/surface modifiers during the synthesis process. Several types of nanostructures have been synthesized so far by varying either the metal precursors or the supercritical solvent system (metals, semiconductors, nitrides, oxides, etc.) at nanometre scale. It is worth highlighting that from the same metal precursor, various types of materials can be obtained. For instance, starting from metal acetylacetonate precursors, it is possible to obtain either metal, oxides, or nitride nanomaterials whether the considered solvent is supercritical CO_2, supercritical water, or supercritical ammonia [28].

The synthesized material characteristics (morphology, structure, composition, organization/stability) are directly linked to the control of the operating parameters: solvent nature (water, alcohols, alkanes, ammonia, mixtures, etc.), pressure, temperature, coordination complex precursors, concentration, residence time, and reactor design (single tubing, coflow, multiple injections, etc.). Continuous synthesis of nanomaterials in supercritical fluids is generally conducted through two main strategies:

(i) *The direct nucleation and growth in flow without any surfactants.* In that case, the nanoparticles are "naked" or functionalized with the ligands coming from the precursor itself or by the solvent molecules [68]. This generally results in the recovery of aggregated NPs, although some defined structures (organization of nanoparticles in larger particles) can be obtained.

(ii) *The addition of a surfactant to the reaction media.* The presence of an organic molecule could greatly affect the nanoparticle morphology (size, shape, composition, and distribution), organization, and stability. It is therefore sometimes advantageous to use in situ or ex situ functionalization to achieve good NP dispersion for their future implementation and use. In situ functionalization can be performed by introducing directly the stabilizing agent in the precursor solution. This results in covalent bonding of the stabilizing agent to the surface, making particle highly stable even after several months of storing. Oppositely, ex situ functionalization can be done by adding a surfactant in a post-synthesis step (at the outlet of the reactor) just after the nucleation/growth steps. In this case, the ligand-NP interactions are rather weak but one can use this approach to separate nucleation/growth from functionalization step, getting rid of any surfactant influence over the NP characteristics. A novel approach (coflow) was recently introduced to combine both advantages by (i) confining the nucleation/growth of the NPs far from the tubing wall in order to prevent for any potential clogging – in particular when working at microscale – due to either NP bridging or constriction effect from wall deposition, (ii) separating nucleation/growth from functionalization steps, and (iii) achieving strong covalent bonding of the surfactants on the NP surface.

The supercritical continuous synthesis of nanomaterials was first reported by Adschiri et al. in supercritical water from metal salts as precursors in the beginning of the 1990s [27]. Various metal oxide nanoparticles have been prepared mainly from nitrates (AlOOH from $Al(NO_3)_3.9H_2O$, for instance), sulfates (TiO_2 from $Ti(SO_4)_2$, for instance), chlorides (αFe_2O_3 from $FeCl_2$, for instance), or hydroxides (CeO_2 from $Ce(OH)_4$, $Ce(NO_3)_3.6H_2O$ or still $(NH_4)_2Ce(NO_3)_6$, for instance). The supercritical hydrothermal synthesis allows today the synthesis of numerous inorganic nanomaterials with controlled sizes from micrometer down to nanometer scale and complex compositions. The use of coordination complexes or metal precursors for a chemistry in water was of course not obvious due to solubility consideration, especially for the continuous injection in the supercritical reactor. They appear with the researches on multicationic oxides like $Ce_{1-x}Zr_xO_2$ ($0 \leq x \leq 1$) by hydrolysis of mixtures of $[NH_4]_2[Ce(NO_3)_6]$ and $[Zr(ac)_4]$ in near-critical water (300°C, 25 MPa) in the appropriate ratios [69]. Highly crystallized $Ce_{1-x}Zr_xO_2$ nanoparticles are obtained in the size range of 3.5–7.5 nm (size determined from PXRD pattern with the Scherrer formula) depending on the material composition. More recently synchrotron in situ studies of the synthesis of nanocrystalline $Ce_{1-x}Zr_xO_2$ ($0 \leq x \leq 1$) in supercritical water (375°C, 23 MPa) were reported to bring a better understanding on the nucleation and growth mechanism [70]. For compositions rich in cerium atoms, the nanoparticle growth is initially limited by surface reaction kinetics. At a size of about 6 nm, the growth changes and becomes limited by the diffusion of monomers to the surface. For compositions rich in zirconium atoms, the initial growth of small particles is limited by diffusion. The growth mechanism changes at a particle size of ~ 3.5 nm, where the growth becomes limited by the surface reaction kinetics. The differences in initial growth kinetics of the CeO_2 and ZrO_2 phases may also be the origin of the much faster initial growth of CeO_2 nanoparticles, compared to ZrO_2 nanoparticles in supercritical water.

As above mentioned, two main kinds of particles can be obtained whether surfactants are used to functionalize the NPs or not. We describe hereafter some examples of materials, which are obtained in both cases.

4.1 Naked Nanoparticles

The first type of NPs directly nucleates and grows without the use of any additional ligands. Oxides have been particularly studied. Regarding the use of coordination complexes for the supercritical flow synthesis of metal oxide nanomaterials, it is important to point out the processing of alkoxides through sol–gel chemistry in supercritical fluids.

4.1.1 Flow Sol–Gel Synthesis in Supercritical Fluids

In the 1990s, in parallel to the development of the supercritical hydrothermal synthesis from salts as aforementioned, sol–gel reactions in supercritical fluids from alkoxides were also reported. There were numerous studies in supercritical CO_2 from alkoxide precursors to synthesize SiO_2, TiO_2, Al_2O_3, ZrO_2 ... [71]. Due to solubility consideration, this was performed in batch reactor which is out of the scope of this chapter. The development of the flow synthesis of oxides from alkoxides passed first through a semicontinuous process for the formation of magnesium powders from the hydrolysis and supercritical treatment of Mg $(OCH_3)_2$ [72]. The experimental setup was constituted of three reactors. Two high-pressure pumps feed a first reactor operating at room temperature (10 MPa) with an alcoholic solution of magnesium methoxide on one line and water on a second line. The mixture is then flowing through a second reactor working under temperature (between T_{amb} and solvent T_c) to enter before entering the third reactor at supercritical conditions fitted with a filter to stop the powder. The first continuous synthesis appeared in 1996 with the production of TiO_2 from Ti $(O\text{-}iC_3H_7)_4$(TTIP) in supercritical isopropanol (300°C, 10 MPa). The proposed mechanism is based on a hydrolytic decomposition of the alkoxide initiated by water formed by the alcohol dehydration. At the end TiO_2 nanoparticles are formed through a sol–gel process with a narrow range of size distribution (20–60 nm) into spherical agglomerates (500–2,000 nm) [73].

There are two main strategies for the formation of oxides from alkoxides in supercritical alcohols: (1) the injection of the alkoxide in the alcohol solvent in one line and water in the other line and (2) the in situ production of water through the dehydration of the alcohol solvent. The first strategy has been explored for the continuous and controlled synthesis of $BaTiO_3$-based materials, these materials being developed for microelectronics, more precisely for capacitors. The continuous synthesis of $BaTiO_3$ was first reported from the transformation of a double alkoxide ($BaTi(O\text{-}iC_3H_7)_6$) in a supercritical water/isopropanol mixture [74]. Two reactors were used: (1) for the alkoxide hydrolysis and (2) for the thermal treatment of the produced $BaTiO_3$ nanoparticles at supercritical conditions. The produced $BaTiO_3$ nanoparticles are characterized with an average size of 10 nm. Over the last 10 years, our research group deeply investigated the supercritical flow synthesis of $BaTiO_3$-based materials, namely BST ($Ba_{1-x}Sr_xTiO_3$ with $0 \leq x \leq 1$) and BTZ ($BaTi_{1-y}Zr_yO_3$ with $0 \leq y \leq 1$) [31] (Fig. 10). The synthesis of the whole BST solid solution from $BaTiO_3$ to $SrTiO_3$ was demonstrated using barium, strontium, and titanium isopropoxides [75, 76]. The flow reaction system is made of two injection lines: one for the alkoxides dissolved in ethanol and the second one for water (preheated at 150°C) in order to favor the precursor's hydrolysis. The two lines are mixed at the inlet of a tubular reactor allowing in (1) a first part to perform the hydrolysis/condensation and (2) a second part (above the critical point of the water/ethanol mixture) to induce the crystallization. Increasing the strontium amount leads to a decrease of the mean particle size; this behavior has been
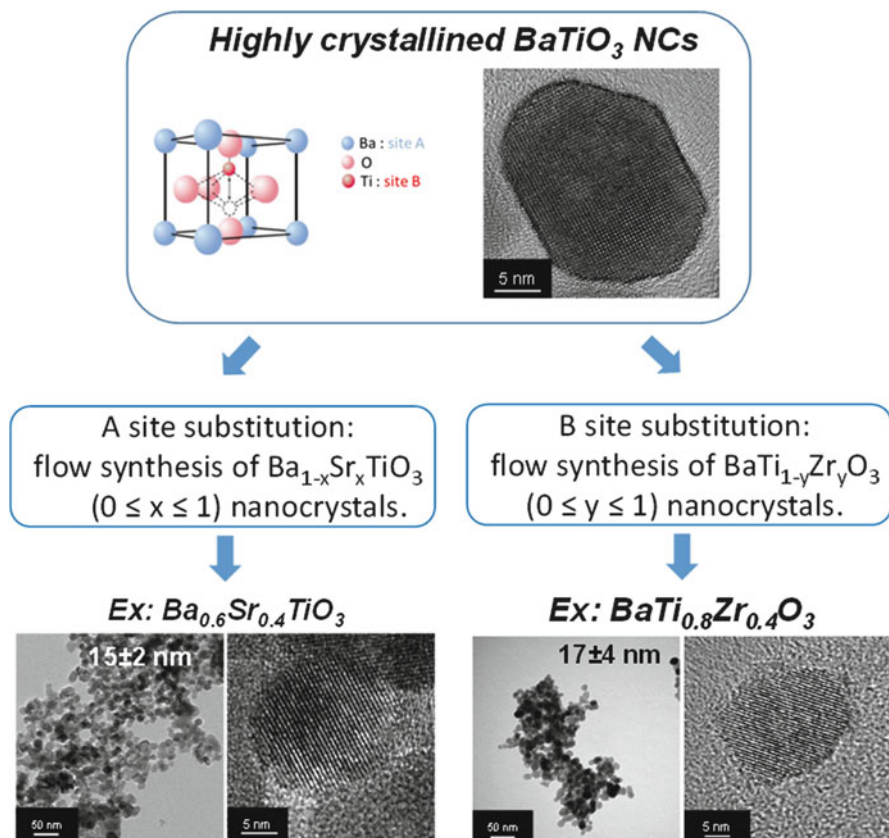
Fig. 10 Supercritical flow synthesis of high-quality BaTiO$_3$-based materials

explained through the coupling of in situ and ex situ investigations [77]. The in situ synchrotron analyses confirmed the influence of the barium substitution by strontium on the nanoparticle growth mechanism. Regarding the ex situ analyses, they showed the presence of surface –OH functions decreasing with the increase of strontium in the BST solid solution. The decrease of surface –OH functions will impact the ability of the precursor to react at the surface of the particles and thus limit the growth.

Replacing strontium isopropoxide with zirconium isopropoxide conducts to the formation of the whole BTZ solid solution from BaTiO$_3$ to BaZrO$_3$(BaTi$_{1-y}$Zr$_y$O$_3$ with $0 \leq y \leq 1$) [78]. Similar as in the case of BST, an increase of zirconium content in the BTZ solid solution induces a decrease in BTZ particle size and size distribution (20 ± 6 nm, for BaTiO$_3$, down to 15 ± 3 nm when increasing the zirconium content up to BaTi$_{0.4}$Zr$_{0.6}$TiO$_3$ and finally reaches 10 ± 2 nm for BaZrO$_3$ nanoparticles).

The flow sol–gel synthesis at supercritical conditions gives access to a high level of control over the synthesis of the entire BST/BTZ solid solutions in terms of

material characteristics (size, size distribution, crystallinity, ...) and properties. We developed also a method to obtain advanced nanostructured ceramics using spark plasma sintering (SPS) with all the obtained powder compositions, especially for BST-based ceramics [79].

One important conclusion of these works on the use of alkoxides in a supercritical flow reactor is that it allows designing highly crystalline nanomaterials, in a short residence time (less than 2 min) at relatively low temperature (400°C); these nanomaterials exhibit high quality and can be considered as unique. Another important advantage of this continuous synthetic route is the versatility; beyond metal oxides, different natures of advanced materials can be produced: metals, nitrides, sulfides ... The case of nitrides was really challenging and is described in the next section.

4.1.2 Nitrides from the Transformation of Coordination Complexes in a Supercritical Flow Reactor

A first tentative to produce in-flow nitrides was reported more than 15 years ago. Cansell et al. investigated the transformation of copper and iron acetylacetonates [$Cu(acac)_2$ and $Fe(acac)_3$, respectively] in supercritical ammonia ($T_c = 132.4°C$, $P_c = 11.1$ MPa) [32]. Ammonia was first saturated with copper or iron acetylacetonates in an extractor (Fig. 5, bottom left) before entering the supercritical reactor. The concentration in metal precursor can be controlled with the ammonia density. As a result, copper nitride Cu_3N with metal copper as impurity was obtained with the transformation of $Cu(acac)_2$. Regarding the decomposition of $Fe(acac)_3$ in supercritical ammonia, it conducts to the formation of Fe_4N with Fe_2O_3 impurities at 180°C and 16 MPa. The experiments have shown that the final particle size depends on the variations of the working conditions (T, P, solute supersaturation, hydrodynamics, etc.). Aggregates of about 50 nm constituted of crystallites with a size below 10 nm are obtained for the Fe_4N–Fe_2O_3 powder. To simplify the procedure, the coordination complexes were dissolved in a cosolvent before injection. In this study methanol was chosen as cosolvent. This way the metal precursor in methanol is injected through one line and the ammonia through another line in the supercritical reactor with a molar ratio of 70 % NH_3–30 % MeOH. The ammonolysis of many coordination complexes was investigated in this supercritical NH_3–methanol mixture in a range of temperatures between 170 and 290 °C at about 16 MPa: $Cr(hfac)_3$ or $Cr(acac)_3$, $Co(hfac)_2$, $Fe(acac)_3$, $Cu(hfac)_2$ and $Ni(hfac)_2$, (hfac meaning hexafluoracetylacetonate) [28]. As far as $Co(hfac)_2$ and $Ni(hfac)_2$ were concerned, Ni_3N and Co_2N particles were produced in shapeless aggregates of a few micrometers. These aggregates were constituted of crystallites between 20 and 100 nm for Ni_3N and 60–120 nm for Co_2N. The ammonolysis of iron and chromium precursors in supercritical NH_3–methanol conducted to the growth of oxide/nitride mixtures, namely Fe_2O_3/Fe_4N (nanodomains of 10 nm organized in spherical particles of about 50 nm) and Cr_2O_3/Cr_2N (as amorphous powder after synthesis). The transformation of gallium, titanium, and aluminum
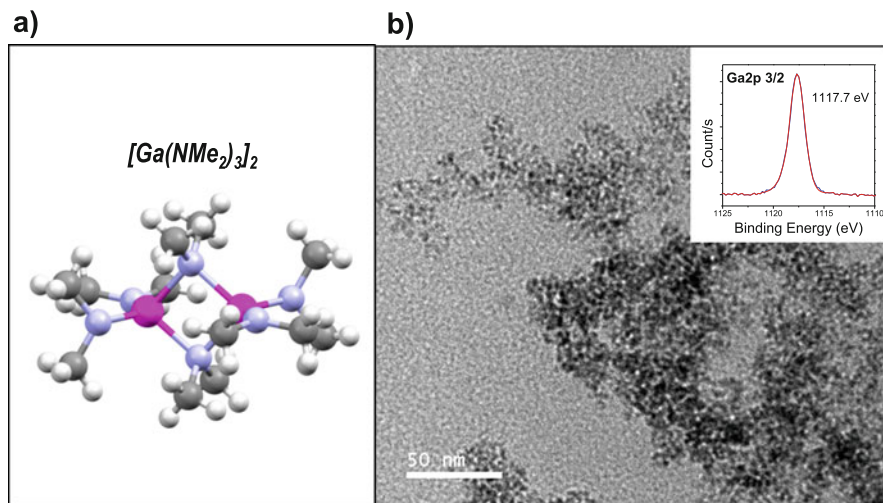
Fig. 11 (**a**) Ga precursor (tris(dimethylamino)Gallium dimer) used for the fast synthesis of GaN QDs and (**b**) TEM micrograph of GaN nanoparticles obtained in a continuous flow reactor (XPS analysis as insert)

precursors ($Ga(acac)_3$, $Al(acac)_3$, and $Ti(OPr^i)_2(acac)_2$) induced the formation of the corresponding oxides (Ga_2O_3, Al_2O_3, and TiO_2, respectively) under the same experimental conditions (supercritical NH_3–methanol at 225–230°C and 16 MPa).

On one hand, metals for which the Gibbs free energy of oxide formation is weak (Cu, Ni, and Co) tend to only form metal nitrides; the ammonolysis of the corresponding coordination complexes is favored relative to the metal oxidation reaction. On the other hand, metals for which the Gibbs free energy of oxide formation is high (Ga, Ti, and Al) lead to metal oxides.

Regarding iron and chromium, their affinity with oxygen is intermediate which involves the formation of mixtures Cr_2O_3/Cr_2N and Fe_2O_3/Fe_4N. Following these studies was the flow synthesis of metal nitrides, for which the Gibbs free energy of oxide formation is high, still challenging; for this GaN as model system was targeted.

The oxidation issue was overcome in (1) removing all traces of oxygen from the solvent/cosolvent system and from the precursor and (2) controlling the reaction environment thanks to supercritical microreactor [80]. GaN nanoparticles were prepared in a tubular microreactor flowing anhydrous supercritical cyclohexane ($T_c = 281$°C, $p_c = 40.7$ bar) at 400 °C and 150 bar (22 s of residence time) from [Ga $(NMe_2)_3]_2$. An alternative process concerns the injection of $[Ga(NMe_2)_3]_2$ in hexane in the presence of ammonia. Three to four nanometer gallium nitride nanoparticles were obtained. The formation of high-purity GaN was confirmed by XPS analysis (see inset of Fig. 11). The as-prepared nanoparticles displayed a strong UV photoluminescence emission centered around 335 nm, which is blue-shifted compared to bulk GaN emission (typically 365 nm) and corresponds to a bandgap increase. The unusual PL properties conjugated with the small size

measured are consistent with the formation of quantum-confined GaN nanoparticles.

This example allows illustrating the versatility in terms of phase nature of the flow synthesis method in supercritical fluids. The next section concerns the interest in coupling chemistry and chemical engineering in supercritical fluids for the development of advanced nanostructured materials.

4.2 Functionalized Nanoparticles

4.2.1 Ex Situ Functionalization for Hybrid Organic/Inorganic Nanostructures

The supercritical fluid method is very efficient in terms of material characteristic control. The flow synthesis allowed by this approach offers the possibility to play with both the process and the chemistry for the design of advanced nanostructured materials. An example is the separation of the step of nanoparticle formation with the step of nanoparticle functionalization. Knowing that it is possible with the supercritical route to control part of the nanomaterial characteristics without the use of surfactants, we proposed few years ago this concept of separation of nucleation/growth and functionalization for the design of hybrid organic/inorganic nanomaterials [81]. This simple concept is represented in Fig. 12.

In this concept naked nanoparticles formed in the supercritical flow (characteristic control thanks to pressure, temperature, residence time, solvent, coordination complex nature, and concentration) are sprayed into a functionalization vessel which contained the surfactant. The separation of the two steps of nucleation/ growth and functionalization offers a huge versatility in terms of inorganic core
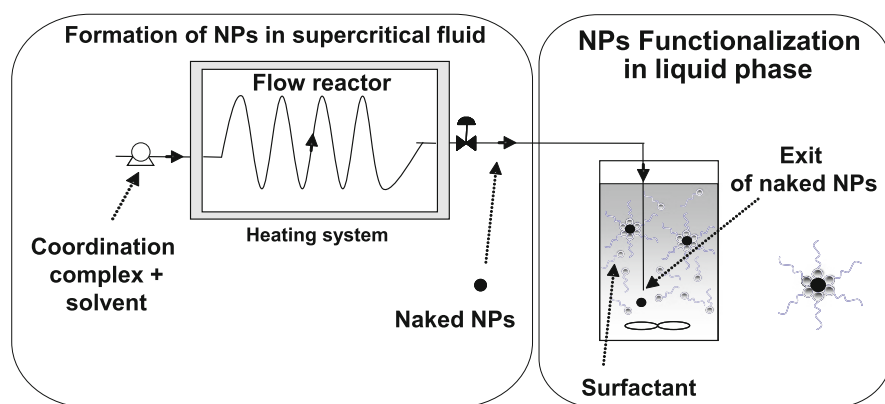
Fig. 12 Process scheme for the synthesis in supercritical fluids of hybrid organic/inorganic nanomaterials through the concept of separation of nucleation/growth and functionalization (adapted from [81])

(as aforementioned with the supercritical flow method) and functionalization agent. As a basic point of view, this process could allow characterizing in situ NP functionalization.

This concept was first demonstrated with the flow synthesis of palladium NPs functionalized with heptadecafluoro-1-decanethiol. In a typical experiment palladium trifluoroacetate(Pd(hfa)$_3$) in acetone is injected in the supercritical flow reactor operating at 20 MPa and 250 °C for a residence time of 10 s. The obtained NPs are sprayed into the functionalization vessel containing heptadecafluoro-1-decanethiol. Our concept was demonstrated thanks to the comparison of this experiment with another test performed without heptadecafluoro-1-decanethiol in the functionalization vessel. Well-dispersed Pd NPs with a narrow size distribution (2.1 ± 0.4 nm) were obtained in the presence of heptadecafluoro-1-decanethiol in comparison with spherical aggregates (98 ± 41 nm) for the non-functionalized PdNPs. The aggregates are formed with Pd NPs of about 3.2 ± 0.7 nm. The experiments with the formation of Pd NPs with and without heptadecafluoro-1-decanethiol as surfactant allow making the proof of concept for the separation of nucleation/growth from functionalization. This first study was supported with the synthesis of Pd NPs stabilized with an ionic liquid: [BMIM]PF$_6$ (1-*n*-butyl-3 methylimidazoliumhexafluorophosphate). Pd NPs prepared in the same conditions as previously reported are sprayed into the functionalization vessel containing the pure ionic liquid. The result is a colloidal solution of Pd NPs/BMIMPF$_6$, Pd NPs presenting a size in good agreement to the one measured with heptadecafluoro-1-decanethiol used as stabilizing agent. Furthermore the activity of these hybrid Pd NPs/BMIMPF$_6$ in the Heck reaction between iodobenzene and styrene (with triethylamine used as a base) proved that there is no passivation of the Pd NPs during the supercritical flow synthesis. The applicability of this concept was extended to the functionalization of Pd NPs with a polymer, namely a cinchonidine-grafted polysiloxane [82]. Cinchonidine being a fluorescent molecule (emission band at 355 nm upon an excitation at 329 nm), meaning sensitive to its environment, we used it as a probe to investigate the functionalization phenomenon. It was observed that the relative fluorescence intensity of cinchonidine gradually decreases with an increase of Pd NPs concentration, proving the interaction between cinchonidine, and so cinchonidine-grafted polysiloxane, and Pd NP surface. Beyond the design of organic/inorganic hybrid nanoparticles, this process can also be used to prepare one of the new generation of catalysts taking benefit of a synergetic effect between a metal element and a nonmetal one like C, P, B, or still N [83]. Following the same procedure, the Pd clusters formed in the supercritical flow reactor are sprayed into the functionalization vessel containing the nonmetal source as metal precursor ligands and solvent. It results in an interaction at room temperature between the highly reactive Pd clusters and the nonmetal source at the origin of the formation of palladium carbide or hydride in the frame of our study. The as-modified Pd NCs present interesting physicochemical properties, opening an avenue towards the formation of other metal/nonmetal material preparation such as phosphides or still borides.

4.2.2   In Situ Functionalization

As opposed to ex situ functionalization, the ligands can be directly introduced inside the initial precursor solution, before its injection in the reactor, leading to in situ functionalization. The main differences are that (1) the ligands will influence the nucleation/growth process of the NPs and (2) the ligand-to-NP bonding will be much stronger.

To highlight these trends, a perfect example concerns the synthesis of superparamagnetic manganese ferrite NPs in supercritical ethanol ($MnFe_2O_4$) at a fairly moderate temperature (260 °C) [84]. The study investigates in particular the role of in or ex situ functionalization over the NP characteristics. The NPs were obtained by mixing acetylacetonate precursors of manganese and iron ($Mn(acac)_2 + Fe(acac)_3$) in ethanol. In a first step, the particles were synthesized by continuously injecting the solution within a supercritical reactor (residence time fixed at 90s). The NPs were further surface-modified by recovering the NPs at the outlet (upon depressurization) in a vessel containing the ligand mixtures (oleic acid + oleylamine) as aforementioned. In a second step, the ligand mixture was coinjected with the precursor solution through a "T" mixer before being flown through the reactor.

The as-obtained nanoparticles present good crystallinity in both cases, sizes below 8 nm, monodispersity, superparamagnetic behavior at room temperature, and high saturation magnetization. However, depending on the capping strategy, the ferrite NPs present different characteristics. First, the synthesis of $MnFe_2O_4$ with in situ functionalization afforded very small crystals (~2 nm), while the ex situ produced NPs of around 7 nm, underlying the major role of the ligand systems and its impact on the nucleation/growth process of the NPs (Fig. 13). Second, the obtained NPs display extended (for in situ-coated NPs) or short term (for ex situ-coated NPs) colloidal stability.

It is also interesting to highlight the different works that have been performed concerning the continuous synthesis of semiconductor quantum dots (QDs) in supercritical fluids. Starting from coordination complex precursors, CdSe and InP QDs were successfully synthesized in short times. As mentioned in the previous section, the main interest in using supercritical fluids compared to liquid solvents is to narrow residence time distribution, which in turn allows narrowing particle size distribution. This characteristic is highly important when considering QDs, since most of the applications require narrow line width emission, directly dependent on the size distribution. For instance, a study demonstrated the synthesis of CdSe QDs in a supercritical microreactor comparing the high-boiling-point squalane solvent with supercritical hexane (sc-hexane). Precursors cadmium oleate [$Cd(oleate)_2$] and trioctylphosphine selenium [TOPSe] in hexane (or squalane) were mixed directly at high temperature and high pressure ($270 < T < 310$°C, $p = 5$ MPa) leading to fast nucleation of QDs. The supercritical fluid synthesis produced a narrower FWHM and particles size distribution than liquid-phase synthesis at the same conditions [63]. In fact, comparison of the data shows that the size distribution percentage
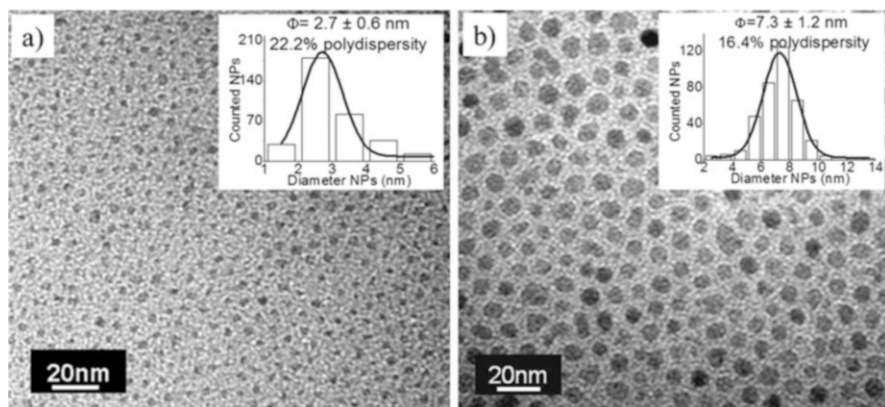
Fig. 13 Superparamagnetic manganese ferrite NPs synthesized continuously in supercritical ethanol with in or ex situ functionalization with oleic acid: (**a**) $MnFe_2O_4$@OAc in situ-functionalized NPs and (**b**) $MnFe_2O_4$ ex situ-functionalized NPs (adapted from [84])

(standard deviation/d_{avg}) for QDs synthesized in sc-hexane, 4–6 % (FWHM: 25–27 nm), is much smaller than for that for QDs synthesized in liquid squalane, 9–12% (FWHM: 41–49 nm). This demonstrates that the use of a supercritical solvent effectively results in homogeneous reaction conditions ideal for nanocrystal synthesis. This is indeed primarily due to the their low viscosity resulting in higher diffusivity coefficient, as demonstrated in a systematic study concerning the synthesis of CdSe QDs using various solvents exhibiting different viscosity values (Fig. 14a) [64].

Similarly, Baek et al. proposed continuous three-stage silicon-based supercritical microfluidic system ($p = 6.5$ MPa) consisting in mixing (130–175°C), aging (200–340°C), and sequential injection stages (80–320°C) for the production of high-quality InP nanocrystals (Fig. 14b) [65]. The first two stages of the reactor were utilized for the systematic study of InP nanocrystal formation. Starting from the mixing of indium myristate [In(MA)$_3$] with tris(trimethylsilyl) phosphine [(TMS)$_3$P] in octane (2:1 ratio) in the first microreactor serving as a mixer, the reacting fluid is then allowed to flow through a second "aging" microsystem at different reaction temperatures. Eventually, the third stage (sequential injection microreactor) aims at growing larger QDs (2–3.2 nm) by injecting additional precursor through six additional side channels, allowing maintaining the precursor concentration below the nucleation threshold, therefore leading to growth process while maintaining a homogeneous size distribution.

Most of these approaches were demonstrated using supercritical microreactors, which do not allow for high production rates. Therefore, recent papers have focused on the investigation of the process scale-up for accessing higher production rates and actually show the promise of such high-quality NPs for their further implementation in devices. In this view, authors report the synthesis of CdSe QDs from a cheap bile-acid-based cadmium precursor (cadmium deoxycholate) in supercritical hexane using a stainless steel millifluidic reactor, allowing producing up to 1 g/day
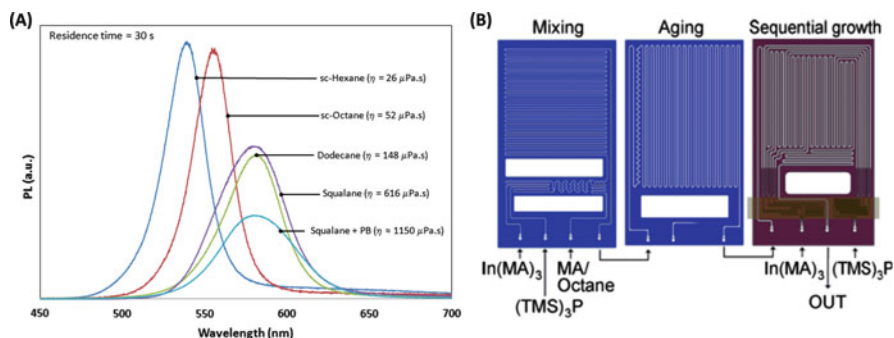
Fig. 14 (**a**) Solvent effect over the final photoluminescence (PL) properties of the as-synthesized CdSe QDs (adapted from [64]). (**b**) Three-stage process for the continuous synthesis of InP QDs in supercritical octane (adapted from [65])

of high-quality QDs [10]. Based on a similar approach, Ippenet al. developed a process using supercritical toluene for the "large scale" production of InP QDs [85].

4.2.3 The Coflow Approach to Separate Nucleation/Growth from Functionalization Steps

As mentioned before, to improve the process reproducibility and to get better control over nanostructure properties, it is advantageous to take benefits of continuous synthetic methods based on supercritical milli/microfluidics. In this view, we have discussed about the interest of a separated control of the nucleation/growth and the functionalization steps, mentioning however that (1) ex situ functionalization provides better control over surface functionalities, but rather poor colloidal stability and are mostly semicontinuous processes, while (2) in situ functionalization leads the NPs' characteristics to be dependent on the chosen ligand system, but provides better stability over time with strong ligand-NP bonds. A question has therefore arisen: could it be possible to couple the advantage of both approaches by taking advantage of a hydrodynamically controlled environment in continuous supercritical synthesis?

In this view, a coaxial continuous supercritical reactor made of two tubing inserted in one another was developed (Fig. 15). In a conventional use, the precursor solution is injected in the inner flow, while the outer flow could be either a pure solvent or a solution containing ligands. The main interests are (1) to separate nucleation/growth occurring in the inner flow before mixing from the functionalization step occurring downstream upon the mixing of the inner and outer flows by inter-diffusion processes at supercritical conditions and (2) to ensure a 3D positioning of the precursor flow at the center of the main tubing, allowing reducing the risk of clogging by focusing the nucleation far from the reactor walls while being able to interchange the capping ligand system without influencing the NC core size or structure.
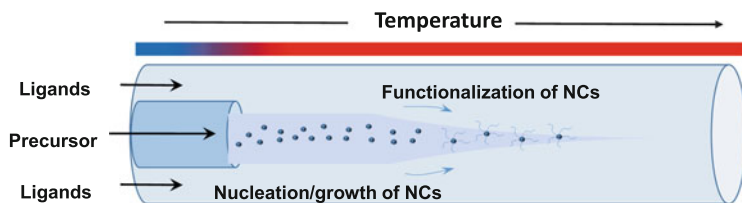
Fig. 15 General concept of the coflow approach using two tubing inserted in one another

This strategy was first demonstrated with the supercritical microfluidics synthesis of ZnO NCs in sc-ethanol at $T = 250°C$, $p = 25$ MPa, and $Rt = 10$ s, which core characteristics (~3.4 nm) were kept constant, while the surface ligands were tuned (trioctylphosphine, oleic acid, oleylamine), demonstrating the successful separation of nucleation/growth from functionalization step in a continuous supercritical process [86]. Further work has investigated the scaling of such a process for increasing the process rate. The switch from submillimeter microfluidic tubing to millifluidic system allows reaching the same quality of materials, as soon as the hydrodynamic behavior is maintained (i.e., flow focusing regime). However, other material characteristics can be obtained when considering flow expanding regime by playing on the ability of the ligands to access more or less rapidly the NC surface by diffusion [87].

Based on this first demonstration, an adapted coflowing setup was further used to synthesize hybrid Pd NC nanocatalysts (Fig. 16a) [88]. The main interest was to modulate the stereoelectronic properties of the Pd NC surface by changing the ligand for boron chemistry catalysis. To prevent from any reducing reagent contamination of the Pd NC surface prior to their functionalization, the palladium precursor (palladium hexafluoroacetylacetonate – $Pd(hfac)_2$) dissolved in toluene was reduced by hydrogen. The low solubility of hydrogen in toluene under the working conditions ($T = 100°C – p = 25$ MPa) was overcome by adding supercritical CO_2 to the system as the main solvent during the nanocatalyst synthesis process. $ScCO_2$ ensured to work in a homogeneous phase, thus getting rid of gas–liquid mass transfer limitations. Various types of ligand systems were considered and successfully linked to the Pd NCs, resulting in the synthesis of a "ready-to-use" nanocatalyst solution in short time (residence time of 17 s) since the fluorous precursor's moieties are removed with the flow of CO_2 upon depressurization at the continuous system outlet. This approach allowed to access a library of nanocatalysts (Fig. 16b), whose catalytic efficiencies were further evaluated towards the C–B coupling process in the Vaultier reaction (Fig. 16c) [89].

The cases of Pd@dppf and Pd@PCy$_3$ (dppf and PCy$_3$ stand for 1,1′-bis(diphenylphosphino)ferrocene and tri(cyclohexyl)phosphane, respectively) were later deeply investigated. Pd NCs synthesized in the presence of dppf (Pd@dppf NCs, size ~ 2.4 nm) were monodispersed, almost spherical, with a narrow size distribution, and exhibited a good crystallinity in contrast to the larger and aggregated Pd NCs obtained in the presence of PCy$_3$ (Pd@PCy$_3$ NCs). The difference was attributed to the type of ligand; dppf, being more bulky, can shield better the formed nuclei,
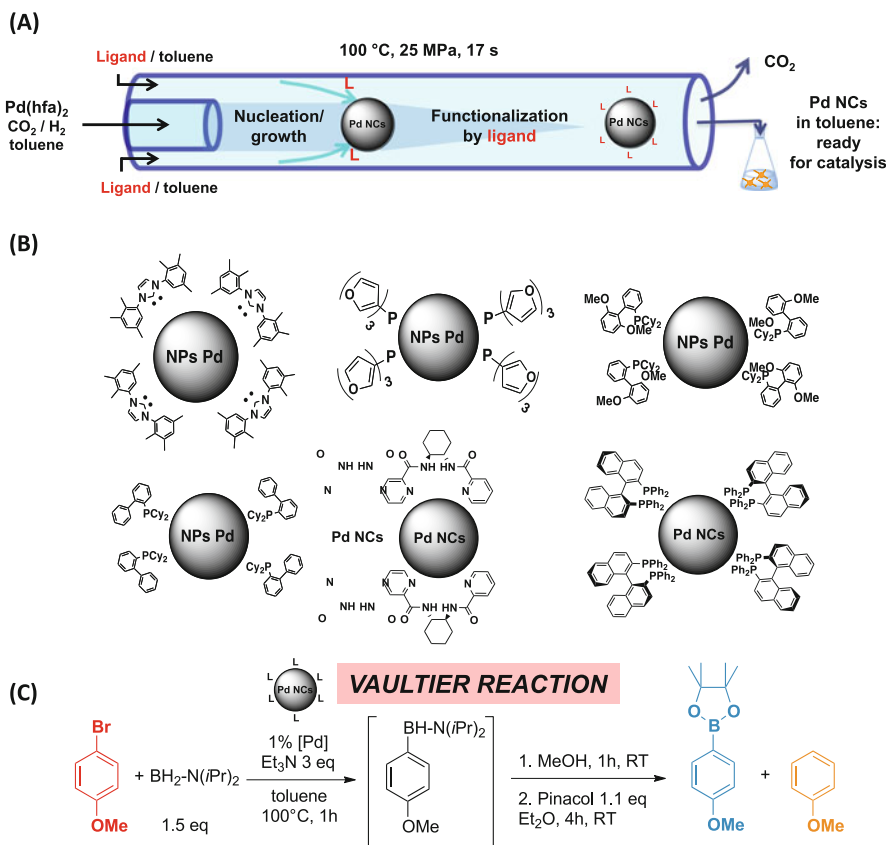
Fig. 16 (**a**) Coflow system used for the synthesis of a library of Pd nanocatalysts; (**b**) general scheme of the obtained NPs, depending on the considered ligand system; and (**c**) description of the Vaultier reaction, in which the Pd nanocatalysts' efficiency was evaluated

therefore impeding a further growth upon mixing. Over time, due to their high reactivity, Ostwald ripening occurs, and larger NPs are formed but at the expense of losing catalytic activity. Oppositely, Pd@PCy$_3$ system behaves completely different, and the already aggregated NCs are stable over time and keep the same catalytic activity [90].

5 Conclusion

Processes using supercritical fluids have attracted increasing interest over the past 30 years, in particular thanks to the capability of some supercritical fluids (SCFs) to replace toxic industrial solvent systems. Additionally, later applications in continuous nanomaterial synthesis in supercritical fluids have taken advantages of the

"hybrid" thermophysical properties of such fluids, intermediate between liquids and gases, which are continuously adjustable with small variations of pressure and temperature for highly specific reactions or separations.

Process speaking, such properties lead to several benefits compared to liquid flow synthesis of nanomaterials such as tunable Reynolds number flows from laminar to almost turbulent, low pressure drop at high flow rate or small scales, fast mixing/heat and mass transfers, and narrow residence time distributions.

Beyond their process versatility allowing accessing various types of materials from a single precursor (metal, oxide, nitrides, etc.), other advantages of SCF synthetic methods stand in the high crystallinity of the obtained materials, the high specific surface area (nucleation is favored over growth), the possible process separation of nucleation/growth from the functionalization step, and the opportunity for new discoveries.

We have presented in here, through selected examples, the huge potential of such continuous synthesis methods from coordination complexes (including organometallic reagents) for various applications from catalysis to energy, imaging, etc.

Although there is to date only few examples of complex nanostructures synthesized through this method, there is an avenue towards its application for the optimized design of nanomaterials, for example, favoring multistep reactions in a single pot. The continuous supercritical synthesis approach offers new opportunities for the synthesis of well-controlled nanomaterials from inorganic to hybrid and more complex architectures such as multifunctional nanomaterials from continuous assemblies or multistep synthesis. To date this promising area of research is still little explored, but it raises many promises for nanomaterial synthesis used as building blocks towards complex devices in a near future.

References

1. Coe S, Woo WK, Bawendi M, Bulovic V (2002) Nature 420:800–803
2. Sharma P, Brown S, Walter G, Santra S, Moudgil B (2006) Adv Colloid Interface Sci 123–126:471–485
3. Bruchez M, Moronne M, Gin P, Weiss S, Alivisatos AP (1998) Science 281:2013–2016
4. Liu W, Howarth M, Greytak AB, Zheng Y, Nocera DG, Ting AY, Bawendi MG (2008) J Am Chem Soc 130:1274–1284
5. Saha K, Agasti SS, Kim C, Li X, Rotello VM (2012) Chem Rev 112:2739–2779
6. Valera FE, Quaranta M, Moran A, Blacker J, Armstrong A, Cabral JT, Blackmond DG (2010) Angew Chem Int Ed 49:2478–2485
7. Shahbazali E, Hessel V, Noel T, Wang Q (2014) Nanotechnol Rev 3:65–86
8. Marre S, Jensen KF (2010) Chem Soc Rev 39:1183–1202
9. Gomez L, Sebastian V, Irusta S, Ibarra A, Arruebo M, Santamaria J (2014) Lab Chip 14:325–332
10. Chakrabarty A, Marre S, Landis RF, Rotello VM, Maitra U, Guerzo AD, Aymonier C (2015) J Mater Chem C 3:7561–7566
11. Hessel V, Kralisch D, Kockmann N, Noel T, Wang Q (2013) ChemSusChem 6:746–789
12. Marre S, Roig Y, Aymonier C (2012) J Supercrit Fluids 66:251–264
13. Cansell F, Aymonier C (2009) J Supercrit Fluids 47:508–516

14. Stouten SC, Noël T, Wang Q, Hessel V (2014) Chem Eng Process Process Intensif 83:26–32
15. Cansell F, Aymonier C, Loppinet-Serani A (2003) Curr Opin Solid State Mater Sci 7:331–340
16. Desimone JM, Maury EE, Menceloglu YZ, McClain JB, Romack TJ, Combes JR (1994) Science 265:356–359
17. Lecoutre C, Guillaument R, Marre S, Garrabos Y, Beysens D and Hahn I (2015) Phys Rev E 91, 060101
18. Abraham FF (1977) Chem Phys Lett 47:179–181
19. Kwang Chu C, Robert LR (1979) Equations of state in engineering and research. American Chemical Society, Washington
20. Pinho B, Girardon S, Bazer-Bachi F, Bergeot G, Marre S, Aymonier C (2014) Lab Chip 14:3843–3849
21. Bazaev AR, Abdulagatov IM, Bazaev EA, Abdurashidova A (2007) J Chem Thermodyn 39:385–411
22. Chrastil J (1982) J Phys Chem 86:3016–3021
23. Kruse A, Vogel H (2008) Chem Eng Technol 31:23–32
24. Kruse A, Vogel H (2008) Chem Eng Technol 31:1241–1245
25. Cochran HD, Cummings PT, Karaborni S (1992) Fluid Phase Equilib 71:1–16
26. Aymonier C, Loppinet-Serani A, Reveron H, Garrabos Y, Cansell F (2006) J Supercrit Fluids 38:242–251
27. Adschiri T, Lee YW, Goto M, Takami S (2011) Green Chem 13:1380–1390
28. Desmoulins-Krawiec S, Aymonier C, Loppinet-Serani A, Weill F, Gorsse S, Etourneau J, Cansell F (2004) J Mater Chem 14:228–232
29. Aymonier C, Erriguible A, Marre S, Serani A and Cansell F (2007) Int J Chem Reactor Eng 5: Article A77
30. Dahl JA, Maddux BLS, Hutchison JE (2007) Chem Rev 107:2228–2269
31. Philippot G, Elissalde C, Maglione M, Aymonier C (2014) Adv Powder Technol 25:1415–1429
32. Cansell F, Chevalier B, Demourgues A, Etourneau J, Even C, Pessey V, Petit S, Tressaud A, Weill F (1999) J Mater Chem 9:67–75
33. Marre S, Aymonier C, Subra P and Mignard E (2009) Appl Phys Lett 95:134105
34. Roig Y, Marre S, Cardinal T and Aymonier C (2011) Angew Chem Int Ed, 50:12071–12074
35. Takami S, Sugioka KI, Ozawa K, Tsukada T, Adschiri T, Sugimoto K, Takenaka N, Saito Y (2015) Phys Procedia 69:564–569
36. Tighe CJ, Gruar RI, Ma CY, Mahmud T, Wang XZ, Darr JA (2012) J Supercrit Fluids 62:165–172
37. Dunne PW, Munn AS, Starkey CL, Lester EH (2015) Chem Commun 51:4048–4050
38. Tiggelaar RM, Benito-Lopez F, Hermes DC, Rathgen H, Egberink RJM, Mugele FG, Reinhoudt DN, van den Berg A, Verboom W, Gardeniers H (2007) Chem Eng J 131:163–170
39. de Mello AJ (2006) Nature 422:394–402
40. Jensen KF, Ajmera SK, Firebaugh SL, Floyd TM, Franz AJ, Losey MW, Quiram D, Schmidt MA (2000) In: Hoyle W (ed) Automated synthetic methods for speciality chemicals. Royal Society of Chemistry, Cambridge, pp 14–24
41. Gervais T, Jensen KF (2006) Chem Eng Sci 61:1102–1121
42. Marre S, Adamo A, Basak S, Aymonier C, Jensen KF (2010) Ind Eng Chem Res 49:11310–11320
43. Oosterbroek RE, Hermes DC, Kakuta M, Benito-Lopez F, Gardeniers JGE, Verboom W, Reinhoudt DN, van den Berg A (2006) Microsyst Technol 12:450–454
44. Trachsel F, Hutter C, von Rohr PR (2008) Chem Eng J 135:S309–S316
45. Goodwin AK, Rorrer GL (2008) Ind Eng Chem Res 47:4106–4114
46. Goodwin AK, Rorrer GL (2009) Energy Fuel 23:3818–3825
47. de la Iglesia O, Sebastian V, Mallada R, Nikolaidis G, Coronas J, Kolb G, Zapf R, Hessel V, Santamaria J (2007) Catal Today 125:2–10
48. Kikutani Y, Hibara A, Uchiyama K, Hisamoto H, Tokeshi M, Kitamori T (2002) Lab Chip 2:193–196

49. Mazurczyk R, El Khoury G, Dugas V, Hannes B, Laurenceau E, Cabrera M, Krawczyk S, Souteyrand E, Cloarec JP, Chevolot Y (2008) Sens Actuators B Chem 128:552–559
50. Jensen KF (2006) MRS Bull 31:101–107
51. Kelley SC, Deluga GA, Smyrl WH (2002) AlChE J 48:1071–1082
52. Sabate N, Esquivel JP, Santander J, Torres N, Gracia I, Ivanov P, Fonseca L, Figueras E, Cane C (2008) J New Mater Electrochem Syst 11:143–146
53. Wu XH, Guo H, Ye F, Ma CF (2009) Prog Chem 21:1344–1348
54. Appelhans D, Ferse D, Adler HJP, Plieth W, Fikus A, Grundke K, Schmitt FJ, Bayer T, Adolphi B (2000) Colloid Surface A 161:203–212
55. Kulkarni SA, Vijayamohanan KP (2007) Surf Sci 601:2983–2993
56. Srinivasan U, Houston MR, Howe RT, Maboudian R (1998) J Microelectromech Syst 7:252–260
57. Lorber N, Sarrazin F, Guillot P, Panizza P, Colin A, Pavageau B, Hany C, Maestro P, Marre S, Delclos T, Aymonier C, Subra P, Prat L, Gourdon C, Mignard E (2011) Lab Chip 11:779–787
58. Couto R, Chambon S, Aymonier C, Mignard E, Pavageau B, Erriguible A, Marre S (2015) Chem Commun 51:1008–1011
59. Gunther A, Jensen KF (2006) Lab Chip 6:1487–1503
60. Song H, Chen DL, Ismagilov RF (2006) Angew Chem Int Ed 45:7336–7356
61. Glasgow I, Aubry N (2003) Lab Chip 3:114–120
62. Levenspiel O (2002) Chem Eng Sci 57:4691–4696
63. Marre S, Park J, Rempel J, Guan J, Bawendi MG, Jensen KF (2008) Adv Mater 20:4830–4834
64. Marre S, Baek J, Park J, Bawendi MG, Jensen KF (2009) JALA 14:367–373
65. Baek J, Allen PM, Bawendi MG, Jensen KF (2011) Angew Chem Int Ed 50:627–630
66. Watkins JJ, Blackburn JM, McCarthy TJ (1999) Chem Mater 11:213–215
67. Moner-Girona M, Roig A, Molins E, Llibre J (2003) J Sol-Gel Sci Technol 26:645–649
68. Slostowski C, Marre S, Babot O, Toupance T, Aymonier C (2012) Langmuir 28:16656–16663
69. Cabanas A, Darr JA, Lester E and Poliakoff M (2000) Chem Commun 901–902
70. Pedersen BL, Yin H, Birkedal H, Nygren M, Iversen BB (2010) Chem Mater 22:2375–2383
71. Sui R, Charpentier P (2012) Chem Rev 112:3057–3082
72. Znaidi L, Chhor K, Pommier C (1996) Mater Res Bull 31:1527–1535
73. Gourinchas Courtecuisse V, Chhor K, Bocquet JF, Pommier C (1996) Ind Eng Chem Res 35:2539–2545
74. Bocquet JF, Chhor K, Pommier C (1999) Mater Chem Phys 57:273–280
75. Reverón H, Elissalde C, Aymonier C, Bidault O, Maglione M, Cansell F (2005) J Nanosci Nanotechnol 5:1741–1744
76. Reverón H, Elissalde C, Aymonier C, Bousquet C, Maglione M, Cansell F (2006) Nanotechnology 17:3527
77. Philippot G, Jensen KMØ, Christensen M, Elissalde C, Maglione M, Iversen BB, Aymonier C (2014) J Supercrit Fluids 87:111–117
78. Philippot G, Albino M, Chung UC, Josse M, Elissalde C, Maglione M, Aymonier C (2015) Mater Des 86:354–360
79. Philippot G, Albino M, Epherre R, Chevallier G, Beynet Y, Manière C, Weibel A, Peigney A, Deluca M, Elissalde C, Maglione M, Aymonier C and Estournès C (2015) Adv Electron Mater 1
80. Giroire B, Marre S, Garcia A, Cardinal T and Aymonier C (2016) React Chem Eng, DOI: 10.1039/C5RE00039D
81. Moisan S, Marty JD, Cansell F, Aymonier C (2008) Chem Commun 1428–1430
82. Dumont MF, Moisan S, Aymonier C, Marty JD, Mingotaud C (2009) Macromolecules 42:4937–4940
83. Pascu O, Moisan S, Marty J-D, Aymonier C (2014) J Phys Chem C 118:14017–14025
84. Pascu O, Marre S, Aymonier C, Roig A (2013) Nanoscale 5:2126–2132
85. Christian I, Benjamin S, Christopher P, Stefan K, Tonino G, Andreas H (2015) Nanotechnology 26:085604
86. Roig Y, Marre S, Cardinal T, Aymonier C (2011) Angew Chem Int Ed 50:12071–12074

87. Ilin ES, Marre S, Jubera V, Aymonier C (2013) J Mater Chem C 1:5058–5063
88. Gendrineau T, Marre S, Vaultier M, Pucheault M, Aymonier C (2012) Angew Chem Int Ed 51:8525–8528
89. Guerrand HDS, Marciasini LD, Gendrineau T, Pascu O, Marre S, Pinet S, Vaultier M, Aymonier C, Pucheault M (2014) Tetrahedron 70:6156–6161
90. Pascu O, Marciasini L, Marre S, Vaultier M, Pucheault M, Aymonier C (2014) Nanoscale 6:9864–9864

Enantioselective Organometallic Catalysis in Flow

Haruro Ishitani, Yuki Saito, and Shū Kobayashi

Abstract Enantioselective chemical transformations using chiral metal catalysts under continuous-flow conditions are described. Although flow methods have several advantages over batch methods in terms of environmental compatibility, efficiency, and safety, synthesis by flow methods is more difficult than by batch methods. Some pioneering efforts on the topic were conducted in the early 1990s; major contributions have been started very recently. While some fruitful results have been reported in enantioselective hydrogenation, other reactions such as enantioselective oxidation, C–X bond formation, and C–C bond formation are still limited. More advances is expected because flow methods are leading candidates for the next generation of manufacturing methods that can mitigate environmental concerns.

Keywords Carbon–carbon bond forming reaction • Chiral catalyst • Continuous-flow • Hydrogenation • Metal catalysis • Oxidation

H. Ishitani
Green and Sustainable Chemistry Social Cooperation Laboratory, Graduate School of Science, The University of Tokyo, Hongo, Bunkyo-ku, Tokyo 113-0033, Japan

Y. Saito
Department of Chemistry, School of Science, The University of Tokyo, Hongo, Bunkyo-ku, Tokyo 113-0033, Japan

S. Kobayashi (✉)
Green and Sustainable Chemistry Social Cooperation Laboratory, Graduate School of Science, The University of Tokyo, Hongo, Bunkyo-ku, Tokyo 113-0033, Japan

Department of Chemistry, School of Science, The University of Tokyo, Hongo, Bunkyo-ku, Tokyo 113-0033, Japan
e-mail: shu_kobayashi@chem.s.u-tokyo.ac.jp

Contents

1 Introduction

Most efforts on enantioselective organometallic catalysis have been conducted by batch methods for a long time. This is a typical and symbolic example that a batch approach is currently by far the most common method in most laboratories of organic chemistry and synthetic organic chemistry. The production of fine chemicals such as active pharmaceutical ingredients (APIs), agrochemicals, electronic chemicals, fragrances, etc. has mostly been carried out by repeating batch methods.

On the other hand, as synthetic procedures, flow methods have several advantages over batch methods in terms of environmental compatibility, efficiency, and safety. Indeed, flow manufacturing is an important technique that is used as a framework for the production of automobiles, electronic devices, steels, and foods. The advantages of flow manufacturing have been reviewed recently [1–9]. In general, however, synthesis by flow methods is more difficult than by batch methods, and it has generally been considered that synthesis by flow methods can be applicable for the production of simple gasses such as ammonia but that it is difficult to apply to the synthesis of more complicated molecules such as APIs. Contrary to this, in the chemical industries, the number of continuous-flow methods that are in use has gradually begun to increase, even in fine chemical industries including the pharmaceutical industry. At the same time, investigations of organic reactions including enantioselective reactions using flow methods at laboratory level have seen an ongoing increase in popularity over the past decades.

This chapter reviews an area of continuous-flow chemical transformations, focusing on enantioselective flow reactions using chiral metal catalysts that will be important for producing bioactive molecules and others. Enantioselective reactions with chiral catalysts containing any metals will be covered. Chiral nonmetal catalysis (chiral organocatalysis) will not be included. Also, enantioselective reactions using chiral organometallic reagents with achiral catalysts will not be discussed.

2 Early Investigations on Enantioselective Organometallic Flow Reactions

The idea of flow reactions appeared in the early 1990s when certain classes of polymer-supported reagents were developed. Itsuno et al. developed polystyrene-based chiral amino alcohol **1**, which was used as a catalyst for the addition of dialkylzinc (**3**) to an aldehyde [10]. They first examined batch reactions and confirmed that the catalyst could operate with sufficiently high enantioselectivity in the ethylation of *p*-chlorobenzaldehyde (**2**). The authors then applied the reaction system to a continuous-flow arrangement and showed that 0.7 mmol of a polymer-supported catalyst packed in a glass column could be used to produce 58 mmol of the desired product **4** with 92% *ee* (Scheme 1).

Later, the same reaction was also examined with soluble polypropylene-based amino alcohol **5** under continuous-flow conditions using an HPLC pump [11]. A membrane reactor bearing an ultrafiltration membrane was used for fixation. The reaction of benzaldehyde (**6**) with **3** proceeded; however, the enantioselectivity of the reaction with respect to product **7** dropped during operation time (Scheme 2).

In 1999, Hodge et al. tested the same reaction by using polymer-supported amino alcohol **8** and found that the initial performance of the catalyst in the reaction of benzaldehyde (**6**) with **3** gave **7** in >94% *ee* (Scheme 3) [12]. However, the performance could not be maintained after 275 h of operation. The results of the study also indicated that partial racemization of the chiral scaffold might occur. Nevertheless, the systematic investigations on the weight of the catalyst, flow rates, and concentrations of substrates are remarkable features of these early attempts to achieve
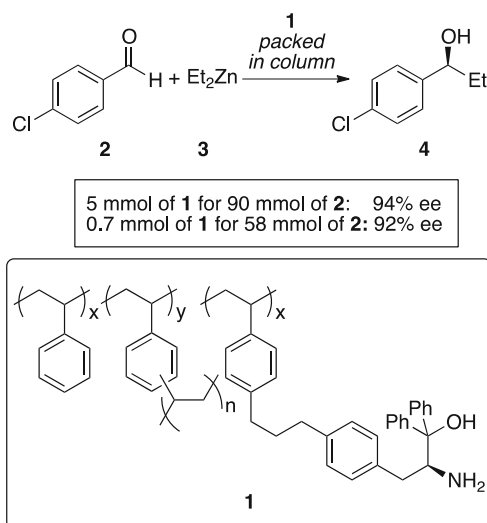
Scheme 1 Enantioselective ethylation (1)
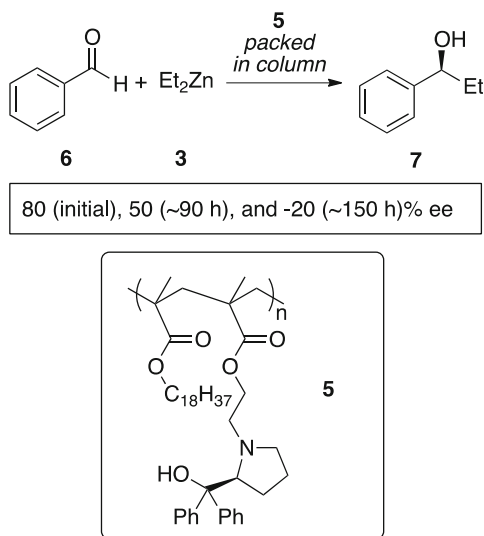
Scheme 2 Enantioselective ethylation (2)
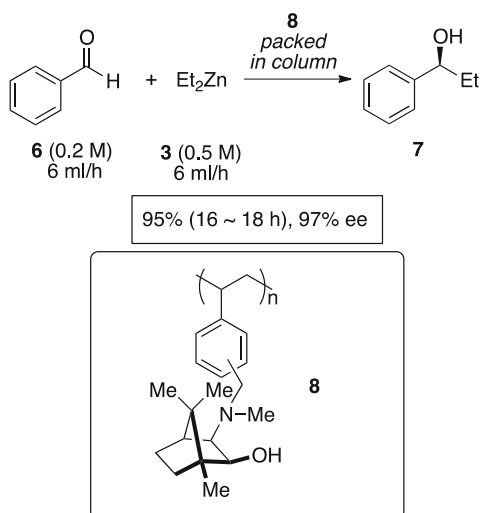
Scheme 3 Enantioselective ethylation (3)

enantioselective catalysis in flow. Clearly, in the latter part of the 1990s, many research groups must have noted this seminal work from the beginning of their research efforts.

In the following four sections, more than 70 works on enantioselective reactions using organometallics or metal complex-mediated enantioselective reactions under continuous-flow conditions are reviewed. Ideas regarding flow techniques and immobilizations are also discussed.

3 Enantioselective Hydrogenation

Hydrogenation reactions of carbon–carbon or carbon–heteroatom double bonds are among the most important transformations for obtaining chiral organic compounds, and relatively large-volume enantioselective hydrogenations under continuous-flow conditions have been reported. Chiral-modified Pt-heterogeneous catalysts for enantioselective hydrogenations are among the most established catalysts in the history of asymmetric catalysts, and continuous-flow reactions with such modified heterogeneous catalysts have certainly been dominant over alternative homogeneous chiral catalysts over the past decade (Fig. 1, Type I). To enable the fine-tuning of asymmetric environments around the metal center, several chiral-catalyst-anchored inorganic materials have also been developed (Type II). One of the impressive characteristics of this stream of investigation is the use of supercritical fluids as a mobile phase; this medium has high affinity for molecular hydrogen and opens new possibilities for the management of molecular catalysts, which has indeed attracted attention (Type III).

3.1 Alkaloid-Modified Platinum Catalysts in Flow

Enantioselective hydrogenations of activated ketones such as pyruvate esters over cinchona alkaloid-modified Pt on solid supports have been widely studied since the pioneering findings of Orito's group (Type I in Fig. 1) [13]. A preliminary investigation of the reaction with a flow reactor was first reported in 1991 by Ibbotson et al. They conducted hydrogenation of methyl pyruvate **13a** using Pt/SiO_2 as a catalyst and cinchonidine as a chiral modifier (Fig. 2). Although conversion of pyruvate was below 10%, the product was obtained in 80% *ee* under flow conditions (Fig. 3) [14]. Baiker et al. demonstrated continuous asymmetric hydrogenation of ketopantolactone (**14**) or ethyl pyruvate (**13b**) over Pt/Al_2O_3 by using a tubular reactor [15, 16]. They fed the substrate with a trace amount of cinchonidine (CD; **12**; 2,800–3,750 ppm relative to the substrate) and showed that the corresponding alcohol was produced in 83.4% *ee* with 94 $mmol/g_{cat}$ h from **14**
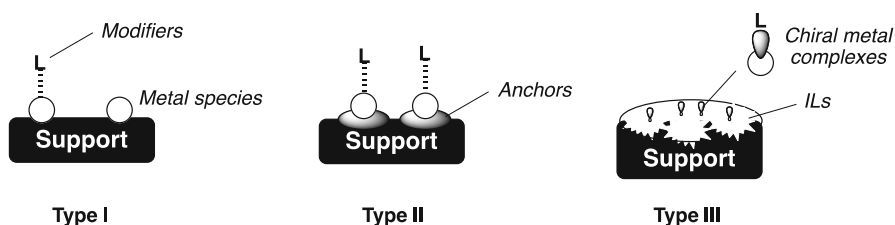
Fig. 1 Types of immobilized catalysts for asymmetric hydrogenation in flow

Fig. 2 Cinchona alkaloids

Quinidine (QD; **9**)   Quininine (Q; **10**)   Cinchonine (C; **11**)   Cinchonidine (CD; **12**)

13a

H_2

12 / Al_2O_3

H_2 **sparger**
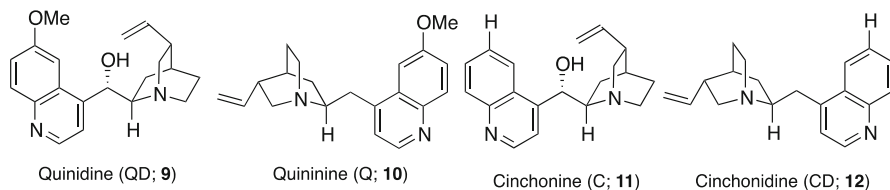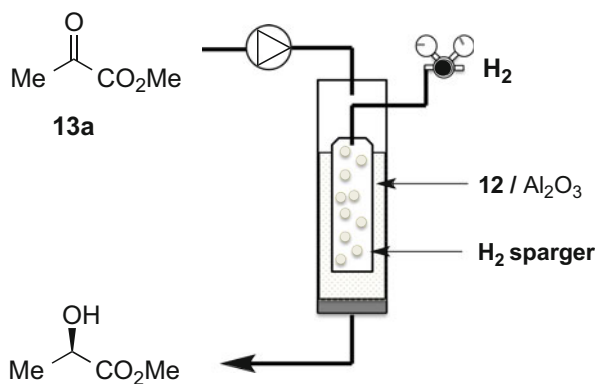
Fig. 3 Ibbotson's flow setup for asymmetric hydrogenation

and in 89.9% *ee* with 23 mmol/g_{cat} h from **13a**. Isopropyl 4,4,4-trifluoroacetate was also used for asymmetric hydrogenation over the same catalyst system [17]. Up to around 90% *ee* and turnover frequency (TOF) of 810 were achieved by using THF as a mobile phase. The same authors demonstrated hydrogenation of ethyl pyruvate (**13b**) in dense ethane as a fluid over a CD-Pt/Al_2O_3 system (Table 1) [18].

Bartók et al. systematically investigated asymmetric hydrogenation of pyruvate esters on Pt/Al_2O_3 with a substrate/modifier solution [19–21]. They also applied their system using an H-Cube high-pressure continuous-flow system with Pd/Al_2O_3 or Pt/Al_2O_3 to asymmetric hydrogenations of α,β-unsaturated carboxylic acids [22] and trifluoroacetophenone [23]. The effects of the structures of the modifiers and additives were disclosed (Table 2).

Murzin et al. investigated continuous production of chiral mandelate ester by flow enantioselective hydrogenation of benzoylformate over Pt/Al_2O_3 with a substrate/modifier solution system [24]. They demonstrated the combination of a hydrogenation reactor and a chromatographic separation to give the pure product (Scheme 4).

Li et al. [25] and Hutchings et al. [26] independently investigated asymmetric hydrogenation of ketoester **18** and methyl pyruvate **13a** over pretreated CD-Pt/Al_2O_3. Li et al. used a 6×100 mm stainless steel column as a fixed bed reactor, and a 0.33 M solution of **18** was fed into the reactor with 1.8 mL/min. Three types of

Table 1 Selected examples of asymmetric hydrogenation of ketoesters over a Pt/Al$_2$O$_3$ system
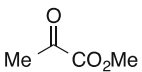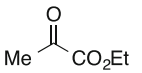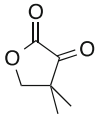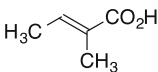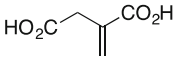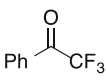
Ketoester	Catalyst	Modifier	Conditions and result	References
(structure) Me–CO–CO$_2$Me **13a**	Pt(6.3 wt%)/ SiO$_2$, 0.4 g	**12** *Pretreated*	20°C, 12 mL/h, ~1 h Conv.: ~10%, 65~80% *ee*	[14]
(structure) Me–CO–CO$_2$Et **13b**	Pt(5 wt%)/ Al$_2$O$_3$, 0.4 g	**12**	rt, in toluene (0.15 M), **13b:12** = 360:1 Yield: 23 mmol/g$_{cat}$, 89.9% *ee*	[16]
(structure) **14**	Pt(5 wt%)/ Al$_2$O$_3$, 0.4 g	**12**	rt, in toluene (0.078 M), **14:12** = 270:1 Yield: 94 mmol/g$_{cat}$, 83.4% *ee*	[15]
13b	Pt(5 wt%)/ Al$_2$O$_3$, 0.9 g	**12**	30°C, 100 bar, ethane: **13b**: H$_2$ = 500:1:10, **13b:12** = 2500:1 Yield: 94 mmol/g$_{cat}$, 83.4% *ee*	[18]

Table 2 Flow enantioselective hydrogenation over Pd- or Pt/Al$_2$O$_3$ catalyst reported by Bartók et al.

Substrate	Catalyst	Conditions	Result	References
(structure) H$_3$C–CO$_2$H, CH$_3$ **15**	Pd(5 wt %)/ Al$_2$O$_3$ 0.3 g	10°C, in toluene (0.05 M) **15:12** = 20:1, 1 mL/min, 5.0 MPa (H$_2$) w/wo benzylamine	wo benzylamine: ~45% *ee* w benzylamine: ~50% *ee*	[22]
(structure) HO$_2$C–CO$_2$H **16**	Pt(5 wt %)/ Al$_2$O$_3$ 0.3 g	10°C, in toluene (0.05 M) **16:12** = 20:1, 1 mL/min, 6.0 MPa (H$_2$) w/wo benzylamine	wo benzylamine: ~5% *ee* w benzylamine: ~40% *ee*	[22]
(structure) Ph–CO–CF$_3$ **17**	Pt(5 wt %)/ Al$_2$O$_3$ 0.1 g	10°C, in toluene/AcOH (9/1, 0.045 M), 1 mL/min, 1.0 MPa (H$_2$)		[23]
		17:9 = 45:1	18% *ee*	
		17:10 = 45:1	30% *ee*	
		17:11 = 45:1	50% *ee*	
		17:12 = 45:1	60% *ee*	

solvents with a variety of hydrogen pressure conditions were tested, and 95% conversion of **18** with 68% *ee* was achieved by using toluene as mobile phase and 6.0 MPa H$_2$ pressure. Hutchings et al. used a 3 mm microreactor, and the maximum enantioselectivity was 51% *ee*, which was observed in the initial stage of the reaction. Later, the same group also tested a 28 × 300 mm trickle bed reactor and found that 70% *ee* was maintained during 120 min when the catalyst was
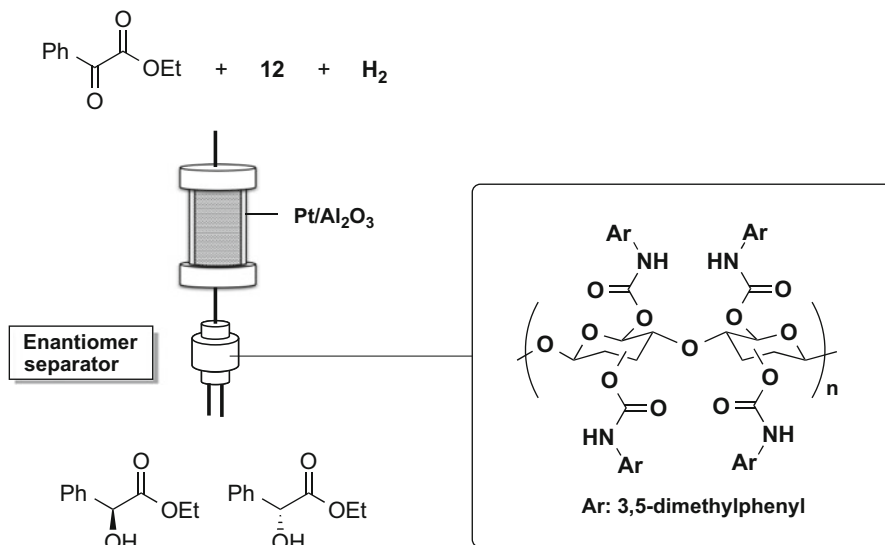
Scheme 4 Murzin's setup for asymmetric hydrogenation and enantiomer separation

Table 3 Asymmetric hydrogenation over a preimmobilized CD-Pt/Al$_2$O$_3$ catalyst

Substrate	Modifier catalyst system	Conditions and result	References
18	**12**@Pt(5 wt%)/ Al$_2$O$_3$ 0.5 g	rt, in toluene, 1.2 mL/h **15**, 0.6 mL/h 6.0 MPa, 60 mL/min (H$_2$) Conv. 99.4%, 68.4% ee	[25]
13b	**12**@Pt(5 wt%)/ Al$_2$O$_3$ 0.4 g, with SiC	25°C, in CH$_2$Cl$_2$ 0.25 M, 1 mL/min, 300 mL/min (H$_2$) ~70% ee	[27]

pretreated with hydrogen and the solvent for 2 h prior to feeding the substrate solution (Table 3) [27].

3.2 Supported Chiral Transition Metal Complex in Flow

Cinchona alkaloids are useful natural chiral auxiliaries; however, the range of applicable substrates is limited, presumably because chemical modification of the alkaloids is relatively challenging. Therefore, the use of other chiral scaffolds combined with heterogeneous transition metal catalysts was also investigated. De Bellefon et al. screened 20 chiral diphosphine ligands with homogeneous
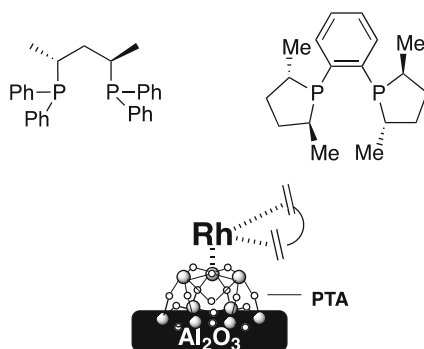
Fig. 4 Schematic of PTA-anchored chiral Rh complexes on Al_2O_3

Table 4 Selected examples of asymmetric hydrogenation over an Rh/PTA/Al_2O_3 system

Substrate	Catalyst	Conditions	Result	References
19a	[Rh(S,S-Skewphos) (nbd)]BF$_4$/PTA / Al$_2$O$_3$	CO$_2$ 1 mL/min, **19a** (in IPA, 2.5 M) 0.25 mL/min, H$_2$ 10 MPa (4 eq), 60°C	Conv. 66% 63% *ee*	[30]
19a	[Rh(R,R-MeDuPhos) (cod)] BF$_4$ (0.02 mmol)/ PTA/Al$_2$O$_3$	**19a** 4.46 mmol (in EtOH) Rh:**19a** = 1:223, 20 mL/min, H$_2$ 100 mL/min, 20°C	Conv. 99% 99.9% *ee*	[31]
19b	[Rh(R,R-MeDuPhos) (cod)] BF$_4$/PTA/Al$_2$O$_3$	**19b** 0.05 mL/min, H$_2$ 5 bar, 0.2 mL/min, rt	98% *ee* 99% purity	[32]
23	[Rh(S-MonoPhos)$_2$ (cod)]BF$_4$/PTA/ Al$_2$O$_3$	**23** (in EtOAc, 0.2 M) 0.1 mL/min, H$_2$ 1 bar, 20°C	Conv. >99 ~63%, 97 ~91% *ee*	[33]

[Rh(cod)$_2$]BF$_4$ complexes for the hydrogenation of (*Z*)-methyl acetamido-cinnamate under microflow conditions [28]. The use of Rh complexes immobilized on solid supports was also tested. A class of such immobilized Rh catalysts was heteropoly acid anchored catalysts on alumina (Type II in Fig. 1) [29]. The unique structure of heteropoly acids such as phosphotungstic acid (PTA) enabled interaction with both metal species and supports (Fig. 4).

Several research groups tried to utilize the metal-PTA-Al$_2$O$_3$ system in asymmetric hydrogenation of itaconate esters (Table 4). Poliakoff et al. first tested such a heterogeneous chiral catalyst for the asymmetric hydrogenation of dimethyl

itaconate (**19a**) under continuous-flow conditions [30]. Moderate conversion and enantioselectivity (66% yield and 63% *ee*) were obtained by using (*S*,*S*)-Skewphos **20** as ligand and supercritical carbon dioxide as mobile phase. The same reaction was also investigated by Simmons et al. in a gas–liquid flow reaction over an Rh/PTA/Al$_2$O$_3$ catalyst by using a trickle bed reactor [31]. They used (*R*,*R*)-Me-DuPhos **21** as chiral ligand, and under the optimized conditions, a substrate/catalyst ratio of 223 under atmospheric pressure at room temperature, 99% conversion and up to 99.9% *ee* were achieved. In 2013, Cole-Hamilton et al. reported highly effective solvent-free enantioselective flow hydrogenation of dibutyl itaconate over an Rh-Me-DuPhos/PTA/Al$_2$O$_3$ catalyst system [32]. More than 99% conversion and 99% *ee* were achieved for the first 23 h, and 68 g of pure (*S*)-dibutyl 2-methylsuccinate (**22b**) was obtained by the use of 41 mg of the chiral Rh catalyst. Bakos's group also reported the application of a similar catalyst system for the asymmetric flow hydrogenation of methyl acetamido acryrate (**23**) [33]. The catalyst system [Rh(COD)((*S*)-MonoPhos)$_2$]BF$_4$ on PTA/Al$_2$O$_3$ was used, and the
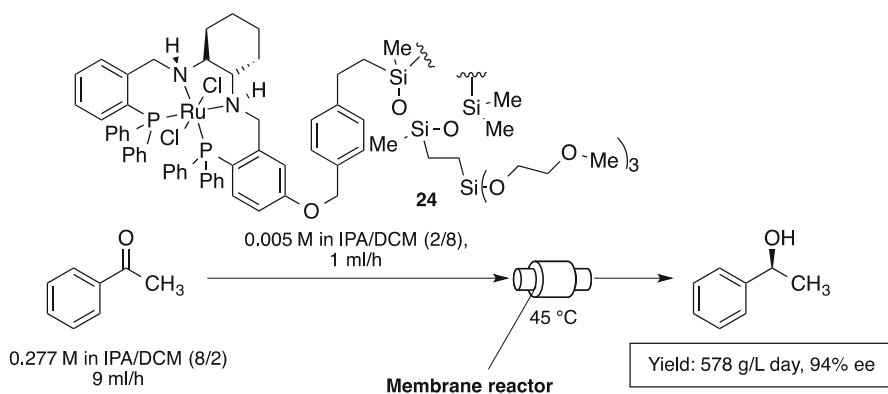
Scheme 5 Asymmetric transfer hydrogenation of acetophenone with a membrane reactor
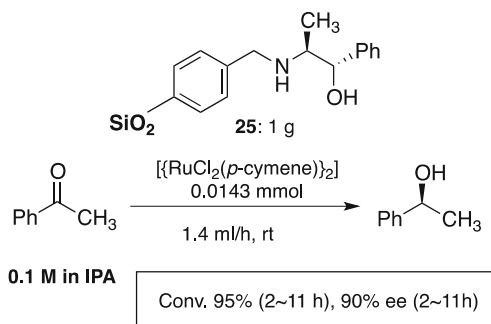
Scheme 6 Asymmetric transfer hydrogenation of acetophenone by using a silica-supported catalyst

desired product was obtained continuously for 12 h with >99% conversion and 96–97% *ee* by using a microfluid-based flow reactor, H-Cube.

Asymmetric transfer hydrogenation of acetophenone over supported metal catalysts under flow conditions was also reported [34, 35]. Soluble polysilane-tethered salen-like P,N-ligand **24** and insoluble silica-supported amino alcohol ligand **25** were, respectively, used for Ru-catalyzed transfer hydrogenations, and high conversion and >90% enantioselectivity were achieved in both cases (Schemes 5 and 6).

3.3 Flow Asymmetric Hydrogenation with Homogeneous Catalysts

Several flow reactions involving homogeneous transition metal catalysts have also been reported. Yamada et al. investigated enantioselective borohydride-mediated reduction of tetralone derivatives by using homogeneous chiral cobalt catalyst **26** with a microflow reactor [36]. Under the microreactor conditions, high reactivity at 10°C was achieved while maintaining high levels of enantios-electivity (Scheme 7). Ley et al. reported diastereoselective asymmetric
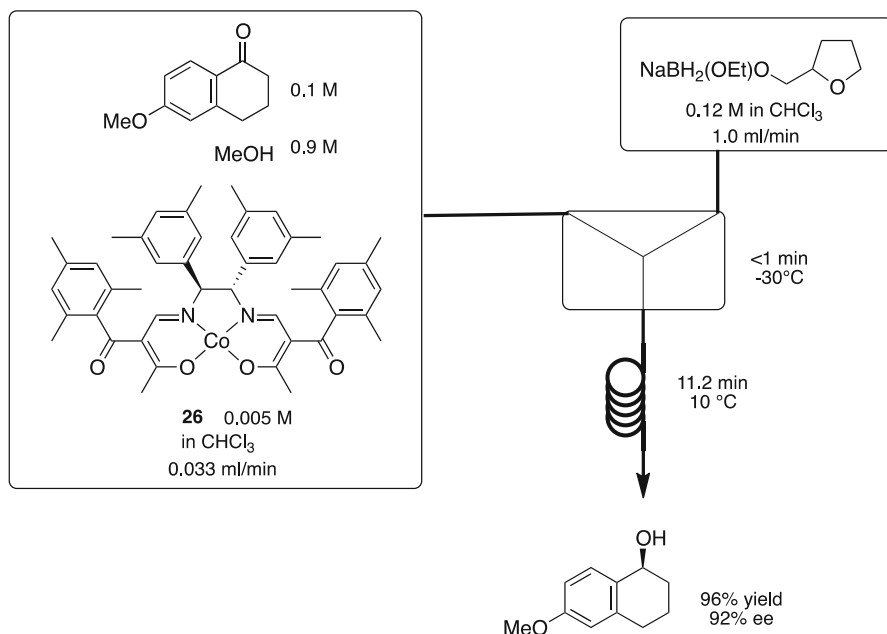
Scheme 7 Homogeneous flow asymmetric borohydride-mediated reduction by using a chiral cobalt catalyst
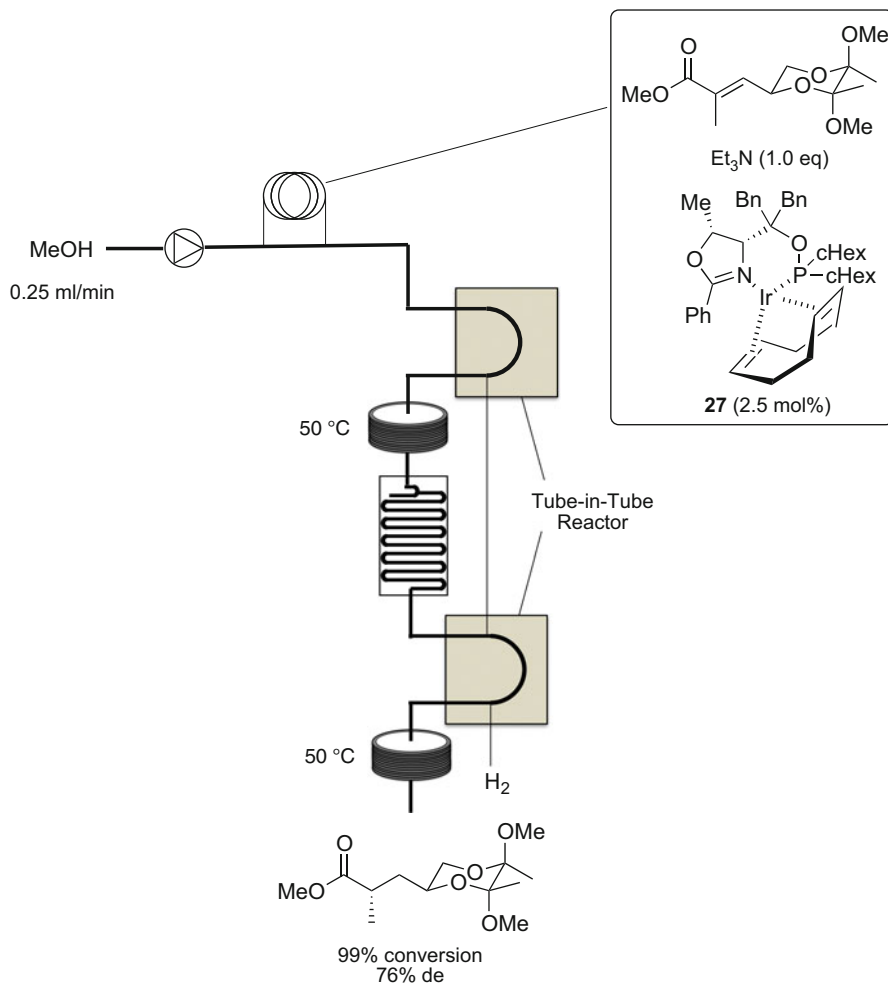
Scheme 8 Homogeneous flow asymmetric hydrogenation with a tube-in-tube reactor

hydrogenation of chiral trisubstituted olefins with chiral Ir catalyst **27** [37]. Two sets of tube-in-tube reactors and a mixer chip were successfully used in this enantioselective hydrogenation reaction, and it enabled rapid catalyst screening to be performed (Scheme 8). In such flow systems using homogeneous catalysts, removal or recycling of chiral metal complexes is important to minimize both contamination of products and loss of expensive chiral scaffolds to waste. Reek's group introduced a reverse-flow adsorption system consisting of two
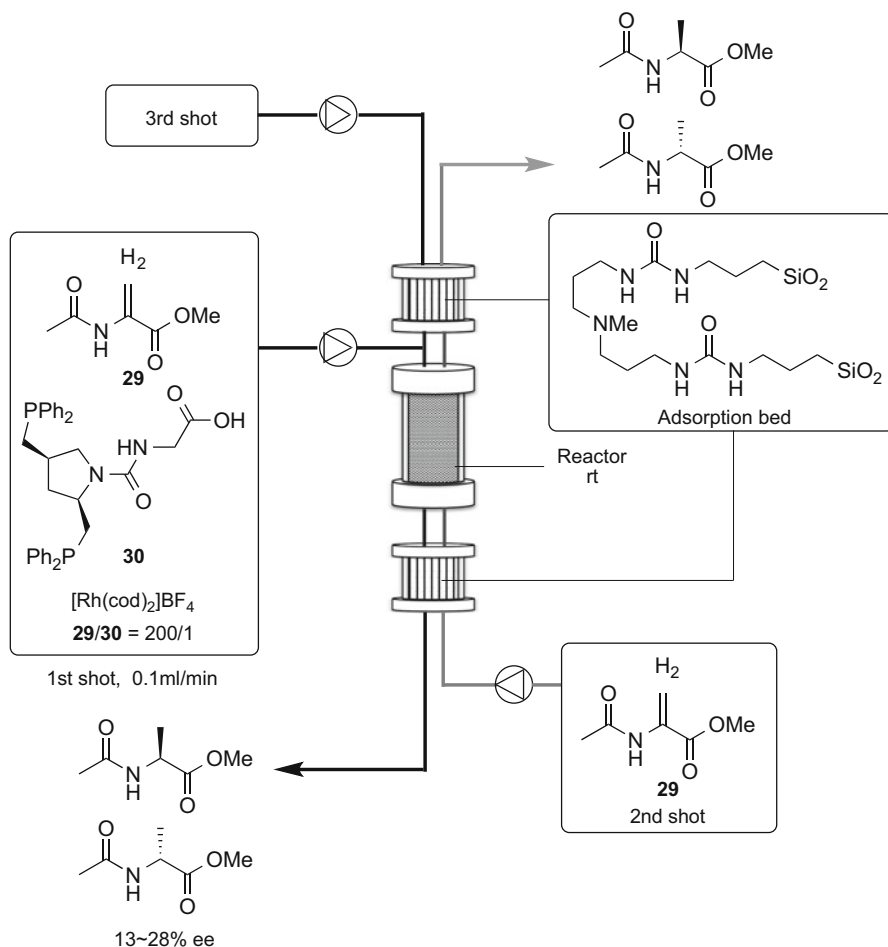
Scheme 9 Schematic of Reek's reverse-flow adsorption system

catalyst adsorption–desorption beds on both ends of a reactor [38]. Silica-immobilized urea **28** was used for the adsorption bed, and hydrogenation of methyl acetamideacrylate (**29**) or hydrosilylation of acetophenone was conducted with several chiral Rh catalysts **30** to demonstrate their system (Scheme 9). Jensen et al. developed a continuous recycling system by using chiral Ru diphosphine/diamine homogeneous catalyst **32** in the asymmetric hydrogenation of tetralone (**31**) [39]. A nanofiltration technique was used for recycling, and the turnover number of the catalyst reached 5,000 in a 24 h operation (Scheme 10).
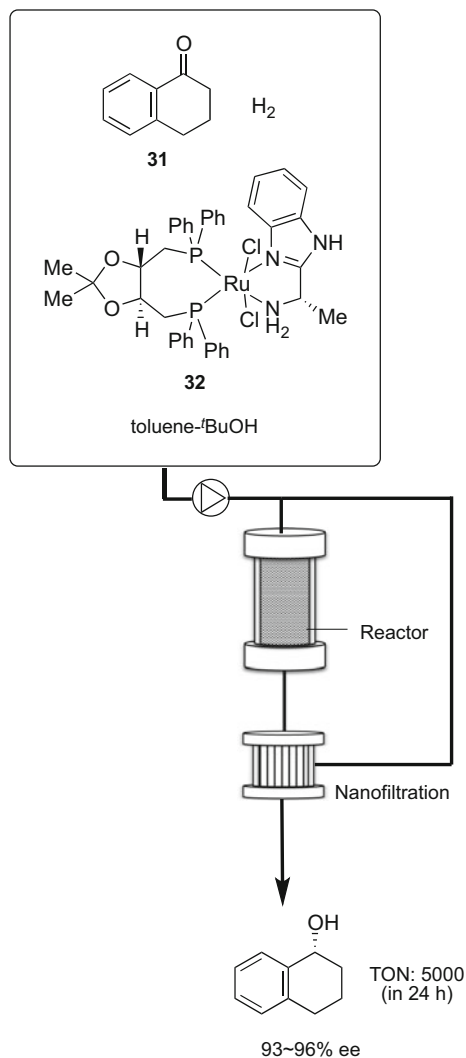
Scheme 10 Jensen's recycling system incorporating a nanofiltration flow system

Since 2010, Leitner's group has successively reported continuous-flow enantioselective hydrogenations of itaconates, β-ketoesters, and enol esters based on their concept of ionic liquid-supported catalysts (Type III in Fig. 1) [40]. The high affinity of a chiral Rh-naphthyl-QUINAPHOS **33** complex with ionic liquid or supported ionic liquid on silica (supported ionic liquid
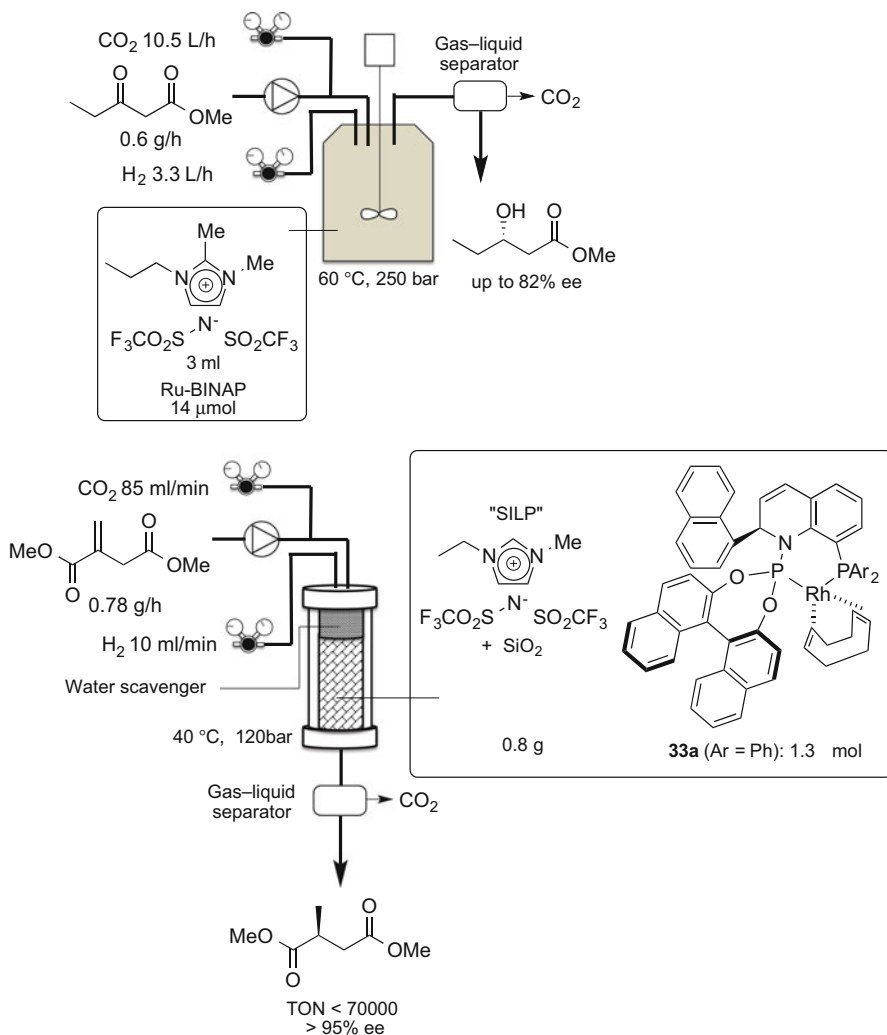
Scheme 11 Leitner's asymmetric hydrogenation with ionic liquid: use of ionic liquid in a batch reactor with a flow system (*top*); use of SiO_2-supported ionic liquid phase with a tubular reactor (*bottom*)

phase, SILP) enables the homogeneous catalyst inside a tubular reactor to be maintained, and an important factor of the immobilization is the use of $scCO_2$ as a mobile phase, which was originally developed by Cole-Hamilton et al. (Scheme 11). Leitner et al. systematically investigated flow conditions, types of ionic liquids, and supports of ionic liquids in the SILP study [41–43]. Typically, turnover numbers (TONs) in their investigation reached more than 140,000, and the *ee* values gradually decreased from >99 to around 70%.

Table 5 Comparison between ionic liquid and SILP systems for Rh-**33b**-catalyzed asymmetric hydrogenation of enol ether **34**

	IL/scCO$_2$	SILP/scCO$_2$
IL (mL)	2.5	1.25
Rh ($\times 10^{-3}$ mmol)	14	7.5
Residence time (min)	17	10
Stability (to keep >60% conv., h)	48	>223
Space–time yield (g/L h)	55	32
TON	11,200	70,400
ee%	80–82	80–84
Rh leaching (ppm)	<1	<1

They also drew a comparison between the IL/scCO$_2$ system and the SILP/scCO$_2$ system from the viewpoint of efficiency (Table 5) [44].

4 Enantioselective Oxidation

Compared with enantioselective flow hydrogenation reactions, only a few examples are known for enantioselective flow oxidations. Liese et al. reported the use of a polyglycerol-supported Mn-salen complex **35**-embedded membrane reactor as a continuous batch reactor [45]. A space–time yield of 458 gL^{-1}d^{-1} and a TOF of 18 were reached in the steady state. The maximum enantioselectivity in epoxidation of 6-cyano-2,2-dimethyl-chromene (**36**) was 92% *ee* (Scheme 12). Later, Hupp et al. developed electrostatic immobilization of a Mn-salen complex onto a mesoporous anodic aluminum oxide membrane through anodic surface–catechol interaction (**37**) [46]. The flow asymmetric epoxidation of 2,2-dimethyl-chromene was conducted, and 67% conversion with 84% *ee* was achieved when the flux was set to 7.5 mL h^{-1}cm^{-2} (Scheme 13).

A chiral V-salen complex attached on polysiloxane **39** was coated inside capillaries for on-column gas chromatographic or liquid-phase sulfoxidation of benzylphenylsulfide **38** [47]. The given enantioselectivities were low; however, this allowed rapid investigation and analysis which in turn enabled the identification of effective catalysts (Scheme 14). A chiral capillary covalently coated with Mn salen (**40**) was also developed by Su et al., and this system was used for kinetic resolution of racemic 1-phenylethanol (Scheme 15) [48].
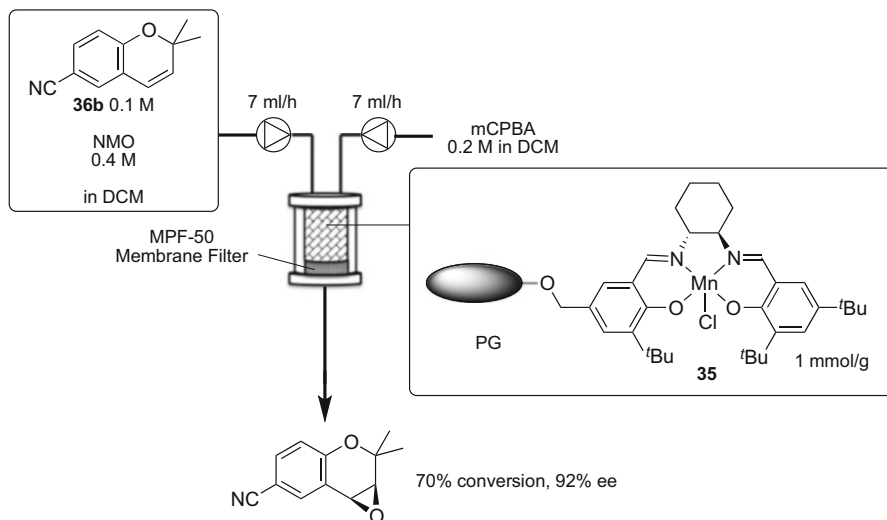
Scheme 12 Asymmetric epoxidation using PG anchored Mn salen with a membrane filter
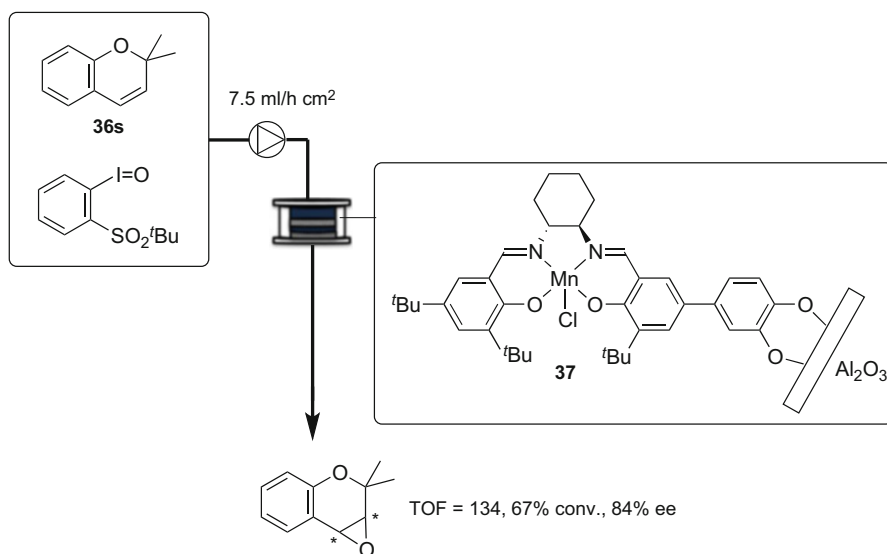
Scheme 13 Asymmetric epoxidation over anodic Al_2O_3-immobilized Mn salen
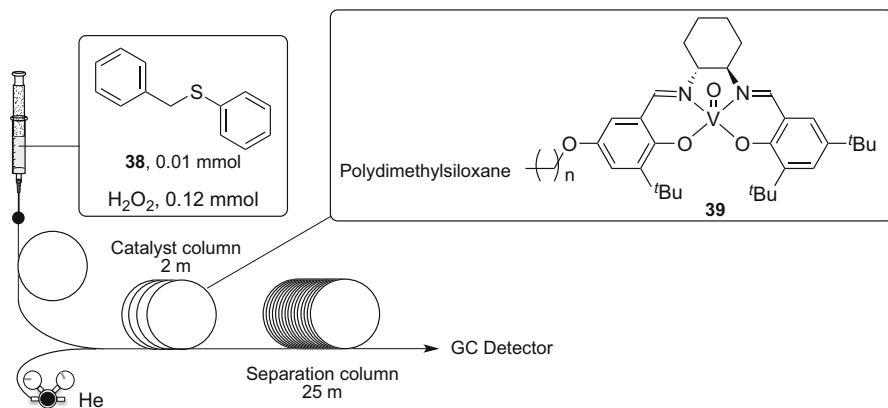
Scheme 14 Flow asymmetric sulfoxidation by using an anchored V-salen catalyst
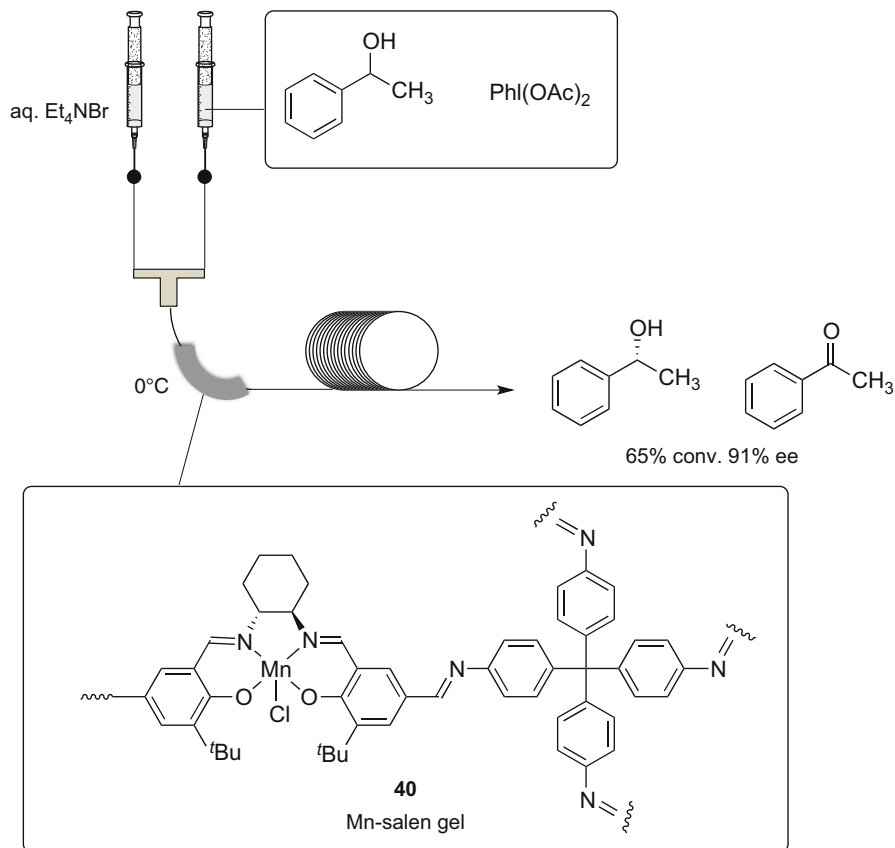
Scheme 15 Oxidative kinetic resolution through a chiral Mn-salen-coated column

5 Enantioselective C–X Bond Formation

Since the early stages of synthetic organic chemistry, C–X (X=O, N, S, and other heteroatoms) bond formation reactions have been studied by many synthetic organic chemists. Such C–X bond formation reactions are fundamental and they enable the synthesis of a wide variety of molecules. Currently, transition metal catalysts are mainly employed to achieve efficient and stereoselective reactions. Some of them are robust and are even employed in industrial processes. Given that flow synthesis has several advantages over batch synthesis, C–X bond formation reactions that are catalyzed by immobilized catalysts under flow conditions are now a hot topic and will be developed further in the future. This chapter focuses mainly on C–O bond formation, which provides important chiral building blocks, chiral alcohols, as the products.
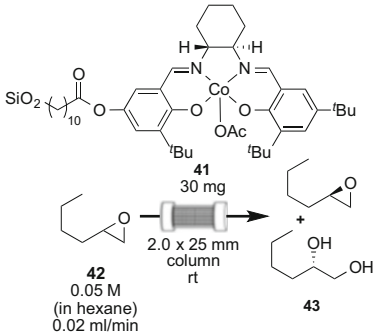
The asymmetric epoxide-opening reaction provides a chiral alcohol with another functional group. In particular, the reaction results in kinetic resolution when conducted with a racemic epoxide. The first asymmetric C–O bond formation catalyzed by a metal complex under continuous-flow conditions was reported by Jacobsen in 1999 [49]. In their report, polymer-supported chiral Co(salen) complex **41** was employed as a catalyst in hydrolytic kinetic resolution of terminal epoxides such as **42**. A chiral salen ligand immobilized on silica was prepared and packed in a column to perform the flow reaction. The product diol **43** was obtained in good yield with excellent enantioselectivity. The catalyst could be recycled simply by washing with THF and water (Table 6).

In 2005, Jacobs et al. reported the asymmetric ring opening of an epoxide with trimethylsilyl azide catalyzed by a Cr(salen) complex immobilized on silica **44** under continuous-flow conditions [50]. In this report, the catalyst was a Cr complex, which was simply impregnated on silica without any covalent bond connection. Two kinds of Cr salen complexes, monomeric and dimeric, were impregnated on silica, and both were packed separately in a column as catalysts for continuous-flow reactions. Although excellent conversion and enantioselectivity were achieved, a significant amount of Cr was lost through leaching. This problem was addressed to some extent by adding pure silica in the column as a scavenger (Scheme 16).

In 2007, Krisching et al. employed a Co(salen) complex immobilized on glass/polymer monolithic composite **46** for the dynamic kinetic resolution of epoxide **47** by hydrolysis [51]. The product was obtained in good yield with high enantioselectivity. The catalyst could be reactivated at least three times by washing with toluene and AcOH (Scheme 17).

More recently, the group of Schulz reported the same reaction with a Co(salen) complex polymer [52]. The yield and enantioselectivity were comparable with those using the PS-Co(salen) catalyst.

In 2010, Reiser et al. reported the kinetic resolution of a 1,2-diol catalyzed by an immobilized Cu-AzaBOX complex on Co/C nanoparticles **49** [53]. The magnetic nature of the nanoparticles meant that they could be agitated by an external rotating magnetic field, which prevented leaching of the catalyst and controlled the fluid dynamics. As a result, product **52** was obtained in high yield with excellent

Table 6 Hydrolytic kinetic resolution of a racemic epoxide

Cycle	Conv. of **42** (%)	*ee* of **42** (%)	*ee* of **43** (%)	K_{rel}	Yield of **43** (%)
1	36	54.0	94.7	63	34
2	39	61.1	94.2	63	39

TMSN$_3$ 0.45 eq., Conv. 40.5%, 85% ee (**45**)
TMSN$_3$ 0.75 eq., Conv. 70.4%, >99% ee (**42**)
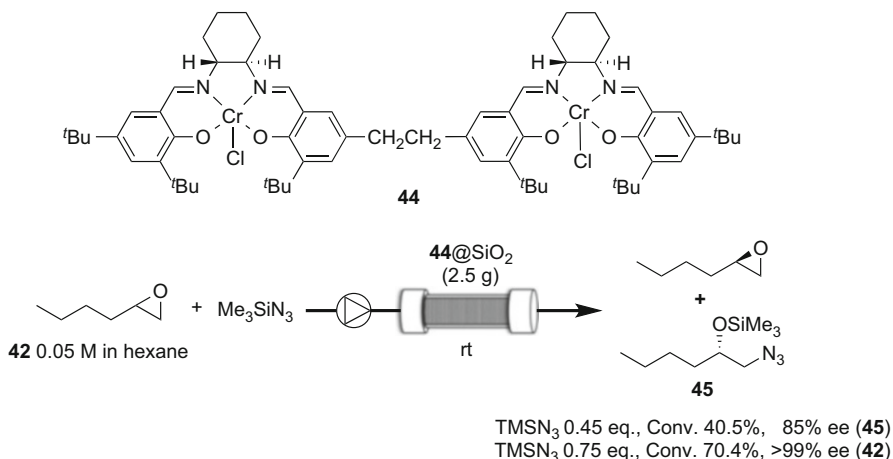
Scheme 16 Asymmetric epoxide ring-opening reaction with trimethylsilyl azide

enantioselectivity, the catalyst maintained its reactivity for at least five runs, and less than 1% catalyst leaching was observed (Scheme 18).

Quite recently, McQuade et al. reported the formation of a Cu-NHC complex under continuous-flow conditions and its catalytic use for boron conjugate addition [54]. Cu$_2$O was first packed in a column with MS4A, and a solution of imidazolium salt **53** was introduced to form a Cu-NHC complex. After the formation of the NHC complex, the solution was mixed with B$_2$(pin)$_2$, Michael acceptor **54**, and a catalytic amount of NaO^{t}Bu to perform the boron conjugate addition. Borylated compound **55** was obtained in high yield and with good enantioselectivity (Scheme 19).
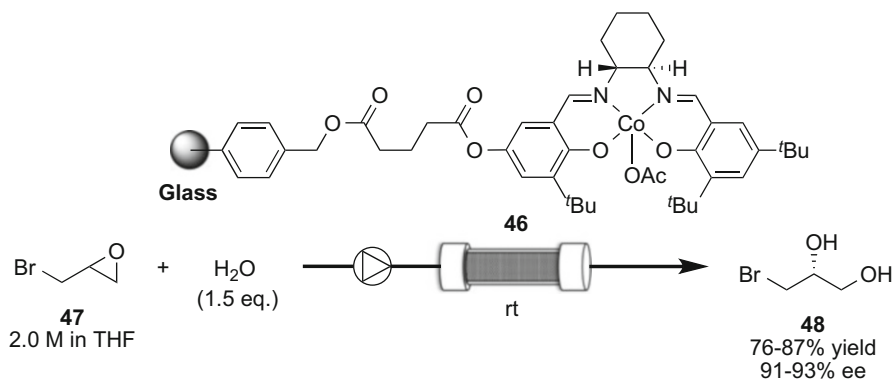
Scheme 17 Hydrolytic kinetic resolution with immobilized Co-salen **46**
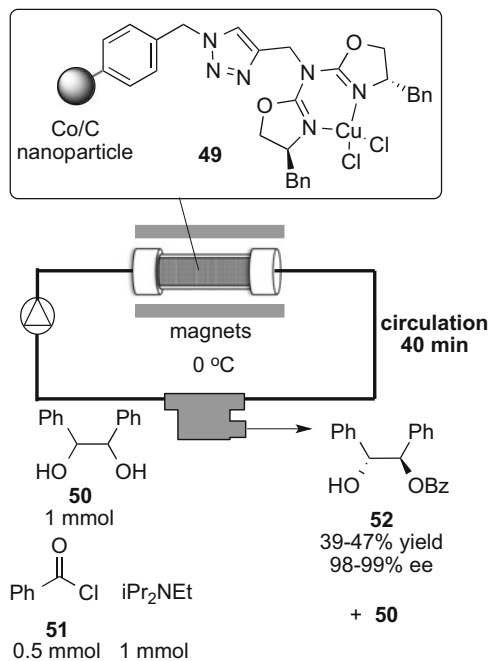
Scheme 18 Kinetic resolution through benzoylation using Co/C nanoparticles **49**
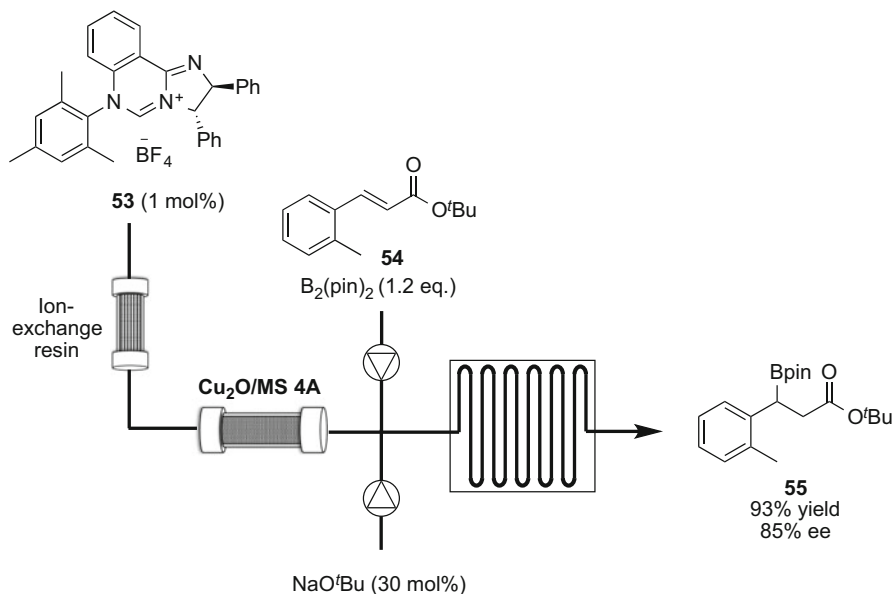
Scheme 19 Asymmetric boron 1,4-addition with a chiral homogeneous Cu-NHC catalyst

6 Enantioselective C–C Bond Formation

C–C bond-forming reactions are among the most important reactions in synthetic organic chemistry to construct the basic skeleton of target molecules. To date, various kinds of reactions including enantioselective reactions have been investigated. Currently, most C–C bond formation reactions depend on metal catalysts to achieve efficient and highly selective coupling. Immobilization of metal complexes and applications to continuous-flow reactions would provide more efficient methods to construct complex molecules.

Hydroformylation is among the most powerful methods to synthesize aldehydes; the approach offers excellent atom economy and uses olefins and carbon monoxide as readily available starting materials. Furthermore, asymmetric variants may be performed by using substituted olefins as starting materials. Many efficient homogeneous catalysts have been developed, with Rh catalysts in particular demonstrating excellent catalyst activities; indeed, some of these catalysts are now employed in industrial processes. Thus, much effort is now devoted to develop immobilized Rh complexes for use in continuous-flow reactions. The first hydroformylation reaction under continuous-flow conditions was reported by Nozaki et al. in 2003 [55]. In their study, Rh-BINAPHOS complex immobilized onto polystyrene **56** was employed for hydroformylation. The olefin was mixed with supercritical CO_2, H_2, and CO and injected into the column packed with the catalyst. Product **57** was finally obtained in moderate yield with good regio- and enantioselectivities with eight types of substrate (Scheme 20).

Et /0.44

0.53

PS-Rh-BINAPHOS **56**

0.0075
+ 0.0225 Free ligand

H$_2$ + CO
(80 - 120 atm)

scCO$_2$

R

56

60 °C

CHO

R

57
5-82 % conv.
l/b =65/35-91/9
60-88% ee
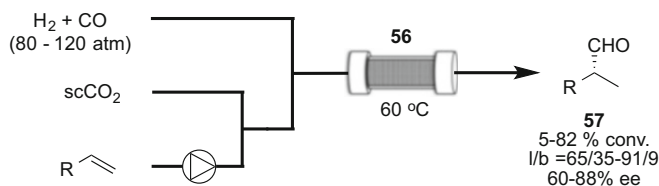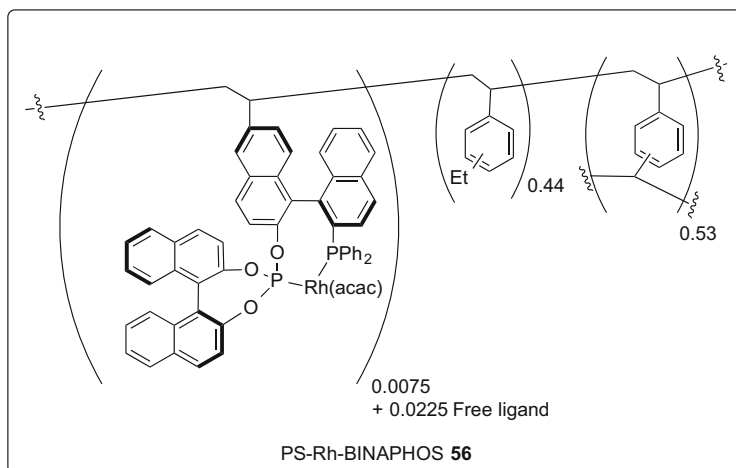
Scheme 20 Asymmetric hydroformylation with PS-Rh-BINAPHOS

Another catalyst system for hydroformylation reactions under continuous-flow conditions was reported by Landis et al. in 2014 [56]. A biphosphine ligand was immobilized on polystyrene beads **58**, which were then applied for the continuous-flow reactions. As a result, the desired aldehyde was obtained in low yield with excellent regioselectivity. However, by employing a circulation system, the conversion could be increased to 100% with a concomitant increase in the regioselectivity. Racemic catalyst **58** was used for the continuous-flow reaction, although excellent enantioselectivity was observed in a batch reaction with the chiral catalyst (Scheme 21).

Cyclopropanation is an important process in synthetic organic chemistry, because the specific structure is often observed in biologically active molecules. However, cyclopropanation reactions require a specified methodology to overcome the high barrier associated with forming the strained ring. Among several kinds of transformations developed to date, carbine transfer reactions catalyzed by transition metals, such as Rh and Cu, are the most versatile because they provide enantioselective reactions. The first cyclopropanation reaction catalyzed by an immobilized metal complex under continuous-flow conditions was reported by Luis et al. in 2007 [57]. The Cu-BOX complex **59** (Fig. 5) was immobilized on polystyrene and employed for the reaction. The yield and the selectivity of formation of the product **66** were strongly dependent on the flow rate. At a flow rate of 5 μL/min, the product was obtained in 61% yield with 71% *ee* (Table 7). However, increasing the flow rate to 200 μL/min resulted in lower
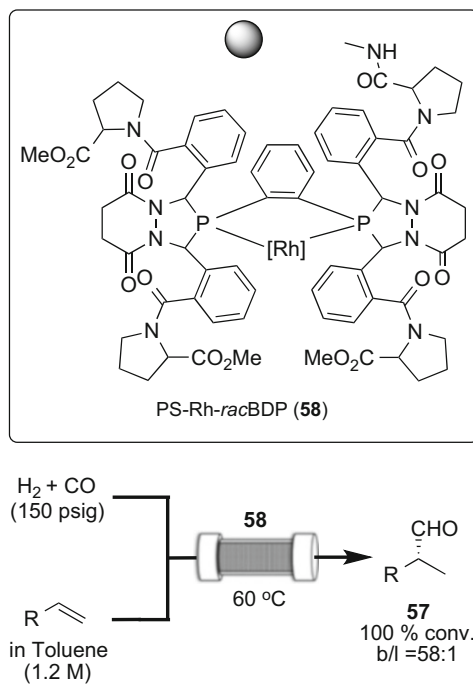
Scheme 21 Flow hydroformylation with catalyst **58**
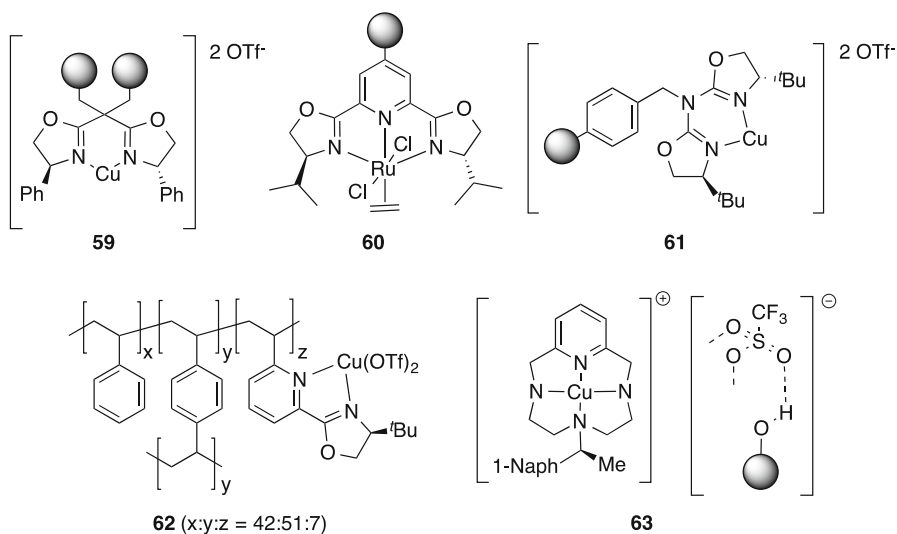
Fig. 5 Chiral heterogeneous catalysts for continuous-flow cyclopropanation

Table 7 Selected examples of continuous-flow asymmetric cyclopropanation reactions

$$\text{Ph} \diagup + \text{N}_2 \diagdown \text{CO}_2\text{Et} \xrightarrow[\text{conditions}]{\text{Catalyst}} \text{Ph} \cdots \text{CO}_2\text{Et (trans-66)} \quad \text{Ph} \cdots \text{CO}_2\text{Et (cis-66)}$$

64 **65** trans-**66** cis-**66**

Catalyst	Conditions	Result	References
59	**64**: 2 M, **65**: 0.5 M (in CH$_2$Cl$_2$), 0.002 mL/min	61% yield 71% ee (*trans*-**66**)	[57]
60	**65**: 1.73 M in **64**, 0.05 mL/min scCO$_2$ 8 MPa: 0.55 mL/min, 40°C	22% yield 89% ee(*trans*-**66**)	[58]
61	**64**: circuling (in CH$_2$Cl$_2$) 5 mL/min	80% yield 93% ee(*trans*-**66**)	[59]
62	**64**:1.5 M, **65**: 0.5 M (in CH$_2$Cl$_2$), 0.023 mL/min	24% yield 60% ee (*cis*-**66**)	[60]
63	**64**: 87.8 mmol, **65**: 17.5 mmol, 0.02 mL/min scCO$_2$ 130 bar: 0.5 mL/min, 40°C	65.5% yield 62% ee (*cis*-**66**)	[61]

yield (29%) and lower selectivity (55% *ee*). Notably, the enantioselectivity achieved under continuous-flow conditions was much higher than those obtained by using a homogeneous catalyst. Solvent-free conditions could also be used with almost the same TOF, albeit with somewhat lower enantioselectivity (57% *ee*). It is interesting that whereas other flow reactions usually suffer from significant metal leaching, in this case, metal leaching was less than 1 ppm.

Another example of cyclopropanation by using Ru-PyBOX immobilized on polystyrene as the catalyst (**60**) was reported by the same group in the same year [58]. Although the use of a higher flow rate decreased both yield and selectivity, the use of scCO$_2$ as solvent dramatically improved both attributes. Later, Lee and Ying et al. reported the use of Cu-AzaBOX complex immobilized on siliceous mesocellular foam (MCF) for the cyclopropanation reaction [59]. A circulating flow allowed both high yield and excellent selectivity. Catalyst **61** was robust enough to perform the reaction as many as 20 times without loss of either yield or selectivity.

In 2011, Ochoa et al. reported a newly designed supported ligand for the cyclopropanation reaction [60]. Pyridine-monooxazoline (=Pyox) ligand was immobilized on polystyrene and employed for the catalysis. It is interesting that the use of the Pyox ligand led to higher catalyst activity compared with reaction with the Box ligand with respect to both reactivity and selectivity. With this new catalyst **62**, the continuous-flow cyclopropanation between **64** and **65** was performed using either dichloromethane or scCO$_2$ as solvent. Although the yield and the selectivity of the product **66** remained moderate, the catalyst remained active after a 1,000 min reaction without loss of either reactivity or selectivity.

More recently, another novel catalyst was designed by Caselli et al. The CuOTf complex with a tetraazacyclic ligand was immobilized on silica through hydrogen-bond interactions. The yield and the selectivity using catalyst **63** were almost the same as those reported previously, and several substrates were employed including substituted styrenes for the construction of a quaternary carbon center. Further-more, the catalyst remained active for up to 25 h without loss of either activity or selectivity, and negligible levels of Cu leaching were observed (0.007%) [61].

Another interesting catalysis system that involves an Rh dimer complex to achieve diazo compound activation has been used to perform carbonyl ylide cycloaddition reactions. In 2011, Hashimoto et al. reported cycloaddition of styrene (**65**) with carbonyl ylide formed in situ from diazo ester **68** under continuous-flow conditions with immobilized Rh dimer catalyst **67** [62]. The product **69** was obtained in high yield with excellent enantioselectivity for as much as 60 h, with a level of Rh complex leaching of 0.013% (Scheme 22).

The Diels–Alder reaction is a powerful method to construct compounds containing a six-membered ring carbon skeleton. Metal catalysts can also provide the desired compound in an enantioselective manner, which can be employed for the synthesis of biologically active compounds. The first Diels–Alder reaction under continuous-flow conditions with an immobilized catalyst was reported in 1996 by Itsuno et al. [63]. In this report, a borane amide immobilized on polysty-rene (**70**) was employed. The reaction of cyclopentadiene **72** with methacrolein **71** afforded cycloadduct **73** in excellent yield with good stereoselectivity (Scheme 23).
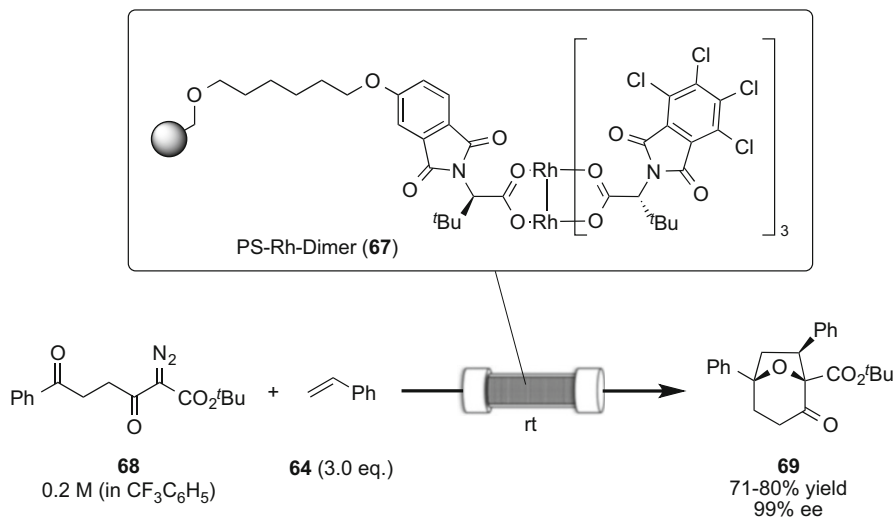
Scheme 22 Continuous-flow asymmetric cycloaddition between **68** and **63**
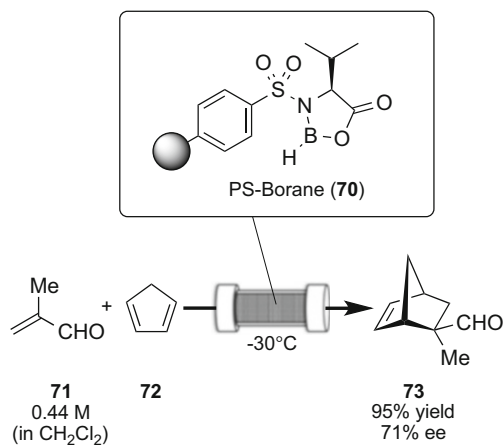
Scheme 23 Continuous-flow asymmetric Diels–Alder reaction with PS-Borane **70**

In 2000, Luis et al. reported another version of the Diels–Alder reaction between cyclopentadiene and crotonoylamide **75** catalyzed by immobilized Ti-TADDOL complex **74** with either a single-path system or a circulation system (Scheme 24) [64]. Although the yield of the desired product **76** was excellent, the enantioselectivity remained moderate. Notably, monolith polystyrene gave better enantioselectivity than grafted polystyrene, whereas the *endo/exo* selectivity remained almost the same.

Another useful class of pericyclic reactions is the Alder–ene reaction. In 2004, Salvadori et al. reported that Cu-BOX immobilized on polystyrene **77** catalyzed a
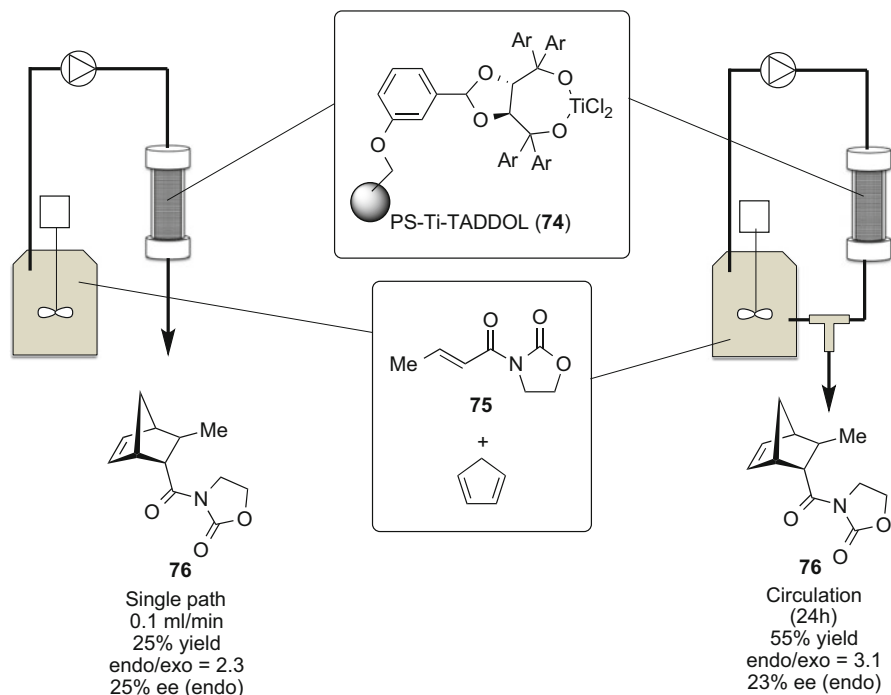
Scheme 24 The PS-Ti-TADDOL-catalyzed continuous-flow asymmetric Diels–Alder reaction

glyoxylate–ene reaction with an alkene (Scheme 25) [65]. Product **80** was obtained by the reaction of **78** with ethyl glyoxylate **79** in good yield with excellent enantioselectivity. Catalyst activity remained for over 80 h without any change in the enantioselectivity.

The 1,2-addition of dialkyl- or diaryl zinc to an aldehyde is a straightforward way to generate an alcohol from an aldehyde. This reaction was mainly developed from the 1990s and various kinds of efficient catalysts have been developed. Under homogeneous catalyst conditions, chiral amino alcohols were found to be excellent catalysts for enantioselective reactions. Therefore, efforts were concentrated on developing immobilized chiral amino alcohols for continuous-flow reactions. As shown in Sect. 2, a particular series of this reaction was investigated in the early 1990s. A recent example of diethyl zinc addition to an aldehyde under continuous-flow conditions was reported by Luis et al. in 2002 [66]. In this report, a β-amino alcohol was immobilized on polystyrene **81** and employed for the reaction. Although the reaction required 24 h circulation to achieve high yield, chiral alcohol **7** was finally obtained in excellent yield with excellent enantioselectivity. The catalyst could be reused at least four times without loss of either reactivity or enantioselectivity (Scheme 26).

In 2008, Pericàs et al. reported another immobilized amino alcohol that was used for the catalytic addition of diethyl zinc to aldehydes [67]. This new catalyst **82** enabled the reaction time to be reduced to as short as 9.8 min to obtain the desired
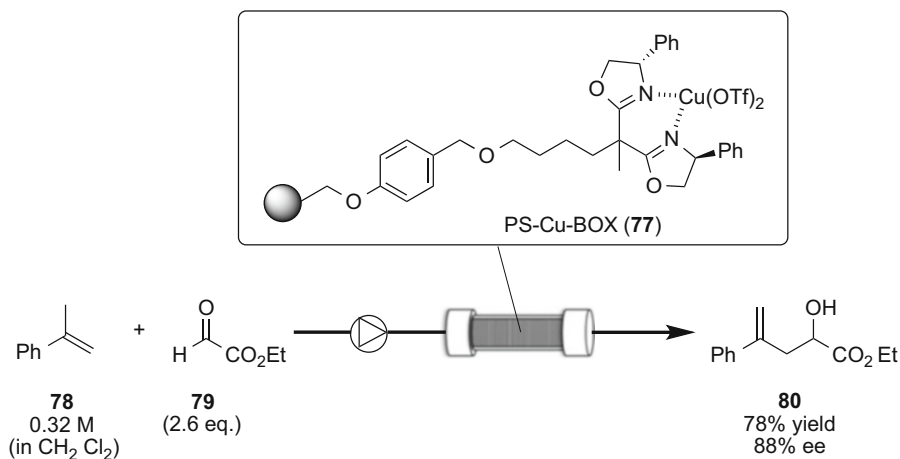
Scheme 25 Continuous-flow ene-type reaction with an immobilized Cu catalyst
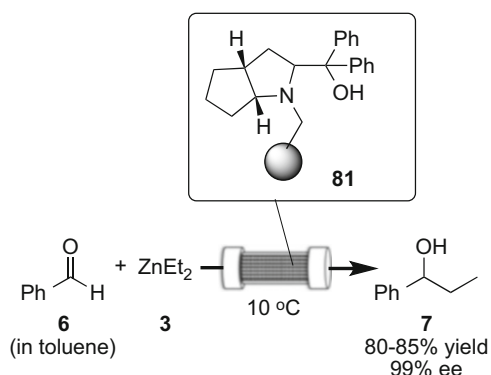
Scheme 26 Continuous-flow diethyl zinc addition to an aldehyde with catalyst **81**

alcohol in excellent yield. The substrate scope of the reaction with respect to the aldehyde was also examined. The same group reported the aryl zinc addition to an aldehyde by using the same catalyst. An excellent yield was again attained, although a slight decrease in the enantioselectivity was observed (Scheme 27) [68].

Cyanation of an aldehyde is also an important C–C bond formation methodology that affords a secondary alcohol. In 2008, Moberg et al. reported the use of a Ti (salen) dimer complex immobilized on polystyrene **83** to catalyze the asymmetric cyanation of an aldehyde [69]. The desired product was obtained in good yield with good enantioselectivity. However, relatively slow feeding of substrates (0.8 mL/min) was required to attain sufficient conversion (Scheme 28).

Another Ti complex was employed for the enantioselective cyanation of an imine. In 2012, Seayad et al. reported the cyanation of a flow-generated imine
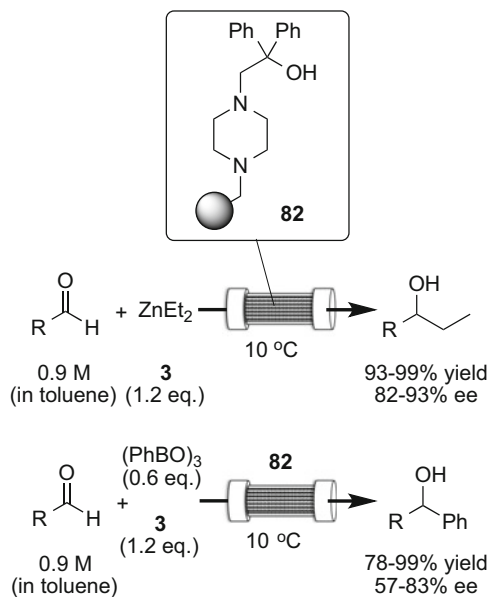
Scheme 27 Continuous-flow diethyl or diaryl zinc addition catalyzed by **82**
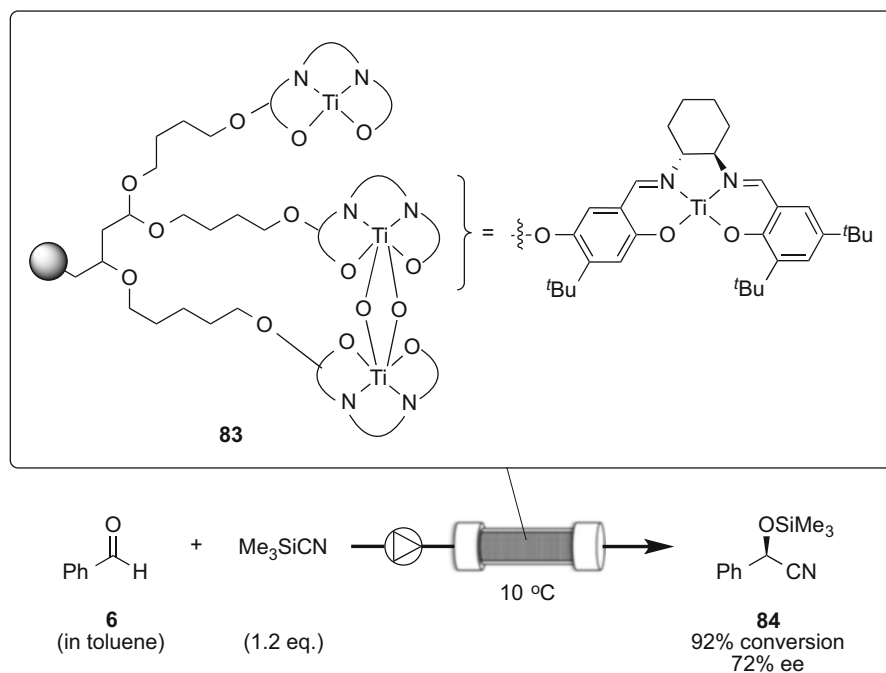
Scheme 28 Continuous-flow asymmetric cyanation catalyzed by immobilized Ti complex **83**
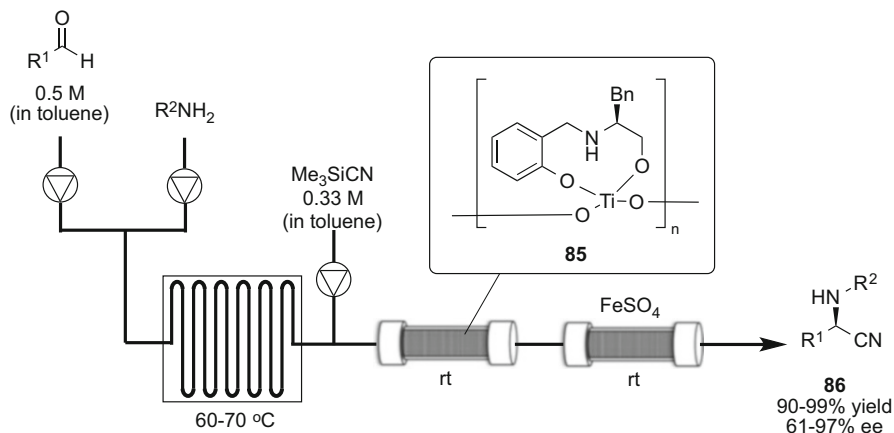
Scheme 29 Two-step continuous-flow reaction to afford chiral secondary amines
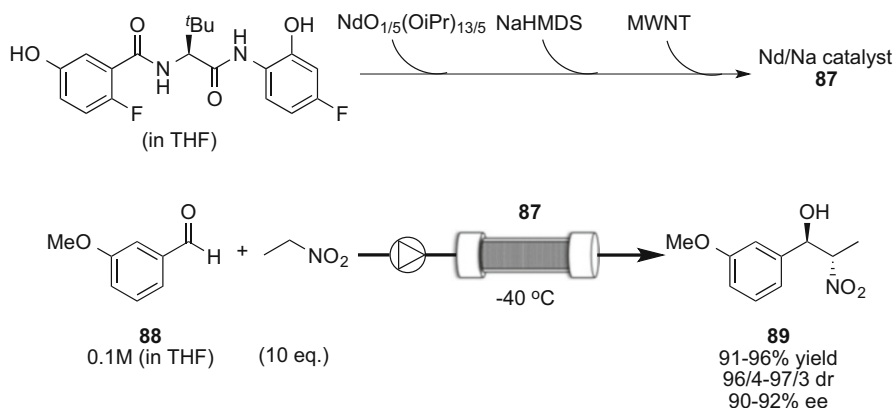
Scheme 30 Asymmetric Henry reaction catalyzed by **87** under continuous-flow conditions

catalyzed by Ti-alkoxide polymer **85** by using an immobilized column reactor system [70]. This system could be used to generate a chiral amine in excellent yield with excellent enantioselectivity, and flow formation of an imine prior to the cyanation would enable the utilization of unstable imines (Scheme 29).

The Henry reaction is a reliable C–C bond formation reaction that can be used to obtain 1,2-nitro alcohols, which are precursors of 1,2-amino alcohols. Shibasaki et al. reported the use of Nd/Na multiwalled carbon nanotube (MWNT) heterogeneous catalyst **87** for the Henry reaction under continuous-flow conditions [71]. First, the catalyst was prepared by mixing a chiral amide, $NdO_{1/5}(O^{i}Pr)_{4/5}$, NaHMDS, and MWNT in THF. The obtained solid was packed in a column, and the Henry reaction between aldehyde **88** and nitroethane was performed under continuous-flow conditions. The Henry adduct **89** was obtained in excellent yield with excellent stereoselectivity for 30 h without any loss of either reactivity or selectivity (Scheme 30).
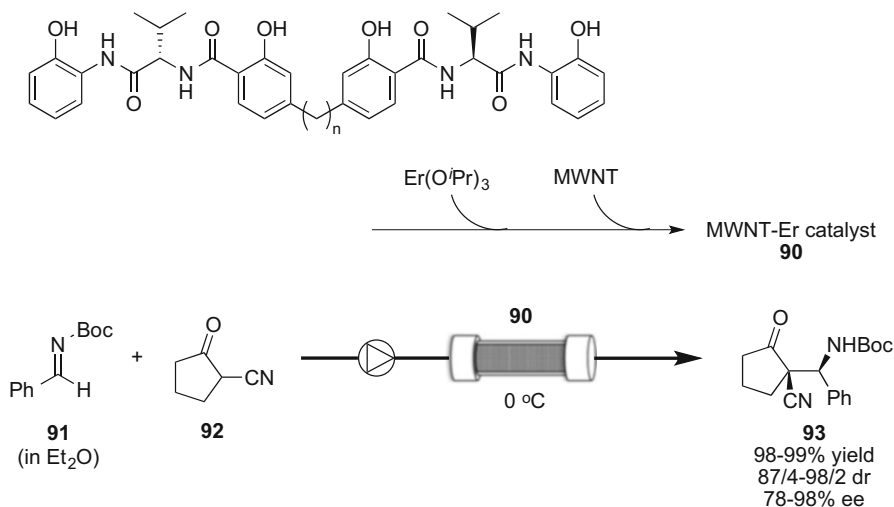
Scheme 31 MWNT-supported catalyst for asymmetric continuous-flow Mannich-type reaction

The same group reported a Mannich-type reaction under continuous-flow conditions by using a MWNT-immobilized catalyst [72]. Again, the europium-based MWNT-supported catalyst **90** was prepared by mixing a chiral ligand, a metal salt, and MWNT. This catalyst demonstrated excellent activity in the Mannich-type reaction of imine **91** with cyano ketone **92** to give the desired chiral amine **93** in excellent yield with excellent stereoselectivity (Scheme 31).

Asymmetric 1,4-addition reaction is another effective method to construct chiral molecules. One successful example was reported by Buchwald et al. in 2012 [73]. In this reaction, an aryl bromide was employed as starting material. First, the aryl bromide was lithiated with *n*-BuLi followed by conversion into an aryl boronate; finally, 1,4-addition reaction with enone **94** was carried out under homogeneous catalysis with Rh-QuinoxP. As a result, the desired 1,4-adduct was obtained in good to excellent yield with excellent enantioselectivity without isolation of the intermediates (Scheme 32).

Another successful example was reported by Kobayashi's group in the same year [74]. In this report, 1,4-addition reaction of malonate **96** with nitroalkene was developed using polystyrene immobilized Ca-PyBOX catalyst **95**. With this catalyst, the 1,4-adduct **97** was obtained in excellent yield with excellent enantioselectivity. Notably, the catalyst remained active for over 200 h without loss of either activity or selectivity (Scheme 33). The multistep flow total synthesis of optically active rolipram was achieved by using this flow asymmetric reaction as one of the key transformations (Scheme 34) [75].
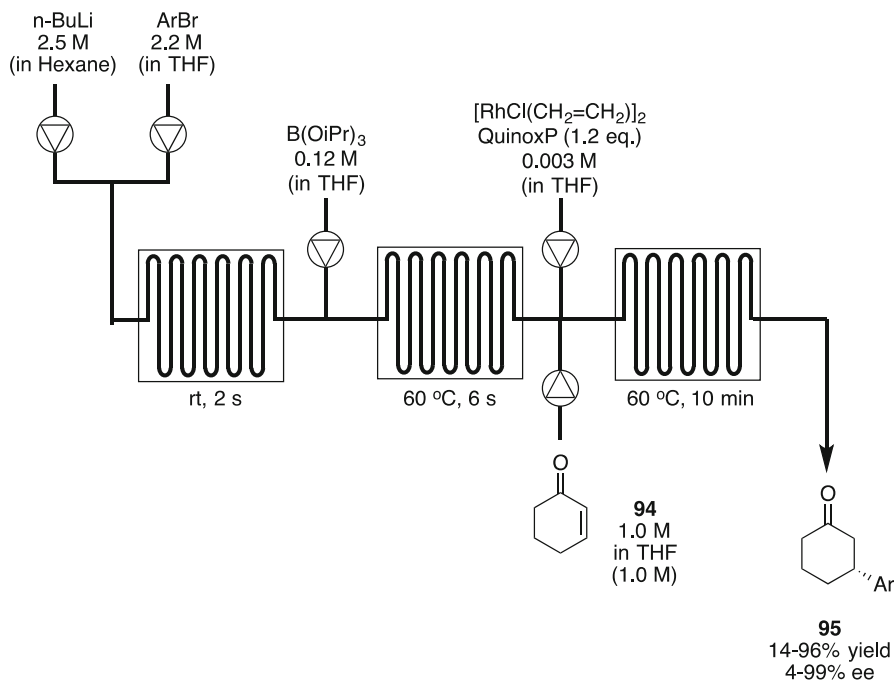
Scheme 32 Setup image of Buchwald's continuous-flow asymmetric 1,4-arylation of an enone
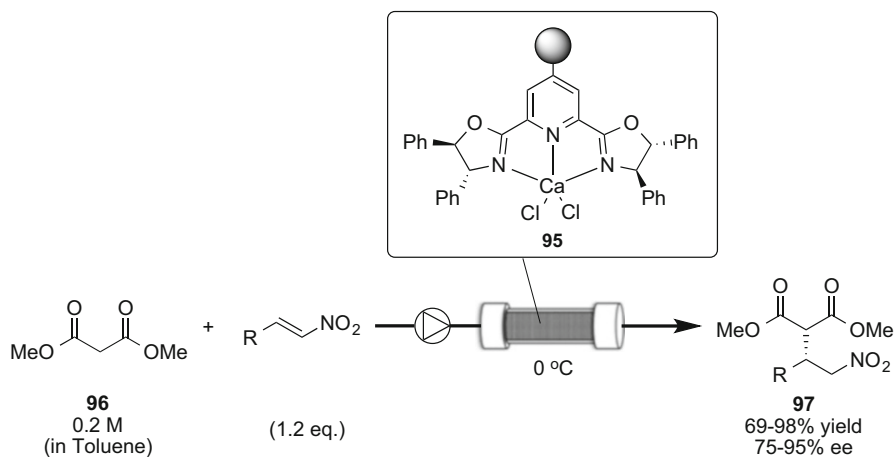
Scheme 33 Flow asymmetric 1,4-addition of malonate to nitroolefin
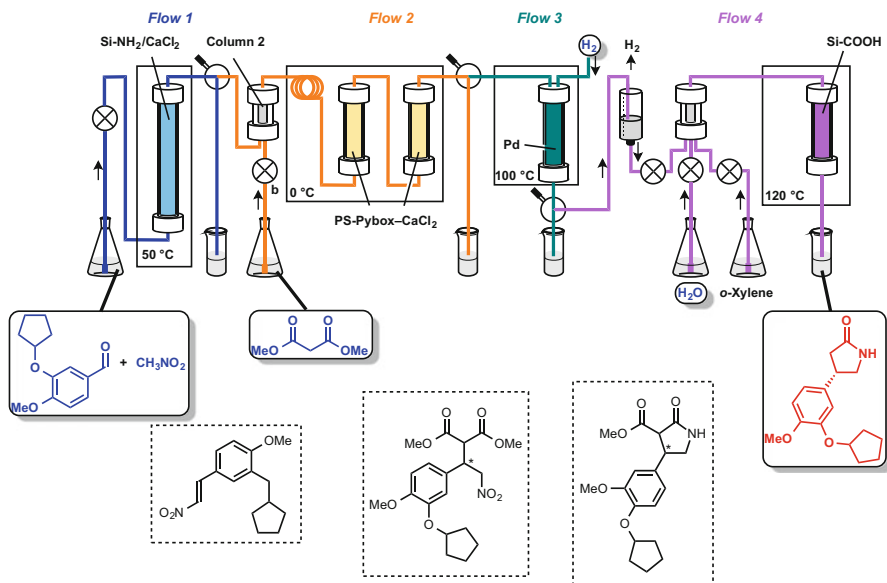
Scheme 34 Continuous-flow asymmetric synthesis of optically active rolipram

7 Conclusion and Perspectives

Enantioselective chemical transformations using chiral metal catalysts under continuous-flow conditions have been described. Although some pioneering efforts were conducted in the early 1990s, major contributions on the topic have been started very recently. While some fruitful results have been reported in enantioselective hydrogenation, other reactions such as enantioselective oxidation, C–X bond formation, and C–C bond formation are still limited, and the area is still at an early stage.

There have been many chiral metal catalysts developed that promote enantioselective chemical transformations, and major activities in this field have been conducted by batch methods for a long time. On the other hand, as synthetic procedures, flow methods have several advantages over batch methods, as noted previously. Therefore, targets of asymmetric synthesis by flow methods should not be limited to enantioselective reactions that cannot be conducted by batch methods, but should be directed toward various types of enantioselective reactions leading to the synthesis of complex chiral molecules such as APIs. Flow methods are leading candidates for the next generation of manufacturing methods that can mitigate environmental concerns [76].

References

1. Mak XY, Laurino P, Seeberger PH (2009) Beilstein J Org Chem 5
2. Webb D, Jamison TF (2010) Chem Sci 1:675
3. Wenger J, Ceylan S, Kirchning A (2011) Chem Commun 47:4583
4. Wenger J, Ceylan S, Kirchning A (2012) Adv Synth Catal 354:17
5. Baxendale IR (2013) J Chem Technol Biotechnol 88:519
6. Tsubogo T, Ishikawa T, Kobayashi S (2013) Angew Chem Int Ed 52:6590
7. Zhao D, Ding K (2013) ACS Catal 3:928
8. Pastre JC, Browne DL, Ley SV (2013) Chem Soc Rev 42:8849
9. Munirathinam R, Huskens J, Verboom W (2015) Adv Synth Catal 357:1093
10. Itsuno S, Sakurai Y, Ito K, Maruyama T, Nakahama S, Frechet JMJ (1990) J Org Chem 55:304
11. Kragl U, Dreisbach C (1996) Angew Chem Int Ed Engl 35:642
12. Hodge P, Sung DWL, Stratford PW (1999) J Chem Soc Perkin Trans 1: 2335
13. Orito Y, Imai S, Niwa S, Nguyen GH (1979) J Synth Org Chem Jpn 37:173
14. Meheux PA, Ibbotson A, Wells PB (1991) J Catal 128:387
15. Künzle N, Hess R, Mallat T, Baiker A (1999) J Catal 186:239
16. Meier DM, Ferri D, Mallat T, Baiker A (2007) J Catal 248:68
17. Künzle N, Mallat T, Baiker A (2003) Appl Catal A 238:251
18. Wandeler R, Künzle N, Schneider MS, Mallat T, Baiker A (2001) Chem Commun 673
19. Szöllösi G, Cserényi S, Balázski K, Fülöp F, Bartók M (2009) J Mol Catal A Chem 305:155
20. Szöllösi G, Cserényi S, Bucsi I, Bartók T, Fülöp F, Bartók M (2010) Appl Catal A 382:263
21. Szöllösi G, Makra Z, Fekete M, Fülöp F, Bartók M (2012) Catal Lett 142:889
22. Hermán B, Szöllösi G, Fülöp F, Bartók M (2007) Appl Catal A 331:39
23. Szöllösi G, Cserényi S, Bartók M (2010) Catal Lett 134:264
24. Martin G, Pereira C, Pettersson F, Saxén H, Murzin DY, Rodrigues A, Salmi T (2015) Chem Eng Technol 38:804
25. Li X, Li C (2001) Catal Lett 77:251
26. Von Arx M, Dummer N, Willock DJ, Taylor SH, Wells RPK, Wells PB, Hatchings GJ (2003) Chem Commun 1926
27. Jenkins RL, McMorn P, Hutchings GJ (2005) Catal Lett 100:255
28. Abdallah R, Meille V, Shaw J, Wenn D, de Bellefon C (2004) Chem Commun 372
29. Augustine RL, Tanielyan SK, Mahata N, Gao Y, Zsigmond A, Yang H (2003) Appl Catal A 256:69
30. Stephenson P, Licence P, Ross SK, Poliakoff M (2004) Green Chem 6:521
31. Al Herz MA, Tsoligkas AN, Simmons MJH, Wood J (2011) Appl Catal A 396:148
32. Duque R, Pogorzelec PJ, Cole-Hamilton DJ (2013) Angew Chem Int Ed 52:9805
33. Madarász J, Farkas G, Balogh S, Szöllösy A, Kovács J, Darvas F, Urge L, Bakos J (2011) J Flow Chem 2:62
34. Sandee AJ, Petra DGI, Reek JNH, Kamer PCJ, van Leerwen PWM (2001) Chem Eur J 7:1202
35. Laue S, Greicer L, Wöltinger J, Liese A (2004) Adv Synth Catal 343:711
36. Hayashi T, Kikuchi S, Asano Y, Endo Y, Yamada T (2012) Org Process Res Dev 16:1235
37. Newton S, Ley SV, Casas Arcé E, Grainger DM (2012) Adv Synth Catal 354:1805
38. Marras F, van Leeuwen PWNM, Reek JNH (2011) Chem Eur J 17:7460
39. O'Neal EJ, Lee CH, Brathwaite J, Jensen KF (2015) ACS Catal 5:2615
40. Hintermair U, Zhao G, Santini CC, Muldoon MJ, Cole-Hamilton DJ (2007) Chem Commun 1462
41. Theuerkauf J, Franciò G, Leitner W (2013) Adv Synth Catal 255:209
42. Hintermair U, Höfener T, Pullmann T, Franciò G, Leitner W (2010) ChemCatChem 2:150
43. Hintermair U, Franciò G, Leitner W (2013) Chem Eur J 19:4538
44. Zhang Z, Franciò G, Leitner W (2015) ChemCatChem 7:1961
45. Beigi M, Haag R, Liese A (2008) Adv Synth Catal 350:919
46. Cho S-H, Walther ND, Nugyan ST, Hupp JT (2005) Chem Commun 5331

47. Sandel S, Weber SK, Trapp O (2012) Chem Eng Sci 83:171
48. Liu H, Feng J, Zhang J, Miller PW, Chen L, Su C-Y (2015) Chem Sci 6:2292
49. Allen Annis D, Jacobsen EN (1999) J Am Chem Soc 121:4147
50. Dioos BML, Jacobs PA (2005) Appl Catal A 282:181
51. Solodenko W, Jas G, Kunz U, Kirschning A (2007) Synthesis 583
52. Hong X, Billon L, Mellah M, Schulz E (2013) Catal Sci Technol 3:723
53. Schätz A, Grass RN, Kainz Q, Stark WJ, Reiser O (2010) Chem Mater 22:305
54. Opalka SM, Park JK, Longstreet ARD, McQuade T (2013) Org Lett 15:996
55. Shibahara F, Nozaki K, Hiyama T (2003) J Am Chem Soc 125:8555
56. Adint TT, Landis CR (2014) J Am Chem Soc 136:7943
57. Burguete MI, Cornejo A, García-Verdugo E, García J, Gil MJ, Luis SV, Martínez-Merino V, Mayoral JA, Sokolova M (2007) Green Chem 9:1091
58. Burguete MI, Cornejo A, García-Verdugo E, Gil MJ, Luis SV, Mayoral JA, Martínez-Merino V, Sokolova M (2007) J Org Chem 72:4344
59. Lim J, Riduan SN, Lee SS, Ying JY (2008) Adv Synth Catal 350:1295
60. Aranda C, Cornejo A, Fraile JM, García-Verdugo E, Gil MJ, Luis SV, Mayoral JA, Martínez-Merino V, Ochoa Z (2011) Green Chem 13:983
61. Castano B, Gallo E, Cole-Hamilton DJ, Dal Santo V, Psaro R, Caselli A (2014) Green Chem 16:3202
62. Takeda K, Oohara T, Shimada N, Nambu H, Hashimoto S (2011) Chem Eur J 17:13992
63. Kamahori K, Ito K, Itsuno S (1996) J Org Chem 61:8321
64. Altava B, Burguete MI, Fraile JM, García JI, Luis SV, Mayoral JA, Vincent MJ (2000) Angew Chem Int Ed 39:1503
65. Mandoli A, Orlandi S, Pini D, Salvadori P (2004) Tetrahedron Asymmetry 15:3233
66. Burguete MI, García-Verdugo E, Vincent MJ, Luis SV, Pennemann H, von Keyserling NG, Martens J (2002) Org Lett 4:3947
67. Pericàs MA, Herrerías CI, Solà L (2008) Adv Synth Catal 350:927
68. Rolland J, Cambeiro XC, Rodriguez-Escrich C, Pericàs MA (2009) Beilstein J Org Chem 5:56
69. Lundgren S, Ihre H, Moberg C (2008) ARKIVOC 6:73
70. Seayad AM, Ramalingam B, Chai CLL, Li C, Garland MV, Yoshinaga K (2012) Chem Eur J 18:5693
71. Hashimoto K, Kumagai N, Shibasaki M (2014) Org Lett 16:3496
72. Hashimoto K, Kumagai N, Shibasaki M (2015) Chem Eur J 21:4262
73. Shu W, Buchwald SL (2012) Angew Chem Int Ed 51:5355
74. Tsubogo T, Yamashita Y, Kobayashi S (2012) Chem Eur J 18:13624
75. Tsubogo T, Oyamada H, Kobayashi S (2015) Nature 520:329
76. Kobayashi S (2015) Chem Asian J. doi:10.1002/asia.201500916

Catalysis in Flow: Why Leaching Matters

King Kuok (Mimi) Hii and Klaus Hellgardt

Abstract The ability to deploy heterogeneous catalysts in continuous flow depends on their stability against deactivation and for reactions in the liquid phase (leaching). This article will discuss the current understanding how leaching can affect catalyst activity and deactivation. Future prospects for the development of the field are proposed.

Contents

K.K. Hii (✉)
Department of Chemistry, Imperial College London, Exhibition Road, South Kensington, London SW7 2AZ, UK
e-mail: mimi.hii@imperial.ac.uk

K. Hellgardt
Department of Chemical Engineering, Imperial College London, Exhibition Road, South Kensington, London SW7 2AZ, UK

1 Introduction

Recent years have seen an increased demand for atom-efficient catalytic methods to be implemented in continuous flow for the manufacture of high-value products such as fine chemicals and pharmaceuticals [1], which relies almost entirely on reactions conducted in the liquid phase. Preferably, the work is carried in multiphasic systems where the catalyst, either molecular or metallic nanoparticles, is immobilised onto an insoluble support, to facilitate separation, removal and recovery from the product stream. However, the loss of catalyst into the reacting fluid (leaching) effectively negates the biggest advantage of using heterogeneous catalysts. Needless to say, irretrievable loss of metal catalyst to the mobile phase is detrimental for the development of catalytic flow strategies.

Even more significantly, particularly for the manufacturing of active pharmaceutical ingredients (APIs), the amount of impurities in the final product, including residual metal, is tightly regulated. For Pd, routinely used in API production, the allowable levels are 10, 1 and 0.1 ppm, respectively, depending on the route of administration (oral, parenteral or inhalation) (http://www.ich.org/fileadmin/Public_Web_Site/ICH_Products/Guidelines/Quality/Q3D/Q3D_Step_4.pdf).   The industrial standard for determining trace metal residues in an API is by inductively coupled plasma spectroscopy (ICP-OES or ICP-AES), where detection of metal concentrations at sub-ppm levels are possible and can be extended to sub-ppb concentrations with ICP-MS. However, the analysis is not always practical or trivial, particularly when a large quantity of organic material is involved, which can affect the behaviour of analytes [2].

There are two general ways an immobilised catalyst can leach from a support: by loss of the molecular entity or nanoparticle into the solution (Fig. 1, pathway i, "migration") or by the slow erosion of molecular or colloidal entities from a nanoparticle surface (Fig. 1, pathway ii, "corrosion"). The former will be directly related to the nature of the insoluble support (organic, inorganic) and the means of immobilisation (adsorption, encapsulation, covalent or dative bonding). The leached species is expected to maintain its primary structure (e.g. a discreet molecular complex or a nanoparticle), which may retain its activity, or is deactivated by irreversible product inhibition, for instance. The second pathway (ii) applies mostly to metallic nanoparticles, where the surface-catalysed process induces the formation of soluble metallic species, either as ligated complexes or colloidal species, which may or may not be catalytically active.

The assessment of a heterogeneous catalyst is typically carried out in batch reactors (frequently in a screw top vial), where catalyst leaching is simply discounted by showing that the recovered catalyst remains active in subsequent runs and no detectable levels of metal residues in the product. There are several potential problems with such an approach, particularly if the reactions were conducted on a small scale with a low TON. For example, the catalyst can act as reservoir for release of homogeneous entities which facilitates a homogeneous reaction. If the catalyst contains sufficient active element or if the active catalyst
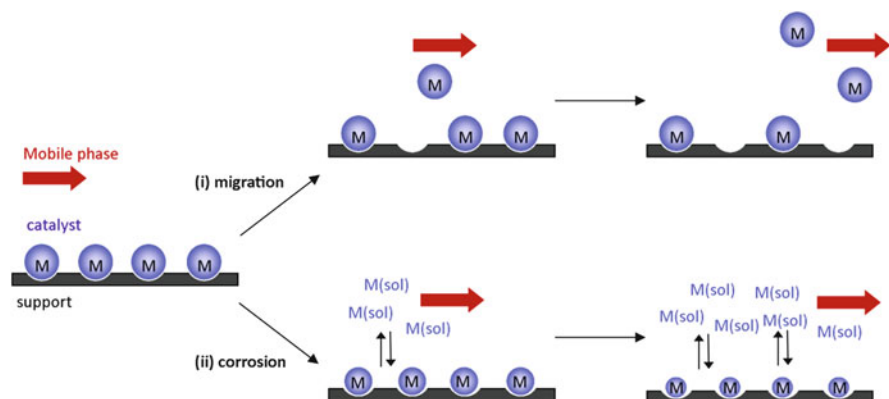
Fig. 1 Possible pathways for catalyst leaching

returns onto the support ("boomerang" or "catch-and-release" catalysis [3]), then leaching can occur during repeated runs which can be misinterpreted as a heterogeneous system that does not experience any activity change. Indeed, this is a primary reason why many catalysts, initially assessed in batch reactors, may not subsequently be suitable for continuous flow under a dynamic flow regime.

Similar caution also needs to be exercised for heterogeneous catalysts employed in continuous flow. In a recent review that discusses methods of utilising supported catalysis in continuous-flow microreactors, catalyst leaching was largely dismissed for most of the processes by ICP analysis [4]. Nevertheless, it is worth noting the (low) level of productivity afforded by microreactors, which may limit the amount of metal detectable by ICP analysis.

Other methods employed to determine leaching, and their possible shortcomings, include [5, 6]:

1. *Hot filtration* of the heterogeneous reaction mixture and testing for continued catalytic activity in the supernatant liquid. The result may depend on the phase separation step. The homogeneous catalyst may be trapped by the filter, giving a false negative; conversely, porous filters, or one that is compromised, may allow fine particulates to pass through, causing false negatives.
2. *Three-phase test* where the reactions were performed using the heterogeneous catalyst, a solubilised reactant and an immobilised reactant. Conversion of the latter into product will indicate leaching of active catalyst into the solution phase. However, the lack of conversion may not necessarily confirm absence of homogeneous catalysts.
3. *Catalyst poisoning*. Traditionally, mercury poison test has been employed to discriminate between homo- and heterogeneous catalytic regimes by sequestering heterogeneous catalysis. This is rarely used nowadays due to the safety and disposal issues associated with the use of elemental mercury. In certain cases, mercury may be catalytically active under the reaction conditions [7]. Conversely, this may also be achieved by the introduction of scavengers known to

bind strongly to the soluble metal catalyst. In this case, reduced catalyst activity will be associated with the presence of catalytically active species in solution. However, it is important to evaluate a number of different scavengers to eliminate false negatives.

It is important to note that all the above tests are invasive and ex situ techniques and are therefore liable to misinterpretation, particularly if they are not performed meticulously. Indeed, it has been demonstrated that mixed results can be obtained in some cases [5]. Critically, none of these tests could distinguish which, if not both, of the two leaching mechanisms (as depicted in Fig. 1) may be operating.

More often than not, the burden of proof depends on conducting the appropriate experiments to prove that catalyst leaching does occur under reaction conditions. In earlier studies mentioned above, analyses are largely based on empirical observations and often not quantitative. However, advances in laboratory hardware, automation and availability of computational resources have greatly facilitated acquisition and handling of data in real time, which has transformed a scientist's ability to design, conduct and interpret the results of a large number of experiments. In the field of catalysis, the development of *Operando* spectroscopy is a particularly exciting emerging area. In essence, it combines spectroscopic characterisation of a material (typically the catalyst) simultaneously with measurement of catalytic performance [8]. For heterogeneous catalysis, such studies are typically performed by observing changes in the catalyst material under working conditions whilst monitoring variations in its activity and selectivity at the same time. In the following sections, both direct and indirect methods for studying catalyst leaching are presented and discussed, with a particular emphasis on reactions that involve C–C coupling reactions in organic solvents.

2 Direct Observation of Catalyst Leaching (*Operando* Spectroscopy)

X-ray absorption spectroscopy (XAS) has emerged as a very powerful technique for catalytic research [9, 10]. It allows the study of a specific element as it undergoes changes in its oxidation state and coordination environment. Most importantly, the technique may be operated in transmission or fluorescence modes and is independent of the physical state of the sample (solid, liquid or gas), which is ideal for the complex reaction environment in which heterogeneous catalysis operates [11]. This was exploited in a catalyst leaching study by the research groups of Grunwaldt and Baiker [12], where a special reaction cell was constructed for Quick-EXAFS (QEXAFS) studies that contains two beam paths allowing for separate monitoring of the catalyst bed and soluble species in the liquid phase (Fig. 2). Using this reactor, the Heck arylation reaction between bromobenzene and styrene catalysed by Pd/Al$_2$O$_3$ was examined (Scheme 1), where the leaching of Pd from the solid into the solution phase can be monitored, simultaneously with reaction monitoring
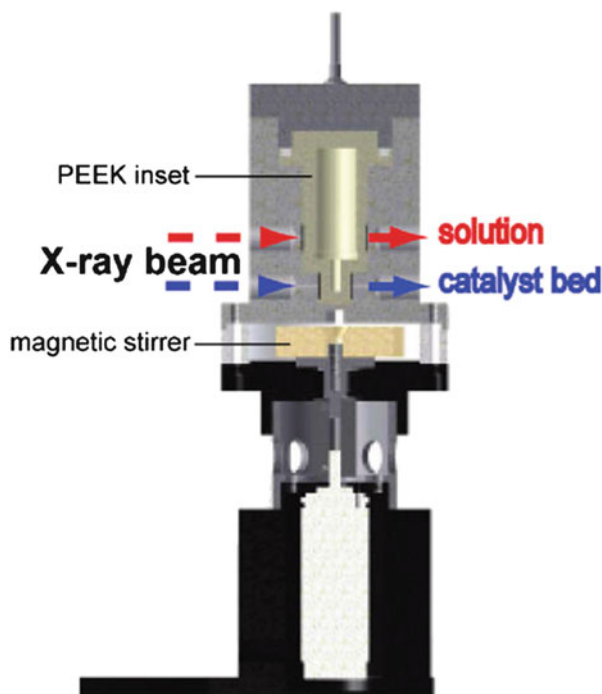
Fig. 2 QuEXAFS (batch) reactor for the examination of Pd leaching (reprint with permission from Reimann et al. [12]. 2011© American Chemical Society)
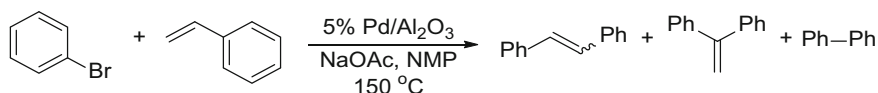
Scheme 1 Heck arylation reaction between bromobenzene and styrene

by gas chromatography (GC). It was found that catalyst activity can be directly correlated to the formation of Pd colloids and complexes such as $[Pd_2Br_6]^{2-}$ or $[PdBr_4]^{2-}$ in the liquid phase, i.e. catalytic activity may be largely attributed to these leached species. Simultaneously, particle size and concentration of Pd were found to remain constant in the catalyst bed, suggesting the operation of a "catch-and-release" mechanism.

In another system, the allylic substitution reaction of (*rac*)-1,3-diphenylallyl acetate with dimethylmalonate catalysed by 5% Pd/Al_2O_3 was examined (Scheme 2) [13]. In the presence of the chiral (*R*)-BINAP ligand/modifier, the reaction was found to be moderately selective (up to 59% ee) under certain conditions. It was suggested that the reaction is largely surface-catalysed when conducted under anaerobic conditions using either THF or dioxane as solvents, as no leached Pd was detected spectroscopically (X-ray absorption near edge
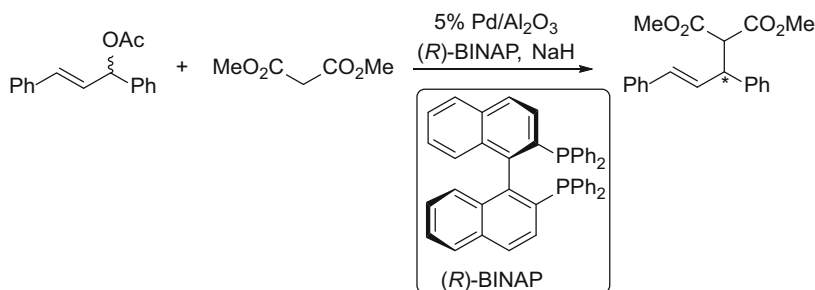
Scheme 2 Asymmetric allylic substation of 1,3-diphenylallyl acetate by dimethyl malonate
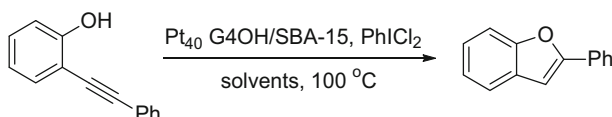
Scheme 3 Hydroalkoxylation reaction catalysed by supported Pt catalyst

structure, XANES) in solution. The use of halogenated solvent such as chloroform, on the other hand, promotes dissolution of Pd and homogeneous catalysis, although the leached species appears to have much lower catalytic activity/selectivity. The roles of the BINAP modifier and reaction temperature were also noted in this study. The general conclusion was that catalyst leaching is minimised in the presence of reducing moieties (malonate, polar solvents, excess BINAP) that can maintain zero oxidation state of Pd for optimal catalyst performance.

In another study, the stability of a silica-supported dendrimer-encapsulated Pt cluster during a hydroalkoxylation reaction was studied in different solvents (Scheme 3) [14]. Using a combination of XAS and kinetic studies, it was suggested that Pt(IV) is the most active form of the catalyst. In contrast to the previous example, the maintenance of the *higher* oxidation state is crucial for catalytic activity. The polar–non-polar repulsive interaction between the catalyst and solvent has been implicated as an important factor in the leaching behaviour of this catalyst. In this case, switching the solvent from non-polar toluene to the more polar dioxane and, even more dramatically, the addition of water caused leaching of catalytically active ionic Pt species into solution, leading to an enhancement of reaction rate.

Selective leaching of one metal from an alloy is a well-known process for the preparation of skeletal catalysts, such as Raney nickel [15]. However, selective leaching may also occur during a catalytic reaction, which can alter the productivity and selectivity of the process. More recently, XAS has also been successfully employed to study the leaching of Pd from SiO$_2$-supported bimetallic Pd/Au catalysts during the synthesis of vinyl acetate from ethylene, carbon monoxide and acetic acid [16]. Under industrially relevant conditions, exposure of the catalyst to acetic acid led to leaching of Pd from the alloy as palladium(II) acetate, leading
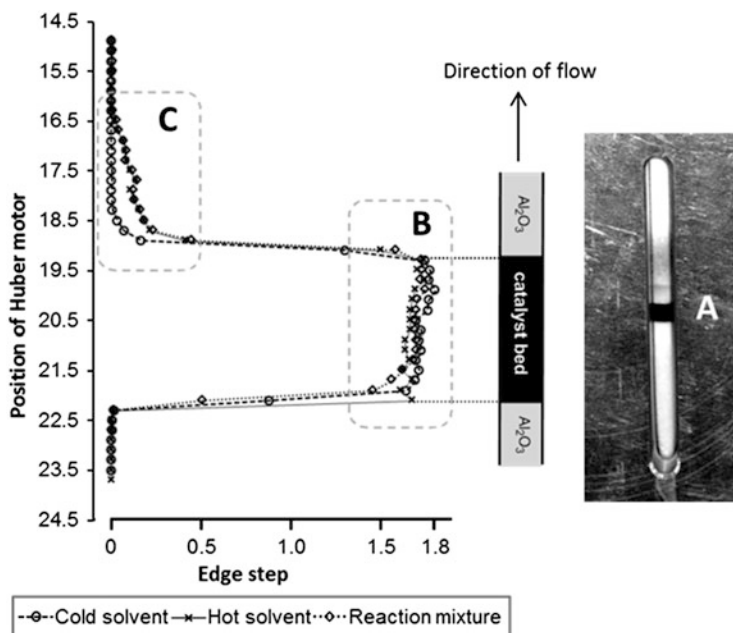
Fig. 3 QEXAFS (flow) reactor for the examination of Pd leaching (reprinted from Brazier et al. [17], with permission from Elsevier.)

to phase separation into Au-rich and Pd-rich phases. The resultant loss of Pt–Au interface causes the catalyst to deactivate eventually.

In an earlier paper, we have found that a sample of 5% Pd/Al_2O_3 undergoes leaching when it was exposed to a heated solution of aqueous ethanol [17]. By employing the heterogeneous catalyst in a packed bed, spatial and temporal evolution of leached Pd species can be resolved by QEXAFS mapping axially along the packed bed. In this case, leaching is clearly visible by the discolouration of the pristine Al_2O_3 packing above the catalyst in the direction of flow (Fig. 3). Subsequent XAS mapping of the catalyst bed revealed a clear migration of Pd species (Fig. 3, region C). XANES analyses revealed a clear redistribution of Pd species along the bed – with an accumulation of Pd(II) species at the entrance of the bed and Pd(0) at the exit. Analysis of the leached Pd species within the alumina bed was also found to consist mainly of Pd(0) species. This is interesting as it also points to a migration of nanoparticles in a convective flow field (Fig. 1, pathway i) due to the destabilisation or disruption of the particle support interaction. Subsequent studies have shown that the smaller Pd nanoparticles (<3 nm) have a tendency to remain oxidised [18].

All of the above examples clearly demonstrate a close correlation between the oxidation state of a catalyst and its leaching behaviour, particularly for Pd systems involving redox processes that lead to the formation of charged or ionic species that
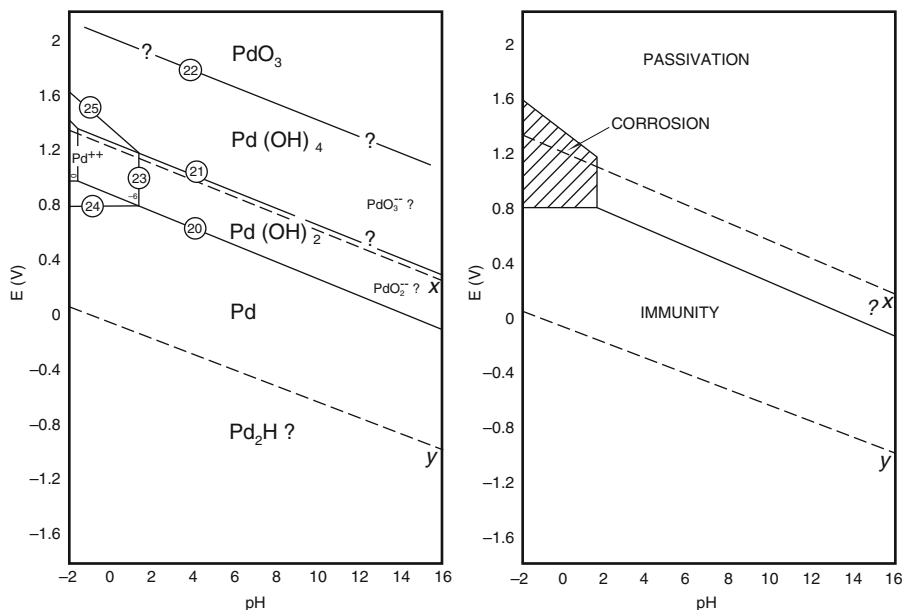
Fig. 4 *Left*: Potential-pH diagram for palladium–water at 25°C. *Right*: theoretical conditions for the corrosion, immunity and passivation of palladium at 25°C. Reproduced from Pourbaix et al. [20], with permission from Johnson Matthey plc

can erode from the catalyst surface into a polar solvent, or conversely of the reduction of such species to form the zero-valent metal, which has the propensity to migrate or coagulate. A better understanding of such processes will lead to more effective preventive strategies against leaching.

This has a great deal of analogy with concepts in corrosion science, where potential/pH (also known as Pourbaix) diagrams are used to indicate the thermodynamic stability, solubility and equilibria of metallic elements and their ions in an aqueous environment [19]. The Pourbaix diagram for palladium is reproduced in Fig. 4 [20]. A simplified diagram is provided on the right, indicating regions of immunity, passivation and corrosion. Immunity denotes the region where the metal is not subject to attack by the aqueous media. Conversely, under highly oxidative condition (top of the diagram), the metal forms a stable protective coating of metal oxides ("passivation"). At lower pH (<2) and potentials of between 0.8 and 1.6 V, palladium corrodes by forming water-soluble cations that can leach into the solution.

Using this diagram, it is perhaps easy to understand why leaching is less of an issue with catalytic hydrogenation reactions – a commonly employed industrial process for the reduction of a wide range of moieties, including alkene, alkyne, nitro, cyano and carbonyl functional groups. These reactions were often conducted in protic solvents, operating via chemisorbed hydride species under a reductive potential ($E° < 0$ V), which fall within the "immunity" region of the diagram.

Currently, Pourbaix diagram is not applicable to reactions occurring in aprotic organic solvents. With greater demand of continuous catalytic flow strategy for organic synthesis, many of which involve redox catalysis, the ability to construct and predict similar phase diagrams for alternative reaction media will undoubtedly be very useful to help identify reaction conditions where catalyst leaching may be avoided.

3 Indirect Methods for Detecting Catalyst leaching

Operando spectroscopy is undoubtedly a very powerful tool for catalytic research, offering unparalleled access to catalytic behaviour on the surface and in solution in real time. However, such experiments require an intense source of X-ray flux accessible only at synchrotron facilities, where special reaction cells will have to be custom-made to afford time-resolved studies under catalytic conditions. The processing and interpretation of XAS data (XANES and EXAFS) are also non-trivial, and the technique is still limited by sensitivity of detectors (<100 ppm of metal will typically be very challenging). Last but not least, for XAS studies, certain catalytic samples may not be stable against exposure to the intense X-ray beam. Careful control experiments are therefore necessary in order to avoid erroneous interpretation of results.

For a modestly resourced laboratory, it may be more practical, at least initially, to rely on reaction profiling and ICP analysis to deduce what might be occurring at the molecular/nano scale. Kinetic analysis can be a powerful method for delineating the intrinsic rate(s) of a catalytic cycle, as well as other underlying processes such as mass transfer, deactivation and leaching. This is achieved by judicious fitting of kinetic models to precise experimental data, preferably generated under different reaction conditions, including varying reaction stoichiometry, concentrations and temperature (for thermodynamic parameters). Indeed, many kinetic models have been developed for the determination of (de)activation mechanisms for both heterogeneous and homogeneous systems [21]. However, the situation is much more complicated when the system includes catalytic turnovers operating both at the surface and in solution. Generally, quantifying the contributions of different pathways is difficult, if not impossible [22].

The most common pitfall for kinetic analysis is inadequate assessment of the reaction parameters under which the experimental data are acquired. For example, NMR spectroscopy is often employed to follow the reaction progress of organic reactions. However, it is important to remember that the average timescale of acquiring a spectrum (typically up to 1 min) can be incompatible with fast catalytic reactions (typically ms or s). Furthermore, for heterogeneous reaction mixtures (either solid–liquid, liquid–liquid, or liquid–gas), the issue of mass transfer is an important consideration [23]. In theory, any heterogeneous reactions would ultimately encounter mass transfer limitations. Using catalytic hydrogenation as a typical example of a fast surface-catalysed reaction, the volumetric mass transfer

Fig. 5 Dynamic behaviour of a catalyst
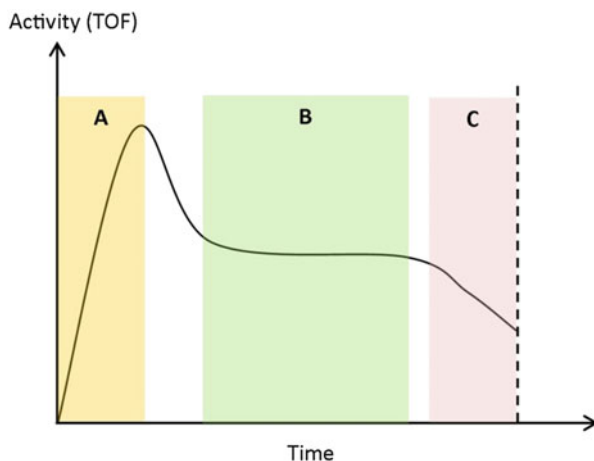
coefficient (k_La) has been estimated to range from 2.1 s^{-1} for a 1 L vessel to 0.05 s^{-1} for a 24,000 L reactor [24]. The use of microreactors to improve heat and mass transfer limitations has been much championed in recent years. Indeed, mass transfer coefficient of a micro-fabricated "packed-bed" device for catalytic hydrogenation reaction was found to range from 5 to 15 s^{-1} [25]. Therefore, any kinetic studies will be restricted by these mass transport limitations, i.e. this will necessarily imply that any TOF greater than these limits is a sign that the reaction may not be occurring solely at the heterogeneous interface.

In practice, all catalysts have a finite lifetime, eventually deactivate and lose activity via a variety of different mechanisms and processes, which may be due to changes in the catalyst structure, or passivation/deactivation as a result of interactions of the catalytic site with the reaction component(s), including reactants, (by)-products and impurities. Transient dynamic behaviour and performance of a catalyst over time can be most accurately assessed by using time-on-stream studies conducted in continuous flow. Some of the many transients a catalytic system may exhibit are depicted in the sketch in Fig. 5, including activation (A), steady state (B) and rapid deactivation (C).

In our earlier paper, we have recorded the different dynamic behaviour of two Pd catalysts (Pd/Al$_2$O$_3$ and PdEncat30) and the solvent effect on catalyst leaching [17]. In a more extensive study by Cantillo, Kappe and co-workers [26, 27], the catalytic behaviour of a number of commercially available immobilised Pd catalysts was directly compared in the C–C coupling reactions of 4-iodobenzonitrile with *n*-butyl acrylate (Heck arylation reaction, Eq. 1), or phenylboronic acid (Suzuki–Miyaura reaction, Eq. 2) (Scheme 4) under different flow conditions, with attendant ICP-MS analysis to determine the level of Pd residue present in the crude reaction mixture.

In all cases, catalyst leaching was observed regardless of the means of support, albeit to different degrees. Generally speaking, the covalent attachment of a phosphine ligand to a silica support appeared to be a more effective way to prevent
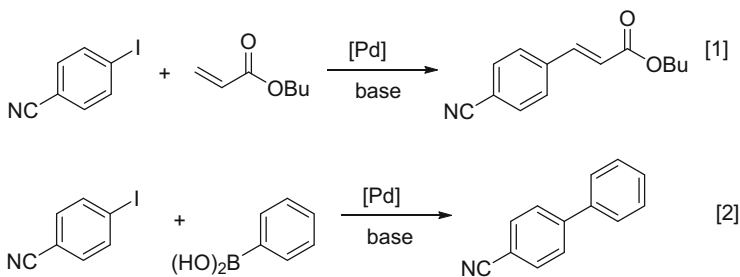
Scheme 4 The Heck arylation and the Suzuki–Miyaura reactions of 4-iodobenzonitrile
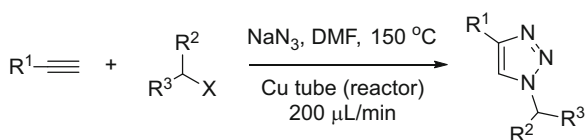
Scheme 5 Huisgen "Click" reaction afforded by a copper tube reaction

leaching, but the loss of Pd can only be really suppressed by using very dilute solutions, which is not a viable option for a chemical process. Thus, it was concluded that as far as these reactions are concerned, homogeneous catalysis may be a more effective strategy.

That said, catalyst leaching may not always be an undesirable process. A copper reactor was utilised as a means of slow release of active catalyst for the alkyne-azide (Huisgen) cycloaddition reaction, for the continuous synthesis of 1,4-disubstituted-1,2,3-triazoles (Scheme 5) [28]. In this case, the amount of Cu present in the solution was found to vary greatly depending on the solvent. The addition of a scavenging resin column reduced the amount of Cu to <5 ppm in the product.

Thus, the slow release of active catalysts that can subsequently perform a homogeneous reaction at high TOF might be in interesting approach towards minimising the total amount of metal contamination in key products.

4   Conclusions

Curiously, there seems to be a general reluctance of the catalytic chemistry community to address the issue of leaching, in particular the identification of truly heterogeneous and homogeneous rates or TONs. Yet, there is ever greater need to understand the phenomenon of catalyst leaching in order to arrive at a true understanding of the underlying catalytic process and, ultimately, for the technology to be adopted for scale-up processes.

Currently, the most reliable way of detecting leaching is by time-on-stream studies, coupled with ICP analysis of the product, which can be performed with relatively modest resources. However, in order to understand the fundamental molecular processes, *operando* spectroscopy has proven itself to be a highly valuable technique, where structure–activity–selectivity relationships can be established under working conditions. Results so far have revealed a compelling relationship between leaching and redox processes. There is sufficient evidence to show that redox catalysis involving oxidative processes can transform the elemental metal into a soluble charged or ionic species, facilitated by the use of polar solvents and oxidative atmospheres. However, more work is needed to understand these processes in greater detail, so that effective mitigation strategies can be devised. If a system could be devised to easily identify leaching via migration or erosion routes (Fig. 1) and to quantify heterogeneous versus homogeneous activity under reaction conditions, then innovation in immobilisation techniques would get a much needed boost.

Here the powerful combination of operand spectroscopy and kinetic analysis may be the vital tool to resolve and deconvolute cause and effect regarding the dynamic behaviour of the catalyst and its consequences for the catalytic reaction itself. To achieve this, both kinetic analysis and concurrent spectroscopy will need to be performed at sub-second timescales. This will require the development of novel in situ cells, fast spectroscopy techniques and more sensitive detectors, as well as the associated online analytical tools, e.g. flow-IR or Raman. In this regard, the increased miniaturisation and commercial availability of these instrumentations in recent years will certainly be very beneficial for the development of these techniques.

At the same time, it may also be necessary to look towards tools and knowledge already accrued in related disciplines that may offer an insight into the fundamental processes governing catalyst leaching, for example, the development of phase diagrams to understand the speciation of metals and their ions in organic solvents. Equally, leaching of metals into a liquid is widely studied in the field of hydrometallurgy, where the aim is to extract or recover valuable metals from mineral ores. During the solvent extraction process, ligands and ion-exchangers are added to facilitate the abstraction of the metal ion into a water-immiscible phase [29]. Whilst catalyst leaching is often considered to be an undesirable process in the chemical industry, there are many lessons that can be learnt from the metal extraction industry (which fields many catalyst manufacturers in its midst), most notably, how the solubility of a metal ion and its separation from a surface may be affected by its interaction with ligands [30].

Last but not least, where catalyst leaching is inevitable, there have to be effective methods for their removal from the reaction stream by optimisation of operating procedures (which could include controlled leaching) and, if this is not possible, by the application of effective metal scavengers [31] or the use of organic solvent nanofiltration (OSN) membranes [32] to retain the homogeneous catalytic component in the reaction vessel. The choice of removal techniques will depend greatly on the type of leaching process (migration or corrosion pathways, Fig. 1); for example,

whilst OSN membranes would be suitable for the removal of nanoparticulate material, metal scavengers may be more effective for the discreet organometallic/colloidal species [33].

References

1. Gutmann B, Cantillo D, Kappe CO (2015) Angew Chem Int Ed 54:6688–6728
2. Cross A: preparation of pharmaceutical samples for metal analysis. https://www.rssl.com/~/media/rssl/en/files/documents/White-Paper/Preparation-of-Pharmaceutical-Samples-for-Metals-Analysis.pdf. Accessed 14 Aug 2015
3. Gruttadauria M, Giacalone F, Noto R (2013) Green Chem 15:2608–2618
4. Munirathinam R, Huskens J, Verboom W (2015) Adv Synth Catal 357:1093–1123
5. Gruber-Woelfler H, Radaschitz PF, Feenstra PW, Haas W, Khinast JG (2012) J Catal 286:30–40
6. Schmidt AF, Kurokhtina AA (2012) Kinet Catal 53:714–730
7. Whitesides GM, Hackett M, Brainard RL, Lavalleye JPPM, Sowinski AF, Izumi AN, Moore SS, Brown DW, Staudt EM (1985) Organometallics 4:1819–1830
8. Bañares M (2009) Top Catal 52:1301–1302
9. Bare SR, Ressler T (2009) Characterization of catalysts in reactive atmospheres by X-ray absorption spectroscopy. In: Gates BC, Knozinger H, Jentoft F (eds) Advances in catalysis, vol 52. Elsevier, San Diego, pp 339–465
10. Bordiga S, Groppo E, Agostini G, van Bokhoven JA, Lamberti C (2013) Chem Rev 113:1736–1850
11. Graefe M, Donner E, Collins RN, Lombi E (2014) Anal Chim Acta 822:1–22
12. Reimann S, Stoetzel J, Frahm R, Kleist W, Grunwaldt JD, Baiker A (2011) J Am Chem Soc 133:3921–3930
13. Reimann S, Grunwaldt JD, Mallat T, Baiker A (2010) Chem Eur J 16:9658–9668
14. Li Y, Liu JHC, Witham CA, Huang W, Marcus MA, Fakra SC, Alayoglu P, Zhu Z, Thompson CM, Arjun A, Lee K, Gross E, Toste FD, Somorjai GA (2011) J Am Chem Soc 133:3527–13533
15. Smith AJ, Trimm DL (2005) Ann Rev Mater Res 35:127–142
16. Simson S, Jentys A, Lercher JA (2015) J Phys Chem C 119:2471–2482
17. Brazier JB, Nguyen BN, Adrio LA, Barreiro EM, Leong WP, Newton MA, Figueroa SJA, Hellgardt K, Hii KK (2014) Catal Today 229:95–103
18. Newton MA, Brazier JB, Barreiro EM, Parry SA, Emerich H, Adrio L, Mulligan C, Hellgardt K, Hii KK (2015) Green Chem. doi:10.1039/C5GC01600B
19. McCafferty E (2010) Introduction to corrosion science. Springer, New York
20. Pourbaix MJN, Van Muylder J, de Zoubov N (1959) Platin Met Rev 3:100–106
21. Argyle MD, Bartholomew CH (2015) Catalysts 5:145–269
22. Schmidt AF, Kurokhtina AA, Larina EV (2012) Kinet Catal 53:84–90
23. Klaewkla R, Arend M, Hoelderich WF (2011) In: Nakajima H (ed) Mass transfer – advanced aspects. InTech, Rijeka, http://cdn.intechopen.com/pdfs-wm/23539.pdf
24. Nerozzi F (2012) Platin Met Rev 56:236–241

25. Losey MW, Schmidt MA, Jensen KF (2001) Ind Eng Chem Res 40:2555–2562
26. Greco R, Goessler W, Cantillo D, Kappe CO (2015) ACS Catal 5:1303–1312
27. Cantillo D, Kappe CO (2014) ChemCatChem 6:3286–3305
28. Bogdan AR, Sach NW (2009) Adv Synth Catal 351:849–854
29. Regel-Rosocka M, Alguacil FJ (2013) Rev Metal 49:292–315
30. Tasker PA, Tong CC, Westra AN (2007) Coord Chem Rev 251:1868–1877
31. Mendonca A (2008) Metal scavengers. In: Tulla-Puche J, Albericio F (eds) The power of functional resins in organic synthesis. Wiley-VCH, Weinheim, pp 227–243
32. Marchetti P, Jimenez Solomon MF, Szekely G, Livingston AG (2014) Chem Rev 114: 10735–10806
33. Gursel IV, Noel T, Wang Q, Hessel V (2015) Green Chem 17:2012–2026

Index